# *Wnt-TCF7L2-dependent transcriptional and chromatin dynamics in cardiac regeneration, homeostasis and disease*

---

Dissertation

for the award of the degree

"Doctor of Philosophy (Ph.D)"

within the doctoral program Molecular Medicine
of the Georg-August University School of Science (GAUSS)
at the Georg-August-Universität-Göttingen

Faculty of Medicine

submitted by
**Lavanya Muthukrishnan Iyer**

from Chennai, India
Göttingen 2018

**Members of the Thesis Committee:**

1. PD Dr. Laura C. Zelarayan
2. Prof. Dr. Steven A. Johnsen
3. Prof. Dr. Heidi Hahn
4. Prof. Dr. Thomas Meyer
5. Prof. Dr. Ralf Dressel
6. Prof. Dr. Jürgen Brockmöller

**Supervisor Name, Institute:** PD Dr. Laura C. Zelarayan, Institute of Pharmacology and Toxicology, University Medical Center (UMG), Robert-Koch Strasse 40, 37075, Goettingen, Germany.

**Second member of the thesis committee Name, Institute:** Prof. Dr. Steven A. Johnsen, Department of General, Visceral and Pediatric Surgery, University Medical Center (UMG), Robert-Koch Strasse 40, 37075, Goettingen, Germany.

**Third member of the thesis committee Name, Institute:** Prof. Dr. Heidi Hahn, Department of Human Genetics, Heinrich-Düker-Weg 12, 37073, Goettingen, Germany.

**Date of Disputation:**

**AFFIDAVIT**

Here I declare that my doctoral thesis entitled *"Wnt-TCF7L2-dependent transcriptional and chromatin dynamics in cardiac regeneration, homeostasis and disease"* has been written independently with no other sources and aids than quoted.

Göttingen, August 2018.

*-Dedicated to my parents Kalyani and Muthukrishnan, and all my teachers.*

*“Happiness can be found even in the darkest of times, if one only remembers to turn on the lights.”*

*-Albus Dumbledore*

**ACKNOWLEDGEMENT**

I express my deepest gratitude for my thesis supervisor Dr. Laura Zelarayan for her continuous support, guidance and motivation throughout all these years. She not only guided my thesis at every step, maintaining the intellectual and scientific quality of experiments, but also provided me with the most ambient resources and environment to develop and grow as a scientist, to be able to have a freedom of ideas, along with a positive scientific spirit. During the course of my PhD, she has constantly been by my side, through all my ups and lows and managed to still keep me optimistic and grounded at the same time. I believe that we both made a strong team together and overcame several obstacles and like many, finally won our own little scientific battles.

This thesis and our success would have been impossible without the help and support of Prof. Dr. Steven A. Johnsen and his entire team. His timely criticisms and an in-depth knowledge and expertise in chromatin biology shaped a significant portion of my thesis, and I am sincerely grateful for the crucial role he played in impacting my career. I also thank Prof. Dr. Heidi Hahn and all the other thesis advisory committee members for their cooperation and support.

A completely unexpected and a major change occurred during my PhD when I grew fascinated towards bioinformatics, becoming skilled at RNA and ChIP-seq data analyses and realized its importance. This was made possible by the superb teaching and a sound technical foundation laid by Dr. Sankari Nagarajan. She not only provided me with all the necessary tools to analyze complicated genomics data, but also ensured as a friend that I truly grasped the concept of each step, gradually making me skilled at this process. Her outstanding guidance later led to several collaborative efforts and projects that I partook in and benefitted from.

Further, I thank Prof. Dr. Wolfram H. Zimmermann and other group leaders of the institute for their discussions and patience in stringently reviewing my thesis regularly during our department seminars.

During my PhD, I was provided with tremendous support to travel for multiple important international conferences in the U.S and Canada, forging excellent collaborations and networking opportunities with world leaders in the field. This was made possible by the German Center for Cardiovascular Research (DZHK). I am deeply thankful to Sylvia Vann and Marion Rappe for managing and arranging finances, making our travels feasible.

I am thankful and lucky that I supervised a sharp and technically-skilled student Sze Ting Pang, who pursued a lab rotation and her master thesis under my guidance. As a result, she assisted me

with several crucial experiments and hence, was immensely helpful during my thesis-completion period.

What is lab without some fun? Scientific growth occurs only in a productive everyday-atmosphere. I truly enjoyed all the fruitful coffees/food and interesting discussions with my colleagues/friends- Norman, Farah, Sebastian, Denise, Franziska, Monique, Claudia, Patapia, and not to forget- some amazing conference (and personal) trips, which made my PhD life far more interesting than I could have possibly imagined.

A PhD does not just affect the life of the person pursuing it, but also indirectly influences the micro-environment of all the family members and friends. Hence, I thank my friends Gaurav, Anusha, Srikkanth, Janani, Abhishek, Srishti, Shobhit and Sundar for tolerating my nonsense and also hormones, at times. I also thank Ravi uncle for being my confidante throughout this phase and for helping me sort my thoughts.

The final and the most important people who have always encouraged and supported me in every possible way are my family. Amma, Daddy, Ramya and Jiju- I love you very much and acknowledge the emotional struggles you have undertaken for me and my career. My stay in Germany and hence, both my masters and PhD degrees would not have been possible without your love and motivation.

Last but not least, I thank the city of Goettingen, with its rich scientific history and accomplishments- for keeping me as crazy and as motivated in science even after all these years. I will dearly miss you and your Gaenseliesel!

## Table of Contents

## Declaration

I, Lavanya Muthukrishnan Iyer, hereby declare that the following doctoral thesis is organized into three chapters, a general abstract, introduction and discussion. These chapters consist of manuscripts either published or are in preparation for immediate submission in peer-reviewed journals.

Lavanya Muthukrishnan Iyer

## Abstract

Wnt/β-catenin-dependent signaling pathway is indispensible for cardiac development, becoming quiescent in the normal adult heart, and re-activated in both regenerative responses post-injury and in cardiac hypertrophy and failure. Many studies have demonstrated the effect of its main nuclear effector- Transcription factor 7-like 2 (TCF7L2) in influencing chromatin landscapes in different malignancies. However, despite being widely studied in the heart, there was little or no evidence for the role of Wnt-TCF7L2 in directly governing cardiac chromatin homeostasis. To address this direct function, we generated transgenic, inducible murine model with cardiomyocytes (CM)-specific B-catenin stabilization, which led to heart failure. We observed increased TCF7L2 expression in both neonatal ((with a regenerative potential, at postnatal day 6 (P6)) as well as in diseased (both experimental and transgenic) cardiac ventricular tissue. Genome-wide mapping of TCF7L2 targets revealed differential occupancies- proximal in neonatal and distal in diseased cardiac ventricles. Integration of genomic with transcriptomic data showed that TCF7L2 directly bound to and primarily regulated aldehyde and fatty acid metabolism in the neonatal; and cardiac developmental and angiogenesis processes in the diseased adult hearts, thereby discerning these two cardiac states. Our search for TCF7L2-cardiac interaction partners revealed remarkable context-specific associations. We identified GATA4 and KLF15 as components of the Wnt-cardiac complex, which repress the pathway for homeostasis in the healthy heart. Conversely, this Wnt-GATA4 interaction was lost in disease progression. Interestingly, despite a high Wnt activity, Wnt-GATA4 interaction persisted in neonatal hearts, suggesting the involvement of other co-factors that can provide this regenerative context. This led to the identification of associations between the Hippo and Wnt pathways in neonatal hearts. Furthermore, lack of cardiac Wnt repressors like KLF15 resulted in gradual cardiac dysfunction, unearthing a so far uncharacterized gene *Shisa3*, in this process. Genomic, transcriptomic and experimental data unraveled that *Shisa3* is a cardiac developmental gene, which is reactivated in heart disease, upon loss of KLF15 and activation of Wnt signaling. Our experiments showed that *Shisa3* belonged to the endothelial reprogramming process during pathological cardiac remodeling. Altogether, results from this dissertation dissected stage-specific nuclear roles of Wnt-TCF7L2, thereby identifying novel cardiac target genes and previously unknown interaction partners. These findings can potentially form the basis for therapeutic interventions promoting cardiac regenerative responses, in a safe, targeted manner.

# 1. Introduction

## 1.1 Cardiac remodeling

Cardiovascular diseases claim millions of lives annually, worldwide. During progression to heart failure following an infarct or injury, the heart attempts to compensate for the insufficient pump function by undergoing a series of gradual changes referred to as 'cardiac remodeling'. Remodeling not only refers to the physical, anatomical changes in the heart, but also to changes at the cellular, molecular, transcriptional and chromatin levels[1].

Cardiac remodeling includes a complex set of biological processes, which results in a gradual increase in left ventricular wall thinning, and a change in cardiac chamber dimensions to a more spherical and a less elongated shape. Although this process is primarily an adaption response of the heart for the functional demand; upon sustained stress, it is usually associated with a continuous decline in ejection fraction (a parameter which indicates the percentage of blood pumped out of the heart with each contraction), culminating in heart failure (Fig. 1)[2]. Myocardial infarction (MI), pressure overload (aortic stenosis, hypertension), inflammatory heart muscle disease (myocarditis), volume overload or idiopathic dilated cardiomyopathy, are some of the numerous causes that trigger pathological cardiac remodeling[3]. In contrast, the heart also undergoes physiological remodeling- a beneficial response to regular exercise and/or pregnancy. Studies have uncovered numerous mechanisms of physiological remodeling including improved cardiomyocytes (CM) differentiation from resident cardiac progenitor stem cells (CPCs)[4].

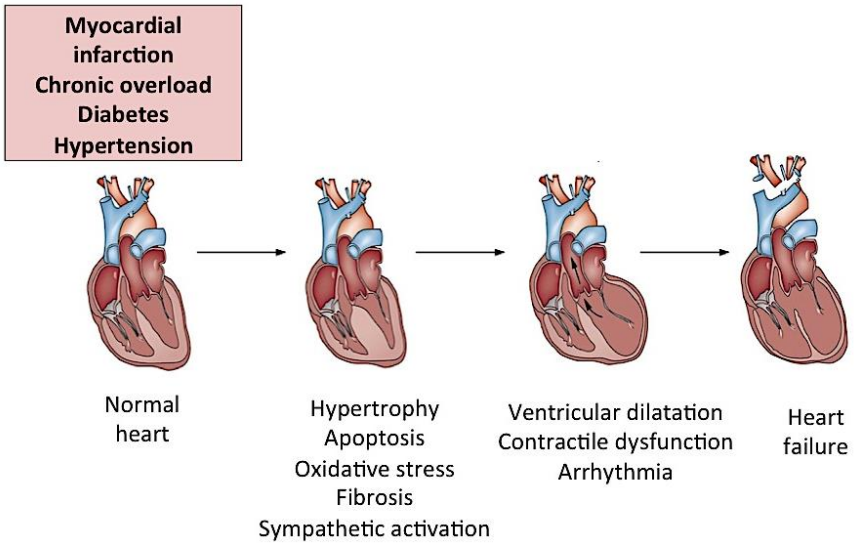


**Fig. 1: The stages of cardiac remodeling.** Upon myocardial infarction or stress, the normal heart undergoes CM hypertrophy and apoptosis along with increased fibrosis. This results in ventricular wall-thinning causing dilatation and contractile dysfunction terminating in arrhythmias and heart failure. Figure adapted from *Fan Jiang et al, 2014* [2].

During an attempt to revert to the normal physiology, the diseased adult myocardium re-activates developmental mechanisms, including gene transcription, cell cycle activation or pathways activated during embryogenesis[5,6]. Researchers in the past have overexpressed cell-cycle regulators like Cyclins and demonstrated that this activation, specifically in the adult myocardium, augments cardiac regenerative potential post-injury, thereby suggesting cell-cycle activation as a defense mechanism during heart disease[7,8]. Thus, given the increased mitosis in fully differentiated cells, cardiac remodeling can also be presumably construed as the 'cancer of the heart'. In this context, Wnt signaling, known to play significant roles in tumor progression[9,10] and metastases and being a predominantly pro-proliferative pathway, plays a crucial, multi-phasic role in both cardiac development as well as adult cardiac homeostasis[11–13].

A crucial aspect of cardiac remodeling is that it displays a hierarchical nature of progression. Starting with chromatin modifications, remodeling triggers transcription factor (TF) co-operativity, thereby leading to gene expression changes. This subsequently results in overall changes in sub-cellular, cellular and organ structure. These accumulating 'disease-programs' culminate in deteriorating heart function[14].

### 1.2 Chromatin responses to cardiac remodeling

Cardiac remodeling begins at the chromatin level, thereby rendering it as a 'root cause' triggering these maladaptive processes[15,16]. The cardiac chromatin acts as an ever-changing scaffold that responds to a multitude of physiological and pathological signals, hence controlling the accessibility of the DNA to environmental cues. Chromatin can be modulated by different factors such as nucleosome remodeling, histone modification and DNA methylation. Chromatin remodelers can associate to histone and DNA-modifying enzymes to mold genomic structure and reprogram gene expression in pathological heart disease[17,18].

There are two major types of enzymes governing chromatin remodeling. One type covalently modifies histone proteins and the other utilizes energy driven by ATP (adenosine triphosphate) consumption- to influence nucleosomes positioning. For example, belonging to the family of ATP-consuming chromatin-remodeling proteins, the SWI/SNF complex regulates transcription, in combination with co-activator and co-repressor complexes in the heart[17]. The SWI/SNF complex includes Brahma-Related-Gene (BRG1) ATPase, which plays crucial roles as chromatin-remodeling machinery during vertebrate heart formation[19,20]. An exciting study revealed a dosage-sensitive synergy between BRG1 and cardiac transcription factors like

GATA4, NKX2-5 and T-box 5 (TBX5). BRG1 haplo-insufficiency in mice hearts led to a reduced TBX5-GATA4 binding to the corresponding promoters of their target genes; suggesting that a relative balance between BRG1 and the master cardiac-TFs was indispensible for proper cardiac gene expression[20,21].

Furthermore, the Bromodomain and Extraterminal (BET) family of chromatin reader proteins (BRD2, BRD3, BRD4, and testis-specific BRDT) recognize and interact with acetylated chromatin; and mediate transcriptional activation by recruiting co-regulatory complexes like mediator and the Positive Transcription Elongation Factor-b (P-TEFb)[22]. An important study reported that BETs are important effectors of pathologic cardiac remodeling, through their ability to activate stress-related cardiac transcriptional programs. An important mechanism by which BETs drive pathological gene induction is through their property of triggering transcriptional pause-release and elongation, thereby co-activating multiple master TFs known to initiate and promote heart failure (HF)[23]. The unraveling of cardiac BET function underscores the relevance of epigenetic reader proteins in heart homeostasis and pathogenesis.

### 1.3 Enhancers and TF-cooperativity in cardiac gene regulation

The cardiac genome encompasses a large number of non-coding regulatory regions comprising insulators and enhancer regions that are responsible for maintaining normal gene expression. Of these regions, enhancers have been shown to act as key cis-regulatory players affecting gene transcription, irrespective of their orientation or distance from the gene body. An active enhancer, marked by histone 3, 27th lysine mono-acetylation (H3K27ac)[24] typically allows for the binding and enrichment of multiple TFs in a cooperative fashion, and regulates transcription from core promoters, mostly through long-range genomic interactions involving chromatin looping and topologically associating domains (TADs) formation. In the recent years, identification of the enhancers partaking in the cardiac developmental, homeostatic and disease programs has been of utmost interest and significance[25–27]. During embryogenesis, heart development occurs through a series of precisely orchestrated genetic programs, which are intertwined at each stage by TFs and chromatin regulators. Any minor aberration(s) in these carefully-structured events lead to congenital heart diseases (CHD), affecting approximately 1% of live births and considered the primary reason for neonatal deaths[21]. Importantly, studies have pointed to the unique and distinct appearances of enhancers during cardiac differentiation. In a mesodermal cell, a pioneer transcription factor (P-TF) binds to an enhancer and primes the locus,

pre-empting the future binding of cardiac TFs to activate gene expression, when the mesodermal cell specifies into a cardiomyocyte (Fig. 2)[27]. Such intricate enhancer dynamics entail a plethora of other investigations, delving deeper into the biology of distal regulatory elements in cardiac development.

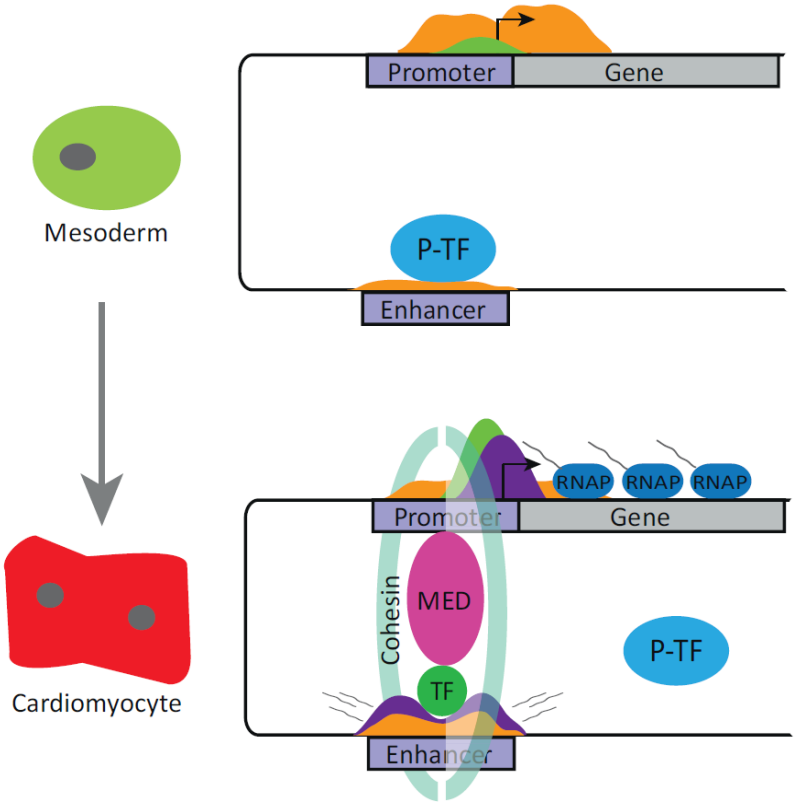


**Fig. 2: Enhancer dynamics during cardiac differentiation.** Maturation towards a differentiated state- a cardiomyocyte (red), from a multi-potent mesodermal cell (green) demands precise and dynamic changes occurring at the chromatin level for gene expression control. Binding of a pioneer transcription factor (P-TF) to the chromatin opens and primes it, pre-empting the region for probable future activation. Open chromatin enables consequent recruitment of the master cardiac TFs, in exchange for P-TF, essential for commitment to the cardiac fate. These TFs then further recruit chromatin modifying enzymes and chromatin architectural proteins like Mediator (MED) and cohesion, along with non-coding enhancer RNAs (eRNAs) produced from the enhancer region, in order to assist in the looping of the enhancers to a gene promoter region and control tissue-specific gene transcription. Yellow, purple and green colors on the promoters and enhancers represent various histone marks enriched during active gene transcription. Figure adapted from *JA Wamstad et al, 2014* [27].

Synergistic interactions between TFs elicit tissue and cell-specific gene expression that governs cell fate, essential for homeostasis. TFs may either activate or repress genes by recruiting co-activators, repressors, mediators or other TFs. These multiple factors along with their interactors serve as convergence points for driving various pathological networks in the myocardium[28–30]. Of note, recently, TFs have been the subject of profound interest owing to their context-specificities. Transgenic murine models have shown that activation of a specific group of TFs- GATA4, Myocyte enhancer factor-2 (MEF2), Nuclear factor κ-light-chain-enhancer of activated B cells (NFATc), and Myelocytomatosis viral oncogene (MYC) play direct and important roles in pathological cardiac remodeling *in vivo*. Moreover, GATA4 and T-box 5 (TBX5) cooperativity has been extensively described in cardiac gene regulation. A missense human

GATA4 mutation G296S was identified in patients with cardiac septal defects and cardiomyopathies. The GATA4-G296S mutation directly interfered with TBX5 binding to cardiac enhancers and resulted in an aberrant regulation of genes leading to defects in cardiac septation. Accordingly, this GATA4-G296S mutation resulted in an inability of GATA4 and TBX5 to suppress non-cardiac genes, thereby promoting opening of the chromatin at endothelial and endocardial gene promoters. These results elegantly unravel the intricate mechanisms of disease-causing mutations that can inhibit transcriptional co-operativity, generate aberrant chromatin landscapes and cellular changes, culminating in phenotypic and structural defects[29]. Although several studies have addressed the association between multiple cardiac master TFs essential for myocyte homeostasis, there is an urgent need to unravel novel TF interactions implicated in heart biology, particularly those that can be effectively, therapeutically targeted. Combining the knowledge of TF synergy along with relevant signaling cascades would help fine-tune and filter specific TF-TF interactions important for a particular context. On that note, Wnt signaling pathway plays crucial roles during cardiac development and disease; and Wnt inhibitors have been effective in treating multiple diseases in various animal models[31]. However, its nuclear and chromatin events were never thoroughly studied in the cardiac context before and hence, deserve further investigation.

### 1.4 Wnt signaling cascade

Wnt glycoproteins are a group of secreted, extracellular growth factors that regulate various intracellular signaling modules, in which the β-catenin-dependent (canonical) Wnt pathway has been extensively studied. Binding of Wnts to the seven transmembrane domain spanning Frizzled (FZD) receptor and the co-receptor Lipoprotein receptor- related 5/6 (LRP5/6) proteins results in the disruption of the cytosolic β-catenin destruction complex, including AXIN2, Adenomatosis polyposis coli (APC), Glycogen synthase kinase 3β (GSK3β) and Casein kinase 1α (CK1α). Post-stabilization and accumulation, β-catenin translocates to the nucleus, where it interacts with TCF (T-cell factor)/LEF (Leukocyte enhancement factor) transcription factors to activate the transcription of Wnt target genes like *Axin2, c-Myc* (Fig. 3)[32]. Activation of tissue-specific target genes is not well described.

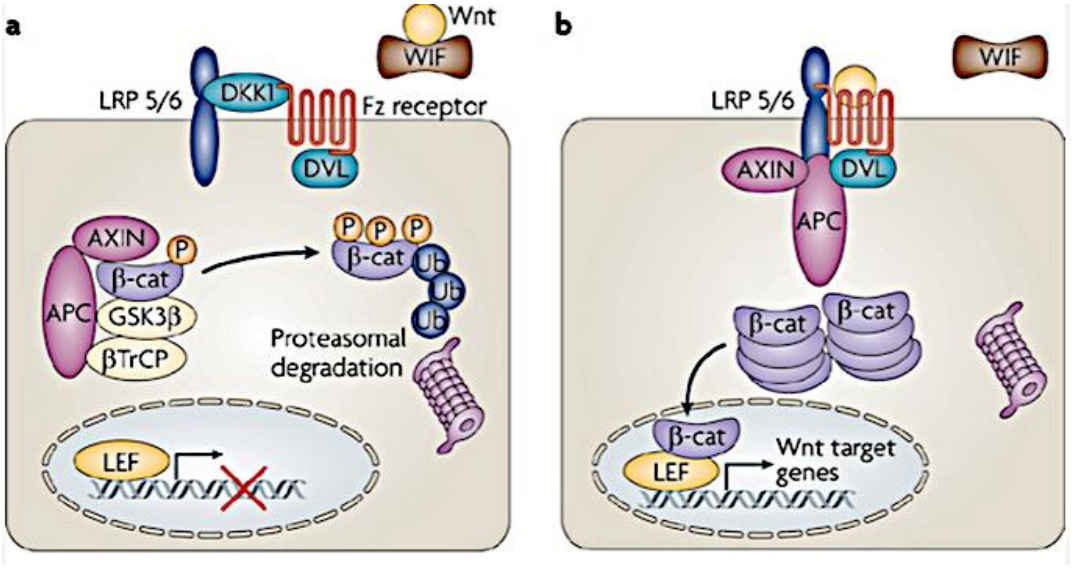


**Fig. 3: The B-catenin-dependent canonical Wnt pathway.** In the inactive state (a), β-catenin bound by AXIN2, APC, GSK3β is degraded. Upon Wnt binding (b) to FZD/LRP receptor, the destruction complex is sequestered causing accumulation of β-catenin and its nuclear translocation; switching on the pathway via TCF/LEF transcription of Wnt target genes. Figure adapted from *Inestrosa et al, 2010* [32].

### 1.5 Wnt signaling in cardiogenesis

Cellular differentiation is meticulously dictated by a complex synergistic network of TFs, which are regulated by effectors of several signaling pathways such as Wnt/β-catenin, ERK, AKT and TGF-β. During progenitor cells differentiation, the precise and dynamic activation of these pathways results in a redistribution of epigenetic modifications genome-wide, causing changes in chromatin architecture and concomitant gene transcription[12]. Wnt signaling is indispensible for vertebrate heart development and maturation[13,33,34]. Many studies have demonstrated the generation of ectopic hearts by conditionally inactivating β-catenin in the mouse embryonic endoderm[35]. However, some recent studies in zebrafish, mouse embryos, and mouse and human embryonic stem cells have uncovered time ad stage-specific roles of Wnt/β-catenin signaling, necessary for the formation of the vertebrate heart. These studies revealed that cardiac specification is initiated by the activation of the Wnt pathway, early during developmental stages, while cardiac induction during maturation/differentiation stages is repressed (Fig. 4)[36]. Correspondingly, addition of Wnt ligands enhances CM differentiation by inducing mesoderm specification in mouse and human embryonic stem cell cultures. Altogether, these results underscore the relevance of Wnt pathway in heart development and maturation, paving way for therapeutic interventions in cardiac repair.

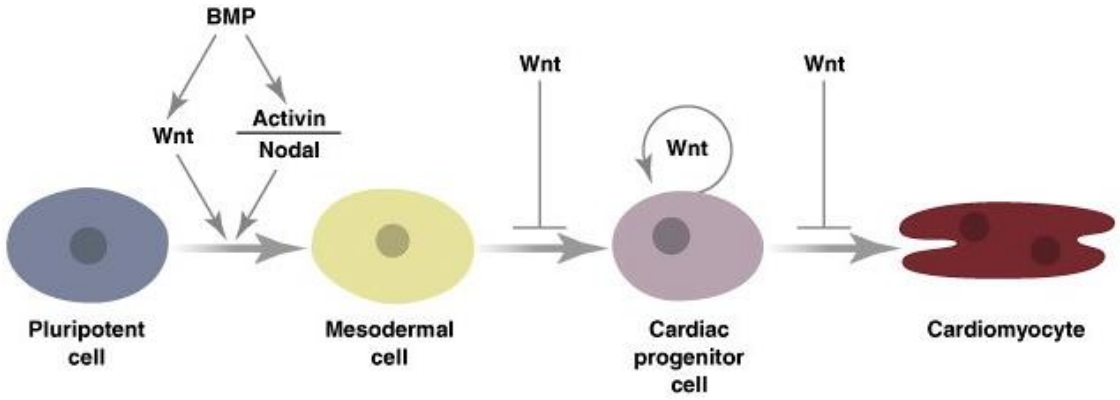


**Fig. 4: Role of Wnt signaling in cardiac development.** While initially Wnt is required for early cardiac mesoderm specification, it is inactivated to promote CPC maturation to CM. Activation at this stage renews CPC population. Figure adapted from *JM Alexander et al, 2010* [36].

### 1.6 Wnt signaling in cardiac regeneration and disease

The capability to repair damaged tissues varies significantly among different vertebrate species. The regenerative capacity of the heart has relevant clinical implications, since adult teleost fish and amphibians can regenerate their hearts, but the mammalian heart is unable to undergo sufficient regeneration upon injury. Interestingly, neonatal mice can also undergo cardiac regeneration, but lose this ability within 7 days after birth[37]. An important case study in 2009 reported complete myocardial functional recovery in a newborn human- born with compromised heart function and ECG, within 4 weeks after birth. This study instilled optimism in the field of human heart regeneration post-injury[38]. In zebrafish and neonatal mice, lost cardiomyocytes are replenished by a re-triggering of proliferation of already-differentiated, pre-existing CMs. While some CM turnover does occur in adult mammals, this CM formation rate is too low to compensate for the massive loss after an injury (Fig. 5)[18,39,40]. However, in response to injury, mammalian hearts retaliate by remodeling spared or remaining ventricular tissue, which ultimately results in pathological CM hypertrophy. On that note, β-catenin-dependent Wnt signaling plays important roles during vertebrate heart development and it is also re-activated in response to cardiac injury[11,41,42]. Regulation of cardiac remodeling by Wnt pathway is pleiotropic, depending on the injury model and the exact stages that have been studied. Furthermore, several components of the Wnt pathway have been shown to play a role in the cardiac injury response. Notably, GSK3β and sFRPs also elicit various functions unrelated to the Wnt pathway, which augments the complexity of attributing clear functional implications of the pathway in the heart. An in depth understanding of the *in vivo* role of Wnt/β-catenin signaling in injured mammalian hearts would help devise efforts towards developing regenerative strategies.

While some findings have demonstrated a similar activation of Wnt/β-catenin signaling during both cardiac regeneration and disease, there is little or no evidence supporting a direct nuclear role of the pathway in these processes. Even though targeting nuclear complexes can be challenging, their increased specificity in comparison to upstream cytosolic counterparts render them as attractive therapeutic avenues. Studying Wnt's chromatin actions in cardiac regeneration and disease would help *discern* these two states, paving way for identification of interesting context-specific targets. Moreover, several studies have shown that inhibiting Wnt pathway post-injury, led to better cardiac outcomes in murine and rat models[31,42,43]. A recent study described the role of Transcription factor 7-like 2 (TCF7L2), a main Wnt nuclear mediator in pathological heart remodeling[44]. However, there was no thorough investigation of its influence on the cardiac chromatin architecture. Our preliminary results revealed that of all the Wnt transcription factors, *Tcf7l2* showed the highest expression in murine cardiac ventricles. Hence, given that TCF7L2 possesses strong chromatin-modulation capabilities previously reported in various cancers, investigating the chromatin-associated roles of TCF7L2 would help distinguish these cardiac states, in a pathway, tissue and context-specific manner.

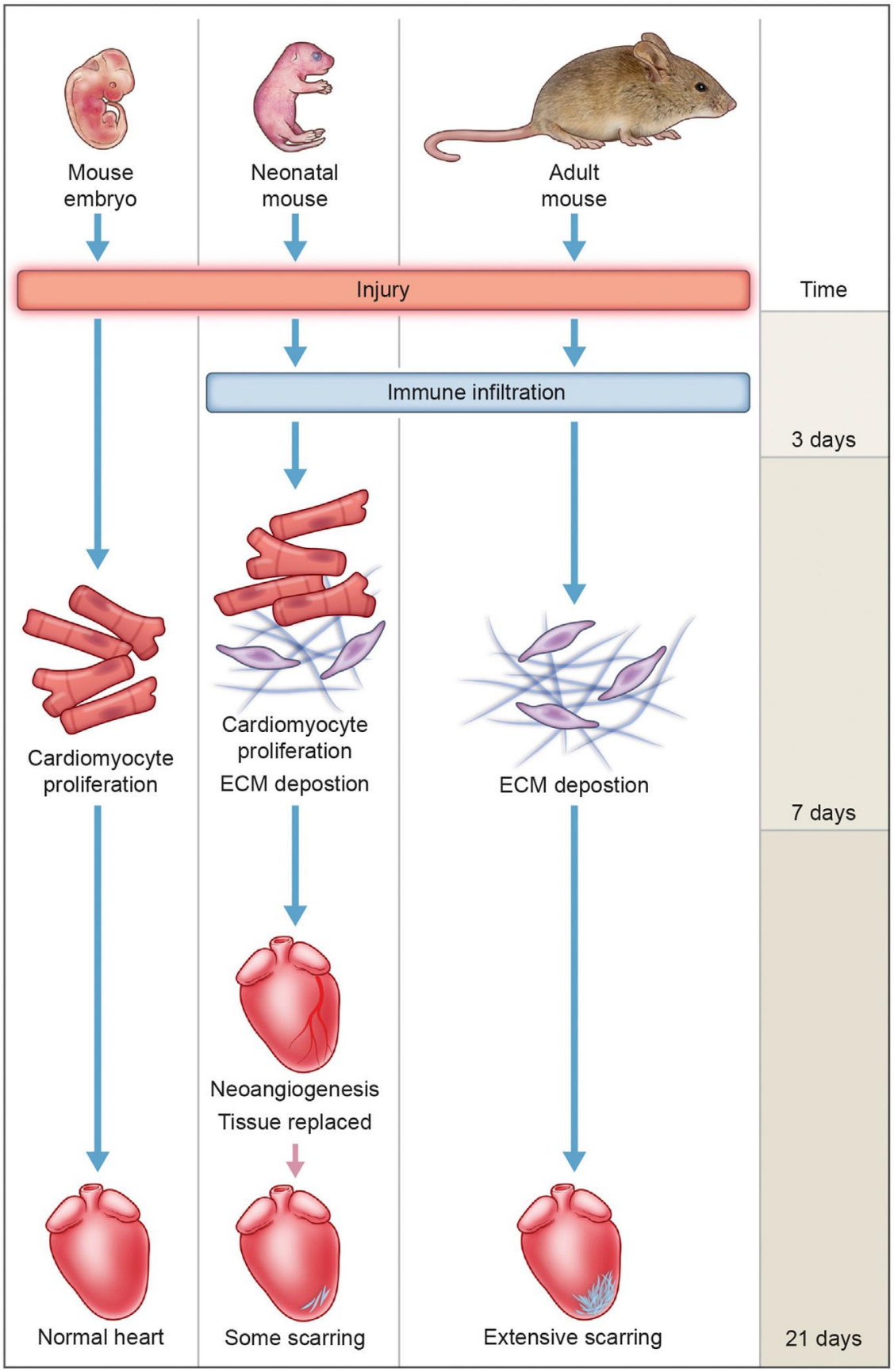
Mouse embryo
Neonatal mouse
Adult mouse
Injury
Immune infiltration
Time
3 days
7 days
21 days
Cardiomyocyte proliferation
Cardiomyocyte proliferation
ECM depostion
ECM depostion
Neoangiogenesis
Tissue replaced
Normal heart
Some scarring
Extensive scarring

**Fig. 5: Cardiac regeneration in fetal, neonatal and adult mammals.** In embryos, compensatory CM growth and proliferation can replenish up to half of the lost tissue. Regenerative neonatal murine heart tissue can replace a majority of lost CMs, with minimal scarring in myocardial infarction and other experimental injury models. Conversely, the adult murine heart tissue fails to replace lost tissue. Inefficient and incomplete CM proliferation and extracellular matrix deposition following injury supersede myocyte replenishment and lead to extensive scarring. *Figure from Uygur and Lee, 2016* [39].

## 1.7 The TCF/LEF family

TCF/LEFs are the main transcription factors that mediate downstream Wnt target gene transcription, in different organs. Unlike in lower order animals (invertebrates), which mostly consist of one TCF/LEF protein that can perform both activating and repressive functions on Wnt target transcription, in vertebrates, gene duplication and isoform complexity of the family have created isoform-specific functions. In Fig. 6, five most conserved domains found in this family: 1. the amino-terminal β-catenin-binding domain, 2. the Groucho binding sequence (GBS), 3. the high-mobility group (HMG) domain, 4. a nuclear localization signal (basic tail), and 5. the C clamp are schematically illustrated[45].

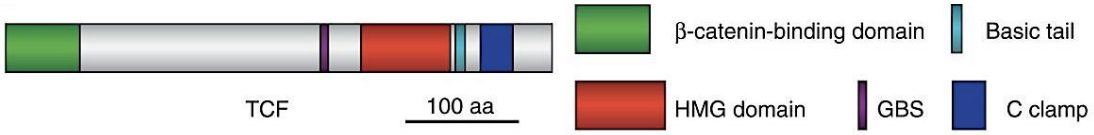


**Fig. 6: Schematic structure showing domains of TCF/LEF proteins**. TCF/LEF transcriptional factors contain five conserved domains in vertebrates. The amino-terminal β-catenin-binding domain, the Groucho binding sequence (GBS), the high-mobility group (HMG) domain followed by a nuclear localization signal (basic tail), and the C clamp can be seen. The specific TCF shown is from the sea urchin *Strongylocentrotus purpuratus. Figure adapted from T. Jin et al, 2008* [46].

Screening and chromatin immunoprecipitation studies involving TCF and B-catenin occupancies across different cell lines and tissue have unraveled a consensus sequence for the TCF/LEF HMG domain: 5′-SCTTTGATS-3′. Fine-tuning of Wnt signaling through TCF-specific functions can be observed in most vertebrates, in which the TCF/LEF family of genes are spread across four loci with alternative promoter usage and messenger RNA (mRNA) splicing[47–49]. These heterogeneous capabilities elicit a variety of tissue and cell-specific gene transcription. In this way, functional outcomes of this variation in these TCF/LEF isoforms can lead to different interpretations of Wnt signals.

### 1.8 Tissue-specific transcriptional actions of TCF7L2

TCF7L2 is robustly expressed in most mammalian organs. However, it elicits tightly controlled, tissue-specific pleiotropic responses in organ homeostasis and disease, by interacting with tissue-specific transcription factors (TF)[50–52]. Studies in the past have demonstrated that TCF7L2 is an important regulator of glucose production *in vitro* and binds directly to genes that are crucial in glucose metabolism pathways in the liver[53]. In pancreas, TCF7L2 is expressed in the beta cells and plays a crucial role in insulin secretion through regulation of the β-cell mass[54]. Importantly, the *TCF7L2* variant rs7903146 in humans was directly associated to the risk of developing type 2-diabetes, by modifying incretins and insulin secretion[55]. In the adult small intestine, *Tcf7l2* was shown to be indispensible for the maintenance of the $Lgr5^+$ stem cells and intestinal crypt homeostasis[56]. A recent study provided evidences for the role of TCFL72 in oligodendroglial maturation and myelination potential, by associating to stage-specific co-regulators Kaiso and Sox10[57]. In 2016, Hou and colleagues showed that TCF7L2 mediates *c-Myc* upregulation during pathological cardiac remodeling and that inhibition of this *c-Myc* axis can be potentially exploited for treating heart failure[44]. However, prior to this thesis study, a thorough, genome-wide mapping of TCF7L2 cardiac disease targets was not performed. Since TCFL72 is expressed in multiple tissues and is known to interact with tissue-specific co-regulators, this thesis aimed to dissect other components of the cardiac Wnt nuclear complex.

### 1.9 Krueppel- like Factor 15 (KLF15): A cardiac Wnt nuclear inhibitor

Krueppel-like factors (KLFs) are multifunctional transcriptional regulators that contain three conserved zinc finger domains within the carboxyl terminus that can bind a putative consensus sequence- 5′-C(A/T)CCC-3′ in numerous gene promoters and enhancers. The amino (N)-terminal functions for transcriptional activation, repression and for protein-protein interactions. Similar to TCF7L2, KLF proteins also regulate transcription by recruiting context-specific regulatory factors in different cell-types. These KLF TFs possess conserved structural homology across species, enabling them to perform similar functions, due to similar protein interaction motifs at their N-terminal domains[58,59].

KLFs can be classified into 3 groups: Group 1 (KLF 3, 8 and 12)- function as transcriptional repressors by associating with the C-terminal Binding Proteins 1 and 2 (CtBP1 and CtBP2). Group 2 (KLFs 1, 2, 4, 5, 6 and 7)- activate transcription. Group 3 (KLFs 9, 10, 11, 13, 12 and 16) members repress transcription by interacting with the known transcriptional co-repressor,

Sin3A. Notably, KLFs 15 and 17 are distantly related, devoid of known protein interaction motifs (Fig. 7). Interestingly, different KLFs were shown to be direct target-TFs regulated by the circadian master regulator –CLOCK[60,61]; and have been shown to have direct roles regulating circadian rhythm across several tissues.

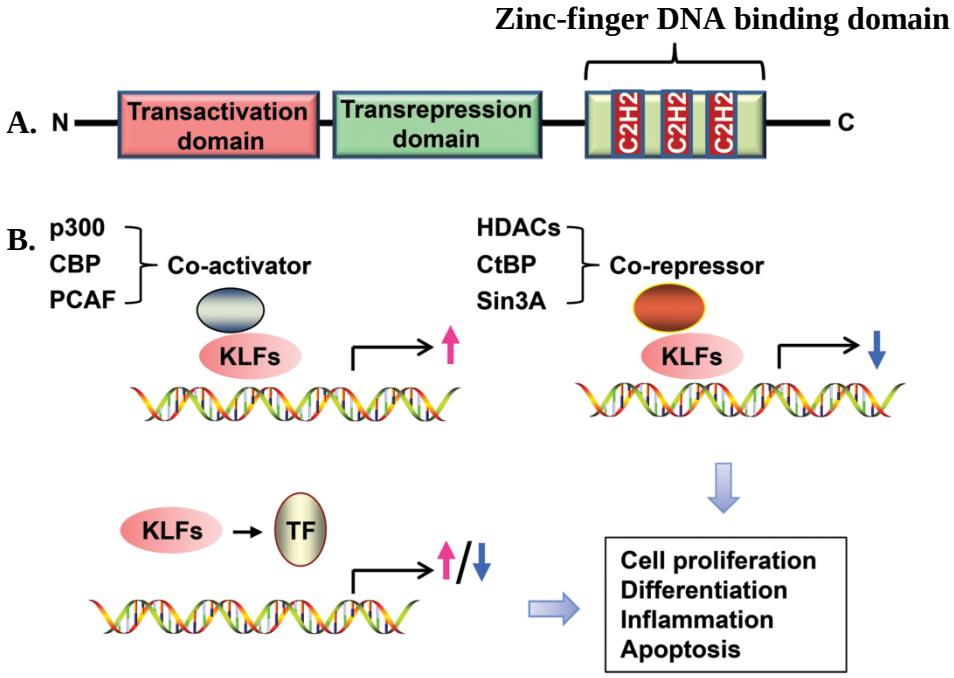


**Fig. 7: Schematic representation of KLF functional domains and gene regulation. A**. N-terminus of KLF proteins encompass transactivation and transrepression domains. C-terminus contains three consecutive zinc-finger (DNA-binding) motifs. **B**. Diagram illustrates mechanisms of KLF in gene transcription. KLFs can activate or repress gene expression in concert with co-activators or co-repressors, or through interaction with other specific TFs. CBP, CREB-binding protein; PCAF, p300/CBP-associated factor; HDACs, histone deacetylases; CtBP, C-terminal-binding protein; Sin3A, SIN3 transcription regulator family member. *Figure adapted from Y. Fan et al, 2017* [62].

Of these KLFs, KLF15 was shown to play a major role in cardiac homeostasis. Previous studies have defined KLF15 as a transcriptional repressor of pathologic cardiac hypertrophy. One study revealed that KLF15 competes with Serum-Response Factor (SRF) for a common docking site within Myocardin (MYOCD), hence suppressing MYOCD to activate cardiotrophic genes in normal adult CM[63]. On the other hand, previous data identified KLF15 as a nuclear, cardiac Wnt repressor affecting cardiac progenitor cell pool in the postnatal heart. This study had also concluded that the absence of KLF15 triggers Wnt/TCF7l2 activation, propelling an endothelial-cell-like program, which is crucial for the control of heart homeostasis and its adaptation to pathological remodeling[64].

In addition to being a significant repressor of cardiac hypertrophic responses, KLF15 is also known to be a crucial mediator of cardiac metabolism and cardiac circadian rhythm control[61,65,66]. In fact, it remains as the only non-core circadian TF to be well described in the adult heart. Interestingly, similar to TCF7L2, KLF15 also exhibits context-specific transcriptional responses by interacting with different TFs. For example, previous studies had described KLF15 binding to B-catenin, NLK as well as TCFL72- all components of the Wnt pathway, essential for cardiac homeostasis[64]. J. Li and colleagues showed that Sp1 and KLF15 interact to regulate basal transcription of the human *LRP5* gene, an important gene which controls osteogenesis and angiogenesis[67].

Apart from detailed research regarding its role in controlling cardiac circadian rhythm, KLF15's stage-specific role explaining its increasing embryonic-to-adulthood expression in the heart was never explored in depth before. Considering its importance in cardiac homeostasis, this particular aspect, in particular itcontribution to Wnt pathway regulation, deserves further investigation; since currently, copious efforts are directed towards targeted cardiac therapies.

### 1.10 Targeting chromatin modelers for therapy

Elucidation of chromatin-dependent cardiac states is currently being rigorously pursued and holds promising opportunities for therapeutic intervention. It is important to remember that basic chromatin research has led to remarkable therapeutic advances in the cancer field. Epigenetic instability caused by aberrant chromatin landscapes has been reported in numerous cancers like colorectal, pancreatic and breast cancer[68]. Such instabilities lead to widespread, global gene silencing with major effects on tumor-suppressor genes. Histone acetyl transferases (HAT) acetylate lysine residues in core histones, reducing DNA compaction, forming a more transcriptionally active chromatin. Conversely, histone deacetylases (HDAC) remove the acetyl groups from the lysine residues, thereby condensing and transcriptionally silencing the chromatin. Studies have exploited this meticulous cellular balance between HATs and HDACs to design targeted strategies with ingenuity. For example, an example is Azacitidine: a chemical analogue of the nucleoside cytidine. It possesses anti-cancer activity via two mechanisms – at low doses, by repressing DNA methyltransferase, causing hypo-methylation of DNA; and at high doses, by its direct cytotoxicity to abnormal hematopoietic cells within the bone marrow by incorporating into DNA and RNA, leading to cell death[69,70]. However, these epigenetic drugs fail to act in a targeted manner, leading to massive side effects. In some cases, they even give rise to

other types of malignancies- teaching us an important lesson that targeting the chromatin globally would be counter-productive. Despite tremendous progress in the field of cardiac chromatin biology, there exists an urgent need to identify and dissect specific machineries modulating the cardiac chromatin in homeostasis and disease.

## 2. Summary of Aims:

### 2.1 Deciphering the chromatin actions of TCF7L2 in the diseased myocardium.

The cardiac genomic occupancy of TCF7L2 was never investigated before at the chromatin level, at any age or context. Considering that Wnt signaling pathway is active during cardiac development and disease, studying the role of its main nuclear effector TCF7L2 would not only enrich our understanding of the core cardiac chromatin-functions of the Wnt pathway, but also identify specific interacting partners in driving heart disease progression. This study further addresses the functional relevance of the newly identified cardiac co-factors within the Wnt-TCF7L2 complex.

### 2.2 Discerning Wnt-TCF7L2 chromatin landscapes in the neonatal, adult and diseased myocardium

The diseased myocardium reactivates developmental machineries (like the Wnt pathway) in order to restore cardiac function. However, in the non-regenerative, mature adult heart, this activation is seldom sufficient to replenish the lost myocytes, post-injury or stress. This suggests the existence of a pathological as well as a regenerative response during heart disease progression. Therefore, unraveling Wnt-associated chromatin states and distinguishing relevant molecular players in the neonatal hearts from diseased hearts could help develop specific strategies inhibitng pathological responses, whilst safely activating regenerative responses during heart disease progression. This study also aims at identifying processes and co-factors that are differentially unique for each stage, driven under Wnt-TCF7L2 transcriptional control.

### 2.3 Role of the Wnt inhibitor, Krueppel-like factor 15 (KLF15) in cardiac homeostasis and disease

Previous work had identified KLF15 as a cardiac Wnt-nuclear repressor, demonstrating that hearts lacking KLF15 develop dysfunction, due to a concomitant Wnt activation. The present study aims at understanding and dissecting stage-specific global transcriptional programs governed by KLF15 in cardiac homeostasis, by investigating hearts with and without KLF15, at different ages. This study also aims at identifying molecular mechanisms that lead to deteriorating cardiac function upon loss of KLF15, by studying novel target genes.

# 3. Author contributions

## Chapter 1

**Individual contribution(s) to published article**

**Applicant (name): Lavanya M. Iyer (first author)**
Individual contribution:

1. **Figures and Sub-figures (actively performed experiments and/or analyzed data)**

**Main:**
**1** B, C, D, E, F, G, H, I, J, K; **2** A, C, F, G, H, I; **3** A, B, C, D, E, F; **4** A, B, C, D, E, F, G, H, I; **5** A, B, C, D, E; **6** A, B, C, D, E; **7** A, B, C, D, E, F, G, H; **8** B, C, D, F.
**Supplementary:**
Table **S1,** Figures- **S1** C, D, E, F, G; **S2** B; **S3** A, B, C, D, E; **S4** A, B, C; **S5** A, B; **S6** A, B, C, D, E; **S7** D, G.

2. **Writing**

**Main:**

a. Title and Abstract
b. Materials and Methods
c. Results
   *All results and discussion were written in association with PD Dr. Laura Zelarayan (corresponding author)
   *also edited the whole manuscript for sentence, grammar and punctuation.
d. Figure legends

**Supplementary:**

a. Experimental procedures
b. Figure legends

3. **Intellectual contributions**

a. Experimental design, especially establishing ChIP-seq for cardiac tissue for TCF7L2, integrative RNA and ChIP-seq data analyses (foundation of data analyses was established in concert with Dr. Sankari Nagarajan and Prof. Dr. Steven A. Johnsen) and interpretation, identification of novel TCF7L2 targets in the heart, discerning cardiac and liver-specific TCF7L2 target genes, identifying the role of GATA4 within the Wnt nuclear complex.
b. Devised main title and result titles.
c. Wrote significant parts of the manuscript.

……
Signature of the applicant

## Chapter 2

**Individual contribution(s) to the manuscript**

**Applicant (name): Lavanya M. Iyer (first author)**
Individual contribution:

1. **Figures and Sub-figures (actively performed experiments and/or analyzed data)**

**Main:**
**1** B, E; **2** A, B; **3** A, B, C, D, E, F; **4** A, B, C, D; **5** A, B, C, D, E; **6** A, B, C, D, E, F; **7** A, B.

**Supplementary:**
Table **S1,** complete figures- **S1 and S2.**

**2. Writing**

**Main:** The whole manuscript including result titles, main title and abstract.

**3. Intellectual contributions**

a. Devised complete experimental set up for the manuscript: testing the neonatal cardiac TCF7L2 expression, immunoprecipitation experiments for GATA4 and B-catenin in the heart across different stages, performing ChIP-seq for TCF7L2, GATA4 and H3K27ac in P6 hearts and analyzed all ChIP-seq and RNA-seq data along with interpretation, identifying differential genomic binding of TCF7L2 across various heart conditions and the corresponding processes regulated, unearthing TEAD2 and its putative role within the cardiac Wnt complex.
b. Prepared all the figures and wrote the entire manuscript.

……
Signature of the applicant

**Chapter 3**

## Individual contribution(s) to the manuscript

**Applicant (name): Lavanya M. Iyer (first author)**
Individual contribution:

1. **Figures and Sub-figures (actively performed experiments and/or analyzed data)**

**Main:**
**2** A, B; **3** A; **4** D; **5** E, H, I; **6** B, C, D, I; **7** E, F.
**Supplementary:**
Figures- **S1** A, B; **S2** C; **S3** A, B; **S6** A, B.

2. **Writing**

**Main:**

a. Parts of materials and methods
b. Results involving own contribution * manuscript was revised after being written by PD Dr. Laura Zelarayan (corresponding author) *also edited the whole manuscript for sentence, grammar and punctuation.
c. Figure legends in association with Claudia Noack (first equally contributed author)

**Supplementary:**

a. Experimental procedures
b. Figure legends for figures involving own contribution

3. **Intellectual contributions**

a. Integration of KLF15 ChIP-seq and RNA-seq to interpret direct, stage-specific target genes; generation of heatmaps and PCA plots to display RNA-seq data; quantification of endothelial-like cell markers in stressed TAC hearts, motif search on the differentially expressed genes in KLF15 KO hearts revealing endothelial transcription factors dysregulation; direct repression of Shisa3 upon KLF15 cardiac expression; testing endothelial markers in KLF15 electroporated hearts; *in silico* binding of KLF15 on *Shisa3* promoter in adult hearts.
b. Devised parts of main title, abstract and result titles.
c. Helped writing results involving own contribution.

……
Signature of the applicant

Declaration by joint-first author: **Dr. Claudia Noack**

……
Signature of the joint-first author

# 4. Chapter 1: Deciphering the chromatin actions of TCF7L2 in the diseased myocardium.

Publication in *Iyer, L. M et al., Nucleic Acids Research 2018 Apr 6; 46(6):2850-2867. doi: 10.1093/nar/gky049.*
Copyright license number from journal: *438148049822.*

**'A context-specific cardiac β-catenin and GATA4 interaction influences TCF7L2 occupancy and remodels chromatin driving disease progression in the adult heart'**

Lavanya M. Iyer[1,2], Sankari Nagarajan[3,4], Monique Woelfer[1,2], Eric Schoger[1,2], Sara Khadjeh[2,5], Maria Patapia Zafiriou[1,2], Vijayalakshmi Kari[2], Jonas Herting[2,5], Sze Ting Pang[1,2], Tobias Weber[1,2], Franziska S. Rathjens[1,2]; Thomas. H. Fischer, MD[2,5], Karl Toischer[2,5], Gerd Hasenfuss[2,5], Claudia Noack[1,2], Steven. A. Johnsen[3] and Laura C. Zelarayán*[1,2]

[1] Institute of Pharmacology and Toxicology, University Medical Center Göttingen, Georg-August University, Göttingen & German Centre for Cardiovascular Research (DZHK) partner site Goettingen, 37075 Germany

[2]German Centre for Cardiovascular Research (DZHK) partner site Goettingen, 37075 Germany

[3] Department of Visceral and Pediatric Surgery, University Medical Center Göttingen, Georg-August University, Goettingen, 37075 Germany

[4]Cancer Research UK (CRUK-CI), Cambridge, CB2 0RE, United Kingdom

[5]Department of Cardiology and Pneumology, University Medical Center Göttingen, Georg-August University, Goettingen

**Abstract**: Chromatin remodeling precedes transcriptional and structural changes in heart failure. A body of work suggests roles for the developmental Wnt signaling pathway in cardiac remodeling. Hitherto, there is no evidence supporting a direct role of Wnt nuclear components in regulating chromatin landscapes in this process. We show that transcriptionally active, nuclear, phosphorylated(p)Ser675-β-catenin and TCF7L2 are upregulated in diseased murine and human cardiac ventricles. We report that inducible cardiomyocytes (CM)-specific pSer675-β- catenin accumulation mimics the disease situation by triggering TCF7L2 expression. This enhances active chromatin, characterized by increased H3K27ac and TCF7L2 occupancies to cardiac developmental and remodeling genes *in vivo*. Accordingly, transcriptomic analysis of β-catenin stabilized hearts shows a strong recapitulation of cardiac developmental processes like cell cycling and cytoskeletal remodeling. Mechanistically, TCF7L2 co-occupies distal genomic regions with cardiac transcription factors NKX2–5 and GATA4 in stabilized-β-catenin hearts. Validation assays revealed a previously unrecognized function of GATA4 as a cardiac

repressor of the TCF7L2/β-catenin complex in vivo, thereby defining a transcriptional switch controlling disease progression. Conversely, preventing β-catenin activation post-pressure-overload results in a downregulation of these novel TCF7L2-targets and rescues cardiac function. Thus, we present a novel role for TCF7L2/β-catenin in CMs-specific chromatin modulation, which could be exploited for manipulating the ubiquitous Wnt pathway.

## Introduction

Wnt signaling is evolutionarily conserved and has key roles in tissue remodeling in embryonic development and adult diseases (1-3). In the postnatal heart, activation of different components of the Wnt/β-catenin pathway was shown upon hypertrophic and ischemic stimuli in different cell types (4-6). Conversely, inhibition of Wnt signaling appears to protect the heart from ventricular remodeling (5,7-9). In the absence of β-catenin or Lymphocyte Enhancer transcription factor (Lef-1) activity, cardiomyocytes (CM) growth is impaired (10). Although functional roles of Wnt/β-catenin signaling in the heart have being studied since about a decade, the epigenetic mechanisms and molecular network driven by its activation are largely unknown.

Wnt canonical signaling activates gene expression by inducing formation of complexes between DNA-binding transcription factors and the co-activator β-catenin, which can be further modulated by tissue-and context-specific repressors or activators (11,12). Upon Wnt receptor activation, increased stability of β-catenin triggers target gene transcription. This is regulated by the interactions of the transcriptionally active form Ser675-phosphorylated ($pSer^{675}$) of β-catenin with members of the TCF/LEF family members through a displacement of repressors from the TCF/LEF complex (13-15). This leads to increased histone acetylation, resulting in chromatin remodeling and gene activation (16,17). TCF/LEF factors are essential for transducing the activation of the Wnt/β-catenin axis. Context-dependent Wnt signaling actions are further fine-tuned by recruiting cell-specific modulators to chromatin complexes (18). TCF transcription factor-7 like 2 (TCF7L2), one of the main transcriptional effector of the Wnt cascade, is expressed in several tissues and was shown to regulate the ubiquitous Wnt target gene Myc in pathological cardiac remodeling (19). Nonetheless, TCF7L2 has been shown to have both tissue- and disease-specific roles concerning distal enhancers. Importantly, enhancers can regulate context-specific gene expression by associating to specific cardiac transcription factors (TFs) (20-23). Overall, the genome-wide tissue-specific regulatory complex of the ubiquitous Wnt

cascade, which may help identify more selectively targetable molecules modulating disease progression, remains mostly poorly understood.

In this study, we show that the very low Wnt/β-catenin activity in the healthy adult heart is increased upon pressure overload in murine and human hearts, which depends on transcriptionally active pSer$^{675}$-β-catenin. Using CM-specific β-catenin stabilization, we mimic all molecular hallmarks of Wnt activation as found upon hypertrophic stimuli, which results in a hypertrophy-like phenotype and severe heart failure. We show that Wnt/β-catenin/TCF7L2 activation leads to increased genome-wide chromatin accessibility and inducible TCF7L2 recruitment to so far unrecognized heart-specific regulatory genomic regions, driving pathological cardiac remodeling. Conversely, β-catenin inactivation post-pressure-overload resulted in a reduced expression of these TCF7L2 novel genes and prevented heart failure development, confirming the validity of our findings. Most importantly, we discovered a role for the hypertrophic transcription factor GATA4 in fine-tuning Wnt/β-catenin/TCF7L2 activation, to maintain adult heart homoeostasis.

## Materials and Methods

### Mouse models

Gain (β-catenin$^{\Delta ex3}$) and loss (β-catenin$^{\Delta ex2–6}$) of function models were achieved by mating *Myh6* merCremer (24) mice with either β-catenin floxed-ex3 (25) and β-catenin floxed$^{\Delta ex2–6}$ (Jackson Lab). For transgenesis induction, heart-specific expression of the Cre recombinase under control of the *Mhy6* promoter was activated by administration of Tamoxifen (T5648, 30 mg/kg body weight/day; Sigma– Aldrich) i.p. for 3 days. Excision of *loxP*-flanked exon 3 of the β-catenin coding region in αMHC-merCremer/β-catenin floxed-ex3 resulted in a non-degradable mutant of β catenin and in αMHC-merCremer/β-cateninfloxed-ex2–6 in non-functional β-catenin. Littermates WT at β-catenin locus and positive for Cre recombinase; and WT without Cre recombinase expression were used as controls. Genotyping primers are listed in Supplemental Table S1.

### Echocardiographic analysis and disease model

Transaortic constriction (TAC) was done in 12-weeks-old mice. Pre-anesthetic and anesthetic agents are listed in Supplemental Table S2. The intervention was performed by tying a braided 5–0 polyviolene suture (Hugo Sachs Electronik) ligature around the aorta and a blunted 26-gauge needle and subsequent removal of the needle. For sham controls, the suture was not tied. To

determine the level of pressure overload by aortic ligation, a high frequency Doppler probe was used to measure the ratio between blood flow velocities in right and left carotid arteries. TAC mice with blood flow gradient <60% were excluded. For echocardiography, mice were anesthetized by 2.4% isoflurane inhalation and ventricular measurements were done with aVisual- Sonics Vevo 2100 Imaging System equipped with a MS400, 30 MHz MicroScan transducer. The observer was unaware of the genotypes and treatments. All these procedures were performed by the SFB 1002 service unit (S01 Disease Models). All animal experiments were approved by the Niedersachsen (AZ-G 15-1840) animal review board.

**Human heart samples**

Left ventricular tissue was used for DNA and RNA isolation. RNA expression of foetal samples was described elsewhere (26). The investigation of human samples conforms to the principles outlined in the Declaration of Helsinki and was approved by the institutional ethics committee of the University Medical Center Goetingen (31 September 2000). DNA and RNA isolation and analyses are described in Supplemental Methods.

**RNA-sequencing (RNA-seq) and data analyses**

RNA-seq was performed at the Transcriptome and Genome Analysis Laboratory, University Medical Center, Goettingen, in biological triplicates. RNA was extracted, quality and integrity was assessed by Bioanalyzer (Agilent). Libraries were prepared and cDNA libraries were amplified

and the size range of final cDNA libraries was determined by applying the DNA 1000 chip on the Bioanalyzer 2100 from Agilent (280 bp). cDNA libraries were sequenced using cBot and HiSeq2000 Illumina (SR; 1 × 50 bp; 51 cycles with single indexing; 6GB ca. 30–35 million reads per sample). Sequence reads were aligned to the mouse reference assembly (UCSC version mm9) using Bowtie 2.0.(27). For each gene, the number of mapped reads was counted and DESeq2 was used to analyze the differential expression (28). Gene ontology (GO) analyses were performed using default parameters and stringency in 'ClueGO': a Cytoscape plug-in.(29) The significant 'GO Biological Processes' were shown with $P \leq 0.05$.

**Chromatin immunoprecipitation (ChIP-seq) and data analyses**

TCF7L2 and H3K27ac ChIPs in murine adult cardiac ventricular tissue were performed by 20 min crosslinking with 1.3% formaldehyde and sonicating for 45 cycles. Inputs were pre-cleared for 45 min at 4◦C using protein-A-sepharose beads. For immunoprecipitation, 2 _g of anti-

TCF7L2, anti-IgG (17–10109, Millipore), anti-GATA4 (sc-25310 X, SantaCruz) or anti-H3K27ac (C15410196, Diagenode) was added to the nuclear extracts and incubated O/N at 4◦C. Antibodies were pulled down using protein-A sepharose beads followed by washing and DNA extraction. For protein complex isolation, proteins were extracted from sepharose beads and supernatants were subjected to immunoblotting. ChIP-seq library preparation was performed using NEB Next Ultra DNA library prep kit for Illumina (E7370) as per manual's instructions. DNA libraries were amplified and sequenced by using the cBot and HiSeq2500 from Illumina (25–30 million reads per sample). Sequence reads were aligned to the mouse reference assembly (UCSC version mm9) using Bowtie2 (30). Peak calling was performed with Model Based Analysis of ChIPseq (MACS2) version 2.1.0.20140616.0 (31). Genes proximal to the bound chromatin regions were identified by GREAT analyses (32). Significant 'GO Biological Processes' were shown with $P \leq 0.05$. Published/public ChIP-seq datasets were used from the following sources: TCF7L2 liver: GSE32513; GATA4, NKX2–5 and TBX3: GSM862697- (33); DNAse-seq: GSM1014166; H3K4me1: GSM769025; RNAPII: GSM918723; H3K27me3: GSM1260017; KLF15: GSM1901940 and CTCF: GSM918756.

**Statistical analyses**

ANOVA single factor analysis was used to calculate the *P* value for qPCR-based analyses. G-Power3.1 was used to determine the sample size for animal studies. For ChIP-seq and RNA-seq analyses, *q*-value (to call peaks) and adjusted *P*-value of ≤0.05 was considered for statistical significance respectively. For motif analyses, *Z*-score and Fisher score (negative natural logarithm of *P*-value) were utilized for showing significant motifs. Unpaired student's test and two way ANOVA with Bonferroni post-test (GraphPad Prism 6.0) were used where appropriate for statistical analysis of epifluorescence measurements of calcium cycling parameters. Again, *P*-values<0.05 were considered statistically significant.

**Results**

**Phospho-Ser$^{675}$β-catenin triggers nuclear Wnt transcriptional reactivation upon cardiac pressure-overload in mice and humans**

The specific contribution of TCF/LEF family members to the Wnt axis in cardiac remodeling is not well defined. We established that TCF7L2 was mainly expressed in adult ventricles and was the highest expressed TCF/LEF member with activating function in the mouse and human left ventricle (Supplementary Figure S1A). In accordance with lowering Wnt activity during

maturation, TCF7L2 decreased from fetal to adult life in mouse and human cardiac tissue (Figure 1A). We next examined the dynamics of re-expression of TCF7L2 and the association to the Wnt/β-catenin activity during the course of transaortic constriction (TAC)-induced hypertrophic remodeling.

Three days after induction of induced pressure overload, β-catenin and TCF7L2 protein were significantly upregulated in left ventricular tissue, compared to sham controls. TCF7L2 remained upregulated 8 weeks post-TAC, although β-catenin levels were normalized, suggesting a sustained, transcriptional Wnt activation. Upregulation of TCF7L2 was confirmed in isolated CMs 3 days post-TAC (Figure 1B). To strictly test β-catenin-dependent transcriptional activation, we firstly analyzed pSer$^{675}$-β-catenin, which possesses high affinity for TCF/LEF family members for target gene regulation (36). Six weeks post-TAC, pSer$^{675}$-β-catenin and TCF7L2 were more abundant in TAC nuclear fractions, while total β-catenin was not significantly changed; in line with the observation 8 weeks post-TAC (Figure 1C).

**Figure 1.**

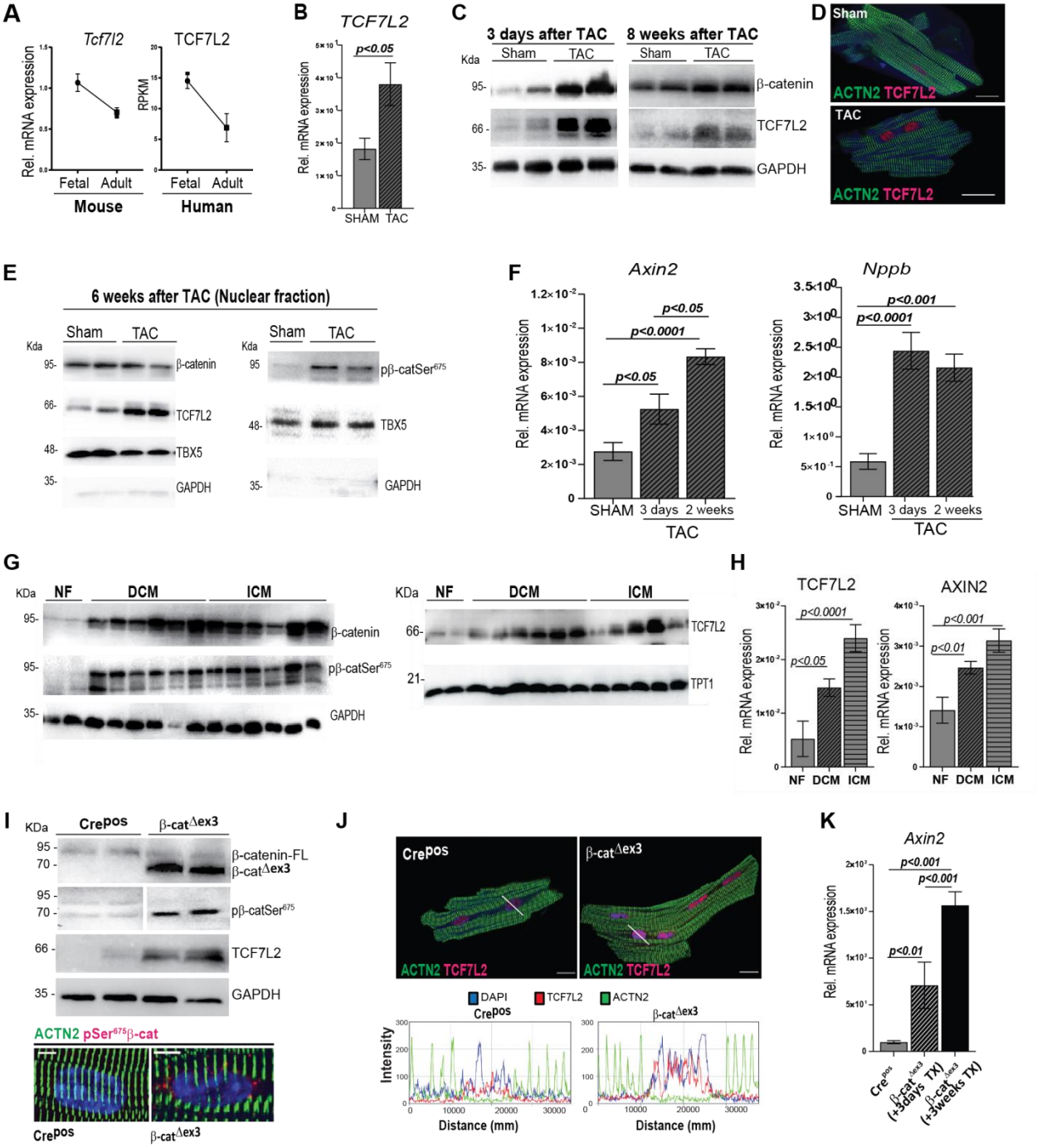


**Figure 1: Nuclear phosphorylated-Ser675 β-catenin triggers Wnt transcriptional reactivation upon cardiac pressure-overload in mice and humans.** (**A**) Normalized transcript expression of murine and RPKMs of human TCF7L2 expression in fetal and adult hearts (*n*=3/per group). (**B**) Relative transcript levels of *Tcf7l2* in 8 weeks post-TAC heart tissue vs. sham control (n≥5). (**C**) Representative immunoblots of TCF7L2 and β-catenin expression 3 days and 8 weeks post-TAC in murine heart ventricles compared to sham (n≥4). (**D**) Immunofluorescence image representing increased TCF7L2 (magenta) in isolated cardiomyocytes (CM) from 3 days post-TAC murine hearts (*n*=3/group). (**E**) Total β-catenin, TCF7L2 and pSer675-β-catenin in nuclear (TBX5-enriched) fraction, 6-weeks post-TAC. (**F**) Relative transcript levels of the classical Wnt target gene, *Axin2*, and CM hypertrophic marker,

*Natriuretic peptide b* (*Nppb*) 3 days and 2 weeks post-TAC in murine ventricular tissue versus sham control ($n \geq 5$). (**G**) Western blots showing total β-catenin, pSer675-β-catenin and TCF7L2 in cardiac ventricular biopsies from ischemic (ICM) and dilated cardiomyopathies (DCM) as compared to non-failing (NF) human hearts (NF: $n = 2$; DCM: $n = 6$; ICM: $n = 6$). (**H**) *TCF7L2* and its target *AXIN2* transcript levels in cardiac ventricular biopsies from DCM and ICM as compared to NF human hearts (NF: $n = 7$; DCM: $n = 15$; ICM: $n = 11$). (**I**) Immunoblot showing stabilized (70 kDa) β-catenin, pSer675-β-catenin and TCF7L2 protein in β-cat$^{\Delta ex3}$ ventricles. Representative immunofluorescence images showing increased perinuclear/nuclear pSer675-β-catenin (lower panel) or (**J**) TCF7L2 (magenta) in isolated CM β-cat$^{\Delta ex3}$ ventricles compared to Cre$^{pos}$ along with corresponding plots below images representing fluorescence intensity profiles over the nucleus. ACTN2 is shown in green, DAPI nuclear staining in blue ($n = 3$/group). The profiles show DAPI (blue) signal overlapping with TCF7L2 (magenta) with a higher intensity in β-cat$^{\Delta ex3}$ CM. (**K**) Relative transcripts of *Axin2* after 3 days and 3 weeks of induction in β-cat$^{\Delta ex3}$ ventricles vs. control Cre$^{pos}$/ β-cat WT (Cre$^{pos}$) hearts ($n = 10$; 3 and 5; respectively). TATA-binding protein (*Tbp)* (B, F) and *GAPDH* (H) were used for transcript normalization. GAPDH and TPT1 serve as protein loading control for whole cell lysate (C, G and I) and GAPDH for cytosolic fraction (E) and TBX5 for nuclear fraction in E. Data are mean ± SEM; *t*-test and ANOVA, Bonferroni's multiple comparison tests. Scale bar: I: 5 μm and D, J: 20 μm.

Secondly, β-catenin/TCF7L2 transcriptional activity was confirmed by upregulation of a classical Wnt target, *Axin2*, along with the hypertrophy marker *Natriuretic peptide b* (*Nppb*), post-TAC induction (Figure 1D). Furthermore, analysis of left ventricular samples from human patients with dilated (DCM) and ischemic cardiomyopathies (ICM) showed upregulation of total β-catenin, pSer$^{675}$-β-catenin and TCF7L2 proteins as well as a transcriptional activation of AXIN2, in comparison to non-failing (NF) heart samples (Figure 1E, F). Altogether, our results show that pSer$^{675}$-β-catenin initiated and maintained a re-expression of TCF7L2 reactivating the main Wnt transcriptional machinery during hypertrophic remodeling in the adult mouse and human heart.

## Phospho-Ser$^{675}$β-catenin induces TCF7L2 expression and promotes heart failure by triggering developmental reprograming in the adult heart

Next, to investigate the mechanisms triggered by β-catenin/TCF7L2-transcriptional activity, we mimicked this activation by inducing β-catenin stabilization specifically in adult CM. Inducible stabilization was achieved by crossing a mouse possessing a *Ctnnb1* (β-catenin) allele with *loxP*-flanked exon 3 (β-catenin$^{floxed\text{-}ex3}$) (25), with a *Myh6*-promoter driven tamoxifen (TX)-inducible-Cre expressing line (24). The recombined allele (β-cat$^{\Delta ex3}$) produces a stabilized GSK3-β-degradation-resistant β-catenin (Figure 1G). Fourteen-week old mice were induced with TX and analyzed for 3 to 4 weeks (Supplementary Figure S1C). To exclude effects of Cre expression and/or TX toxicity, two control groups were used for functional analyses including *Myh6*-merCREmer/β-cat$^{wt}$ (Cre$^{pos}$) and β-cat$^{flox\text{-}ex3}$ (Cre$^{neg}$), respectively. β-cat$^{\Delta ex3}$ hearts showed a significant increase in stabilized β-catenin protein compared to Cre$^{pos}$ controls. Similar to the

observations in TAC-induced remodeling in mouse, TCF7L2 and pSer$^{675}$-β-catenin protein were significantly increased in β-cat$^{\Delta ex3}$ cardiac tissue. Maximum transcriptional activation was observed 3 weeks post-induction (Figure 1H, I and Supplementary Figure S1D).

β-cat$^{\Delta ex3}$ mice phenotypically resembled experimentally-induced hypertrophy with increased heart sizes, cardiac mass, myocyte cross-sectional area and fibrosis (Figure 2A-D).

**Figure 2.**

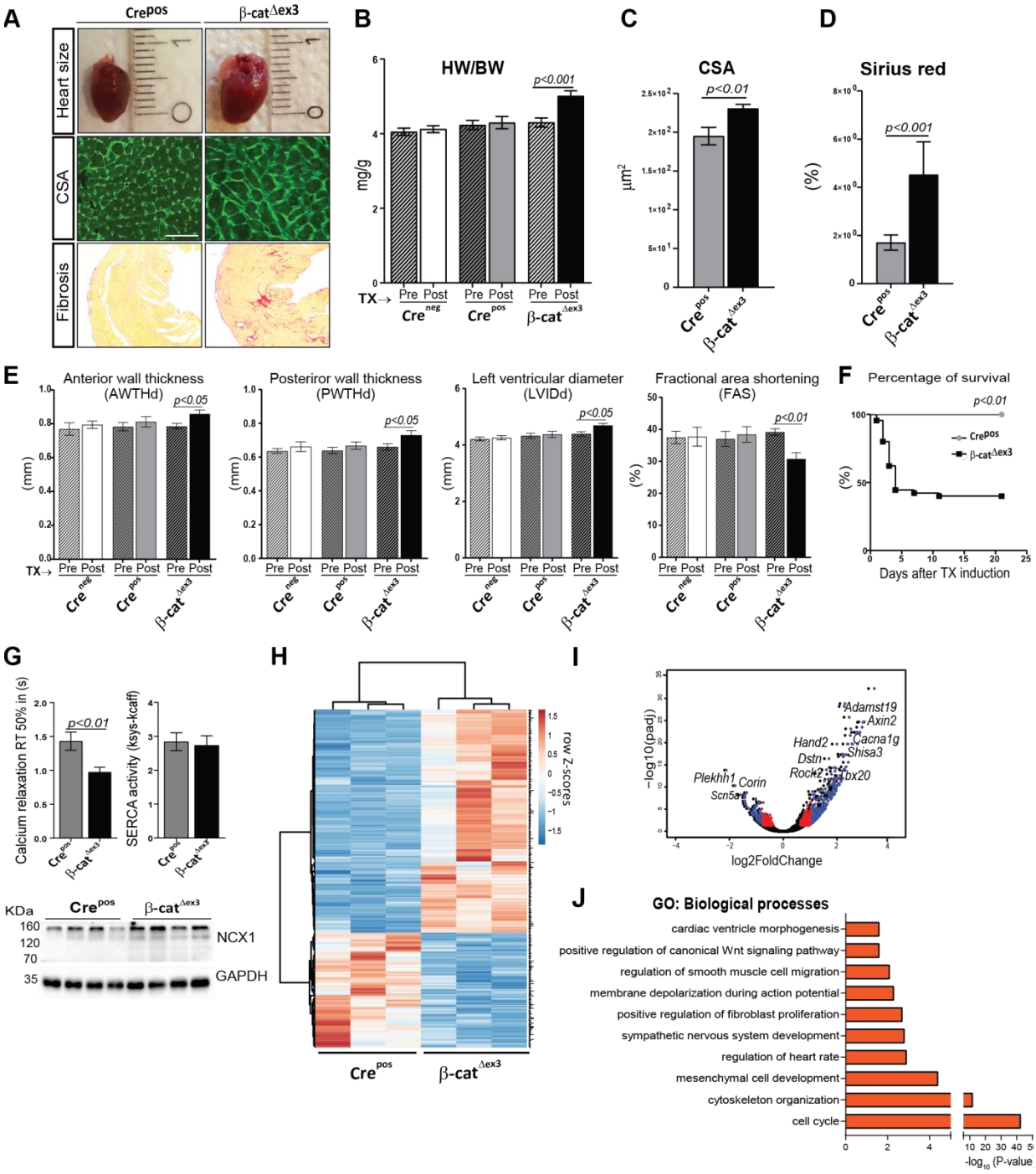


**Figure 2: Wnt activation promotes heart failure by triggering developmental reprogramming in the adult heart.** Representative images (**A**) and quantification showing increased- (**B**) heart-to-body weight ratios (HW/BW, $n \geq 15$/group), (**C**) CM cross-sectional area by WGA-FITC staining ($n = 3$; 150 cells/mouse) and (**D**) fibrosis by Sirius Red staining ($n = 3$/group) in β-cat$^{\Delta ex3}$ versus control Cre$^{pos}$. (**E**) Echocardiographic analyses showing anterior and poster wall thickness diameters (AWTHd, PWTHd), left ventricular inner diameter (LVId) and fractional area shortening (FAS), 3 weeks post-TX induction in β-cat$^{\Delta ex3}$ mice compared to Cre$^{pos}$ and Cre$^{neg}$/ β-cat WT (Cre$^{neg}$) controls (n≥15/group). (**F**) Kaplan–Meier survival curve post-TX induction, $n \geq 21$. (**G**) Half-times of intracellular calcium relaxation (RT50%) of caffeine induced-Ca2+-transients along with SERCA2 activity in β-cat$^{\Delta ex3}$ and Cre$^{pos}$

CMs (*n* = 6/4–21 cells per mouse). Ventricular protein expression of Na+–Ca2+ exchanger (NCX) in β-cat$^{\Delta ex3}$ and Cre$^{pos}$ hearts, n = 4. GAPDH serves as loading control in G. (**H**) Heatmap representing row *Z*-scores of RPKM values of all 572 differentially expressed genes (DEGs) with a cut-off: $log_2FC \pm 0.5$, $P < 0.05$ in Cre$^{pos}$ and β-cat$^{\Delta ex3}$ cardiac ventricles. Upregulated genes and downregulated genes are depicted in red and blue respectively (*n* = 3/group). (**I**) Volcano plot depicting the DEGs. Blue: DEGs with $log_2FC \geq 0.9$ and $p \leq 0.05$; red: $log_2FC \leq 0.9$ and $P \leq 0.05$; black: unregulated genes. (**J**) Gene Ontology (GO) biological processes of upregulated ($P \leq 0.05$) genes. Data are mean ± SEM; *t*-test and ANOVA, Bonferroni's multiple comparison test. Scale bar in A: 20 μm.

Maladaptive cardiac remodeling was indicated by increased anterior and posterior wall thickness and left ventricular chamber diameter along with decreased fractional area shortening and higher mortality in β-cat$^{\Delta ex3}$ mice compared to Cre$^{pos}$ and Cre$^{neg}$ controls (Figure 2E, F). We investigated calcium homoeostasis and observed significantly faster elimination kinetics of caffeine induced-$Ca^{2+}$-transients in β-cat$^{\Delta ex3}$ CMs, while SERCA2 activity remained unchanged in β-cat$^{\Delta ex3}$ compared to Cre$^{pos}$ CMs. Accordingly, expression of the Na(+)-Ca2+ exchanger (NCX) was higher in β-cat$^{\Delta ex3}$ CMs (Figure 2G), which may be part of the genetic reprogramming in cardiac remodelling (37). Amplitude of systolic and caffeine-induced $Ca^{2+}$-transients at increased half-time relaxation rate was unchanged in β-cat$^{\Delta ex3}$ CMs, suggesting that NCX may contribute to the faster $Ca^{2+}$-elimination in β-cat$^{\Delta ex3}$ (Supplementary Figure S1E). Thus, activating β-catenin/TCF7L2-dependent transcription alone is sufficient to initiate adverse cardiac remodeling in the adult heart.

To explore the cellular events triggered by β-catenin/TCF7L2 activation, we performed RNA-sequencing analysis using ventricular tissue. Wnt-activated β-cat$^{\Delta ex3}$ ventricles showed 376 upregulated and 196 downregulated genes compared to control Cre$^{pos}$ (n=3, $p<0.05$ and $log_2FC \geq 0.5$) (Figure 2H). The most differentially regulated genes included targets of the Wnt/β-catenin-dependent (i.e. *Axin2, Lef1, Cacna1g*); and -independent pathways (*Rock2*); cardiac development (*Hand2, Tbx20)* and pathological genes related to heart disease condition ((*Destrin (Dstn), Corin, Adamst19)*) (Figure 2I). Gene ontology (GO) analysis clustered the upregulated genes into cell cycle, tissue remodeling including cytoskeleton organization, cardiac and mesenchymal development (Figure 2I, J). Downregulated genes included heart rate processes (Supplementary Figure S2A).

### β-catenin/TCF7L2 transcriptional activation results in increased CM cell cycling and cytoskeletal remodeling in the adult heart

In line with the role of the Wnt canonical pathway in development (38,39), β-cat$^{\Delta ex3}$ hearts showed a re-expression of a developmental gene cluster coordinating second heart field/right

ventricle and mesenchymal/interstitial cell development, including *Sox4, Tbx20, Hand2, Bambi, Edn3, Dact3* and *Shisa3*. Re-expression of fetal forms of calcium voltage-gated channel and myosin heavy chain (*Cacna1g, Myh7*) as observed in hypertrophic remodeling, was also detected in β-cat$^{\Delta exon3}$ hearts (Figure 3A, B).

**Figure 3.**

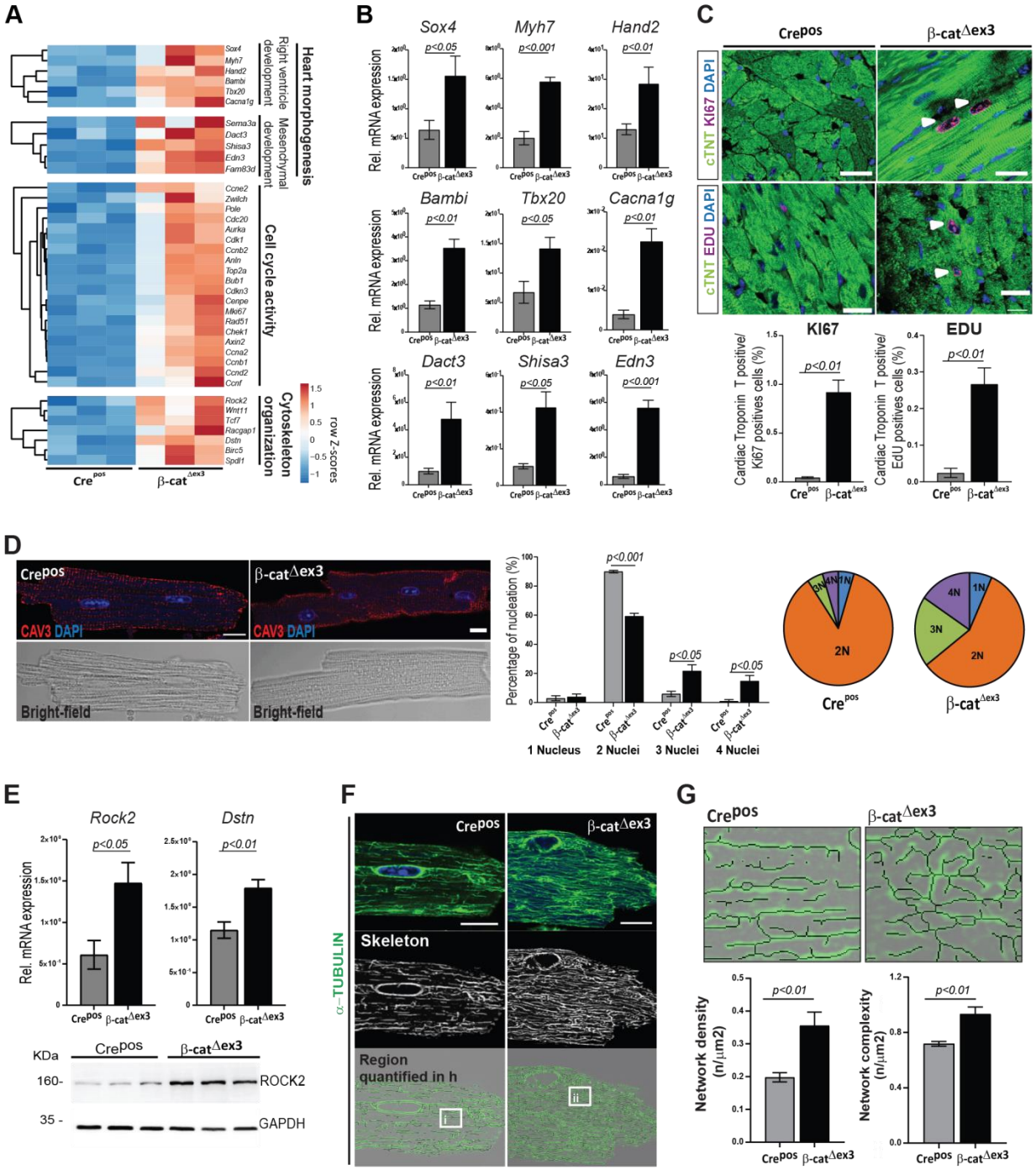


**Figure 3: Wnt transcriptional activation results in increased CM cell cycling and cytoskeletal remodeling in the adult heart.** (**A**) Heatmaps depicting row Z-scores of RPKMs of upregulated genes involved in heart morphogenesis, cell cycling and cytoskeleton organization in β-cat$^{\Delta ex3}$ ventricles; with (**B**) corresponding qPCR validations β-cat$^{\Delta ex3}$ $n$ = 4; Cre$^{pos}$ $n$ = 5). (**C**) Confocal images of KI67 or EdU (magenta) immunostainings with quantification of double positive cTNT/KI67 and EdU cells ($n$ = 3; >400 cells/mouse). White arrows indicate KI67 and EDU positive CM. (**D**) Immunostainings for Caveolin 3 (red), DAPI (blue) in single CM along with quantification of nuclei/CM ($n$ = 3; ≥90 cells/CM per mouse). (**E**) qPCR validating increased cytoskeletal regulators *Rock2* and *Dstn*; and immunoblot showing increased ROCK2 in β-cat$^{\Delta ex3}$ ventricles β-cat$^{\Delta ex3}$ $n$ = 4; Crepos $n$ = 5).

(**F**) Confocal images and (**G**) quantification of microtubule network density and complexity in single CMs ($n$ = 3; 5–8 cells/mouse; i-ii represent higher magnification in F). Images are an overlay of α-TUBULIN images (green) with corresponding extracted skeletons (black). *Tbp* was used for normalization in B and E and GAPDH was loading control in F. Scale bar C: 20 µm, E, G: 10 µm. Confocal images were re-colored for color-safe combinations.

In line with the expression data and the role of Wnt in cell cycle regulation, we found a significantly increased expression of KI67 in cardiac troponin T (cTNT)-positive cells in myocardial tissue and isolated CMs from β-cat$^{\Delta ex3}$ hearts. *In vivo* 5-ethynyl-2'-deoxyuridine (EdU) DNA uptake in cTNT-positive cells was increased in β-cat$^{\Delta ex3}$ myocardial cells (Fig. 3C and Supplementary Figure S2B). Cell cycle genes (*Ccna2, Ccnb1, Ccnb2 and Ccnd2*), previously implicated in hypertrophic remodeling and CM cell cycle re-entry, (40,41) were found increased in β-cat$^{\Delta ex3}$ ventricles. Increased KI67 expression in cTNT-positive cells as well as *Ccna2, Ccnb1 and Ccnb2* expression were also confirmed in TAC-induced hearts (Supplementary Figure S2C). This was accompanied by a switch in CM nucleation towards 3- and 4-nuclei in β-cat$^{\Delta ex3}$ hearts with decreased frequency of bi-nucleation as compared to Cre$^{pos}$ CM (Figure 3D).

Interestingly, genes involved in cytoskeletal organization such as β-catenin-independent Wnt pathway (*Wnt11, Rock2, Tcf7, Wif1*) and Destrin (*Dstn)* (42), also upregulated in human cardiomyopathies were significant upregulated in β-cat$^{\Delta ex3}$ hearts Cre$^{pos}$ (Figure 3E). To visualize a possible effect of cytoskeletal organization genes regulation, we analyzed the CM cytoskeleton, which showed an increased network density and complexity in β-cat$^{\Delta ex3}$ CMs as compared to Cre$^{pos}$ (Figure 3F, G). Adherens junctions structures show no major alterations in β-cat$^{\Delta ex3}$ CMs (Supplementary Figure S2D, E). These results suggest a cross-talk between Wnt/β-catenin-dependent and -independent signaling, which may regulate cytoskeletal rearrangements contributing to pathological changes in adult CMs.

## Induced TCF7L2 and H3K27ac occupancies at disease-associated enhancers defines the cardiac epigenome upon β-catenin stabilization

We showed that TCF7L2 was (*I*) the highest TCF/LEF member expressed in the mouse and human heart and (*II*) re-expressed in both mouse and human cardiomyopathies. Hence, we explored the transcriptional involvement of TCF7L2 in Wnt-mediated chromatin remodeling in the adult heart. ChIP-seq analyses was performed for endogenous TCF7L2 and Histone 3 lysine 27$^{th}$ acetylation (H3K27ac), an established chromatin mark for active enhancers and transcriptionally active regions (43), in β-cat$^{\Delta ex3}$ and Cre$^{pos}$ ventricles. TCF7L2 occupancy was

low, albeit detectable in wild-type ventricles, which correlates to the very low Wnt transcriptional activity in healthy hearts (~222 regions). Validating this ChIP, TCF7L2 occupancy was detected at the known target gene promoters of *Axin2* and *SP5*. A 20-fold enrichment of TCF7L2 occupancy on the *Axin2* promoter was confirmed by qPCR (Supplementary Figure S3A, B). Upon β-catenin stabilization, genome-wide TCF7L2 binding was markedly increased, indicating an inducible occupancy, owing to its upregulation. An inducible recruitment of TCF7L2 and H3K27ac at the *Tcf7l2* gene locus was observed in β-cat$^{\Delta ex3}$ hearts indicating a positive feedback regulation (Supplementary Figure S3C).

**Figure 4.**

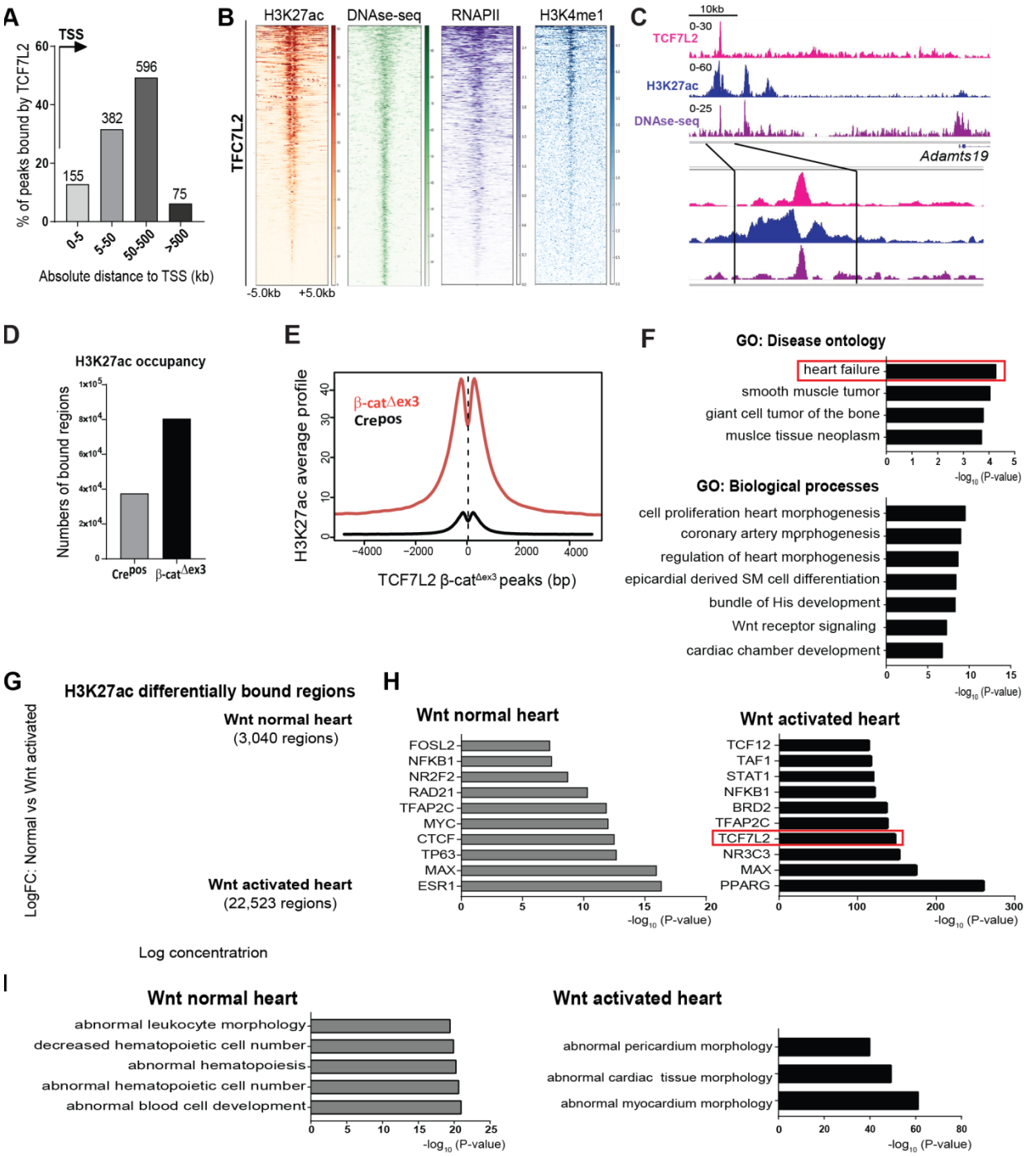


**Figure 4: Induced TCF7L2 and H3K27ac recruitment to disease-associated enhancers defines the β-cat$^{\Delta ex3}$ cardiac epigenome.** (**A**) Genomic distribution of TCF7L2 occupancy in β-cat$^{\Delta ex3}$ ventricles in number of regions and as distance from TSS (arrow) in kb. (**B**) Heatmaps of H3K27ac in β-cat$^{\Delta ex3}$ ventricles and high sensitivity DNAse-sequencing (DHS), -RNAPII, -H3K4me1 occupancy in normal adult heart, on TCF7L2 occupied regions in β-cat$^{\Delta ex3}$ ventricles, aligned according to their maximum signal of TCF7L2 occupancy. Scale depicts normalized RPKM values for heatmaps. (**C**) Exemplary occupancy profiles of TCF7L2, H3K27ac and DHS on an identified distal enhancer of *Adamts19*. (**D**) Total number of H3K27ac bound-regions as well as (**E**) average signal profiles of H3K27ac on TCF7L2 occupied loci in Cre$^{pos}$ and β-cat$^{\Delta ex3}$ ventricles. (**F**) GO disease ontologies of TCF7L2 bound

regions in β-cat$^{\Delta ex3}$ ventricles. (**G**) Binding affinity plot of 25,563 differential ChIPseq-H3K27ac enriched regions (pink dots) in the Wnt normal (3,040 regions, log FC > +0.5, *n* = 3) and in β-cat$^{\Delta ex3}$ (Wnt activated) (22,523 regions, log FC < –0.5, *n* = 2) hearts. (**H**) Motif analysis on differentially enriched distal H3K27ac regions (5,748 from 22,523) in 'Wnt activated' and control 'Wnt normal'. TCF7L2 motif occurrence is highlighted in an orange box. (**I**) Disease Ontologies are for the regions in H. For heatmaps regions ± 5 kb are shown.

We identified 1209 regions associated with 977 genes, occupied by TCF7L2 in β-cat$^{\Delta ex3}$ hearts. Among these, approximately 80% of TCF7L2-bound regions were located distal to transcription start sites (TSS) (Figure 4A). TCF7L2 occupancy was closely associated with H3K27ac in β-cat$^{\Delta ex3}$ hearts and with DNAse hypersensitive (DHS) regions, H3K4me1 and RNAPII binding, all marks of accessible chromatin, in the adult heart (Figure 4B, C). Global H3K27ac occupancy was markedly increased in β-cat$^{\Delta ex3}$ when compared to Cre$^{pos}$ control ventricles; notably also on TCF7L2-bound β-cat$^{\Delta ex3}$ regions (Figure 4D, E). GO analysis of TCF7L2-bound regions revealed "heart failure" as the most significant disease ontology along with developmental remodeling processes (Figure 4F).

In order to understand the relevance of differential H3K27ac occupancy in normal and β-cat$^{\Delta ex3}$ hearts, we identified 25,563 differentially-enriched genomic regions, which were specifically enriched in β-cat$^{\Delta ex3}$ hearts ("Wnt activated hearts": 22,523 regions) or in normal hearts ("Wnt normal hearts": 3,040 regions) (Figure 4G). Since TCF7L2 occupancy occurred predominantly at distal regions, we focused on the distally-enriched regions. Of the 22,523 regions in Wnt activated hearts, 5,748 of the β-cat$^{\Delta ex3}$-specific regions were located > ±5kb from the nearest gene. We identified an extensive overlap of published TCF7L2 data (-log10 p-value=141.209) with β-cat$^{\Delta ex3}$-specific distally-occupied H3K27ac regions, which was absent in the H3K27ac-bound distal regions enriched in the normal heart, (Figure 4H). Functional categorization of H3K27ac-bound distal regions revealed enrichment of processes involved in hematopoietic cell biology in in the normal heart, whereas Wnt activated hearts showed processes involved in abnormal cardiac muscle morphology (Figure 4I). This data indicate a particularly important chromatin-associated role of TCF7L2 in response to β-catenin stabilization in the adult heart in pathological condition.

**TCF7L2 elicits tissue-specific gene regulation in pathological heart remodeling**

Integrative analyses of 977 TCF7L2-bound and 376 upregulated genes (RNAseq, $log_2FC>0.5$, $p<0.05$) upon β-catenin stabilization, showed that TCF7L2 occupied and regulated the expression of a subset of 68 genes. Similar to the categorization of transcriptome data, these genes annotated to cardiac developmental tissue remodeling, cytoskeletal rearrangement and mesenchymal developmental processes in β-cat$^{\Delta ex3}$ hearts (Figure 5A).

**Figure 5.**

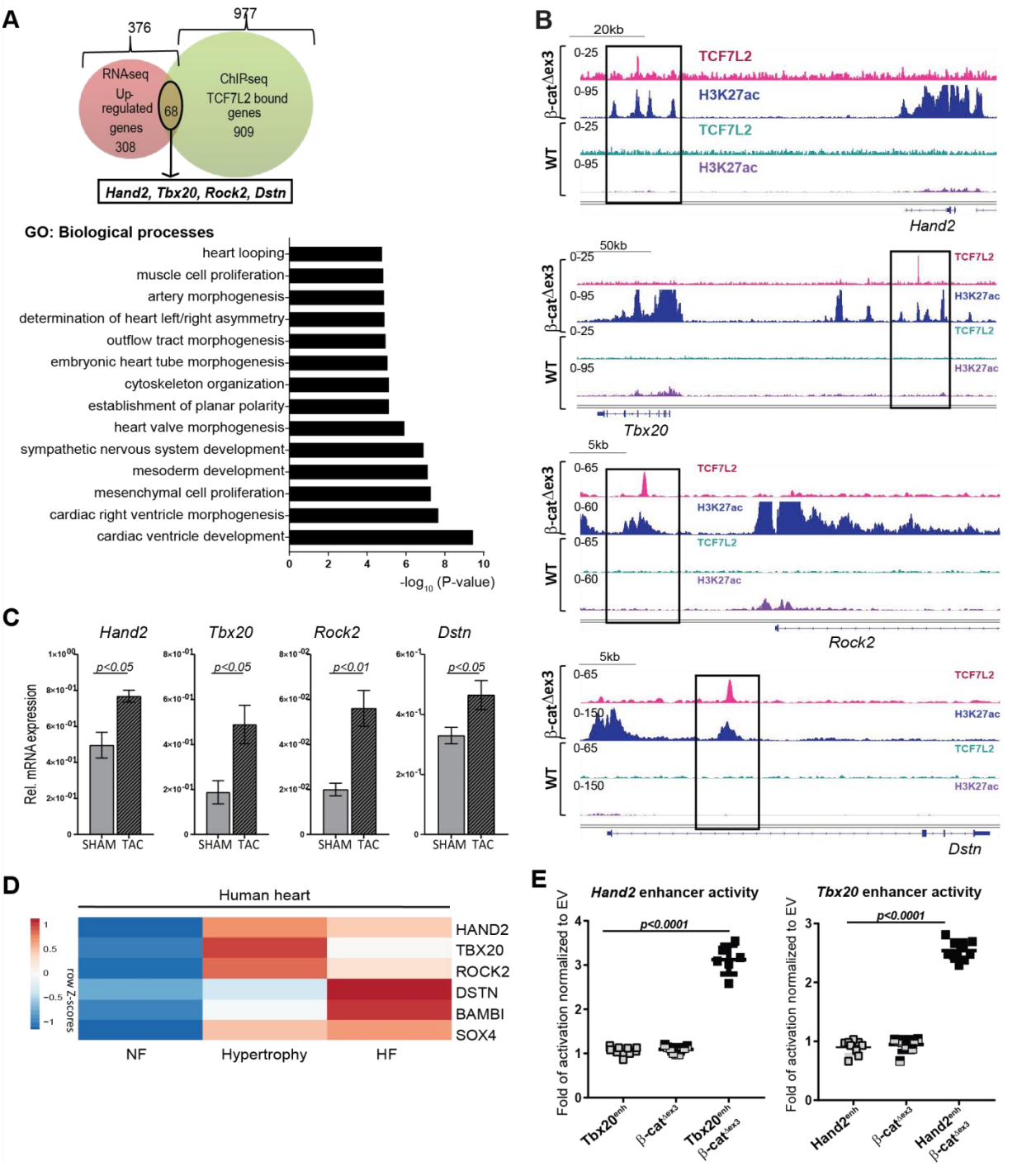


**Figure 5: TCF7L2 elicits tissue-specific gene regulation in pathological heart remodeling.** (**A**) Venn diagram of genes bound by TCF7L2 (green, 977) and upregulated (red, 376; $\log_2FC \geq 0.5$, $P \leq 0.05$) in β-cat$^{\Delta ex3}$ ventricles. GO biological processes annotation of the 68 common genes at the intersection. *Hand2*, *Tbx20*, *Rock2* and *Dstn* are part of these common genes. (**B**) Occupancy profiles of TCF7L2 and H3K27ac in β-cat$^{\Delta ex3}$ and Cre$^{pos}$ ventricles on the identified putative enhancers upstream of *Hand2*, *Tbx20*, *Rock2* and *Dstn*. (**C**) *Hand2*, *Tbx20*, *Rock2* and *Dstn* relative transcript levels in ventricles upon TAC-induced hypertrophy and sham controls, $n \geq 5$. (**D**) Heatmaps showing row Z-scores of RPKMs of dysregulated genes in human ventricular tissue from non-failing (NF), hypertrophic and failing hearts (HF). (**E**) Luciferase reporter assays for *Hand2* and *Tbx20* identified enhancers upon

Wnt activation by β-catenin stabilization in HEK293 cells normalized to empty vector (Renilla luciferase was used as transfection control, *n* = 3⁄independent experiments). *Tbp* was normalization control in C. Data are mean ± SEM; *t*-test.

Upregulated genes that did not intersect with TCF7L2 binding in β-cat$^{\Delta ex3}$ hearts were enriched for DNA replication processes (Supplementary Figure S4). Genes at the upregulated intersection included *Hand2, Tbx20, Rock2 and Dstn*. Significant occupancy of TCF7L2 and H3K27ac on the distal sites of these genes was observed in β-cat$^{\Delta ex3}$, but not in normal hearts (Figure 5B). In line with previous observation (44,45), we observed their upregulation upon cardiac remodeling in the mouse and in the human heart (Figure 5C, D).

For functional confirmation of TCF7L2-dependency of these novel target, we tested *Hand2* and *Tbx20* enhancer regions (containing 4 and 2 TCF/LEF consensus sites, respectively) upon expression of stabilized β-catenin$^{\Delta ex3}$, which mimics our β-cat$^{\Delta ex3}$ mouse model *in vitro*. Luciferase assays showed a 3- (*Hand2*) and 2.5-fold (*Tbx20*) increase in luciferase activity (n=3, Figure 5E). Altogether, these results identified novel β-catenin/TCF7L2 cardiac enhancers and highlight their significance in pathological remodeling in the adult myocardium.

To further investigate the cardiac-specificity of TCF7L2 chromatin occupancy, we compared the binding profiles of endogenous TCF7L2 found in our CMs-β-cat$^{\Delta ex3}$ model, with a published hepatocyte-specific β-catenin stabilized mouse model (46). TCF7L2-bound regions *only* found in β-catenin stabilized hepatocytes (compared to CMs), were associated with metabolic processes, lipid and cholesterol homeostasis. Whereas, TCF7L2-bound regions *only* found in β-catenin stabilized CMs were associated with cardiac developmental processes (Figure 6A). Overlapping binding regions were only found in promoter regions of classical Wnt target genes such as *Axin2* and *Lef1*, while non-overlapping genomic locations belonging to *Hand2, Tbx20, Rock2* and *Dstn* were observed only in β-cat$^{\Delta ex3}$ hearts (Figure 6B). These results strongly point to the tissue-specific functions of TCF7L2 at distal regions (23).

**TCF7L2 cooperates with cardiac-TFs to enable heart-specific gene regulation**

We next aimed to investigate the mechanism, which enabled TCF7L2 to elicit CM-specific responses. Cardiac-TFs including GATA, NKX, TBX and MEF have been shown to collaborate with other factors to direct cardiac-specific gene expression programs (47).

**Figure 6.**

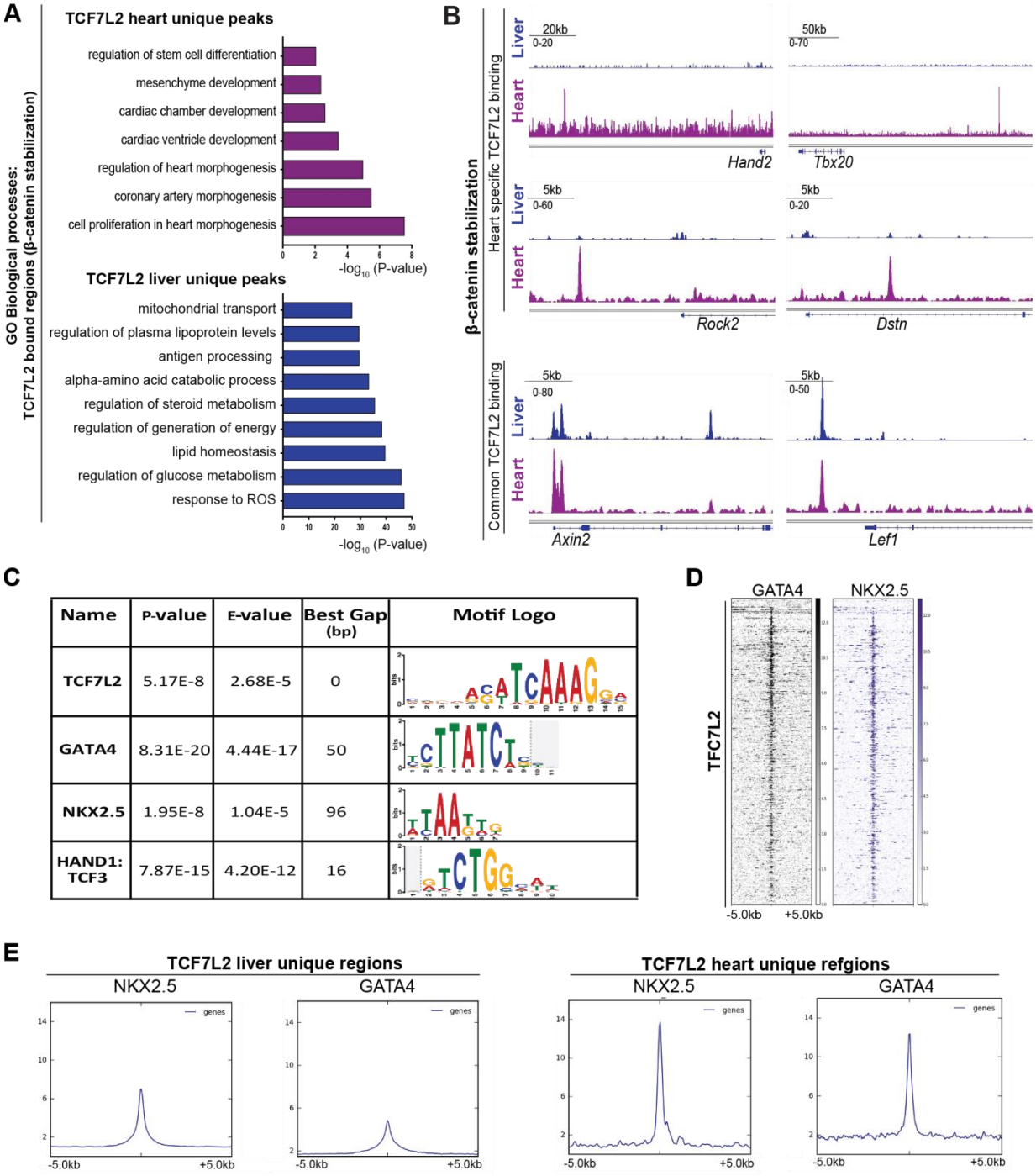


**Figure 6: TCF7L2 cooperates with cardiac-TFs to enable heart-specific gene regulation.** (**A**) Comparison of TCF7L2-bound regions in *in vivo* models of β-catenin stabilization (β-cat$^{\Delta ex3}$) in CMs and hepatocytes. GO biological processes for unique regions in CM (magenta) and hepatocytes (blue). (**B**) TCF7L2 occupancy profiles on identified *Hand2*, *Tbx20*, *Rock2* and *Dstn* enhancers and common Wnt targets *Axin2* and *Lef1* in β-catenin stabilized CM (magenta) and hepatocytes (blue). (**C**) Table enlisting the transcription factors (TFs) enriched on TCF7L2-bound regions in β-cat$^{\Delta ex3}$ ventricles by *de-novo* motif search using MEME-SpaMo. (**D**) Heatmap depicting the occupancy of cardiac-TFs GATA4 and NKX2.5 in the normal heart on regions occupied by TCF7L2 in β-cat$^{\Delta ex3}$

hearts. Regions ± 5 kb are shown. (**E**) Average profiles of GATA4 and NKX2.5 occupancy on TCF7L2-bound liver and heart-specific regions. Data are mean ± SEM; *t*-test.

*De novo* motif analyses revealed that TCF7L2-bound chromatin regions in β-cat$^{\Delta ex3}$ hearts showed a significant enrichment for GATA4 (Gap=50bp, p=8.31E-17), NKX2.5 and HAND1/TCF3 motifs (Figure 6C). This was confirmed by comparing published ChIP-seq datasets for GATA4 and NKX2.5 in the normal adult heart (48) with the TCF7L2-bound regions identified in our study (Figure 6D). Accordingly, *heart-specific* TCF7L2-bound regions showed a higher correlation to NKX2.5 and GATA4 occupancy as compared to their lower association with liver-specific regions (Figure 6E), further confirming its tissue-specific roles.

Among the analyzed cardiac-TFs, GATA4 binding in the normal heart showed the highest correlation (r=0.67) to TCF7L2-bound regions in the β-cat$^{\Delta ex3}$ hearts (Figure 7A, Supplementary Figure S5A). Next, motif analysis was performed on the genes both bound by TCF7L2 and upregulated in β-cat$^{\Delta ex3}$ hearts (68 genes), using BETA-plus, showing again, a significant enrichment of the GATA motif (p value=3.44E-3). The association with downregulated RNA-seq genes showed different motifs including TP53 (Figure 7B). Given the strong correlation of GATA4 and TCF7L2, genes co-occupied by both GATA4 and TCF7L2 in heart tissue were analyzed. Of the 2,258 GATA4-bound (48) and our 977 TCF7L2-bound genes in β-cat$^{\Delta ex3}$ hearts, 319 (~30% of TCF7L2-bound genes) were common, including *Hand2* (Figure 7C). These genes were enriched in heart developmental processes, supporting the relevance of TCF7L2 and GATA4 co-occupancy in cardiac gene regulation (Supplementary Figure S5B).

**GATA4 interacts with β-catenin and contributes to the molecular switch driving adult heart disease progression *in vivo***

To get an insight into the mechanism of regulation of GATA4 on Wnt signaling, we tested the potential physical interaction of GATA4 with nuclear Wnt components in the healthy and Wnt activated (genetically and induced by pressure-overload) adult heart. GATA4 was immunoprecipitated, followed by chromatin-associated protein complex isolation and immunoblotting in the normal, β-cat$^{\Delta ex3}$ and in 6 weeks post-TAC ventricular tissue. The suitability of the anti-GATA4 antibody was validated both by ChIP-qPCR on a known target gene, *Natriuretic peptide a (Nppa)*, and by protein detection (Supplementary Figure S5C). We observed that GATA4 and β-catenin interacted in the normal, but *not* in the β-cat$^{\Delta ex3}$ or TAC ventricular tissue (Figure 7D). Although β-catenin was clearly present in the nucleus

(Supplementary Figure S5D), it was not transcriptionally active in the healthy heart, based on the low p-β-cat$^{Ser675}$. Phosphorylated-β-cat$^{Ser675}$, which was found abundantly enriched in the nuclei of β-cat$^{\Delta ex3}$ and in TAC tissue (Figure 7E), suggesting that GATA4 could bind *only* to transcriptionally inactive β-catenin.

**Figure 7.**

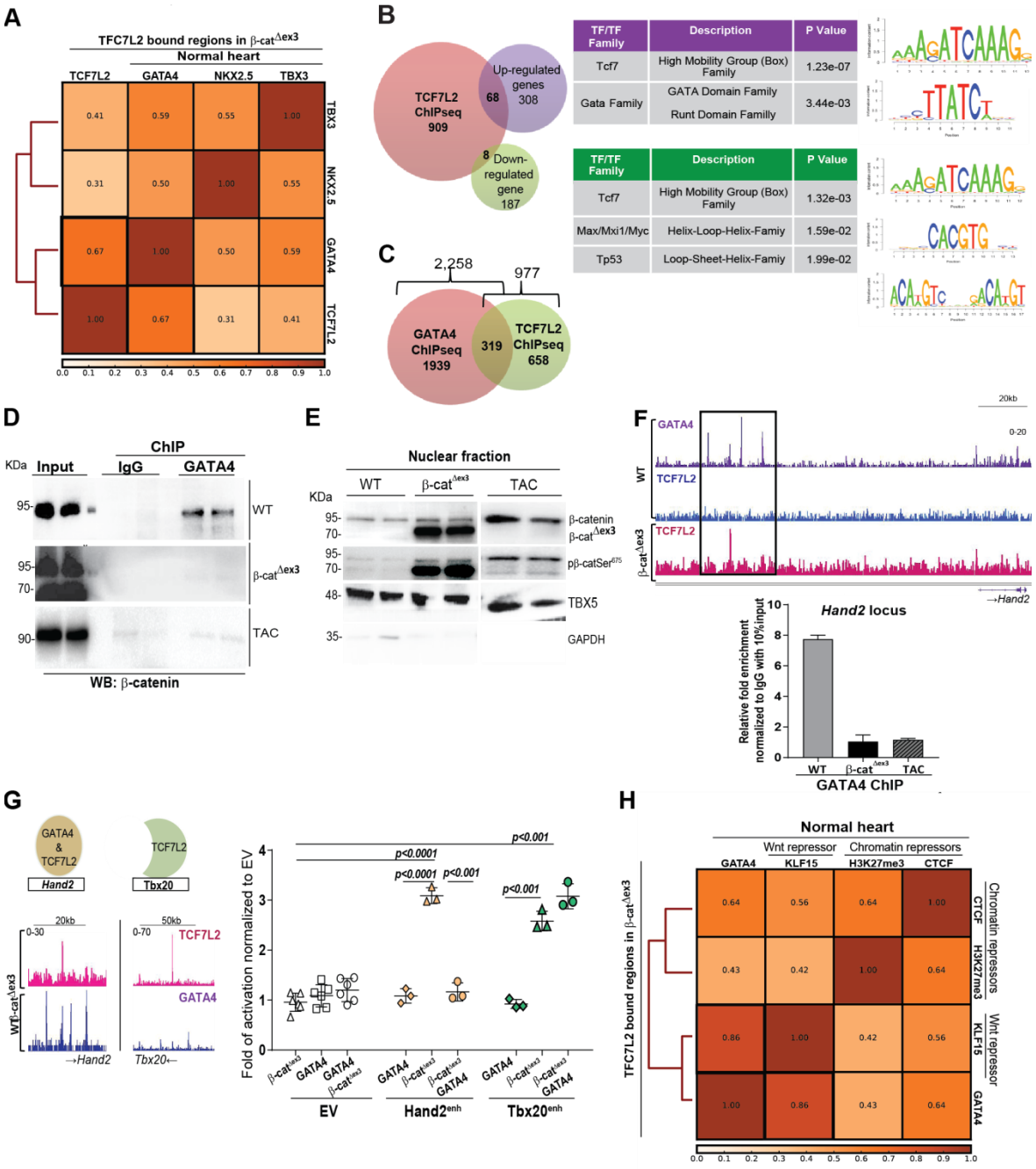


**Figure 7: GATA4 interacts with β-catenin and fine-tunes the molecular switch driving adult heart disease progression *in vivo*.** (**A**) Spearman's correlation plot of TCF7L2 co-occupancy with GATA4, NKX2.5 and TBX3, highlighting highest correlation with GATA4 (black box). (**B**) Venn diagram of genes bound by TCF7L2 (orange) with upregulated (violet) or downregulated (green) genes with $\log_2$FC≥0.5, p≤0.05 in β-cat$^{\Delta ex3}$ ventricles and corresponding motif enrichment of the intersections. (**C**) Venn diagram showing commonly bound genes (319) between TCF7L2 in β-cat$^{\Delta ex3}$ hearts and GATA4 in normal hearts. (**D**) Immunoblot of GATA4 with β-catenin co-immunoprecipitation in WT, β-cat$^{\Delta ex3}$ and 6 weeks post-TAC hearts. Input represents the total, sheared chromatin-protein complexes before immunoprecipitation, (*) protein ladder. (**E**) Immunoblot of total β-catenin and active pSer675-β-catenin in the nuclear fractions of control, β-cat$^{\Delta ex3}$ and 6 weeks post-TAC hearts. TBX5 and GAPDH

were used to detect nuclear and cytosolic enrichments respectively. (**F**) IGV binding profiles for TCF7L2 occupancy in β-cat$^{\Delta ex3}$ hearts along with GATA4 co-occupancy in normal hearts on *Hand2* enhancer locus; ChIP-qPCR for GATA4 binding on *Hand2* enhancer in normal (WT), 6 weeks post-TAC (WT TAC) and β-cat$^{\Delta ex3}$ hearts. Relative fold enrichment was calculated to IgG control, normalized to 10% input chromatin (n = 3 hearts/ChIP) (**G**) Profiles of enhancers with GATA4 and TCF7L2 overlapping occupancy (*Hand2*) and with only TCF7L2 occupancy (*Tbx20*). Luciferase reporter assay for *Hand2* enhancer (-enh) and *Tbx20*-enh upon β-catenin stabilization, GATA4 overexpression or both normalized to empty vector (EV). (Renilla luciferase was the transfection control, *n* = 3⁄independent experiments). Data are mean ± SEM; *t*-test and ANOVA, Bonferroni's multiple comparison test. (**H**) Spearman's correlation plot depicting high correlations between GATA4 and repressive elements KLF15, H3K27me3 and CTCF in normal hearts specifically on TCF7L2-bound regions in β-cat$^{\Delta ex3}$ hearts.

To further investigate the functional role of GATA4 in this complex, we analyzed the regulation of *Hand2,* displaying co-occupancy of GATA4 (in WT healthy hearts) and TCF7L2 (in β-cat$^{\Delta ex3}$ hearts) and *Tbx20,* displaying TCF7L2, but not GATA4 occupancy (Figure 7F). By performing luciferase assays, we show that GATA4 co-expression prevented β-cat$^{\Delta ex3}$-mediated *Hand2*- but not *Tbx20*-enhancer activation (Figure 7G). This supports a repressive role of GATA4 on a subset of Wnt target disease genes in the adult normal heart.

## β-catenin loss of function in CM confirmed the rescue of Wnt-dependent pathological gene regulation *in vivo*

As a proof of concept, we analyzed murine hearts with CMs specific inducible β-catenin loss of function (β-cat$^{\Delta ex2\text{-}6}$) with a confirmed, reduced total β-catenin expression (Figure 8A and Supplementary Figure S6A) subjected to TAC-induced hypertrophy (Figure 8B). Supporting a beneficial effect of blocking Wnt- transcriptional activation, reduction of fractional area shortening and upregulation of the hypertrophic marker *Nppb* was prevented in β-cat$^{\Delta ex2\text{-}6}$ upon TAC (Figure 8C, D). Upregulation of pSer$^{675}$-β-catenin protein expression was attenuated in β-cat$^{\Delta ex2\text{-}6}$ upon 6-weeks post-TAC (Figure 8E). Accordingly, Wnt-mediated transcriptional activation was significantly decreased, as demonstrated by lower *Axin2* expression in β-cat$^{\Delta ex2\text{-}6}$ sham and TAC mice, whereas *Axin2* activation was corroborated upon TAC in Cre$^{pos}$ ventricles (Figure 8F). In line, with the low activity of Wnt in the adult heart, β-catenin loss of function did not significantly affect the expression of novel disease genes at baseline (Supplementary Figure S6B). Finally, activation of the identified novel Wnt associated disease-enhancers *Tbx20, Dstn; Hand2* and *Rock2* was decreased 6-weeks after TAC in β-cat$^{\Delta ex2\text{-}6}$ hearts (Figure 8G and Supplementary Figure S6C).

**Figure 8.**

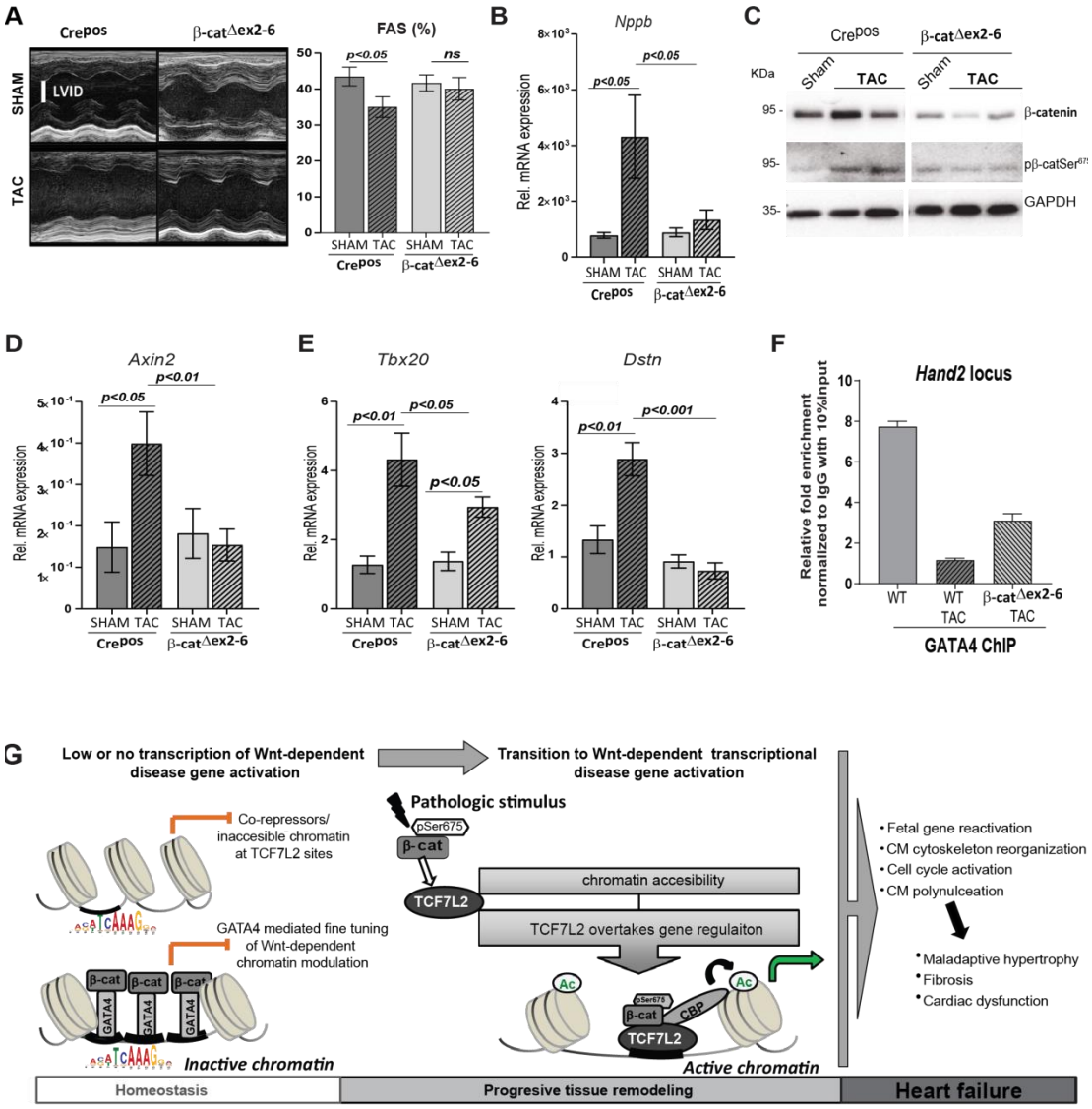


**Figure 8: β-catenin loss of function in CM rescues Wnt-dependent pathological gene regulation *in vivo*.** (**A**) Representative examples of M-mode echocardiograms, and quantification of fractional shortening (FAS) by echocardiographic analysis of 3 weeks TAC-induced Crepos control and β-cat$^{\Delta ex2–6}$ mice, $n \geq 7$. (**B**) Relative transcript levels of hypertrophic marker *Nppb* in β-cat$^{\Delta ex2–6}$ and controls Crepos; sham and TAC (n≥8/per group). (**C**) Immunoblot depicting total β-catenin and pSer675-β-catenin upon TAC in β-catenin loss of function (β-cat$^{\Delta ex2–6}$). GAPDH was protein-loading control (n=2/group). Relative transcript levels of (**D**) classical Wnt target *Axin2* and (**E**) newly identified *cardiac* Wnt targets *Tbx20* and *Dstn*, 6 weeks post-TAC in β-cat$^{\Delta ex2–6}$ and controls, n≥7. Data are mean ± SEM; ANOVA, Bonferroni's multiple comparison test. *Tbp* was used for transcript normalization. (**F**) ChIP-qPCR for GATA4 binding on *Hand2* enhancer in normal (WT), 6 weeks post-TAC (WT TAC) and β-cat$^{\Delta ex2–6}$ TAC hearts. Relative fold enrichment was calculated to IgG control, normalized to 10% input chromatin ($n$ = 3 hearts/ChIP). (**G**) Schematic representation of the findings of this study. In the healthy adult heart, β-catenin/TCF7L2-dependent loci are inactive, inaccessible or bound by transcriptional repressors, resulting in low transcription. On a subset of these loci, GATA4 binds to transcriptionally *inactive* β-catenin, fine-tuning Wnt-

dependent transcription. This chromatin state guaranties normal homeostasis in the adult heart. Pathological stimuli leading to active pSer675-β-catenin accumulation activates Wnt signaling and the epigenetic state switches on to 'active', replaced by transcriptionally active pSer675-β-catenin bound to TCF7L2, leading to enriched H3K27ac occupancy and a highWnt transcriptional activity. This results in the expression of disease-associated genes leading to adverse remodeling and heart failure.

## Discussion

Activation of the Wnt/β-catenin signaling occurs upon heart remodelling (5,7,19) by mechanisms, which are so far not well-understood. In this study, we elucidate the mechanisms by which Wnt signalling activity regulates chromatin remodelling and further identify the cellular processes mediated by this activation in in CMs of the adult mammalian heart. We established the relevance of TCF7L2 as a transducer of global Wnt/β-catenin-dependent transcription, controling this process. In the adult mouse and human heart, we showed that TCF7L2 is the mainly expressed TCF/LEF family member, with known transcriptional activating functions, confirming its relevance in Wnt-mediated functions in this tissue, as also reported elsewhere (19). In accordance with decreasing Wnt activity during heart maturation, TCF7L2 expression decreases from fetal to adulthood and is elevated upon pathological remodeling in the mouse and human heart ventricles. This data categorizes TCF7L2 in the fetal gene reprograming of the adult stressed heart in an evolutionary conserved manner. Despite low Wnt activity, we detected β-catenin and TCF7L2 in the nucleus of CMs in the adult healthy heart. Our data suggest that inactivity of the pathway could be explained by low levels in the healthy heart, in contrast to the abundant p-β-cat$^{Ser675}$ in the hypertrophic murine and human hearts. Increased p-β-cat$^{Ser675}$ may subsequently trigger TCF7L2 activation and recruitment to the chromatin. Further amplifying the signaling, our data strongly support a positive feedback regulation on TCF7L2 expression following β-catenin/TCF7L2 activation. Thus, p-β-cat$^{Ser675}$ initiates and sustains pathological heart remodeling (scheme, Figure 8H). Importantly, all this regulation is evolutionarily conserved in the human heart, allowing us to confidently address the relevance of Wnt/TCF7L2-mediated transcription in adult tissue remodeling in the murine heart model.

Previous studies showed that in neonatal rat CM, in which β-catenin was upregulated upon hypertrophic stimuli, adenovirus-mediated stabilization of β-catenin induces CM growth *in vitro* (49). However, it is becoming clear that mechanisms of Wnt regulation in neonatal CM may significantly differ from adult CM due to the different expression patterns of the transcriptional

co-activators and the chromatin accessibility in an immature CM. Our study shows that β-catenin stabilization in the adult heart not only results in CM hypertrophy, but also in CM de-differentiation, a feature of pathological remodelling, leading to severe heart failure. This is mediated by subsequently p-β-cat$^{Ser675}$; TCF7L2 and Wnt target gene activation. As a part of de-differentiation phenotype, β-cat$^{\Delta ex3}$ hearts showed upregulation of genes participating in heart morphogenesis, more confined to second heart field development and expansion, in line with the role of Wnt during embryogenesis in these processes (38,39).

In heart development, initial activation of Wnt/β-catenin signaling (canonical) is followed by an activation of the Wnt/β-catenin-independent (non-canonical) pathway, which represses the canonical signaling and regulates cell polarity (38). In line with this, β-catenin stabilization in adult CM was followed by an upregulation of ROCK2, a Wnt/planar cell polarity (PCP) non-canonical component and key regulator of the cytoskeleton. Additionally, we identified *Destrin*, an actin dynamizing factor previously involved in rearrangements of cytoskeletal filaments and in human cardiomyopathies and heart failure (42) as novel Wnt target in cardiac tissue. This regulation was reflected by a major reorganization of CM cytoskeleton as indicated by more dense and interlinked cytoskeletal structures in β-catenin stabilized hearts. Disorganization of cytoskeleton is a feature of hypertrophic and failing CM, which contributes to alterations in intracellular signaling and CM function (50) and may explain the increased mortality in β-cat$^{\Delta ex3}$ mice. Thus, our study showed a so far unappreciated cross-talk between components of Wnt signaling branches and uncovered a direct TCF7L2 regulation on *Rock2* and the novel Wnt target *Dstn,* driving cytoskeleton reorganization in pathological cardiac remodeling. Additionally, activation of Wnt signaling in CM induces changes in mesenchymal cell remodeling, suggesting a cellular cross-talk leading to whole heart tissue remodeling.

In line with activation of cell cycling genes, increased CM cycling, as indicated by KI67 expression and EdU incorporation, was observed in β-cat$^{\Delta ex3}$ similarly to post-induced TAC hearts, the latter supporting previous studies (51). Interestingly, increased cell cycle in β-cat$^{\Delta ex3}$ CM resulted in multi-nucleated cells, suggesting endo-reduplication, rather than newly formed myocytes. Stabilization of β-catenin in neonatal rat CM did not affect cell cycle (49), most probably due to a physiological cell cycling in this period of life. Inactivation of GSK3β, which allows for β-catenin accumulation, showed increased cycling in adult CM *in vitro*, which previously allowed the conclusion that Wnt signaling pathway is a potential target for

stimulating cardiac regeneration (52). Of note, one-day postnatal murine CM, which maintains a high regenerative potential (53), showed enriched gene networks associated with the Wnt signaling after ischemic heart injury (54). Since Wnt signaling becomes inactivated in the postnatal heart during later stages, it is tempting to speculate that reactivation of the signaling will confer regenerative capacity to the adult mature heart (54). However, our results show that sustained CM cycling and reprograming stimulated by Wnt activation, leads to organ functional decay and *not* to tissue regeneration. Similarly, persistent activation of the Hippo-pathway leads to cell cycle reactivation in adult CM accompanied by loss of cardiac function (55). Thus, activation of the Wnt pathway in the adult heart triggers a program of CM dedifferentiation and remodeling. This may implicate an initial protective mechanism of the stressed heart to preserve CM function and structure, which fails eventually upon sustained activation of the pathway. Hence, Wnt activation although it triggers similar biological processes as in the developing heart, is rather detrimental for the adult heart function. This may be explained by a low developmentally permissive transcriptional state of the adult CM in comparison to the early postnatal stages (54).

The ability of the Wnt pathway to elicit a large variety of transcriptional responses requires that β-catenin and TCFs distinguish between genes to be activated and genes to remain silent in a specific context. We explored the so far uninvestigated chromatin landscape modifications (23) upon increased transcriptionally active β-catenin and TCF7L2 in the adult heart. This activation resulted in increased transcriptionally active chromatin, both genome-wide and at TCF7L2-bound regions as indicated by an enhanced H3K27ac genomic recruitment in β-cat$^{\Delta ex3}$ hearts. We detected stronger signal intensity and an increase in TCF7L2 binding sites. Consistent with our transcriptomic data, TCF7L2 occupied active enhancers of genes involved in heart failure and cardiac developmental remodeling. Furthermore, distal regions differentially enriched for H3K27ac in β-cat$^{\Delta ex3}$ were associated with TCF7L2 binding. This is in line with stronger TCF7L2 recruitment to distal regions upon Wnt stimulation (23), possibly by increased DNA-binding affinities of TCF7L2 bound to the transcriptionally active p-β-cat$^{Ser675}$. TCF7L2 binding could thus create a local chromatin environment that allow for enhanceosome formation, promoting activation of normally silenced genes (23).

Although most Wnt targets are tissue- and context-specific, a surprisingly short list of confirmed specific targets is known (56). A previous study associated TCF7L2 activation with the

ubiquitous Wnt target c-Myc in the heart (19). Using integrative, unbiased genome-wide analyses, we identified and validated novel TCF7L2 cardiac-specific direct target genes involved in adult tissue development and tissue remodeling such as *Hand2, Tbx20, Rock2* and *Dstn* (42,44,45,57). β-catenin stabilization induced TCF7L2 recruitment to distal regions of these novel targets in the heart but not in liver, whereas recruitment of TCF7L2 to proximal regions of ubiquitously described Wnt targets *Axin2* and *Lef1* was induced in both tissues. This demonstrated the cardiac-specific association of TCF7L2 to the distal regulatory regions of these genes according to its tissue-specificity functions at enhancer distal regions. To further validate the implication of the Wnt signal activation on these identified targets, we used a CM-β-catenin loss of function *in vivo* model. In line with previous finding, β-catenin deletion in CM results in preserved cardiac function upon TAC (8,10,58,59). Here, we showed that reduced level of p-β-cat$^{Ser675}$ upon pathological stimuli prevented Wnt nuclear activation and disease-specific upregulation of our identified novel Wnt targets upon blunted Wnt/β-catenin activation. This strongly supports their dependency on Wnt/TCF7L2 activation during pathological remodeling and their influence on functional deterioration.

A striking finding of our present study is the repressive function of GATA4 on disease-associated-enhancers co-occupied by GATA4 and TCF7L2. We uncovered a chromatin-bound Wnt nuclear complex including GATA4 and β-catenin in the healthy adult heart. Cooperation of GATA3 was shown to repress TCF7L2-mediated transcription in cancer cells (21), suggesting a tissue specific cooperation of members of the GATA family with TCF7L2. Moreover, different GATA factors dictate transcription in a cell type-specific manner. In hematopoietic system GATA1 and 2 are known to regulate cell development, maturation and malignancies, indicating its contribution to physiological and pathological states. Moreover, GATA1 has been involved in context-dependent regulation at the chromatin level, indicating that the GATA factors are cell- and context specific cofactors controlling homeostasis and diseases (60,61). Our findings support the notion that tissue-specific Wnt-independent TFs, such as GATA4, collaborate with β-catenin to modulate chromatin activity (23). This highlights the role of the inactive nuclear β-catenin in the healthy heart, where quiescent Wnt/β-catenin-dependent transcription maintains normal homeostasis. Accordingly, GATA4 is necessary for maintenance of adult homeostasis, since its loss of function resulted in hypertrophic remodeling (62,63). This suggests that cooperation of GATA4 and Wnt signaling may contribute to inhibition of pathological cascades in the normal

heart. Aberrant activation of p-β-cat$^{Ser675}$ followed by TCF7L2 positive feedback activation in disease condition induces a shift towards active chromatin, by increased accessibility and by replacement of repressors at the Wnt complex. Consequently, de-repression of normally silenced genomic regions, leading to CM dedifferentiation, occurs. This results in pathological heart remodeling and culminates in heart failure upon sustained activation (scheme, Fig. 8H). Accordingly, a dynamic, context-specific GATA4 occupancy in heart homeostasis and disease has been demonstrated (64). Approaches stabilizing GATA4/β-catenin repressive functions may help to maintain cardiac homeostasis and prevent adverse remodeling.

Overall our study presents the first genome-occupancy mapping of heart-specific targets of *TCF7L2 in vivo*. This enabled us to provide a novel mechanistic insight showing a nuclear cardiac-specific regulatory complex driving tissue and context-specific Wnt-dependent transcriptional switches at the transition of disease initiation in pathological heart remodeling. This is mediated by a context and tissue-specific epigenetic function of β-catenin/TCF7L2, which cooperate with specific co-regulators to activate reprogramming and tissue remodeling. More broadly, the identification of TCF7L2-specific regulation may provide us a framework to identify novel therapeutic avenues to reduce the increased activity of the ubiquitously expressed Wnt pathway in a tissue specific manner for preventing heart damage and heart failure progression.

## ACCESSION NUMBERS

Sequencing data files have been deposited in NCBI GEO (https://www.ncbi.nlm.nih.gov/geo/query/acc.cgi?acc=GSE97763) under accession GSE97763. ChIP-seq datasets: GSE97761**, RNA-seq datasets: GSE9776**2

## SUPPLEMENTARY DATA

Supplementary Data are available at NAR online.


## ACKNOWLEDGEMENT

The authors thank Ines Mueller and Daniela Wolter for superb technical assistance; Collaborative Research Center (CRC) (Sonderforschungsbereiche (SFB)) 1002 service units (S01 Disease Models for echocardiography measurements and analysis; S02 High resolution fluorescence microscopy for advancing cell staining and cytoskeleton analysis and INF Information infrastructure for providing platform structure) and Dr. Gabriela Salinas (Head of Transcriptome and Genome Analysis Laboratory, University of Goettingen) for advices on

RNAseq. The authors thank Prof. W.-H. Zimmermann (WHZ) for revising the article and providing helpful advice.

**FUNDING**

This work was supported by the Deutsche Forschungsgemeinschaft (DFG) grant (to LCZ grant number: ZE900-3); CRC 1002 (Project C07 to LCZ); and the German Center for Cardiovascular Disease (DZHK). The founders had no role in study design, data collection, analysis and/or decision to publish. Funding for open access charge: Internal institutional funding (UMG).

*Conflict of interest statement*. None declared.

## References

1. van Amerongen, R. and Nusse, R. (2009) Towards an integrated view of Wnt signaling in development. *Development*, **136**, 3205-3214.
2. Ozhan, G. and Weidinger, G. (2015) Wnt/beta-catenin signaling in heart regeneration. *Cell regeneration*, **4**, 3.
3. Gessert, S. and Kuhl, M. (2010) The multiple phases and faces of wnt signaling during cardiac differentiation and development. *Circulation research*, **107**, 186-199.
4. Hermans, K.C. and Blankesteijn, W.M. (2015) Wnt Signaling in Cardiac Disease. *Comprehensive Physiology*, **5**, 1183-1209.
5. van de Schans, V.A., Smits, J.F. and Blankesteijn, W.M. (2008) The Wnt/frizzled pathway in cardiovascular development and disease: friend or foe? *Eur J Pharmacol*, **585**, 338-345.
6. Nakagawa, A., Naito, A.T., Sumida, T., Nomura, S., Shibamoto, M., Higo, T., Okada, K., Sakai, T., Hashimoto, A., Kuramoto, Y. *et al.* (2016) Activation of endothelial beta-catenin signaling induces heart failure. *Scientific reports*, **6**, 25009.
7. Dawson, K., Aflaki, M. and Nattel, S. (2013) Role of the Wnt-Frizzled system in cardiac pathophysiology: a rapidly developing, poorly understood area with enormous potential. *J Physiol*, **591**, 1409-1432.
8. van de Schans, V.A., van den Borne, S.W., Strzelecka, A.E., Janssen, B.J., van der Velden, J.L., Langen, R.C., Wynshaw-Boris, A., Smits, J.F. and Blankesteijn, W.M. (2007) Interruption of Wnt signaling attenuates the onset of pressure overload-induced cardiac hypertrophy. *Hypertension*, **49**, 473-480.
9. Xiang, F.L., Fang, M. and Yutzey, K.E. (2017) Loss of beta-catenin in resident cardiac fibroblasts attenuates fibrosis induced by pressure overload in mice. *Nature communications*, **8**, 712.
10. Xin Chen, S.P.S., Eileen Hsich, Lei Cui, Syed Haq, Mark Aronovitz, Risto Kerkelä, Jeffery D. Molkentin, Ronglih Liao, Robert N. Salomon, Richard Patten, and Thomas Force. (2006) The β-Catenin/T-Cell Factor/Lymphocyte Enhancer Factor Signaling Pathway Is Required for Normal and Stress-Induced Cardiac Hypertrophy. *Molecular and cellular biology*, **26**, 4462-4473.
11. Hatzis, P., van der Flier, L.G., van Driel, M.A., Guryev, V., Nielsen, F., Denissov, S., Nijman, I.J., Koster, J., Santo, E.E., Welboren, W. *et al.* (2008) Genome-wide pattern of TCF7L2/TCF4 chromatin occupancy in colorectal cancer cells. *Molecular and cellular biology*, **28**, 2732-2744.
12. Cadigan, K.M. (2008) Wnt-beta-catenin signaling. *Current biology : CB*, **18**, R943-947.

13. Li, Y., Shao, Y., Tong, Y., Shen, T., Zhang, J., Li, Y., Gu, H. and Li, F. (2012) Nucleo-cytoplasmic shuttling of PAK4 modulates beta-catenin intracellular translocation and signaling. *Biochimica et biophysica acta*, **1823**, 465-475.
14. Hino, S., Tanji, C., Nakayama, K.I. and Kikuchi, A. (2005) Phosphorylation of beta-catenin by cyclic AMP-dependent protein kinase stabilizes beta-catenin through inhibition of its ubiquitination. *Molecular and cellular biology*, **25**, 9063-9072.
15. Gordon, M.D. and Nusse, R. (2006) Wnt signaling: multiple pathways, multiple receptors, and multiple transcription factors. *The Journal of biological chemistry*, **281**, 22429-22433.
16. van Veelen, W., Le, N.H., Helvensteijn, W., Blonden, L., Theeuwes, M., Bakker, E.R., Franken, P.F., van Gurp, L., Meijlink, F., van der Valk, M.A. *et al.* (2011) beta-catenin tyrosine 654 phosphorylation increases Wnt signalling and intestinal tumorigenesis. *Gut*, **60**, 1204-1212.
17. Nusse, R. (2005) Wnt signaling in disease and in development. *Cell research*, **15**, 28-32.
18. Xin, N., Benchabane, H., Tian, A., Nguyen, K., Klofas, L. and Ahmed, Y. (2011) Erect Wing facilitates context-dependent Wnt/Wingless signaling by recruiting the cell-specific Armadillo-TCF adaptor Earthbound to chromatin. *Development*, **138**, 4955-4967.
19. Hou, N., Ye, B., Li, X., Margulies, K.B., Xu, H., Wang, X. and Li, F. (2016) Transcription Factor 7-like 2 Mediates Canonical Wnt/beta-Catenin Signaling and c-Myc Upregulation in Heart Failure. *Circulation. Heart failure*, **9**.
20. Papait, R., Cattaneo, P., Kunderfranco, P., Greco, C., Carullo, P., Guffanti, A., Vigano, V., Stirparo, G.G., Latronico, M.V., Hasenfuss, G. *et al.* (2013) Genome-wide analysis of histone marks identifying an epigenetic signature of promoters and enhancers underlying cardiac hypertrophy. *Proceedings of the National Academy of Sciences of the United States of America*, **110**, 20164-20169.
21. Frietze, S., Wang, R., Yao, L., Tak, Y.G., Ye, Z., Gaddis, M., Witt, H., Farnham, P.J. and Jin, V.X. (2012) Cell type-specific binding patterns reveal that TCF7L2 can be tethered to the genome by association with GATA3. *Genome biology*, **13**, R52.
22. Norton, L., Chen, X., Fourcaudot, M., Acharya, N.K., DeFronzo, R.A. and Heikkinen, S. (2014) The mechanisms of genome-wide target gene regulation by TCF7L2 in liver cells. *Nucleic acids research*, **42**, 13646-13661.
23. Mosimann, C., Hausmann, G. and Basler, K. (2009) Beta-catenin hits chromatin: regulation of Wnt target gene activation. *Nature reviews. Molecular cell biology*, **10**, 276-286.
24. Sohal, D.S., Nghiem, M., Crackower, M.A., Witt, S.A., Kimball, T.R., Tymitz, K.M., Penninger, J.M. and Molkentin, J.D. (2001) Temporally regulated and tissue-specific gene manipulations in the adult and embryonic heart using a tamoxifen-inducible Cre protein. *Circ.Res.*, **89**, 20-25.
25. Harada, N., Tamai, Y., Ishikawa, T.-o., Sauer, B., Takaku, K., Oshima, M. and Taketo, M.M. (1999) Intestinal polyposis in mice with a dominant stable mutation of the beta -catenin gene. *EMBO J.*, **18**, 5931-5942.
26. Langmead, B. and Salzberg, S.L. (2012) Fast gapped-read alignment with Bowtie 2. *Nature methods*, **9**, 357-359.

27. Anders, S. and Huber, W. (2010) Differential expression analysis for sequence count data. *Genome biology*, **11**, R106.
28. Bindea, G., Mlecnik, B., Hackl, H., Charoentong, P., Tosolini, M., Kirilovsky, A., Fridman, W.H., Pages, F., Trajanoski, Z. and Galon, J. (2009) ClueGO: a Cytoscape plug-in to decipher functionally grouped gene ontology and pathway annotation networks. *Bioinformatics*, **25**, 1091-1093.
29. Langmead, B. (2010) Aligning short sequencing reads with Bowtie. *Current protocols in bioinformatics*, **Chapter 11**, Unit 11 17.
30. Zhang, Y., Liu, T., Meyer, C.A., Eeckhoute, J., Johnson, D.S., Bernstein, B.E., Nusbaum, C., Myers, R.M., Brown, M., Li, W. *et al.* (2008) Model-based analysis of ChIP-Seq (MACS). *Genome biology*, **9**, R137.
31. McLean, C.Y., Bristor, D., Hiller, M., Clarke, S.L., Schaar, B.T., Lowe, C.B., Wenger, A.M. and Bejerano, G. (2010) GREAT improves functional interpretation of cis-regulatory regions. *Nature biotechnology*, **28**, 495-501.
32. Zhang, L., Prosdocimo, D.A., Bai, X., Fu, C., Zhang, R., Campbell, F., Liao, X., Coller, J. and Jain, M.K. (2015) KLF15 Establishes the Landscape of Diurnal Expression in the Heart. *Cell reports*, **13**, 2368-2375.
33. Wagner, E., Brandenburg, S., Kohl, T. and Lehnart, S.E. (2014) Analysis of tubular membrane networks in cardiac myocytes from atria and ventricles. *Journal of visualized experiments : JoVE*, e51823.
34. Nock, R. and Nielsen, F. (2004) Statistical region merging. *IEEE transactions on pattern analysis and machine intelligence*, **26**, 1452-1458.
35. Arganda-Carreras, I., Fernandez-Gonzalez, R., Munoz-Barrutia, A. and Ortiz-De-Solorzano, C. (2010) 3D reconstruction of histological sections: Application to mammary gland tissue. *Microscopy research and technique*, **73**, 1019-1029.
36. Valenta, T., Hausmann, G. and Basler, K. (2012) The many faces and functions of beta-catenin. *The EMBO journal*, **31**, 2714-2736.
37. Sipido, K.R., Volders, P.G., Vos, M.A. and Verdonck, F. (2002) Altered Na/Ca exchange activity in cardiac hypertrophy and heart failure: a new target for therapy? *Cardiovascular research*, **53**, 782-805.
38. Cohen, E.D., Tian, Y. and Morrisey, E.E. (2008) Wnt signaling: an essential regulator of cardiovascular differentiation, morphogenesis and progenitor self-renewal. *Development*, **135**, 789-798.
39. Ai, D., Fu, X., Wang, J., Lu, M.F., Chen, L., Baldini, A., Klein, W.H. and Martin, J.F. (2007) Canonical Wnt signaling functions in second heart field to promote right ventricular growth. *Proceedings of the National Academy of Sciences of the United States of America*, **104**, 9319-9324.
40. Senyo, S.E., Lee, R.T. and Kuhn, B. (2014) Cardiac regeneration based on mechanisms of cardiomyocyte proliferation and differentiation. *Stem cell research*, **13**, 532-541.
41. Ahuja, P., Sdek, P. and MacLellan, W.R. (2007) Cardiac myocyte cell cycle control in development, disease, and regeneration. *Physiological reviews*, **87**, 521-544.
42. Kubin, T., Poling, J., Kostin, S., Gajawada, P., Hein, S., Rees, W., Wietelmann, A., Tanaka, M., Lorchner, H., Schimanski, S. *et al.* (2011) Oncostatin M is a major mediator of cardiomyocyte dedifferentiation and remodeling. *Cell stem cell*, **9**, 420-432.

43. Creyghton, M.P., Cheng, A.W., Welstead, G.G., Kooistra, T., Carey, B.W., Steine, E.J., Hanna, J., Lodato, M.A., Frampton, G.M., Sharp, P.A. *et al.* (2010) Histone H3K27ac separates active from poised enhancers and predicts developmental state. *Proceedings of the National Academy of Sciences of the United States of America*, **107**, 21931-21936.
44. Dong, M., Liao, J.K., Fang, F., Lee, A.P., Yan, B.P., Liu, M. and Yu, C.M. (2012) Increased Rho kinase activity in congestive heart failure. *European journal of heart failure*, **14**, 965-973.
45. Dirkx, E., da Costa Martins, P.A. and De Windt, L.J. (2013) Regulation of fetal gene expression in heart failure. *Biochimica et biophysica acta*, **1832**, 2414-2424.
46. Gougelet, A., Torre, C., Veber, P., Sartor, C., Bachelot, L., Denechaud, P.D., Godard, C., Moldes, M., Burnol, A.F., Dubuquoy, C. *et al.* (2014) T-cell factor 4 and beta-catenin chromatin occupancies pattern zonal liver metabolism in mice. *Hepatology*, **59**, 2344-2357.
47. He, A., Kong, S.W., Ma, Q. and Pu, W.T. (2011) Co-occupancy by multiple cardiac transcription factors identifies transcriptional enhancers active in heart. *Proceedings of the National Academy of Sciences of the United States of America*, **108**, 5632-5637.
48. van den Boogaard M, W.L., Tessadori F, Bakker ML, Dreizehnter LK, Wakker V, Bezzina CR, 't Hoen PA, Bakkers J, Barnett P, Christoffels VM. (2012) Genetic variation in T-box binding element functionally affects SCN5A/SCN10A enhancer. *J Clin Invest.*, **122**, 2519-2530.
49. Haq, S., Michael, A., Andreucci, M., Bhattacharya, K., Dotto, P., Walters, B., Woodgett, J., Kilter, H. and Force, T. (2003) Stabilization of beta-catenin by a Wnt-independent mechanism regulates cardiomyocyte growth. *Proceedings of the National Academy of Sciences of the United States of America*, **100**, 4610-4615.
50. Sequeira, V., Nijenkamp, L.L., Regan, J.A. and van der Velden, J. (2014) The physiological role of cardiac cytoskeleton and its alterations in heart failure. *Biochimica et biophysica acta*, **1838**, 700-722.
51. Liu, Z., Yue, S., Chen, X., Kubin, T. and Braun, T. (2010) Regulation of cardiomyocyte polyploidy and multinucleation by CyclinG1. *Circulation research*, **106**, 1498-1506.
52. Tseng, A.S., Engel, F.B. and Keating, M.T. (2006) The GSK-3 inhibitor BIO promotes proliferation in mammalian cardiomyocytes. *Chemistry & biology*, **13**, 957-963.
53. Porrello, E.R., Mahmoud, A.I., Simpson, E., Hill, J.A., Richardson, J.A., Olson, E.N. and Sadek, H.A. (2011) Transient regenerative potential of the neonatal mouse heart. *Science*, **331**, 1078-1080.
54. Quaife-Ryan, G.A., Sim, C.B., Ziemann, M., Kaspi, A., Rafehi, H., Ramialison, M., El-Osta, A., Hudson, J.E. and Porrello, E.R. (2017) Multi-Cellular Transcriptional Analysis of Mammalian Heart Regeneration. *Circulation*.
55. Tian, Y., Liu, Y., Wang, T., Zhou, N., Kong, J., Chen, L., Snitow, M., Morley, M., Li, D., Petrenko, N. *et al.* (2015) A microRNA-Hippo pathway that promotes cardiomyocyte proliferation and cardiac regeneration in mice. *Science translational medicine*, **7**, 279ra238.
56. Parker, D.S., Ni, Y.Y., Chang, J.L., Li, J. and Cadigan, K.M. (2008) Wingless signaling induces widespread chromatin remodeling of target loci. *Molecular and cellular biology*, **28**, 1815-1828.
57. Mittal, A., Sharma, R., Prasad, R., Bahl, A. and Khullar, M. (2016) Role of cardiac TBX20 in dilated cardiomyopathy. *Molecular and cellular biochemistry*, **414**, 129-136.

58. Haq, S., Michael, A., Andreucci, M., Bhattacharya, K., Dotto, P., Walters, B., Woodgett, J., Kilter, H. and Force, T. (2003) Stabilization of beta -catenin by a Wnt-independent mechanism regulates cardiomyocyte growth. *Proceedings of the National Academy of Sciences of the United States of America*, **100**, 4610-4615.
59. Zelarayan, L.C., Noack, C., Sekkali, B., Kmecova, J., Gehrke, C., Renger, A., Zafiriou, M.P., van der Nagel, R., Dietz, R., de Windt, L.J. *et al.* (2008) Beta-Catenin downregulation attenuates ischemic cardiac remodeling through enhanced resident precursor cell differentiation. *Proceedings of the National Academy of Sciences of the United States of America*, **105**, 19762-19767.
60. Emery H. Bresnick*, K.R.K., Hsiang-Ying Lee, Kirby D. Johnson and Archibald S. Perkin. (2012) Master regulatory GATA transcription factors: mechanistic principles and emerging links to hematologic malignancies. *Nucleic acids research*, **40**, 5819–5831.
61. Bresnick, K.R.K.a.E.H. (2017) The GATA factor revolution in hematology. *Blood*, **129**, 2092-2102.
62. Oka, T., Maillet, M., Watt, A.J., Schwartz, R.J., Aronow, B.J., Duncan, S.A. and Molkentin, J.D. (2006) Cardiac-specific deletion of Gata4 reveals its requirement for hypertrophy, compensation, and myocyte viability. *Circulation research*, **98**, 837-845.
63. Bisping, E., Ikeda, S., Kong, S.W., Tarnavski, O., Bodyak, N., McMullen, J.R., Rajagopal, S., Son, J.K., Ma, Q., Springer, Z. *et al.* (2006) Gata4 is required for maintenance of postnatal cardiac function and protection from pressure overload-induced heart failure. *Proceedings of the National Academy of Sciences of the United States of America*, **103**, 14471-14476.
64. He, A., Gu, F., Hu, Y., Ma, Q., Ye, L.Y., Akiyama, J.A., Visel, A., Pennacchio, L.A. and Pu, W.T. (2014) Dynamic GATA4 enhancers shape the chromatin landscape central to heart development and disease. *Nature communications*, **5**, 4907.

## Supporting Data

Supporting table S1 related to Experimental Procedures
Supporting table S2 related to Experimental Procedures
Supporting experimental procedures
Supporting references
Supporting figures and figures legends

**Supporting table S1 related to Experimental Procedures**

Primers used in the direction of 5'-3' orientation for qPCR.

| **Name of the genes** | **Sequence** | **Comments/Use** |
|---|---|---|
| **HUMAN** | | |
| *AXIN2* forward (F) | GTGTGAGGTCCACGGAAACT | qPCR |
| *AXIN2* reverse (R) | AATCATCCGTCAGCGCATCA | qPCR |
| *GAPDH* F | AAGGCTGTGGGCAAGGTCATC | qPCR |

| | | |
|---|---|---|
| *GAPDH* R | GCGTCAAAGGTGGAGGAGTGG | qPCR |
| *TCF7L2* F | CAGACCTGAGCGCTCCTAAG | qPCR |
| *TCF7L2* R | TCAGTCTGTGACTTGGCGTC | qPCR |
| **MOUSE** | | |
| *Axin2* intron F | CAGGCTGGGACTGAATGAAG | qPCR |
| *Axin2* intron R | AAACAAGCATGGGACCACACC | qPCR |
| *Axin2* promoter F | GAGCGCCTCTGTGATTGGC | qPCR |
| *Axin2* promoter R | ACAGCAAAGCTCTCCTTTGGG | qPCR |
| *Axin2* F | AGCCGCCATAGTC | qPCR |
| *Axin2* R | GGTCCTCTTCATAGC | qPCR |
| *Cacna1g* F | AAAGAGAAGGAGTAAGGAGAAGCAG | qPCR |
| *Cacna1g* R | ATCTGGGGCTGCTGGTAATG | qPCR |
| Cre (Hgh) F | GTCTGACTAGGTGTCCTTCT | Genotyping |
| Cre (Hgh) R | CGTCCTCCTGCTGGTATAG | Genotyping |
| *Dstn* F | ACCCATGCACTCCCCTTAAC | qPCR |
| *Dstn* R | CTGAACTCCTGAGGCCATGTT | qPCR |
| *Gapdh* F | ATGTTCCAGTATGACTCCACTCACG | qPCR |
| *Gapdh* R | GAAGACACCAGTAGACTCCACGACA | qPCR |
| *Hand2* F | GCCGACACCAAACTCTCCAAG | qPCR |
| *Hand2* R | CCTCCGCCTCTCCGTTCTG | qPCR |
| *Myh7* F | ATGTGCCGGACCTTGGAA | qPCR |
| *Myh7* R | CCTCGGGTTAGCTGAGAGATCA | qPCR |
| *Nppa* promoter F | CGATGAATCAGGTGTGAAGC | qPCR |
| *Nppa* promoter R | TGTCAGGGGCTCCAAATAAG | qPCR |
| *Rock2* F | AGAGTCTGCTGGATGGCTTAAA | qPCR |
| *Rock2* R | TTCACCAAAAGCACCTCTTCC | qPCR |
| *Shisa3* F | CAGGGCAACTATCACGAGGG | qPCR |

| | | |
|---|---|---|
| *Shisa3* R | GACATAGACAGGTTGCGCGG | qPCR |
| *Sox4* F | GTGTTGAGCTTAGGGGAGCA | qPCR |
| *Sox4* R | ATGTCCATTTCCGAGGCTGG | qPCR |
| *Tbp* F | CCAGAACAACAGCCTTCCACC | qPCR |
| *Tbp* R | CAACGGTGCAGTGGTCAGAGT | qPCR |
| *Tbx20* F | AGAAGGAGGCAGCAGAGAACAC | qPCR |
| *Tbx20* R | GCACAGAGAGGATGAGGATGGG | qPCR |
| *ΔNCat* F | GCTGCTGTGACACCGCTGCGTGGAC | Genotyping |
| *ΔNCat* R | CACGTGTGGCAAGTTCCGCGTCATCC | Genotyping |

**Supporting table S2 related to Experimental Procedures**

Anesthetics and preanesthetics used in this study.

| **Intervention** | **Drug** | **Applications-route** | **Dosis** | **Applications-time** |
|---|---|---|---|---|
| **TAC** | Metamizole | Oral | 1,33 mg/ml in Drink water | 2 days before and 7 days after operation (OP) |
| | Buprinorphine | Subcutaneous injection | 0.05-0.1 mg/kg Boby weight | 30 min before and after OP |
| | Midazolame | Subcutaneous injection | 5 mg/kg body weight in 0,9% NaCl | During OP |
| | Fentanyl | Subcutaneous injection | 0,05 mg/ body weight in 0,9% NaCl | |
| | Medetomidin | Subcutaneous injection | 0,5 mg/ body weight in 0,9% NaCl | |
| | Atipamezole | Subcutaneous injection | 2,5 mg/kg body weight in 0,9% NaCl | After OP |
| | Flumazenil | Subcutaneous injection | 0,5 mg/kg body weight in 0,9% NaCl | |
| **Echocardiography** | Isoflurane | Inhalation | 2% [vol/vol] Isoflurane | During meassurements |

## Supporting experimental procedures

### DNA, RNA isolation and quantitative real-time PCR

Ventricular tissue was macro-dissected and used for DNA and RNA isolation. DNA and RNA were isolated using NucleoSpin Tissue genomic DNA and RNA kit (Macherey-Nagel), respectively, as described elsewhere (1). Tissue samples were immediately snap frozen and

stored at -80°C till RNA or DNA preparation. Nucleic acid quantification was assessed using Nanodrop photometer (Thermo Scientific). 500ng RNA was used for cDNA synthesis using 0.5 µg Oligo(dT)20 primer and 100 U M-MLV reverse transcriptase (Promega) for 1h 42°C. Quantitative real-time PCR (qPCR) analyses were performed with SYBR Green (Promega) on a 7900-HT Real-time cycler (Applied Biosystems) using the primers listed in Supporting table S1. Gene expression was normalized to the indicated housekeeper in every experiment. Copy numbers were calculated using the SDS2.4 software with a relative standard curve obtained using the log dilutions of cDNA of gene of interest. All reactions were run in triplicates and normalized to reference control genes. Primers are listed in Supplemental Table S1.

**Cellular fractionation**

Cardiac tissue was homogenized in a hypotonic buffer containing 10 mM HEPES, 10 mM KCl, 2 mM MgCl2, 0.1 mM EDTA and 1 mM DTT with protease inhibitors. After 10 min ice incubation, NP-40 was added to a final concentration of 1% followed by 5 min ice incubation. Lysates were centrifuged at 4000rpm for 5 min at 4°C. Supernatants were cytosol-enriched fractions. To the pellets, a hypertonic buffer containing 50 mM HEPES, 50 mM KCl, 300 mM NaCl, 0.1 mM EDTA, 1 mM DTT and 10% glycerol with protease inhibitors was added and incubated on ice for 25 min. NP-40 was added to a final concentration of 1% followed by 10 min ice incubation. Lysates were centrifuged at 13000rpm for 5 min at 4°C. Supernatants were nuclei-enriched fractions.

**Epifluorescence microscopy and calcium measurements**

CM was isolated as described above. Cells were plated on laminin-coated recording chambers and left to settle for 20 min, followed by incubation with a Fura-2 AM loading buffer (10 µmol/L, Molecular Probes) for 15 min. After staining, the CMs were superfused with experimental solution for 5 min before measurements were started to enable complete de-esterification of intracellular Fura-2 and allow cellular rebalance of Ca2+ cycling properties. Experimental solution contained (in mmol/L): KCl 4, NaCl 140, MgCl2 1, HEPES 5, glucose 10, 5 CaCl2 1 (pH 7.4, NaOH, room temperature). During measurements, CMs were continuously superfused with experimental solution. Measurements were performed with a Motic AE32 microscope (Speed Fair Co. Ltd, Hong Kong) provided with a fluorescence detection system (ION OPTIX Corp., Milton MA). Cells were excited at 340 and 380 nm, and the emitted fluorescence was collected at 510 nm. The intracellular Ca2+ level was measured as the ratio of fluorescence at 340 and 380 nm (F340 / F380, in ratio units). Systolic Ca2+ transients were

recorded at steady-state conditions under constant field stimulation (1, 2, and 3 Hz). To assess the SR Ca2+ content, the amplitude of caffeine-induced Ca2+ transients was measured. After stopping the stimulation during steady-state conditions at 1 Hz, caffeine (10 mmol/L, Sigma-Aldrich, St Louis, MO, USA) was applied directly onto the cell, leading to immediate and complete SR Ca2+ release. The recorded Ca2+ transients were analyzed

with the software IONWizard® (ION OPTIX Corp.). As a measure of SERCA2a-dependent Ca2+ reuptake into the SR, the decay constant k (reciprocal of Tau) of caffeine-induced Ca2+ transients was subtracted from the decay constant k of systolic Ca2+ transients at 1 Hz (ksys - kcaff).

**Chromatin immunoprecipitation (ChIP-seq) and data analyses (extended)**

ChIP was optimized for the cardiac ventricular tissue. TCF7L2 and H3K27ac ChIPs in cardiac ventricular tissue from 3 weeks post-induced β-catΔex3 mice were performed by 20 minutes crosslinking with 1.3% formaldehyde and first sonicated for 20 cycles with the buffer containing 150 mM NaCl, 20 mM EDTA (pH 8.0), 0.5 % sodium deoxycholate, 50 mM Tris-HCl (pH 8.0), 1% (v/v) NP-40, 20 mM Sodium Fluoride, 0.1% SDS and protease inhibitors. The lysates were centrifuged at 12000 x g at 4°C for 2 min and supernatants were collected and stored. To the pellets the above buffer was added again and sonication was repeated for 25 cycles. These supernatants from the second centrifugation per sample were pooled and pre-cleared with sepharose beads for 45 min to reduce unspecific binding. For IP, 2 µg of anti-TCF7L2, anti-IgG (17-10109, Millipore), anti-GATA4 (sc-25310 X, SantaCruz) or anti-H3K27ac (C15410196, Diagenode) was added to the nuclear extracts and incubated O/N at 4°C on a rotor. Antibodies were pulled down using protein-A-sepharose beads followed by washing and DNA extraction. For sequencing, the DNA was isolated using phenol chloroform extraction. For this purpose, 50 µl of 10 mM Tris HCl pH 8.0 containing 10 µg of RNAse A was added to the already washed chromatin-bound beads as well as the input samples and incubated for 30 min at 37°C. Then, 50 µl of buffer containing 100 mM Tris-HCl (pH 8.0), 20 mM EDTA (pH 8.0), 2% SDS and 20 µg of Proteinase K were added and the

samples were incubated overnight at 65°C with a subsequent centrifugation step at 2,000g for 2 min at

RT. The supernatant was collected, and the beads were rinsed again with 100 µl of 10 mM Tris pH 8.0. The samples were centrifuged and the supernatant was added to the first one. For extraction, 10 µl of 8 M LiCl, 4 µl co-precipitant (linear polyacrylamide) and 200 µl

phenol/chloroform/isoamyl alcohol (25:24:1) were added, samples were vortexed for 30 sec and centrifuged for 2 min at full speed. The aqueous phase was collected and the phenol phase was back extracted with 200 µl 10 mM Tris HCl pH 8.0 and 400 mM LiCl. After vortexing and centrifugation, the second aqueous phase was pooled with the first one and precipitation was performed by addition of 100% ethanol and incubation for 2 h at -80°C. After that, samples were centrifuged at maximal speed for 30 min (4°C), pellets were washed with 70% ethanol, dried and re-dissolved in 40 µl of water. 5 µl of the DNA was used for qRT-PCR to confirm efficient chromatin immunoprecipitation and 35 µl for sequencing. DNA concentration was measured using a Qubit dsDNA HS assay on a Qubit® 2.0 Fluorometer. To identify protein complexes bound to the chromatin, proteins were extracted from protein-A-sepharose beads by directly adding protein lysis buffer to the beads, incubating at 95°C for 10 min with constant shaking. Samples were centrifuged and supernatants were used for immunoblotting and/or analysed with mass spectrometry. The efficiency of sonication was determined by performing a shearing check. Briefly, 10 µl of sheared chromatin was used for phenol chloroform extraction. After re-suspension of the DNA in 15 µl of 10 mM Tris HCl pH 8.0, 100 µg/ml RNAse A was added and the mixture was incubated for 1 h at 37°C (700 rpm). The DNA was then run on a 1.5% agarose gel and analyzed on the gel documentation. Efficient shearing consisted of a smear from about 150bp to 1 kb with a maximum around 150- 300 bp. ChIP-seq library preparation was performed using NEB Next Ultra DNA library prep kit for Illumina (E7370) as per manual's instructions. 5 - 50 ng of

fragmented DNA from ChIP was re-sonicated for 15 min in Bioruptor to ensure small fragments suitable for sequencing. End preparation was performed by adding end prep enzyme mix and end repair reaction buffer (10X) to a final reaction volume of 65 µl. Samples were placed on a thermocycler with cycles of 20°C for 30 min and 65°C for 30 min followed by adaptor ligation with blunt/TA ligase master mix, NEB Next adaptor and ligation enhancer to a final volume of 83.5 µl. Samples were incubated at 20°C for 15 min, then 3 µl of User enzyme was added and placed at 37°C for 15 min. Adaptor – ligated DNA was cleaned up using 0.9x AMPure XP beads on magnetic stand and finally DNA was resuspended in 28 µl of 10 mM Tris pH 8.0. From this, 23 µl of DNA was used for PCR amplification followed by clean-up of PCR amplified product using AMPure XP beads. The DNA was resuspended in 33 µl of 10 mM Tris pH 8.0 and analyzed on Bioanalyzer. Quantitation of DNA libraries was done on an Invitrogen Qubit 2.0 Fluorometer

and the size range of DNA libraries was performed on an Agilent Bioanalyzer 2100 (High Sensitivity DNA Assay). DNA libraries were amplified and sequenced by using the cBot and HiSeq2500 from Illumina (20-25 million reads per sample). Sequence reads were aligned to the mouse reference assembly (UCSC version mm9) using Bowtie (*2*). Peak calling was performed with Model Based Analysis of ChIPseq (MACS2) version 2.1.0.20140616.0, which is the updated version of MACS (*3*). Genes proximal to the bound chromatin regions were identified by GREAT analyses (*4*) using 'Basal plus extension' method where each genomic region is overlapped with genes which are 5kb upstream and 1 kb downstream (proximal), plus up to 1000 kb (distal). To integrate ChIP-seq with differential gene regulation i.e RNA-seq, BioVenn web application was used to compare, create and analyse Venn diagrams showing commonly or differently bound genes between two or more datasets (*5*). Gene ontology/pathway analyses for gene lists were performed using default parameters and stringency in 'ClueGO': a Cytoscape plug-in (*6*) and the significant 'Gene Ontology Biological Processes' were shown with $p \leq 0.05$. Published/public ChIP-seq datasets were used from the following sources: TCF7L2 liver: GSE32513, GATA4, NKX2-5 and TBX3: GSM862697-(*7*), DNAse-seq: GSM1014166, H3K4me1: GSM769025 and RNAPII: GSM918723.

**CM isolation and immunocytochemistry**

For CM (CM) isolation, hearts were retrogradely perfused by a modified Langendorff solution (NaCl 120.4 mM, KCl 14.7 mM, KH2PO4 0.6 mM, Na2HPO4 0.6 mM, MgSO4 1.2 mM, Na-HEPES 10 mM, NaHCO3 4.6 mM, taurine 30 mM, 2, 3-butanedione-monoxime 10 mM, collagenase type II (600 U/ml), glucose 5.5 mM, pH 7.4) for 7 min at 37°C at a flow rate of 4 ml/min. The residual tissue was removed by using a 100- μm cell strainer (BD Falcon, 352360). Bovine calf serum (10%) and 12.5 μM CaCl2 in perfusion buffer was used to inhibit collagenase activity. For immunofluorescence, isolated myocytes were plated on laminin (L2020, Sigma)- 2 coated glass coverslips, fixed with 4% PFA, followed by PBS washing and permeabilization with 0.2%BSA and 0.3%Triton in PBS for 10 min. CM were then blocked with 5%BSA and 0.1%Triton at RT. Primary and secondary antibodies (listed in Supplementary methods) were diluted in 2%BSA and 0.1%Triton in PBS. Coverslips were mounted with ProLong Gold medium containing DAPI (Invitrogen) and imaged in Zeiss LSM 710 NLO confocal microscope.

**Histology and immunohistochemistry**

Immunohistochemistry was performed as described previously (*8*). Hearts were dissected, rinsed in PBS, fixed in 4% PFA O/N at 4°C, embedded in paraffin and sectioned at 3 μm thickness in

Leica RM2255 microtome. Sections were de-paraffinized, rehydrated and antigen was unmasked by microwaving sections for 10min in 10mM sodium citrate buffer at pH 6.0. For immunofluorescence (IF), sections were blocked at RT for 1hr with 5%BSA in PBS + 0.1% Triton. For IF, primary antibodies were incubated O/N at 4°C as follows: anti-Cardiac Troponin T (ab8295, Abcam, 1:200), anti-β-catenin (610153, BD Transduction labs, 1:120), anti-Ki67 (ab15580, Abcam, 1:50), anti-acTub (ab24610, Abcam, 1:500), anti-Caveolin3 (ab30750, Abcam, 1:500), anti-TCF7L2 (ab76151, Abcam, 1:50), anti-Shisa3 (HPA054754, Sigma, 1:20), anti-Ncadherin (sc-7939, SantaCruz, 1:100) in 1% BSA in PBS+0.1% Triton. Next, sections were washed in PBS and incubated with secondary anti-rabbit IgG-Alexa 594 or anti-mouse IgG-Alexa 488(1:200; Molecular Probes) antibodies. For assessing proliferation in vivo, 200 μg of 5-ethynyl-2'-deoxyuridine (EdU) EdU per mouse was applied by a single i.p. injection on the same day as TX induction. 3 weeks post-induction, hearts were analyzed by immunofluorescence (IF) with Click-it EdU Assay kit (Invitrogen) according to the manufacturer's instructions. For assessing cross-sectional area (CSA) of CM, sections were stained with 20 mg/ml lectin wheat germ agglutinin (WGA) FITC (Sigma–Aldrich) and mounted with Prolong Gold (Invitrogen), random fields were photographed and 150 cells were counted to calculate CSA using semiautomatic AxioVision software (Zeiss). Microscopic images were captured with a digital microscope (IX70, Olympus). All sections were stained with Hoechst 55532 (Sigma-Aldrich) to visualize nuclei. Sections were stained with DirectRed80 for 1 h (Sigma–Aldrich) for Sirius Red staining. Fibrosis was quantified using ImageJ.

**Analysis of the microtubule network**

To analyze the density and complexity of microtubule networks as well as the orientation of individual network components, a published protocol (*9*) for the analysis of membrane networks in CMs was adapted using the image processing program Fiji. Probe preparation and data analysis was done with the help of SFB 1002 service unit (S02 High resolution fluorescence microscopy and integrative data analysis). Confocal images of fixed, α-tubulin stained ventricular myocytes were used for the microtubule network analysis. Initially, ROIs that enclosed the microtubule network were defined. After background subtraction and smoothing, a statistical region merging algorithm (*10*) was applied to these ROIs. Next, the ROIs were converted into binary images by application of a defined threshold. Binary images of the processed ROIs were then skeletonized using the Fiji plugin "Skeletonize (2D/3D)". Successful skeletonization was confirmed by superposition of the original α-tubulin images and the

skeletonized image as shown in Fig. 3G. Quantitative skeleton properties like length and the number of network junctions were automatically analyzed with the plugin "Analyze Skeleton (2D/3D)" (*11*) and normalized to the area of each ROI.

**Luciferase reporter assay**

Genomic regions of interest were amplified and cloned upstream of a minimal promoter in KpnI and XhoI digested pGL4.25 (Promega). A fragment located ~150 kb upstream of the Tbx20 gene and of ~120 kb upstream of the Hand2 gene (containing two and four TCF/LEF consensus sites, respectively) was cloned for luciferase assay into the pGL4.25 vector system. TSA201 cells were co-transfected with pGL4.25- Hand2 enhancers (enh) and -Tbx20enh, pCDNA3.1-β-cateninΔex3 and pBabeX-Gata4 expression vectors with Turbofect (Thermo Scientific) transfection reagent. Empty plasmids were used for adjustment of equal DNA content per transfection. 40 h after transfection the dual luciferase assay were performed and measured in a GloMax-96 Microplate Luminometer (Promega). Luciferase activity was normalized to Renilla luciferase activity and expressed as fold change against the empty vector pGL4.25. Every experiment was done in technical and biological triplicates.

**Supporting references**


1. C. Noack *et al.*, Krueppel-like factor 15 regulates Wnt/beta-catenin transcription and controls cardiac progenitor cell fate in the postnatal heart. *EMBO Mol Med* **4**, 992 (Sep, 2012).
2. B. Langmead, Aligning short sequencing reads with Bowtie. *Current protocols in bioinformatics* **Chapter 11**, Unit 11 7 (Dec, 2010).
3. Y. Zhang *et al.*, Model-based analysis of ChIP-Seq (MACS). *Genome biology* **9**, R137 (2008).
4. C. Y. McLean *et al.*, GREAT improves functional interpretation of cis-regulatory regions. *Nature biotechnology* **28**, 495 (May, 2010).
5. T. Hulsen, J. de Vlieg, W. Alkema, BioVenn - a web application for the comparison and visualization of biological lists using area-proportional Venn diagrams. *BMC genomics* **9**, 488 (Oct 16, 2008).
6. G. Bindea *et al.*, ClueGO: a Cytoscape plug-in to decipher functionally grouped gene ontology and pathway annotation networks. *Bioinformatics* **25**, 1091 (Apr 15, 2009).
7. L. Zhang *et al.*, KLF15 Establishes the Landscape of Diurnal Expression in the Heart. *Cell reports* **13**, 2368 (Dec 22, 2015).

## Supporting figures

## Figure S1.

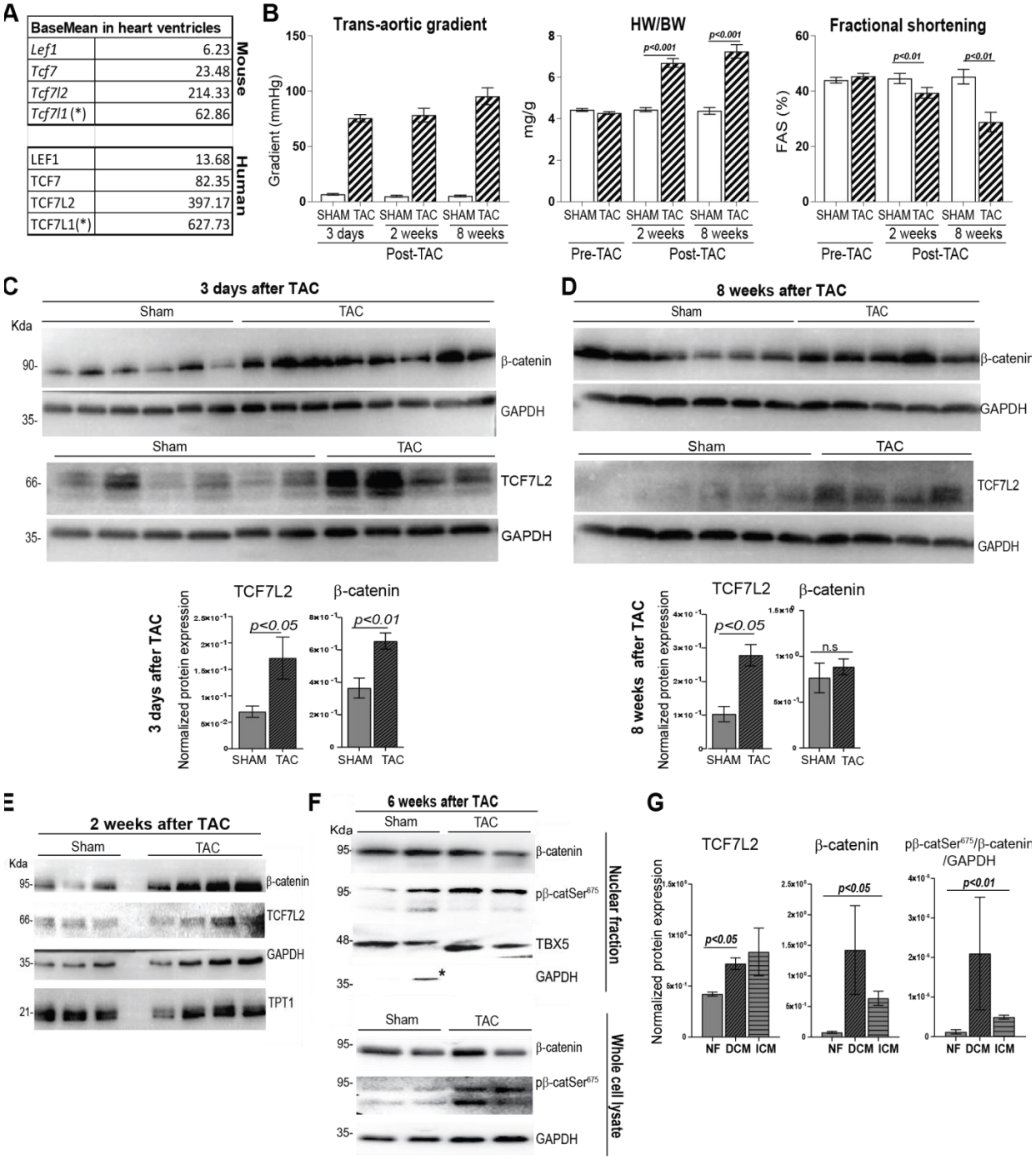


**Figure S1: Regulation of Wnt nuclear components upon cardiac pressure-overload.** (**A**) Base mean values representing the normalized read counts for each transcript by DESeq2, for TCF/LEF factors in the murine and human normal adult heart. **(B)** Validation of the TAC-induced mouse model. Trans-aortic gradient measurements for controlling successful banding; echocardiography analysis showing heart-to-body weight (HW/BW) ratio and fractional area shortening (FAS) in 3-days, 2-weeks and 8-weeks post- TAC mice compared to sham controls, n≥5. (**C, D**) Additional immunoblots depicting protein expression of β-catenin and TCF7L2 in 3 days and 8 weeks-post TAC heart tissue and their densitometry quantification (n≥4). (**E**) Immunoblots depicting protein expression of β-

catenin and TCF7L2 in 2 weeks-post TAC heart tissue (n≥3). (**F**) Immunoblots depicting nuclear and whole lysates protein expression of β-catenin and pSer675-β-catenin in 6 weeks-post TAC heart tissue (n≥3). (**G**) Densitometric quantification of β-catenin and pSer675-β-catenin and TCF7L2 protein normalized to GAPDH in human ventricular biopsies for Figure 1G (NF: n=2; DCM: n=6; ICM: n=6). GAPDH was used as protein loading control in C, D and E. TPT1 was used additionally as a loading control in E. TBX5 and GAPDH were used for nuclear and cytosolic fractions as controls respectively, in F.

## Figure S2.

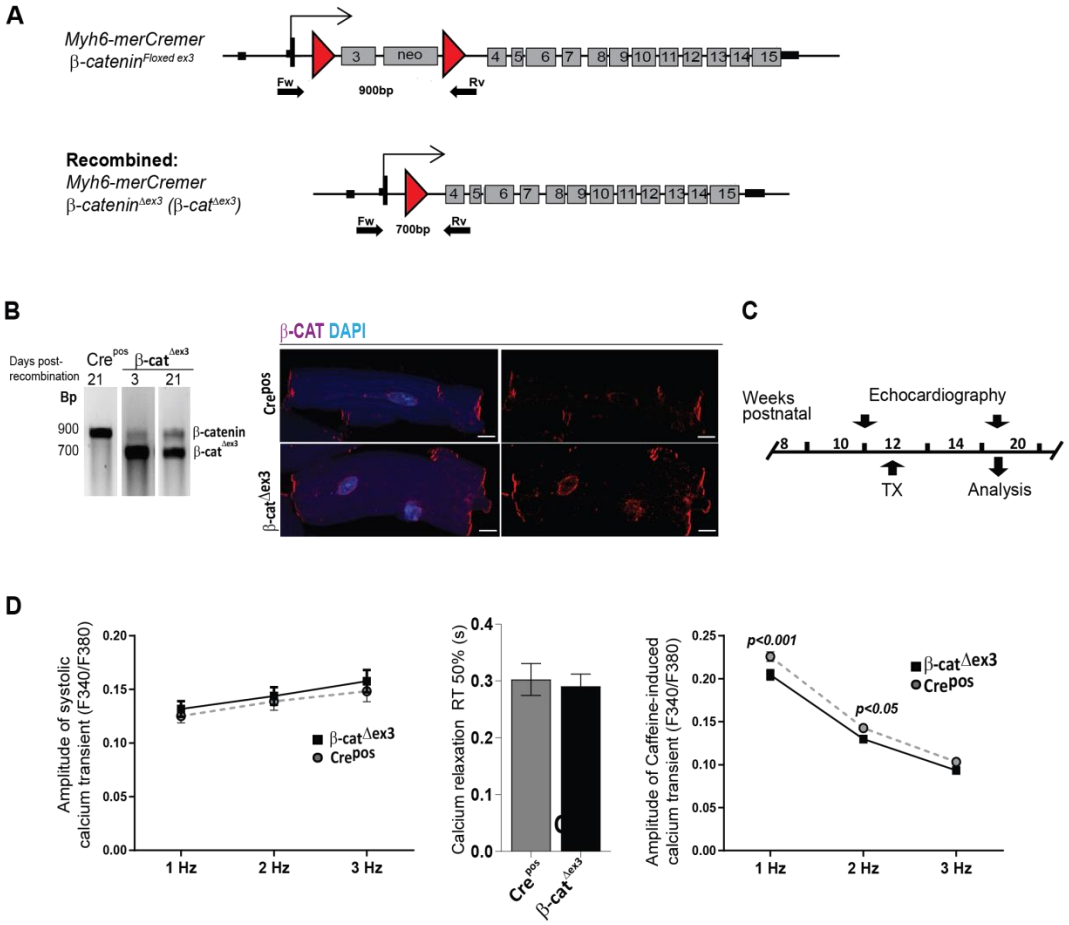


**Figure S2: Validation of β-catΔex3 model.** (**A**) Scheme showing inducible CM-specific β-catenin stabilization by crossing a mouse possessing a *Ctnnb1* allele with *loxP*-flanked exon 3 (β-cateninfloxed-ex3), with a *Myh6*-promoter driven tamoxifen (TX)-inducible-Cre expressing line. The recombined allele (β- catΔex3) produces a stabilized truncated GSK3β-degradation-resistant β-catenin. (**B**) PCR indicating successful recombination 3 and 21 days post-TX induction in Crepos and β-catΔex3 cardiac ventricles. 900 bp: WT β-catenin; 700 bp: truncated β-catenin. Confocal image of β-catenin (magenta) and DAPI (blue) in Crepos and β-catΔex3 isolated CM showing perinuclear/nuclear accumulaiton, n=3. (**C**) Scheme illustrating the time-points of analyses post-tamoxifen (TX) administration in Myh6-merCREmer/β-cat wild-type (WT) (Crepos), β-catflox-exon3 (Creneg) controls and Myh6-merCREmer/β-catflox-exon3 (β-catΔex3) mice. (**D**) Systolic, caffeine-induced Ca2+- transients and systolic half-times intracellular calcium relaxation (RT50%) in β-catΔex3 and Crepos cardiomyocytes. Data are mean ± SEM; ANOVA, Bonferroni's multiple comparison test. Scale bar: 10 µm.

**Figure S3.**

A

| GOID | GOTerm (Downregulated genes log2fold>1.0) | Term P Value |
|---|---|---|
| GO:0086043 | action potential | 9.20E-05 |
| GO:0050433 | regulation of catecholamine secretion | 6.00E-04 |
| GO:0060078 | regulation of postsynaptic membrane potential | 4.30E-03 |
| GO:0086010 | membrane depolarization during action potential | 9.60E-03 |
| GO:0055117 | regulation of cardiac muscle contraction | 1.60E-02 |
| GO:0090280 | positive regulation of calcium ion import | 2.70E-02 |
| GO:0031644 | regulation of neurological system process | 3.90E-02 |
| GO:0017158 | regulation of calcium ion-dependent exocytosis | 4.20E-02 |
| GO:0042312 | regulation of vasodilation | 4.30E-02 |

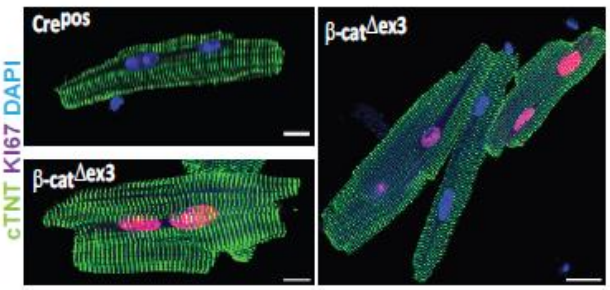


C

| | | log2FC | padj |
|---|---|---|---|
| β-catΔex3 | *Ccna2* | 1.75 | 2.73E-14 |
| | *Ccnb1* | 1.36 | 1.27E-05 |
| | *Ccnb2* | 1.36 | 1.04E-05 |
| post-TAC | *Ccna2* | 3.04 | 5.62E-42 |
| | *Ccnb2* | 3.17 | 3.75E-36 |
| | *Ccnb1* | 3.10 | 7.36E-17 |

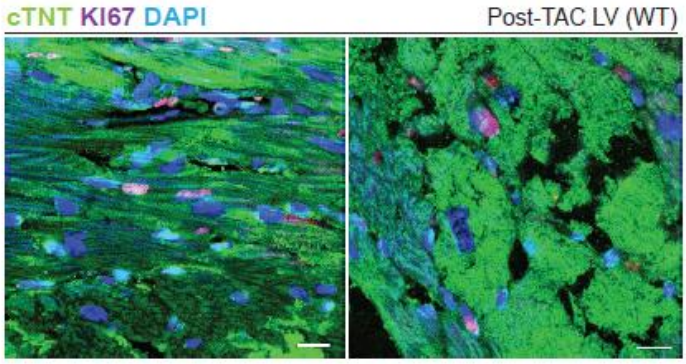


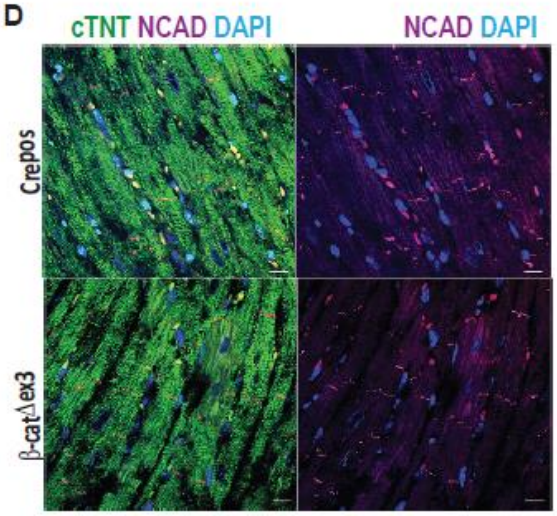


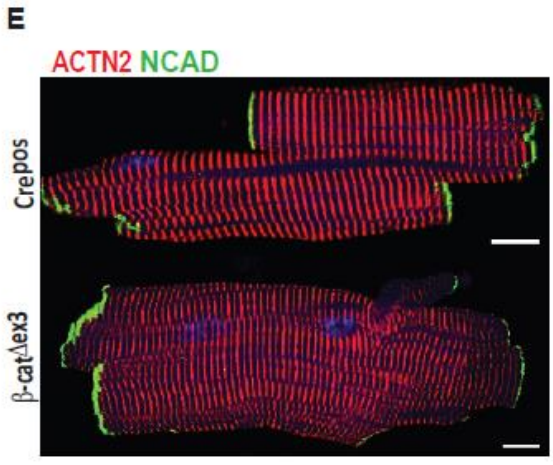


**Figure S3: Cell cycle activity and cytoskeletal structure analyses in β-catΔex3 CM.** (**A**) Gene Ontology (GO) biological processes of downregulated genes (log2FC< -0.5, p<0.05) in β-catΔex3 ventricles. All enriched pathways depicted are significant with p≤0.05. (**B**) Representative immunofluorescence images of cardiac Troponin T (CTNT, green) and KI67 (magenta) in isolated CM in β-catΔex3 and Crepos control. (**C**) Table showing cell cycling genes upregulated in ventricles of β-catΔex3 and TAC-induced hearts along with immunofluorescence staining of CTNT (green), KI67 (magenta) in 6-weeks post-TAC myocardium. (**D**) CTNT (green) and N-cadherin (NCADH, magenta) in Crepos and β-catΔex3 cardiac ventricular tissue and (**E**) Alpha-ACTININ (ACTN2) (magenta) and NCADH

(green) in isolated CM from β-catΔex3 and Crepos control. DAPI was used as a nuclear stain (blue). Scale bar (b, c and d) 20 μm; (E) 10 μm.

## Figure S4.

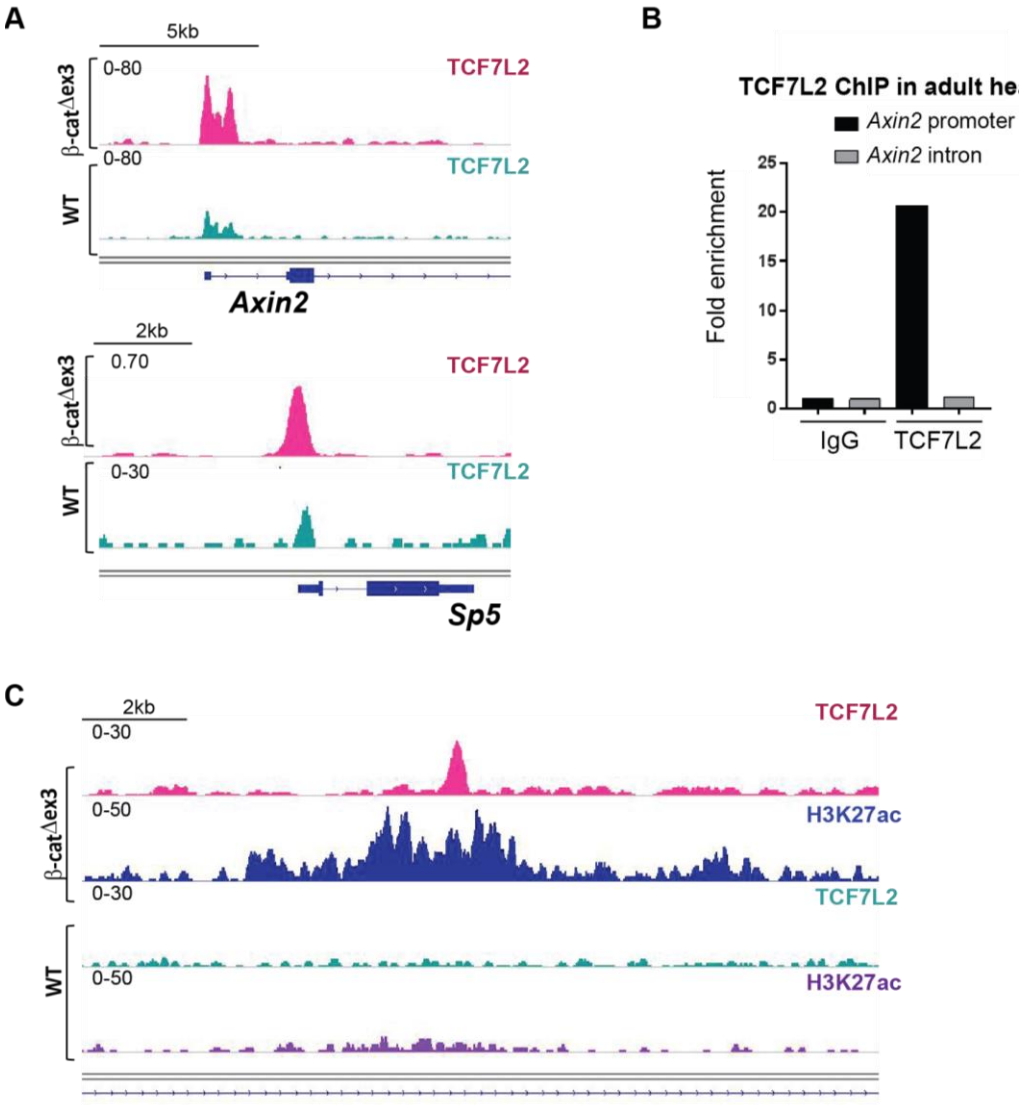


**Figure S4: TCF7L2 occupancy profiles and qPCR validations in the adult heart.** (**A**) Occupancy profiles of TCF7L2 on *Axin2* and *SP5* classical Wnt target genes in the normal (green) and β-catΔex3 hearts (pink). (**B**) Fold enrichment of TCF7L2 at *Axin2* binding site in comparison to IgG in adult hearts validating the TCF7L2-ChIP protocol. (**C**) Occupancy profiles of TCF7L2 and H3K27ac on *Tcf7l2* gene in the normal and β-catΔex3 hearts.

**Figure S5.**

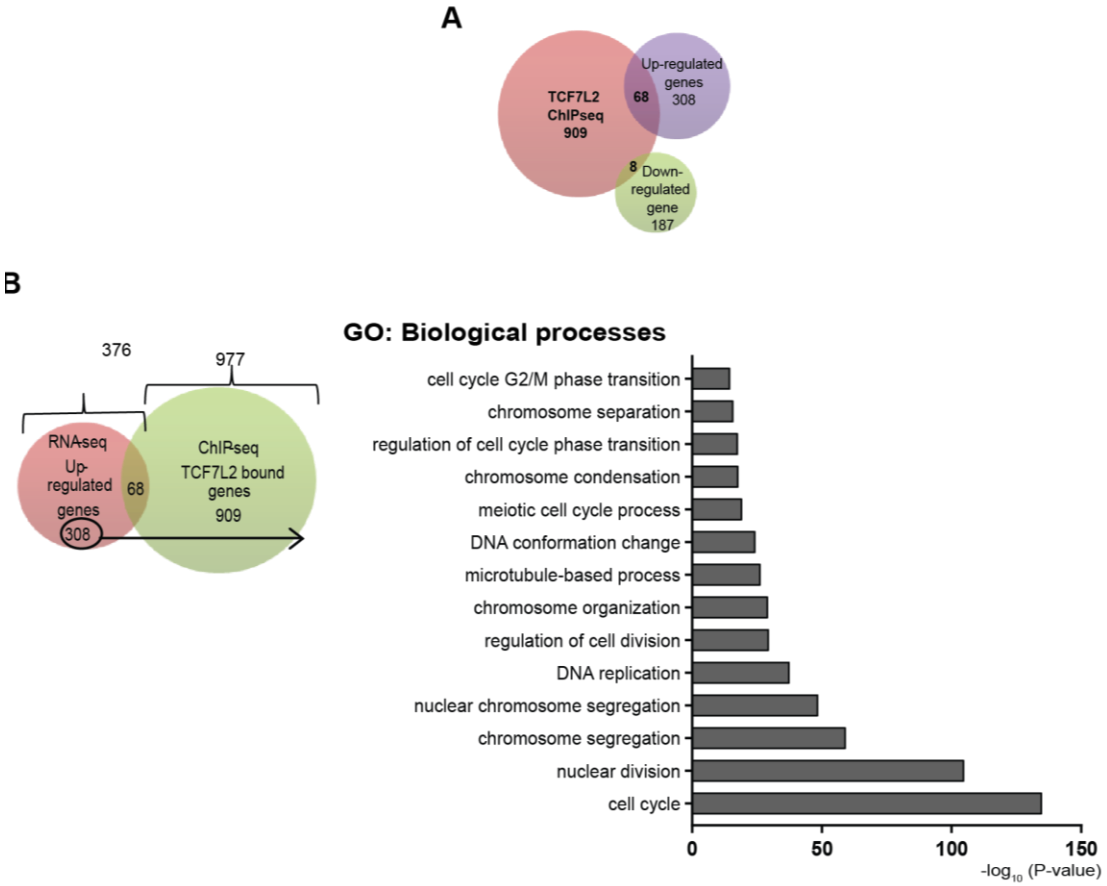


**Figure S5: Downregulated genes not directly bound to TCF7L2 in β-catΔex3 ventricles.** (**A**) Venn diagram of genes bound by TCF7L2 (orange) with upregulated (violet) or downregulated (green) genes with log2FC≥0.5, p≤0.05 in β-catΔex3 ventricles. (**B**) Venn diagram depicting genes bound by TCF7L2 (green, 977) and upregulated with log2FC≥0.5, p≤0.05 (red, 376) in β-catΔex3 ventricles. Black arrow represents upregulated genes but not bound by TCF7L2, which annotated to mitotic and cell cycle processes.

**Figure S6.**

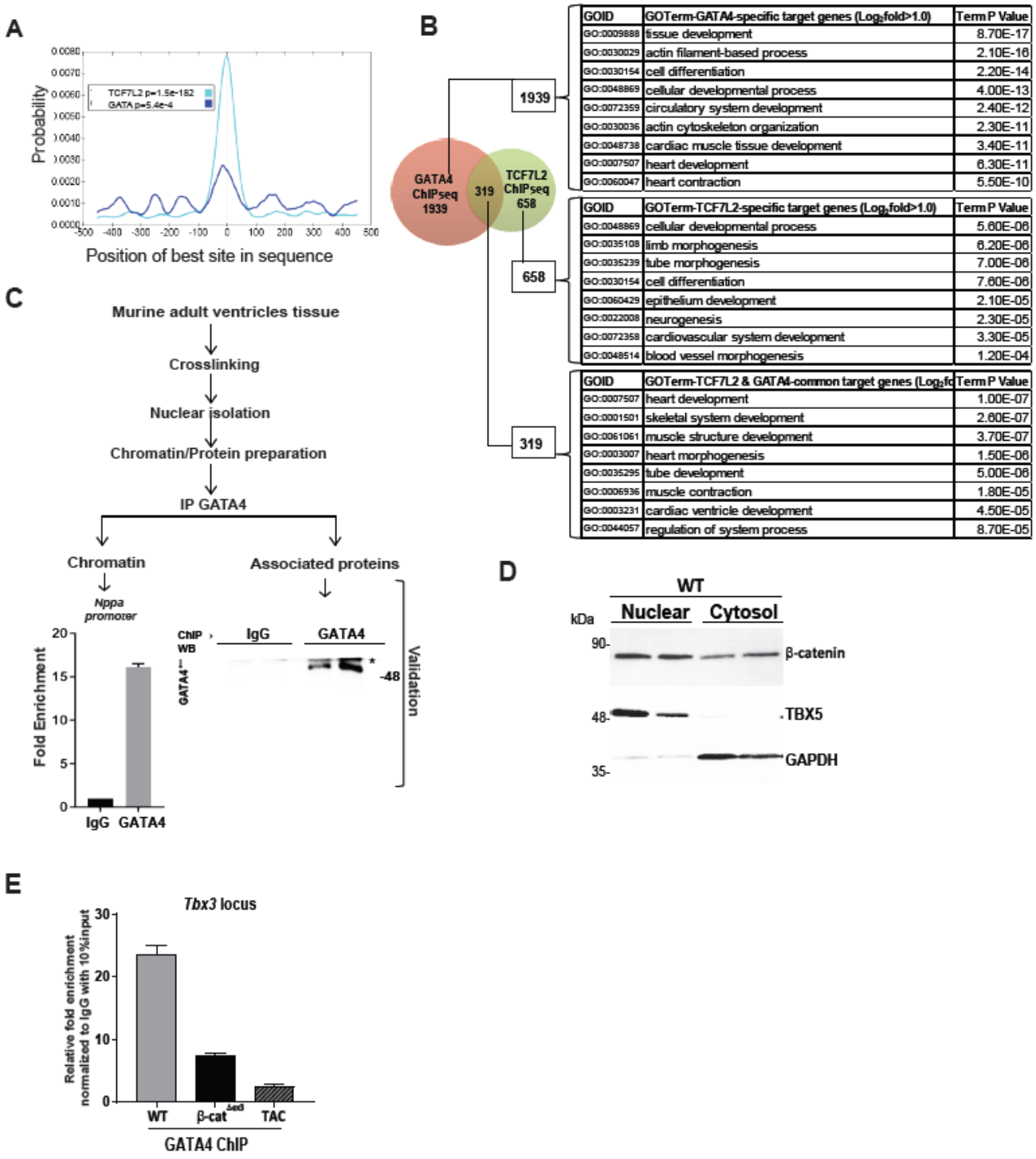


**Figure S6: GATA4 co-occupancy and co-regulation with TCF7L2.** (**A**) CentriMo motif density search on TCF7L2-bound regions in β- catΔex3 hearts showing GATA motif significantly enriched (p=5.4E-4). (**B**) GO biological processes of GATA4-specific, TCF7L2-specific and GATA4-TCF7L2 commonly bound genes. (**C**) Scheme illustrating ChIP-protein isolation and validating the GATA4-ChIP. Enrichment of GATA4 on its known target promoter *Nppa* is shown, n=2. Validation of anti-GATA4 IP depicted by a correct pull-down as detected by GATA4 immunoblot is shown (*heavy chain). (**D**) Immunoblot showing β-catenin expression in both nuclear and

cytosolic fractions of healthy cardiac ventricular tissue, n=2. GAPDH and TBX5 were used as cytosolic and nuclear fraction controls respectively. (**E**) ChIP-qPCR analyses for GATA4 binding to *Tbx3* enhancer locus in β-catΔex3 and 6 weeks post-TAC (Wnt-active) hearts (n=3). Relative fold enrichment was calculated with respect to IgG control, normalized to 10% input chromatin.

## Figure S7.

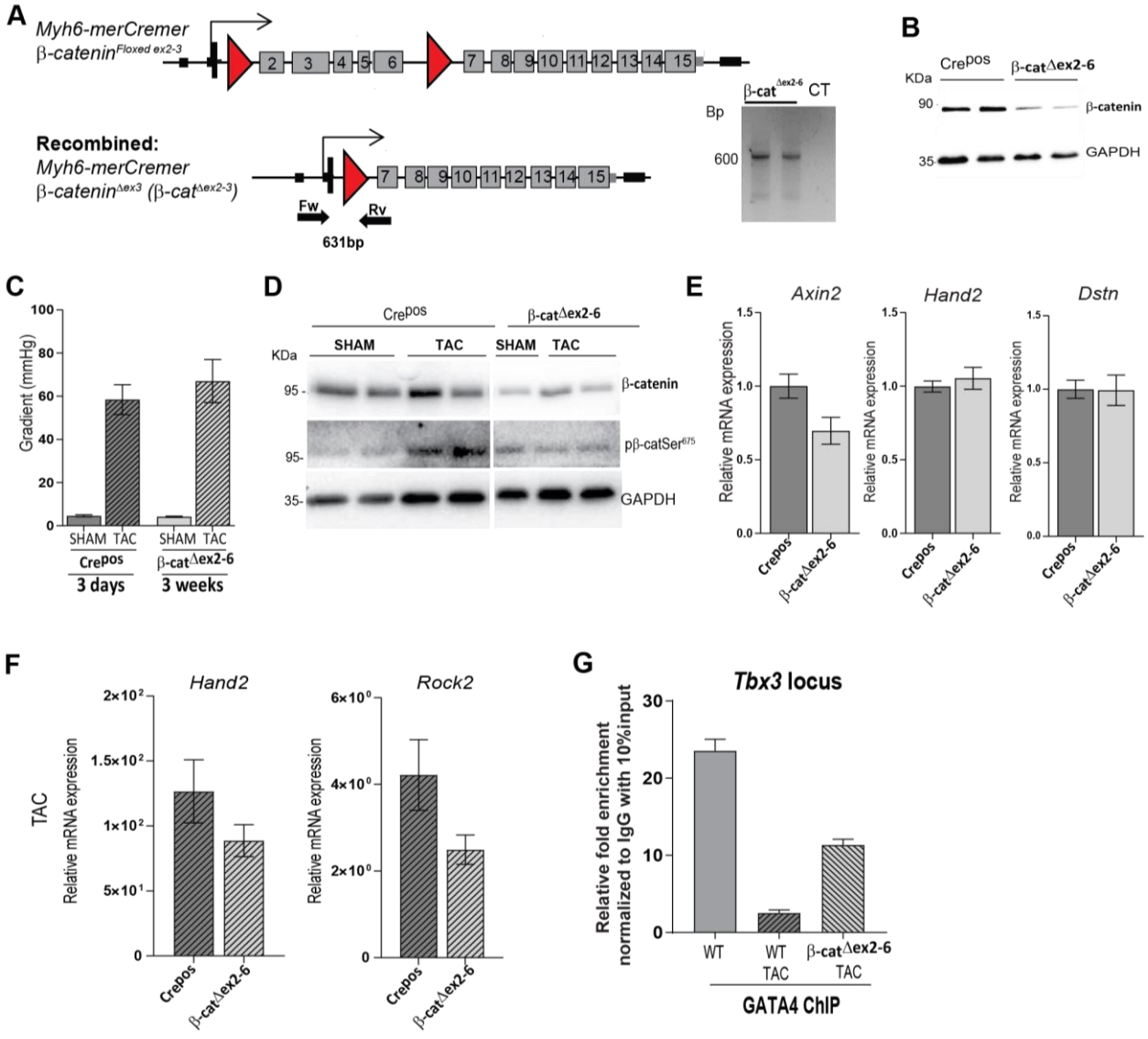


**Figure S7: β-catenin loss of function inducible model.** (**A**) Scheme of the CM-specific β-catenin loss of function (β-catΔex2-6) mouse model, depicting the locus truncation and primer binding sites for genotyping with corresponding recombination PCR. (**B**) Immunoblot showing reduction in total β-catenin in β-catΔex2-6 ventricular tissue compared to Crepos controls. (**C**) Trans-aortic gradient measurements post-TAC confirming a homogenous induced-pressure overload in all groups for validation of functional data. (**D**) Immunoblots showing expression of β-catenin and pSer675-β-catenin in 6 weeks post-TAC and sham controls in Crepos and β-catΔex2-6 heart lysates. (**E**) Relative (Rel) transcript levels of *Axin2, Hand2 a*nd *Dstn* in β-catenin downregulation and control cardiac ventricles, n≥7. (**F**) Relative transcript levels of

*Hand2* and *Rock2* upon β-catenin downregulation in late stages post-TAC (6-weeks) and corresponding controls, n≥7. (**G**) ChIP-qPCR analyses for GATA4 binding to *Tbx3* enhancer locus in normal (WT), 6 weeks post-TAC (WT) and β-catΔex2-6 TAC hearts (n=3). Relative fold enrichment was calculated with respect to IgG control, normalized to 10% input chromatin. *Tbp* was used for transcript normalization in E and F. GAPDH was used as loading control in B and D.

# 5. Chapter 2: Discerning Wnt-TCF7L2 chromatin landscapes in the neonatal, adult and diseased myocardium

## 'Distinct TCF7L2 genomic occupancies discern chromatin states in the neonatal, adult and diseased mammalian myocardium'

Lavanya M. Iyer [1,2], Sze Ting Pang [1,2], Eric Schoger [1,2], Monique Woelfer [1,2] and Laura C. Zelarayan [1,2].

Affiliations:

[1] Institute of Pharmacology and Toxicology, University Medical Center Goettingen, Georg-August University, Goettingen, Germany

[2]DZHK (German Center for Cardiovascular Research), partner site Goettingen, Germany

**Abstract:** During disease, the heart unsuccessfully attempts to compensate by reactivating regenerative responses, characterized by a re-employment of developmental signaling pathways and chromatin remodeling. Our previous work had demonstrated the role of Transcription factor 7-like 2 (TCF7L2), a Wnt pathway effector, in heart disease progression; revealing GATA4 as a Wnt-repressor in the healthy adult heart. However, Wnt-chromatin landscapes were never investigated in the neonatal myocardium. In this study, we observed GATA4-B-catenin interaction in the neonatal (high Wnt activity), similar to the healthy adult (low Wnt activity); and contrary to its loss in diseased hearts (high Wnt activity). Strikingly, TCF7L2 displayed unique genomic occupancies: proximal in neonatal and distal in diseased hearts. Integration of genomic and transcriptomic data showed that TCF7L2 differentially occupied and regulated metabolic genes in the neonatal; and cardiac developmental and vasculogenesis genes in the diseased hearts. Further, *de-novo* motif search analyses identified TEAD2 as a commonly enriched motif in both TCF7L2 and GATA4-bound regions in the neonatal hearts, suggesting its potential role in providing a regenerative context to the GATA4-B-catenin interaction in these hearts. Altogether, this study mapped for the first time, novel genome-wide TCF7L2 and GATA4 targets in the neonatal hearts and identified a stage-specific role for the Wnt-GATA4 complex in different cardiac states.

## Introduction

Heart failure is the most common cause of mortality worldwide. Myocardial infarction is usually accompanied by a loss of CM content in the heart, forming a scar which results in progressive deterioration of cardiac function and ultimately, death[1,2]. Unlike the liver[3,4], mammalian heart is a post-mitotic organ, incapable of robust regenerative responses post-injury or stress[5,6]. This response is usually mediated in the other organs by a massive increase in cell-cycling of the major organ cell-types[7]. Most available cardiovascular therapeutic options include usage of anti-hypertensive drugs, which can only partially and temporarily alleviate symptoms. Hence, there is an urgent need to develop therapies aimed at replenishing the lost pool of CM post-injury. Taking cues from other regenerative systems like satellite cells of the skeletal muscle[8], several studies have unearthed the existence of a cardiac progenitor cells (CPCs)-like niche in the adult heart, which could be potentially triggered to proliferate and populate the lost CM mass, post-infraction. A few studies have also provided evidences showing existing CM de-differentiation in response to injury[9,10]. Previous studies demonstrated that downregulating Wnt/B-catenin cascade in the adult heart led to increased CPC differentiation towards CM, whereas its upregulation owing to a loss of the transcriptional repressor KLF15 led to increased CPC proliferation[11–13]. These findings hint at the existence of a potential regenerative response in the adult heart.

Interestingly, neonatal murine hearts possess a remarkable regenerative capacity until a week after birth (P7)[14]. This ability is attributed to the unique proliferative capacity of the CM at this age-window. This capacity is gradually and completely lost during transition to adulthood, where the CMs are rendered post-mitotic and unresponsive to cell-cycle signals[15]. Further, upon experimental myocardial infarction (MI) in neonatal murine hearts, Wnt signaling, a pro-proliferative developmental pathway was upregulated[15]. Moreover, a groundbreaking case study in 2009 by Poonai and colleagues revealed that a human neonate born with compromised cardiac function could completely cure the infarct scar within 4 weeks after birth. This provided an optimistic basis for human cardiac regeneration post-injury in neonates, for the first time[16].

During disease initiation, CMs exhibit increased cell-cycling, along with cytoskeletal reorganization and an activation of a regeneration-like response[17]. Accordingly, this response is also mirrored in global cardiac chromatin states- wherein, neonatal H3K27ac occupancies are partially recapitulated during disease progression, suggesting a common reactivation mechanism integrating signaling pathways, chromatin modifiers and transcriptional signatures.

However, despite trying to activate regeneration, the adult heart miserably fails to regain homeostasis. This could be due to the lack of a suitable environment to manifest this response fully- to achieve functional restoration. Therefore, distinguishing between these two cardiac states in terms of specific molecular players could help design specific and efficient strategies.

On that note, Wnt signaling pathway is active both, in the neonatal regenerative heart as well as in the diseased adult heart, but not in the normal adult heart[18–20]. However, the role of Wnt nuclear components like TCF7L2 and nuclear B-catenin on cardiac chromatin homeostasis pertaining to neonatal hearts with a regenerative potential had not been investigated before. Durinng the course of this study, TCF7L2 occupancies in the diseased Wnt-activated hearts were elucidated, identifying GATA4 as an important nuclear Wnt repressor, crucial for maintaining homeostasis in the normal adult heart, wherein, it's binding to Wnt-chromatin loci was lost upon disease[17]. Furthermore, we sought to decipher and compare neonatal and disease-specific cardiac TCF7L2/Wnt chromatin landscapes and the role of GATA4 within the Wnt nuclear complex in the neonatal hearts.

We report that TCF7L2 displays a robust expression in the CMs of the neonatal hearts, specifically at postnatal day 6 (P6). Surprisingly, despite an elevated Wnt transcriptional activity and TCF7L2 expression at P6, we observed a clear interaction between GATA4 and B-catenin. Notably, genomic occupancy profiles identified strikingly unique TCF7L2 cardiac occupancies: being proximal in neonatal and distal in diseased hearts. Further, we observed that TCF7L2 bound to and activated the transcription of metabolic genes in the neonatal; and cardiac developmental and angiogenesis processes in the diseased hearts. From neonatal life to adulthood, TCF7L2 loses GATA4 co-occupancy. However, their association on the chromatin also seems stage-specific, since TCF7L2-GATA4 co-occupied loci are enriched for H3K27ac in the neonatal hearts. This suggests an active transcriptional state of these regions at this age, contrary to its repressive role that we had identified in the normal adult heart, indicating a putative recruitment of co-factors providing the correct context for this interaction, at each stage. Overall, we characterized stage-specific chromatin roles of TCF7L2 in the heart, thereby underscoring its transcriptional significance at each stage in the mammalian myocardium.

## Materials and Methods

### Murine cardiac tissue

All animals used for this study belong to the C57BL/6 strain. All animal experiments were approved by the Niedersachsen (AZ-G 15-1840) animal review board.

### DNA, RNA isolation and quantitative real-time PCR

Ventricular tissue was macro-dissected and used for DNA and RNA isolation. DNA and RNA were isolated using NucleoSpin Tissue genomic DNA and RNA kit (Macherey-Nagel), respectively, as described elsewhere. Tissue samples were immediately snap frozen and stored at -80°C till RNA or DNA preparation. Nucleic acid quantification was assessed using Nanodrop photometer (Thermo Scientific). 300-500ng RNA was used for cDNA synthesis using 0.5 µg Oligo(dT)20 primer and 100 U M-MLV reverse transcriptase (Promega) for 1h 42°C. Quantitative real-time PCR (qPCR) analyses were performed with SYBR Green (Promega) on a 7900-HT Real-time cycler (Applied Biosystems) using the primers listed in Supporting table S1. Gene expression was normalized to the indicated housekeeper in every experiment. Copy numbers were calculated using the SDS2.4 software with a relative standard curve obtained using the log dilutions of cDNA of gene of interest. All reactions were run in triplicates and normalized to reference control genes. All primers are enlisted in Supplemental Table S1.

### Immunoblotting

Proteins were extracted from tissues by addition of lysis buffer containing 150 mM sodium chloride**,** 1.0% NP-40 or Triton X-100, 0.5% sodium deoxycholate**,** 0.1% SDS (sodium dodecyl sulfate)**,** 50 mM Tris, and pH 8.0, along with protease and phosphatase inhibitors; homogenizing and centrifuging at 4000 rpm for 20 min at 4 º C. The supernatants were protein lysates. This was followed by quantification with Bradford assay. Bio-Rad system was used to run the blots, at constant 120 V, followed by semi-dry transfer at constant 140 mA. 5% non-fat dried milk in TBST was used to block the membranes. The following primary antibodies were used: anti-TCF7L2 (17-10109, Millipore, 1:1000), anti-GAPDH (60004-1-Ig**,** Proteintech, 1:50000), anti-Tubulin (ab4074, Abcam, 1:1000), anti-B-catenin (610153, BD Transduction Labs, 1:1000) and anti-TEAD2 (MBS846045, MyBioSource, 1:1000).

**Histology and immunohistochemistry**

Hearts were dissected, rinsed in PBS, fixed in 4% PFA O/N at 4°C, embedded in paraffin and sectioned at 3 μm thickness in Leica RM2255 microtome. Sections were de-paraffinized, rehydrated and antigen was unmasked by microwaving sections at 600 W for 10min in 10 mM sodium citrate buffer at pH 6.0. For immunofluorescence (IF), sections were blocked at RT for 1h with 5%BSA in PBS + 0.1% Triton. For IF, primary antibodies were incubated O/N at 4°C as follows: anti-Cardiac Troponin T (ab8295, Abcam, 1:200), anti-TEAD2 (MBS846045, MyBioSource, 1:50), anti-Ki67 (ab15580, Abcam, 1:50) and anti-TCF7L2 (ab76151, Abcam, 1:50) in 1% BSA in PBS+0.1% Triton. Next, sections were washed in PBS and incubated with secondary anti-rabbit IgG-Alexa 594 or anti-mouse IgG-Alexa 488(1:200; Molecular Probes) antibodies. Microscopic images were captured with a digital microscope (IX70, Olympus). All sections were stained with Hoechst 55532 (Sigma-Aldrich) to visualize nuclei.

**RNA-sequencing (RNA-seq) and data analyses**

P6 hearts RNA-seq was performed at Transcriptome Analysis Laboratory (TAL), Goettingen, in biological triplicates. This data was combined and re-analyzed along with our published data for adult and diseased hearts. RNA was extracted, quality and integrity was assessed by Bioanalyzer (Agilent). Libraries were prepared and cDNA libraries were amplified and the size range of final cDNA libraries was determined by applying the DNA 1000 chip on the Bioanalyzer 2100 from Agilent (280 bp). cDNA libraries were sequenced using cBot and HiSeq 4000 Illumina (SR; 1 × 50 bp; 51 cycles with single indexing; 6GB ca. 30–35 million reads per sample). Sequence reads were aligned to the mouse reference assembly (UCSC version mm9) using Bowtie 2.0. For each gene, the number of mapped reads was counted and DESeq2 was used to analyze the differential expression. Gene ontology (GO) analyses were performed using default parameters and stringency in 'ClueGO': a Cytoscape plug-in. The significant 'GO Biological Processes' were shown with $P \leq 0.05$.

**Chromatin immunoprecipitation (ChIP-seq)**

ChIP was optimized for P6 (regenerative), adult and Wnt-activated (disease) cardiac ventricular tissue. Approximately, 10 P10 hearts were pooled to obtain n=1 per ChIP experiment (i.e for 4 IPs described below), whereas for all adult hearts, 1 heart was used for n=1 per ChIP experiment. TCF7L2, GATA4 and H3K27ac ChIPs in these tissues were performed by 20 minutes crosslinking with 1.3% formaldehyde (in PBS, with protease inhibitors) and first sonication for

30 cycles (30sec ON/30sec OFF pulses) in Diagenode Bioruptor Next-Gen with the buffer (Sonication buffer) containing 150 mM NaCl, 20 mM EDTA (pH 8.0), 0.5 % sodium deoxycholate, 50 mM Tris-HCl (pH 8.0), 1% (v/v) NP-40, 20 mM NaF, 0.1% SDS and protease inhibitors. The lysates were centrifuged at 12000 x g at 4°C for 2 min and supernatants were collected and stored. To the pellets, sonication buffer was added again and sonication was repeated for 25 cycles with the same pulse-frequency. These supernatants from the second centrifugation per sample were pooled, combined with the first set and pre-cleared with protein-A coated sepharose beads for 45 min to reduce unspecific binding. 700µl of this pre-cleared chromatin was used per IP and corresponding 10% i.e 70µl was used as total input chromatin. For IP, 2 µg of anti-TCF7L2, anti-IgG (17-10109, Millipore), anti-GATA4 (sc-25310 X, SantaCruz) or anti-H3K27ac (C15410196, Diagenode); and 500ul of IP buffer ((150 mM NaCl, 20 mM EDTA (pH 8.0), 50 mM Tris-HCl (pH 7.5), 1% NP-40, 20 mM NaF, 0.5% sodium deoxycholate and 0.1% SDS, with protease inhibitors)) was added to the chromatin extracts and incubated O/N at 4°C on a rotor. Antibodies were pulled down using 80µl protein-A-sepharose beads followed by extensive washing. 2 washes with IP buffer, 2 washes with wash buffer ((0.5 M LiCl, 20 mM EDTA (pH 8.0), 100 mM Tris-HCl (pH 8.5), 1% NP-40, 20 mM NaF and 1% sodium deoxycholate)), 2 washes with IP buffer again and last 2 washes with TE buffer ((10 mM Tris-HCl (pH 8) and 1 mM EDTA (pH 8.0)) . For each wash, 800µl of the buffer was added and tubes with inverted thrice and centrifuged at 6000 x g at 4°C for 2 min.

DNA-protein complexes were extracted by adding 200µl elution buffer (7.88 g/l Tris-HCl, 1.46 g/l EDTA, 2.92 g/l NaCl, 10 g/l SDS, pH 7.5) at 65°C for 1.5h with constant and vigorous shaking at 1200 rpm. Elution buffer was added also to the input chromatin. Once these complexes were isolated, 12µl of 5M NaCl and 4µl of 20mg/ml Proteinase K were added and incubated O/N at 62°C with constant shaking at 800 rpm. The next morning, DNA was isolated using the Buffer NTB (suitable for high SDS-containing samples) and NucleoSpin Gel and PCR Clean-up kit (Macherey-Nagel) with 30µl of the kit elution buffer.

DNA concentration was measured using a Qubit dsDNA HS assay on a Qubit® 2.0. Library preparation and sequencing were performed at the TAL, Goettingen. For library preparation, TruSeq ChIP Library Preparation Kit - Set A (12 indexes, 48 rxns) Cat N° IP-202-1012 (according to manufacturer's recommendations) was used. The size range of DNA libraries was performed on an Agilent Bioanalyzer 2100 (High Sensitivity DNA Assay). DNA libraries were

amplified and sequenced by using the cBot and HiSeq 4000 from Illumina (25-30 million reads per sample).

**ChIP-seq data analyses**

Sequence reads were aligned to the mouse reference assembly (UCSC version mm9) using Bowtie2. Peak calling was performed with Model Based Analysis of ChIPseq (MACS2) version 2.1.0.20140616.0, which is the updated version of MACS. Genes proximal to the bound chromatin regions were identified by GREAT analyses using 'Basal plus extension' method where each genomic region is overlapped with genes which are 5kb upstream and 1 kb downstream (proximal), plus up to 1000 kb (distal). To identify differentially bound regions, 'DiffBind' tool in Galaxy was used, with default settings. This identifies all regions that are not only differentially occupied, but also for regions with same occupancy but different binding intensities. *De-novo*, sequence based motif search was performed using MEME-ChIP. Gene ontology/pathway analyses for gene lists were performed using default parameters and stringency in 'ClueGO': a Cytoscape plug-in and the significant 'Gene Ontology Biological Processes' were shown with $p \leq 0.05$. BioVenn web application was used to compare, create and analyse Venn diagrams showing commonly or differently bound genes between two or more datasets. Published/public ChIP-seq datasets

**ChIP-qPCR validation**

For ChIP validation, ChIP-qPCRs were performed for the regions bound by the respective TFs by designing primers (70-100 bp product size range, mm9 reference genome) flanking the region. Percentage input and fold enrichment were calculated for each IP relative to IgG control. Always, n=3 samples were used for all validations.

**Chromatin-enriched proteins isolation**

In order to identify protein complexes bound to the chromatin, the same protocol as above was followed until the protein-A sepharose beads washing step. After the last wash, protein complexes were extracted from protein-A-sepharose beads by directly adding standard protein lysis buffer to the beads, incubating at 95°C for 10 min with constant shaking. Samples were centrifuged and supernatants were used for immunoblotting and/or were analyzed with mass spectrometry.

**Statistical analyses**

ANOVA single factor analysis was used to calculate the *P* value for qPCR-based analyses. G-Power3.1 was used to determine the sample size for animal studies. For ChIP-seq and RNA-seq analyses, *q*-value (to call peaks) and adjusted *P*-value of ≤0.05 was considered for statistical significance respectively. For motif analyses, *Z*-score and Fisher score (negative natural logarithm of *P*-value) were utilized for showing significant motifs. Unpaired student's test and two way ANOVA with Bonferroni post-test (GraphPad Prism 6.0) were used where appropriate for statistical analysis of epifluorescence measurements of calcium cycling parameters. Again, *P*-values<0.05 were considered statistically significant.

**Results**

**TCF7L2 is robustly expressed within the regenerative window of the neonatal murine heart**

The murine postnatal heart has shown to have a regenerative potential until 7 days post-birth[14]. In order to study Wnt chromatin dynamics, we first tested the expression of TCF7L2 the main nuclear Wnt mediator, by immunoblotting and its corresponding target gene *Axin2* by quantitative real-time PCR (qPCR) in different embryonic and postnatal stages of cardiac ventricular tissue. Immunoblots revealed a low TCF7L2 protein expression at the embryonic stage (E14.5) and a gradual postnatal increase peaking at P6; reducing in the adult heart and getting activated upon disease induced by transgenic Wnt-stabilization in the adult CMs (model described earlier), n=2. qPCR validations revealed a consistent expression of *Axin2* in the fetal and early neonatal heart stages, peaking between P6-10, and then drastically decreasing in adulthood, n=3, (Fig. 1B). *Tcf7l2* mRNA quantifications are usually inconclusive due to the presence of several spliced transcript isoforms in different tissues and contexts[21,22]. Moreover, *Tcf7l2* mRNA was not upregulated in the Wnt-activated adult hearts, whereas the protein expression was highly enriched[17]. Therefore, we used TCF7L2 protein expression as readout for Wnt transcriptional activity (also in Chapter 1). Consistently, immunofluorescence experiments revealed increased TCF7L2 expression (red) in cardiac Troponin T (TNNT2)-positive (green) CMs in P3 and P6 ventricular myocardium (white arrows indicate expression), as opposed to low expression at P0, confirming immunoblot results (Fig. 1C). Given that Wnt signaling and TCF7L2 are strongly implicated in cell proliferation during organ development[23,24], we wondered whether this peculiar CM-expression of TCF7L2 at P6 could be attributed to possible ongoing cell-cycling activity in the CMs and hence, performed KI67 immunostainings. We

observed indeed, KI67-positive CMs in both P3 and P6 ventricular myocardium, clearly demonstrating ongoing CM-cell-cycling at this age, n=3 (Fig. 1D). These results demonstrate a high Wnt pathway transcriptional activity in both regenerative (P6) and the diseased myocardium.

**GATA4 interacts with B-catenin driving homeostatic responses in the neonatal heart**

Considering that we observed a robust interaction between GATA4 and B-catenin in the healthy adult heart (with low Wnt activity) and its loss upon disease (with high Wnt activity)[17], we questioned whether this interaction was maintained or lost in the neonatal hearts with the highest TCF7L2 protein expression at P6. Interestingly, despite a high Wnt activity at P6, we still observed a clear interaction between GATA4 and B-catenin (red arrow), suggesting that this interaction was predominantly homeostatic and ensures proper transcriptional landscapes in maintaining normal cardiac function at these states (Fig. 1C).

**Figure 1.**

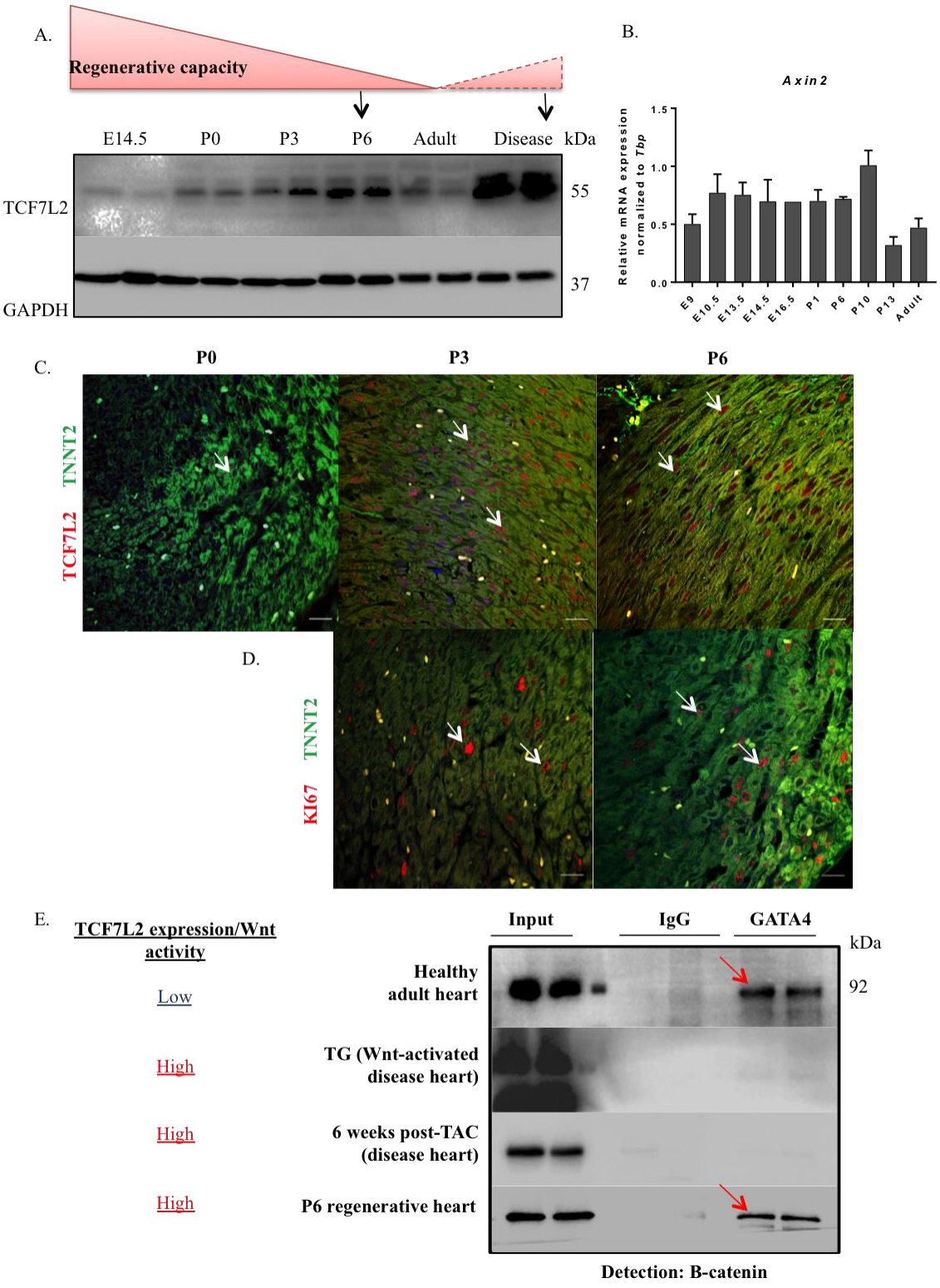


**Fig. 1: TCF7L2 expression and GATA4-B-catenin interaction dynamics in different cardiac stages.** A. Scheme illustrating lowering regenerative capacity as the murine heart grows and matures; and the corresponding protein expressions of TCF7L2 and housekeeping control protein GAPDH, at embryonic day 14.5 (E.14.5) and different

neonatal/postnatal ages. Black arrows indicate increased TCF7L2 protein expression at P6 and diseased cardiac stages, n=2. B. *Axin2* transcript quantification across murine developmental and postnatal stages, n=3. C, D. Corresponding immunofluorescence stainings show increased TCF7L2 and KI67 expression in cardiac Troponin T (cTnT)-positive CMs at P3 and P6, compared to P0. White arrows indicate nuclear TCF7L2 and KI67 expression, n=3. E. Immunoblots depicting nuclear fraction-enriched immunoprecipitation (IP). Input refers to the total protein; IgG was used as negative control; IP was performed for GATA4 and detection for B-catenin. IPs were performed in healthy adult heart (low Wnt), Wnt-activated transgenic and 6 weeks-post trans-aortic constriction (TAC) diseased hearts (high Wnt) and for postnatal day 6 regenerative hearts (high Wnt). Red arrows indicate a positive interaction between GATA4-B-catenin in healthy adult and P6 regenerative hearts, n=2. Scale bars in A: 20µm.

## Neonatal regenerative hearts possess distinct transcriptomic signatures in comparison to the diseased hearts

Postnatal day 6 represents a unique stage in murine cardiac development and maturation wherein, both proliferative as well as homeostatic processes function synergistically in order to populate and increase cardiac mass and at the same time generate mature cardiomyocytes. At P7, the CM cell-cycle is arrested and the ability to regenerate post an injury is lost[14]. Several studies have pointed out that during pathological remodeling upon stress, the adult heart tries to recapitulate a regenerative response and hence activates a plethora of developmental processes[17,20,25]. Hence, intrigued by the cardiac status based on the high CM-TCF7L2 expression *and* the GATA4-B-catenin interaction observed at P6, we performed RNA-seq in these cardiac ventricular tissues (n=3) and compared their transcriptomic signatures to our previously published normal and Wnt-activated diseased adult hearts. Despite similar Wnt activities and processes enriched in the regenerative and diseased myocardium, we observed distinct clustering of P6 hearts versus both normal and diseased adult hearts. This indicates that P6 hearts indeed possess a unique transcriptional status- indicated by PCA plot (biological replicates are encircled with dashed circles) as well as correlation plots (the lower the distance between the samples, the darker is the color and higher the correlation) (Fig. 2A).

## Common and unique processes regulated in neonatal and diseased hearts

To determine common and unique differentially expressed genes (DEGs) between the different groups i.e P6, adult and Wnt-activated (diseased) hearts, we compared all the DEGs (significantly up- $\log_2FC>0.5$ or down- $\log_2FC<-0.5$, $p<0.05$) in these 3 groups. P6-regulated (P6-Up/Down) and Disease-regulated (Dis-Up/Down) DEGs were obtained by comparing to the normal adult heart transcriptome. Further, P6-Up was intersected with Dis-Up to identify commonly upregulated genes between the two stages, compared to the normal adult heart. Firstly, we identified 4651 P6-Up genes, 443 Dis-Up genes and 678 commonly P6-Dis-

upregulated genes. Fig. 2B depicts a heatmap showing all the 443 upregulated DEGs in diseased hearts (compared to normal adult heart) across all 3 groups. A sub-group, which is commonly upregulated in both P6 and disease compared to normal hearts, can be visualized.

To further understand the biological relevance of these unique transcriptional signatures at P6, we performed gene ontology analyses and observed that Dis-Up genes regulated immune processes, hypertrophic cell growth, vasculature development and cardiac fetal gene reactivation. It is intriguing to find cardiac fetal program enriched in Dis-Up, since one would expect that it annotated more in the neonatal hearts, where the CMs can still proliferate. On the other hand, P6-Up genes annotated mainly for cellular metabolic processes. Interestingly, the Wnt pathway, along with cell cycle activation, cytoskeletal reorganization and chromatin modulations were enriched in the commonly upregulated group of genes. These results are in line with previous studies including ours (in Chapter 1) showing that cell cycle and chromatin events are commonly reactivated during both heart development and disease, where Wnt signaling is highly active. These transcriptomic results hint towards a specifically active metabolic state at P6, wherein the heart can still regenerate, while proceeding towards maturation at the same time. Whereas, in the diseased heart, considering hypoxia as a contributing factor[26], angiogenesis and hypertrophic gene programs are triggered[27,28]. This state initiates maladaptive responses, including an activation of fetal programs leading to the production of immature CMs, incapable of functionally compensating for the lost CM pool.

**Figure 2.**

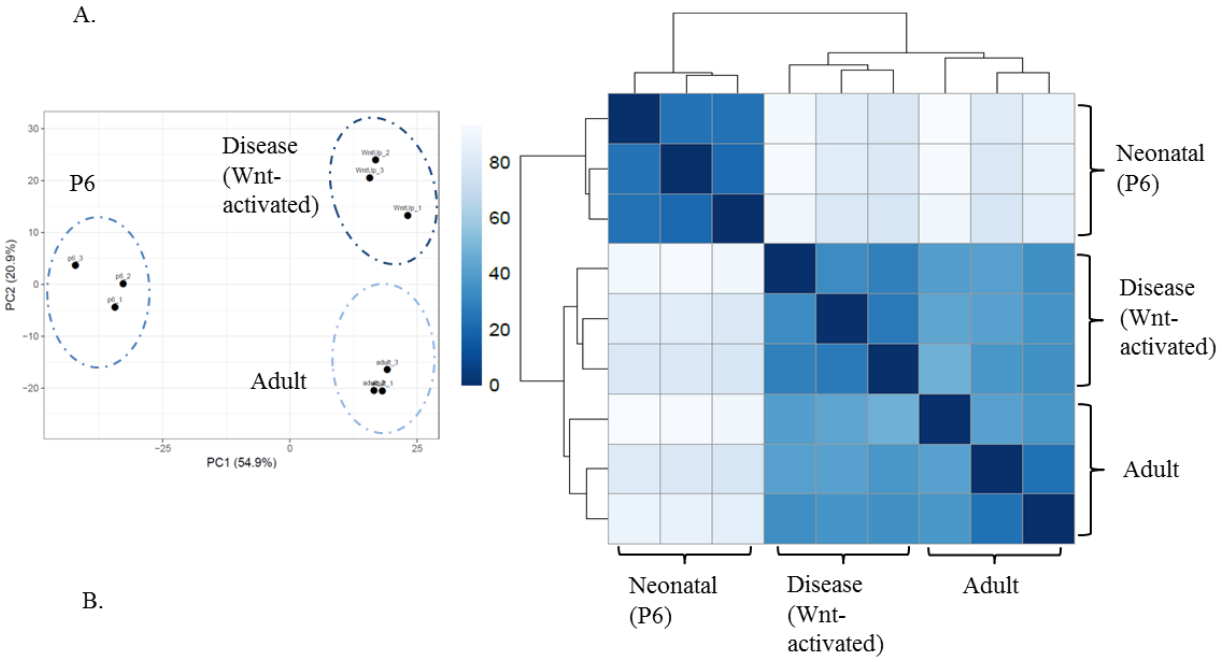


B.

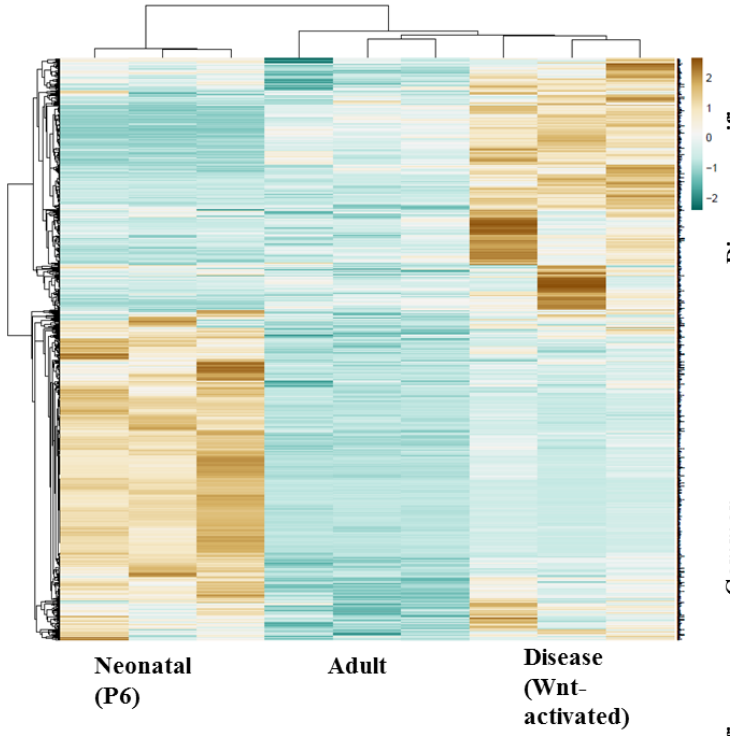


| GO Term | -log$_{10}$(P-value) | |
|---|---|---|
| immune system process | 3.585027 | Disease-specific |
| cell growth | 2.69897 | |
| **vasculature development** | **2.481486** | |
| **muscle cell development** | **1.769551** | |
| mesenchyme development | 1.481486 | |
| **cell cycle** | **71.82391** | Common |
| microtubule cytoskeleton organization | 21.20066 | |
| chromatin organization | 2.031517 | |
| **Wnt signaling pathway** | **1.79588** | |
| **cellular metabolic process** | **29.49485** | Neonatal-specific |
| neurological system process | 29.46852 | |
| epithelium development | 19.27572 | |
| cell communication | 16.31876 | |

**Fig. 2: Transcriptomic profiles of regenerative, normal adult and diseased adult hearts.** A. PCA and correlation plots illustrating distinct grouping of P6 in comparison to normal and diseased adult hearts, n=3. B. Heatmap showing row Z scores of normalized counts from DEGs upregulated in disease compared to normal hearts,

for all three groups. A commonly upregulated sub-group can be observed. Corresponding gene ontology biological processes and their $-\log_{10}$(P-values) are shown in the table.

**TCF7L2 occupies proximal regions in neonatal and distal enhancers in diseased hearts**

Having studied the global transcriptomic profiles of regenerative, homeostatic and diseased hearts, we next aimed to investigate the Wnt-associated chromatin machineries in these states. Owing to high TCF7L2 expression in both P6 (neonatal) and disease (Wnt-activated transgenic and TAC models), we next asked whether the TCF7L2 genomic occupancies were similar too. Further, previous results including Fig. 1C underscored the significance of GATA4 in maintaining the Wnt- chromatin, in a stage-specific manner in the heart. Hence, we performed chromatin immunoprecipitation and sequencing (ChIP-seq) for TCF7L2, GATA4 and H3K27ac (a histone mark to distinguish active enhancers from poised ones) in P6 cardiac ventricular tissue, n=2 per ChIP. We identified 1191 TCF7L2-occupied regions (1280 genes) in P6 hearts, similar to the number we had observed in the Wnt-activated diseased hearts (1209 regions, 976 genes).

Despite its similar expression and number of bound regions in P6 and diseased hearts, we observed a striking difference in TCF7L2 genomic occupancies in the regenerative and diseased myocardium. While our previous findings identified clear, distal enhancer TCF7L2 occupancy in the diseased heart, to our surprise, we observed its remarkable proximal promoter-based occupancy in P6 hearts (Fig. 3A, B). This suggests recruitment of specific proximal and distal transcriptional machineries by TCF7L2 to elicit a stage-specific cardiac gene regulatory response. Interestingly, TCF7L2 is known to occupy both proximal and distal loci, depending on the context in different cancer cell lines and tissues, via recruitment of specific factors[29–31]. However, this was never investigated in the heart in a stage-specific manner before. Further, in regenerative hearts, TCF7L2-bound genes annotated to important and relevant biological processes like heart development, metabolism, vasculature development, Wnt signaling pathway and cell cycle (Fig. 3E), again stressing its importance in stage-specific cardiac function.

**GATA4 controls cardiac contraction and CM structural genes in the neonatal heart**

GATA4 is undisputedly one of the most important TFs required for cardiac development and maintenance[32,33]. It is also shown to play major roles driving hypertrophic responses in pathological remodeling, by associating to specific TFs. Although embryonic and adult GATA4 genome occupancies were reported before[34], its role in the neonatal, regenerative hearts was not studied. Moreover, since GATA4 interacted with B-catenin in the healthy adult and P6 hearts,

we sought to characterize its chromatin occupancy. Our results indicate that GATA4 consistently occupied distal genomic regions from neonatal life to adulthood. However, it occupied a much larger proportion of genomic regions in the P6 neonatal (17786 regions, 9050 genes), in comparison to its previously published occupancy in the adult diseased heart (1618 regions, 2243 genes) (Fig. 3C, D).

In line with its crucial roles in cardiac specification and homeostasis in adulthood, GATA4 occupied regions important for cardiac muscle structure development, contraction and metabolism- all indispensable for cardiac function (Fig. 3F).

**Figure 3.**

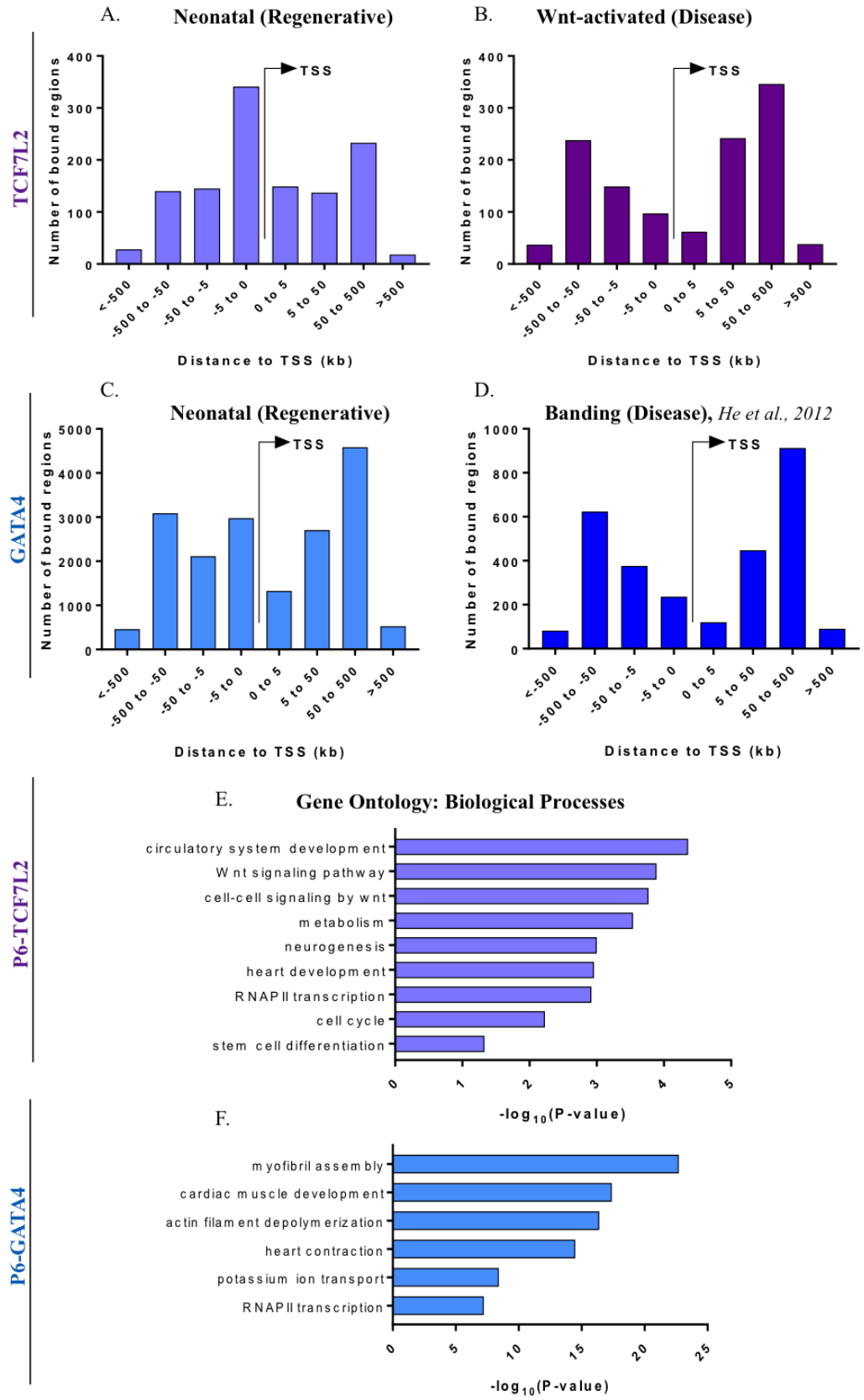
TCF7L2
A.
Neonatal (Regenerative)
B.
Wnt-activated (Disease)
Number of bound regions
TSS
<-500
-500 to -50
-50 to -5
-5 to 0
0 to 5
5 to 50
50 to 500
>500
Distance to TSS (kb)
GATA4
C.
Neonatal (Regenerative)
D.
Banding (Disease), He et al., 2012
P6-TCF7L2
E.
Gene Ontology: Biological Processes
circulatory system development
Wnt signaling pathway
cell-cell signaling by wnt
metabolism
neurogenesis
heart development
RNAPII transcription
cell cycle
stem cell differentiation
-log10(P-value)
P6-GATA4
F.
myofibril assembly
cardiac muscle development
actin filament depolymerization
heart contraction
potassium ion transport
RNAPII transcription

**Fig. 3: TCF7L2 and GATA4 genome occupancies in neonatal hearts.** A, B. Overview of TCF7L2 occupancies in P6 and Wnt-activated diseased hearts; indicating proximal in P6 and distal occupancies in disease, respectively. C, D. Overview of GATA4 occupancies in P6 and published data in diseased hearts; indicating consistent distal occupancies from neonatal life to adulthood. E, F. Gene ontology biological processes of the regions bound by TCF7L2 (pink) and GATA4 (blue) in neonatal P6 hearts. All processes depicted here are within the top 10 and are significant ($P<0.05$).

### TCF7L2 bound regions are enriched for H3K27ac in both neonatal and diseased hearts

Since, we know that Wnt signaling is transcriptionally active during both cardiac regenerative responses and disease; we aimed to investigate the chromatin landscapes for H3K27ac occupancies, specifically at TCF7L2-occupied regions in these two states (P6 and disease). Expectedly, we observed a marked biphasic enrichment of H3K27ac on TCF7L2-bound regions in both P6 and diseased hearts (Fig. 4A), in line with high Wnt transcription. It is interesting to observe that despite TCF7L2 occupies the chromatin differentially in regenerative and diseased myocardia, there is always a recruitment of H3K27ac- further augmenting the activating role of TCF7L2 in Wnt-mediated transcription. H3K27ac enrichments were further validated by ChIP-qPCRs for proximal P6 loci *(Aldh3a2, Mars, Ormdl3, Rnf5* and *Sptlc2)* as well as for distal disease loci *(Ang, Angpt1, Hand2, Tbx3* and *Vav1)*. All values depicted are fold enrichments relative to negative IgG control set at 1, normalized to 10% input (Fig. 4B). TCF7L2 and H3K27ac occupancy profiles are illustrated for some relevant genes in Fig. 4C and D.

**Figure 4.**

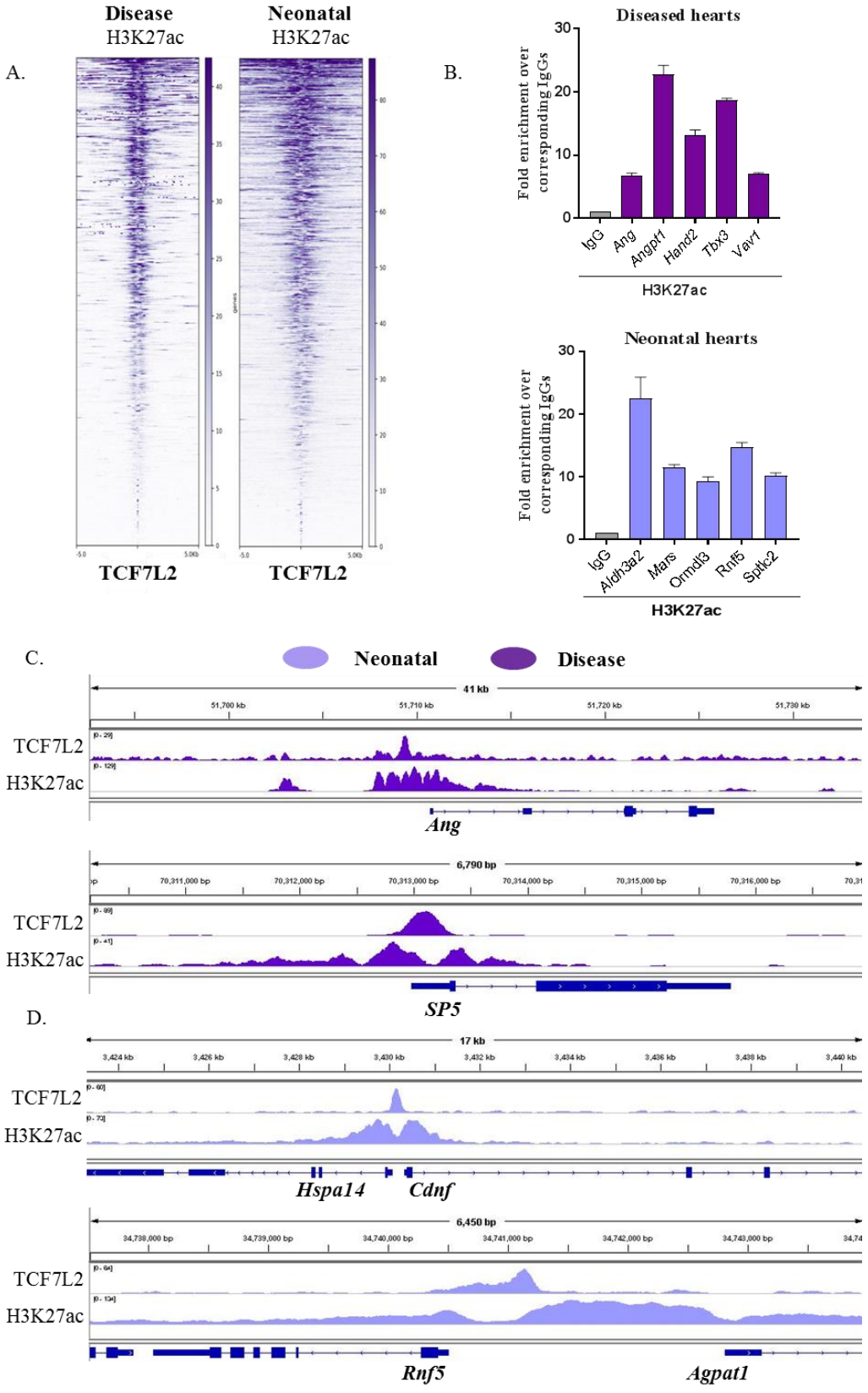
A.
Disease
H3K27ac
Neonatal
H3K27ac
TCF7L2
TCF7L2
B.
Diseased hearts
Fold enrichment over corresponding IgGs
IgG
Ang
Angptl
Hand2
Tbx3
Vavl
H3K27ac
Neonatal hearts
Fold enrichment over corresponding IgGs
IgG
Aldh3a2
Mars
Ormdl3
Rnf5
Sptlc2
H3K27ac
C.
Neonatal
Disease
TCF7L2
H3K27ac
Ang
TCF7L2
H3K27ac
SP5
D.
TCF7L2
H3K27ac
Hspa14
Cdnf
TCF7L2
H3K27ac
Rnf5
Agpat1

**Fig. 4: TCF7L2-bound genomic loci are enriched in H3K27ac in both neonatal and diseased hearts.** A. Heatmaps depicting bamcoverage RPKM-normalized bigwigs on TCF7L2-occupied regions in the regenerative and diseased myocardium. Regions ± 5kb are shown. B. ChIP-qPCRs for P6 and diseased heart H3K27ac-enriched genes validating the enrichment, n=3. C. IGV occupancy profiles depicting TCF7L2-occpied regions enriched for H3K27ac in P6 and diseased hearts.

## TCF7L2 regulates metabolism specifically in the neonatal hearts and cardiac developmental reprogramming in the diseased hearts

Encouraged by the markedly unique occupancy patterns, we performed TCF7L2 differential binding analyses in P6 and diseased hearts. We identified 83 regions (106 genes) enriched in P6 hearts (P6-En) and 170 regions (231 genes) enriched (Dis-En) in the Wnt-activated diseased hearts (Fig. 5A). Notably, similar to the overall occupancy profiles in Fig 3. A and B, P6-En regions were proximal and Dis-En were distal (Fig. 5B). While P6-En annotated to metabolism and RNAPII transcription (e.g *Acyp1, Aldh3a2, Rnf5, Sptlc2, Mars*), Dis-En annotated to vasculogenesis and cardiac developmental remodeling (e.g *Angpt1, Vav1, Tbx20, Hand2, Fzd3*) (Fig. 5C). Fig. 5D, E and Fig. S1 A demonstrate ChIP-qPCR validation and occupancy profiles of TCF7L2-bound P6-En (*Aldh3a2, Mars*) and Dis-En (*Angpt1, Ang*) regions.

**Figure 5.**

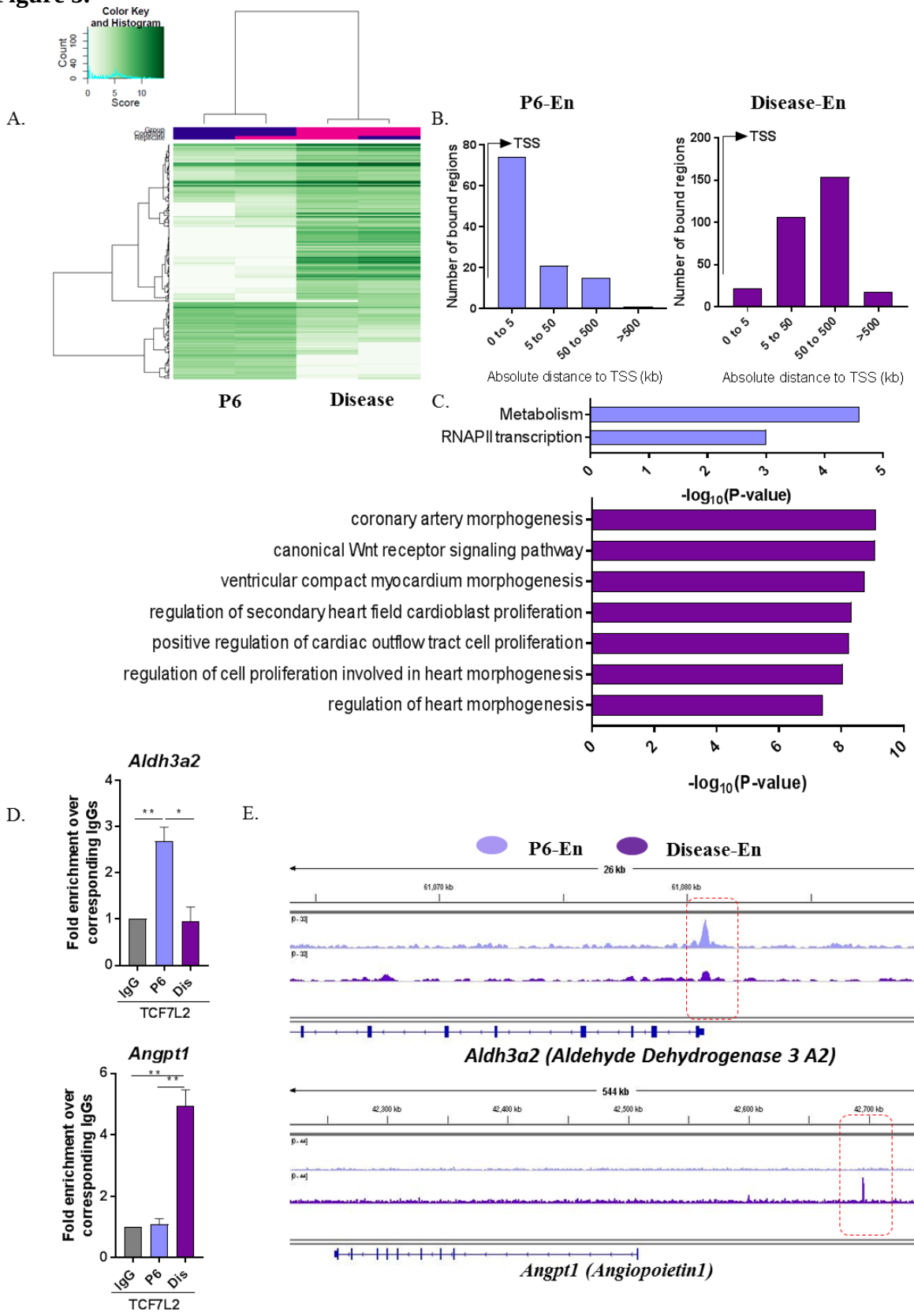
A.
Color Key and Histogram
Count
Score
P6
Disease
B.
P6-En
Disease-En
Number of bound regions
TSS
0 to 5
5 to 50
50 to 500
>500
Absolute distance to TSS (kb)
C.
Metabolism
RNAPII transcription
-log10(P-value)
coronary artery morphogenesis
canonical Wnt receptor signaling pathway
ventricular compact myocardium morphogenesis
regulation of secondary heart field cardioblast proliferation
positive regulation of cardiac outflow tract cell proliferation
regulation of cell proliferation involved in heart morphogenesis
regulation of heart morphogenesis
D.
Aldh3a2
Fold enrichment over corresponding IgGs
IgG
P6
Dis
TCF7L2
Angpt1
E.
P6-En
Disease-En
Aldh3a2 (Aldehyde Dehydrogenase 3 A2)
Angpt1 (Angiopoietin1)

**Fig. 5: Differential TCF7L2-bound regions in neonatal and diseased hearts.** A. Differential binding plot depicting TCF7L2-bound regions in P6 and diseased hearts. B. Overall genomic occupancy profiles of P6-En (proximal) and Dis-En (distal) TCF7L2 regions. C. Gene ontology biological processes of TCF7L2-bound differential genes. D, E. ChIP-qPCR validating and occupancy profiles showing TCF7L2 enrichment at *Aldh3a2* and *Angpt1* loci. The bound regions are highlighted with dashed boxes in red. $P<0.05$, data are mean ± SEM.

Among metabolic genes, TCF7L2 bound mainly to aldehyde, nucleotide and fatty acid metabolic genes like *Aldh3a2* and *Sptlc2*; and importantly, *not* to glucose metabolic genes in the neonatal heart. Moreover, it is known that the heart switches to fatty acid from glucose metabolism with increased maturation[35,36]. In line with this, Wnt signaling is known to play crucial roles in regulating metabolic processes in different contexts[37]. In order to further understand the age-specific neonatal cardiac metabolic transcriptomes, qPCRs were performed for a few exemplary genes like *Aldh3a2*, *Sptlc2 (*both bound by TCF7L2*)* and *Ldhb (not* bound by TCF7L2*),* each representing aldehyde, glucose and fatty acid metabolic processes respectively. While an increasing trend was observed for *Aldh3a2* and *Sptlc2* expressions during progression to adulthood/maturation; *Ldhb* expression expectedly displayed a decreasing trend (Fig. S1B). Along with genomic occupancy data, these findings augment the importance of TCF7L2 in the metabolic maturation of the neonatal heart.

**GATA4 loses TCF7L2 co-occupancy but continually provides cardiac specificity to TCF7L2 from neonatal life to adulthood**

We also observed a marked overlap between P6-TCF7L2 and GATA4-bound regions (944/1191: 75% of all TCF7L2 bound regions), all annotating to cardiac developmental processes, similar to what we had observed in the adult hearts. Exactly like in the adult, even in these neonatal P6 hearts, TCF7L2-GATA4 co-occupied regions (encoding genes- *Rasip1, Mamstr, Myh6, Myl2, Smarca4* etc.) annotated for cardiac development and muscle differentiation-related processes (Fig. 6A, B). These regions were predominantly proximal (Fig. S2A).

In contrast, only 25% (321/1206) of P6-TCF7L2 regions overlapped with published adult (healthy) GATA4 cardiac regions, illustrating decreasing co-occupancy from neonatal life to adulthood (Fig. 6A). These regions were mostly distal (Fig. S2B). We compared the intersections between P6-TCF7L2; and P6 and healthy adult cardiac GATA4 regions because we had observed an interaction between GATA4 and B-catenin only in P6 and healthy adult hearts; and not in diseased hearts. Further, we compared the two intersections and identified 647 out of 944 (68%) P6 TCF7L2-P6 GATA4 co-occupied genes that were lost from neonatal life to adulthood; and 24 out of 321 (7%) P6 TCF7L2-adult GATA4 genes that were newly co-occupied. There

were 297 out of 944 (31%) genes that were consistently co-occupied (Fig. 6C). Remarkably, the co-occupied sites that are maintained throughout were enriched mainly for cardiac developmental and heart-related processes (Fig. 6D). This suggests that irrespective of the cardiac status, GATA4 always mediates the cardiac-specific transcriptional actions of TCF7L2.

GATA4 is a crucial cardiac master-TF and this is evident also in the neonatal hearts, since we observed a high enrichment of H3K27ac on GATA4-bound regions (Fig. S2C). Moreover, the TCF7L2- GATA4 co-occupied regions were also highly enriched for H3K27ac in neonatal hearts- suggesting a potential transcriptionally activating function of GATA4 on TCF7L2-bound regions in the neonatal regenerative heart (Fig. 6E). This is an important finding for two reasons: 1. we had observed a clear interaction between GATA4 and B-catenin in both neonatal and healthy adult hearts; 2. we previously demonstrated the repressive role of GATA4 on TCF7L2-bound Wnt loci in the healthy adult hearts. Considering that the GATA4-B-catenin interaction occurs in both the cases, the enrichment of H3K27ac on these TCF7L2-GATA4 intersect regions in the neonatal hearts suggests a putative recruitment of other context-specific co-factors to the Wnt-GATA4 loci, enabling the regenerative status of the cardiac chromatin, at this stage. Fig. 6E displays occupancy profiles of TCF7L2, GATA4 and H3K27ac for *Myl2* and *Nr3c2* loci in neonatal (P6) hearts.

**Figure 6.**

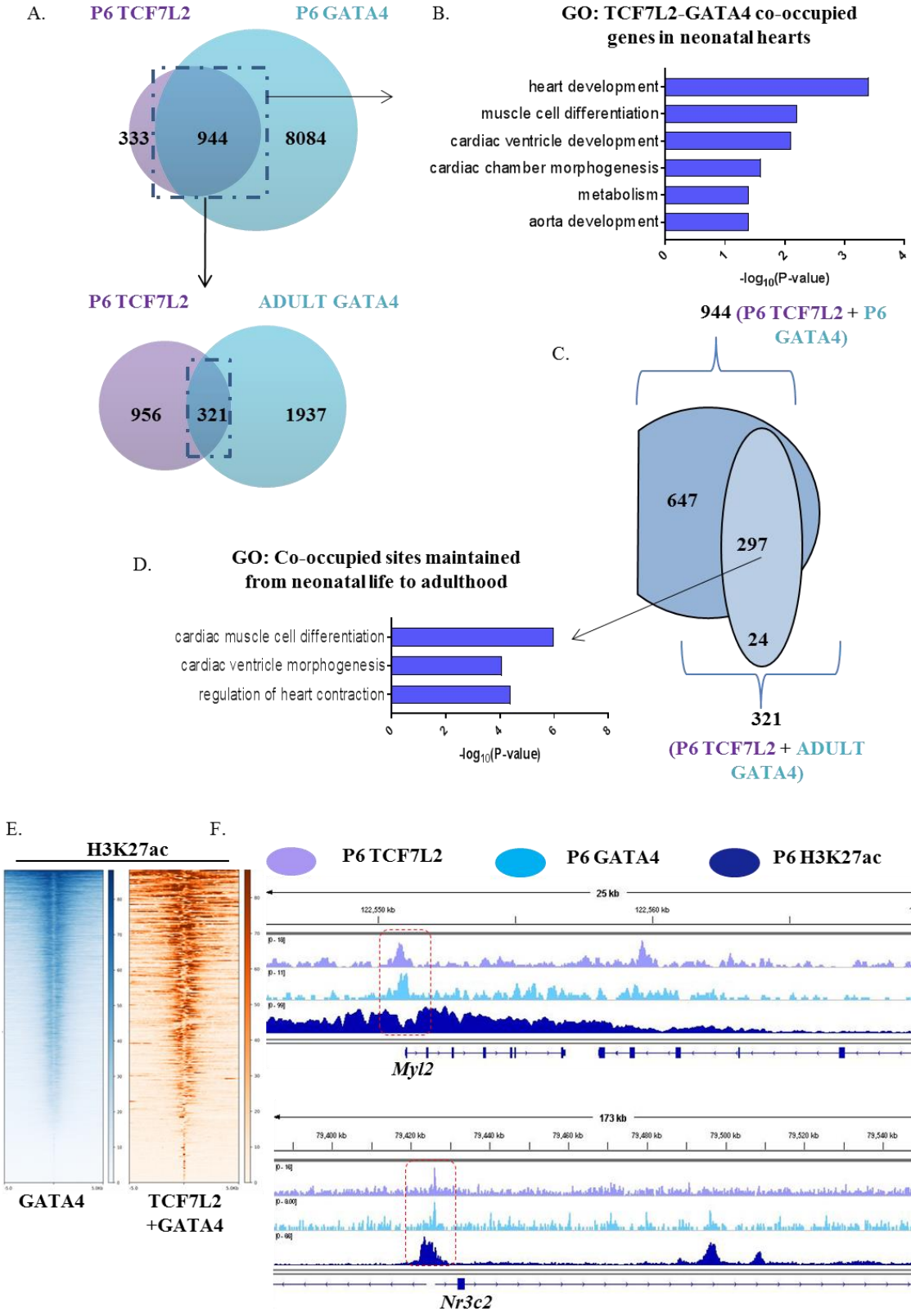


**Fig. 6: GATA4 provides cardiac specificity to TCF7L2 in the neonatal, regenerative heart.** A. Venn diagrams showing decreasing TCF7L2-GATA4 co-occupancies from neonatal life (~75%) to adulthood (~25%). B. Gene

ontologies depicting biological processes regulated by genes co-occupied by TCF7L2 and GATA4 in the neonatal heart. C. Intersects illustrating all TCF7L2-GATA4 co-occupied genes, with arrow indicating gene ontologies for genes that remain co-occupied from neonatal life to adulthood (D). E. Heatmaps showing RPKM-normalized H3K27ac bigwigs enrichment on GATA4 (blue) and TCFL2-GATA4 co-occupied (brown) regions in the neonatal heart. Regions ± 5kb are shown. F. Occupancy profiles of TCF7L2, GATA4 and H3K27ac on cardiac genes *Myl2* and *Nr3c2* promoters in neonatal (P6) hearts.

**TEAD2 is a novel, putative, neonatal-specific cardiac co-factor of the Wnt-GATA4 complex**

GATA4-TCF7L2 co-occupied regions were enriched for H3K27ac (transcriptionally active regions) in the neonatal heart, whereas GATA4 played a repressive role on the Wnt loci in the healthy adult heart. Importantly, a clear interaction was observed between GATA4 and B-catenin in both these cases, despite a potentially different relevance. Hence, we wondered whether other context-specific co-factors were recruited in order to execute appropriate transcriptional responses. To that end, upon performing *de-novo*, sequence-based motif search, we identified a significant enrichment of TEAD2 motif in both TCF7L2 as well as GATA4-bound regions in the neonatal heart (Fig. 7A). TEAD2 is a potentially interesting candidate in the neonatal cardiac context for a variety of reasons: a. It is mainly expressed only during developmental stages and not in adult tissues[38,39]. b. It is an important effector of the Hippo pathway, which is known to play crucial roles in heart regeneration[40,41]. Moreover, TEAD2 was never investigated previously in the heart. Owing to these reasons, we performed immunoprecipitation experiments and unraveled indeed, an interaction between TEAD2 and B-catenin in neonatal, but not in the diseased hearts, augmenting the putative significance of TEAD2 within the GATA4-Wnt complex in driving neonatal, regenerative responses. Anti-IgG and anti-WNT5b IPs were used as negative controls, n=2 (Fig. 7B).

**Figure 7.**

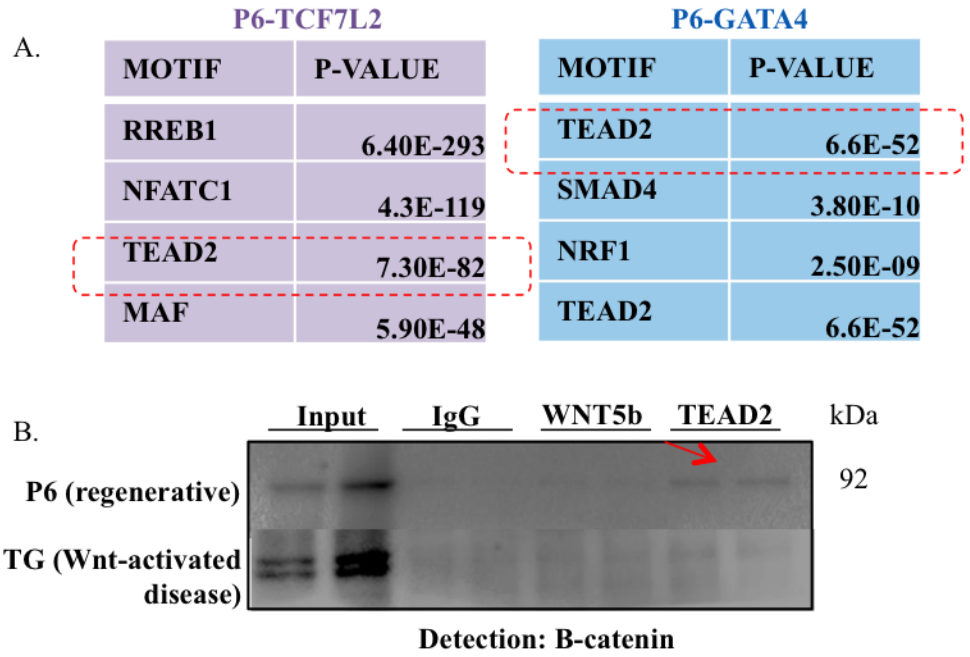


**Fig. 7: TEAD2 in the neonatal cardiac Wnt complex.** A. *De-novo* motif search analyses revealing common TEAD2 motifs (highlighted in dashed red boxes) in both TCF7L2 and GATA4-occupied regions in the neonatal heart. B. Immunoprecipitation depicting a mild interaction between TEAD2 and B-catenin in neonatal hearts (P6) (red arrow), and its loss in diseased hearts, n=2.

## Discussion

The mammalian heart is the first anatomical structure to be formed during embryonic development. This complex process involves precise and meticulous combination of gene transcription events, elicited by temporal recruitment of transcription factors to the cardiac chromatin[42,43]. The gradual growth in organ size during development is largely attributed to the robust ongoing cell cycle activity. Several mature organs like the liver, retain this ability to proliferate and re-populate lost cells, both during homeostasis and disease[3]. However, post-mitotic cells like the neurons and CM arrest their ability to divide and maintain this state throughout adulthood[44,45]. In this context, it is interesting to observe that certain organs possess a striking capacity to regenerate, after an injury. On the other hand, the murine heart loses its regenerative potential post-injury, around postnatal day 7 (P7); and the cardiac chromatin also responds accordingly, by recruiting molecular machineries repressing the transcription of mitotic genes and activating cardiac maturation programs[14,15].

Since current cardiovascular therapies are vastly aimed at symptomatic alleviation, rather than directly interfering with the CM pool, there is an urgent need to invent strategies improving the regenerative capacity of the adult heart. Interestingly, several studies including ours, have demonstrated a re-triggering of the adult CM cell cycle and developmental programs during injury/stress[15,17]. However, despite this developmental re-activation, the injured heart failed to regain complete homeostasis, ultimately leading to cardiac dysfunction. Therefore, in this present study, we decided to distinguish between the two cardiac states: to identify processes unique to regenerative and diseased hearts. Previous studies have investigated global cardiac chromatin and transcriptomic changes across different CM stages by studying histone and chromatin accessibility profiles[46–48]. However, we focused on specific molecular players and identified their stage-specific roles within the cardiac chromatin.

The Wnt signaling pathway is known to be crucial for cardiac development, and its quiescence is needed for CM differentiation. Several studies have shown a reactivation of its cytosolic components (like GSK3β and PKA); and WNT ligands/Frizzled (FZD) receptors in heart disease[20,25,49,50]. However, the specific nuclear transcriptional roles were never investigated before in the heart, especially in a stage-specific manner. Transcription factor 7-like 2 (TCF7L2) is the most important nuclear effector of the pathway and studies have recently shown its transcriptional role in driving heart disease progression, also by influencing the chromatin landscape[17]. Notably, TCF7L2 is predominantly context-specific, wherein it associates to unique tissue-specific interaction partners to elicit appropriate transcriptional regulation. For example, TCF7L2 interacts with HNF4α and FOXO1 in liver, regulating metabolic homeostasis in hepatocytes[29,51]; and with SOX4 in oligodendroglia driving their maturation[52].

Hence, we chose TCF7L2 as our TF of interest; characterized its function in the regenerative, neonatal myocardium and compared its roles on the chromatin in neonatal, adult and diseased heart tissues. In our previous study, we had identified the cardiac master TF GATA4 as a cardiac Wnt repressor in the healthy adult heart, whereby we reported a clear interaction between GATA4 and nuclear B-catenin, along with a significant overlap with TCF7L2 genomic occupancies in the adult heart[17]. In this study, we sought to decipher the role of the Wnt-TCF7L2 cardiac complex and its interaction partners in a different context- the regenerative myocardium.

Our results demonstrated increased TCF7L2 expression in the ventricular CM of neonatal P6 murine hearts, decreasing in adulthood and increasing again in disease. Given that TCF7L2 is extensively correlated to cell proliferation and tumor metastases[53,54], its increased expression

specifically in P6 hearts is particularly interesting. This is because around postnatal day 6, the murine heart initiates CM maturation processes[55], whilst still promoting heart growth (based on KI67 expression in TNNT2-positive CMs at this age). Moreover, we observed again, an interaction between GATA4 and B-catenin in P6 cardiac tissue, similar to the observation in the healthy adult heart. These results suggest the presence and co-dominance of both developmental as well as maturation processes at postnatal day 6. Intrigued by the unique cardiac status at P6, we performed RNA-seq in P6 cardiac ventricular tissue and compared their transcriptomes with those of adult and diseased (Wnt-activated) hearts. This analysis indeed categorized P6 as a unique cardiac stage, since they transcriptionally grouped distinctly as compared to both adult and diseased hearts, while simultaneously possessing commonly upregulated genes with the diseased in comparison to the adult heart. Expectedly, these commonly enriched genes in P6 and diseased hearts annotated to chromatin reorganization, cell cycle and Wnt signaling pathway- establishing that these responses belong to the regenerative circuit within the diseased myocardium. On the other hand, genes upregulated only in P6 or in disease annotated mainly to metabolic process or immune response, angiogenesis and cardiac developmental processes; suggesting that these processes distinguish the two states.

In order to identify the role of TCF7L2 as well as GATA4 within these specific transcriptional responses, ChIP-seq experiments were performed. These results unraveled striking tendencies of TCF7L2 genomic occupancies in the heart- being proximal in P6 and distal in diseased cardiac ventricular tissue, despite occupying similar *number* of regions. These regions annotated to a variety of important cardiac processes like metabolism, cell cycle, angiogenesis, neurological process and expectedly, Wnt pathway activation. GATA4 is a master cardiac TF and true to its significance, GATA4-occupied a large portion of the genome in P6 hearts- mostly annotating to heart muscle development and contraction processes.

In order to understand the stage-specific, chromatin-associated roles of TCF7L2 in P6 and diseased hearts, we performed differential binding analyses, which identified regions specifically enriched for TCF7L2, in each case. P6-enriched regions were proximal, largely annotating to metabolism. Accordingly, disease-enriched TCF7L2 regions were distal and annotated to vascular and cardiac developmental processes (both in line with transcriptomics data). The enrichment of cardiac fetal genes in Dis-En suggests that the heart unsuccessfully attempts to restore its function by triggering the generation of new, immature CM, which do not contribute to the improvement, but rather initiate fibrotic and pathological responses, culminating in heart

failure. On the other hand, enrichment of metabolic processes in P6-En indicates the role of TCF7L2 in directing CM maturation- since neonatal hearts require elevated metabolism in order to establish a fully functional, contractile myocardium. While the proximal nature of TCF7L2 occupancy in P6 hearts could suggest its putative association to promoter-acting TFs like PPAR[56,57] to regulate metabolism; the distal, enhancer-based occupancy in diseased hearts is suggestive of interaction with enhancer-associated TFs like BRD4 and BRG1- both known to propel heart disease progression[58–60].

Further, we observed a marked overlap between TCF7L2 and GATA4 occupancies (about 75%) in P6 hearts, enriched for H3K27ac- indicating a transcriptionally active state of these regions. This is surprising, since a. the TCF7L2-GATA4 overlap was only 30% in the adult heart, where the Wnt pathway is quiescent, and b. the recently reported repressive role of GATA4 on Wnt loci in the adult heart[17]. Given that GATA4 interacted with B-catenin in both P6 (high Wnt) and healthy adult (low Wnt), and not in diseased (high Wnt) hearts, we envisaged the presence of neonatal-specific co-factors, which provided the basis for the regenerative context, at this age. Hence, upon performing *de novo,* sequence-based motif search analyses of these regions, we identified an enrichment of TEAD2 in both TCF7L2 and GATA4-occupied loci in P6 hearts. TEAD2 is an important downstream mediator of the Hippo pathway- a pathway often implicated in cardiac regenerative responses[40,41]. Moreover, TEAD2 was never studied in a cardiac context before. Our results revealed an interaction between TEAD2 and B-catenin only in P6 hearts, strengthening our hypothesis regarding its potential relevance, specifically at this stage within the cardiac Wnt complex.

Altogether, our study presents for the first time, evidence for the transcriptional roles of TCF7L2 and GATA4 in the neonatal heart and identified their direct target genes and novel co-factors mediating this response, crucial for regeneration.

## Supplementary information

### Supporting table S1

Primers used in the direction of 5’-3’ orientation for qPCR.

| Name of the genes | Sequence | Comments/Use |
|---|---|---|
| **MOUSE** | | |

| | | |
|---|---|---|
| *Axin2* F | AGCCGCCATAGTC | qPCR |
| *Axin2* R | GGTCCTCTTCATAGC | qPCR |
| *Mars peak* F | GTTGAAGTGGTATCGCACGC | ChIP-qPCR |
| *Mars peak* R | CTAAATGCATCGCCACGCTC | ChIP-qPCR |
| *Ormdl3 peak* F | CCACCCTGACGCAATAGTGA | ChIP-qPCR |
| *Ormdl3 peak* R | CTTGTGCAACACGTGAAGGG | ChIP-qPCR |
| *Aldh3a2 peak* F | CCTGCTAACGACAAAGTGCG | ChIP-qPCR |
| *Aldh3a2 peak* R | TCCCGCGGCTAGATTAGAGG | ChIP-qPCR |
| *Rnf5 peak* F | AGGTTCAAAGGCCTCGACTC | ChIP-qPCR |
| *Rnf5 peak* R | GTAAACCGCCCAATCAAGCG | ChIP-qPCR |
| *Sptlc2 peak* F | GCGGGGTCTATCGGCTATTG | ChIP-qPCR |
| *Sptlc2 peak* R | GATGTCTGCAAGCCGCTTTT | ChIP-qPCR |
| *Angpt1 peak* F | GAGAGTCCAGCCCACTACAA | ChIP-qPCR |
| *Angpt1 peak* R | ATTGAAGGCACTGAGTGGGAG | ChIP-qPCR |
| *Vav1 peak* F | AGGCCCTCTCCGTCAGG | ChIP-qPCR |
| *Vav1 peak* R | GGACTTGTTCCAAAGGGGCT | ChIP-qPCR |
| *Ang peak* F | GTCTTTTGGGCTCTCAACCC | ChIP-qPCR |
| *Ang peak* R | GGACGAGCAATGATCAACCAAA | ChIP-qPCR |

| | | |
|---|---|---|
| *Hand2 peak* F | TCATCTTTCAGTCGTGCCGT | ChIP-qPCR |
| *Hand2 peak* R | CTGAGTAGTGCACATGACAGC | ChIP-qPCR |
| *Tbx3 peak* F | TCGGGGTTAGGCCTTGATAAC | ChIP-qPCR |
| *Tbx3 peak* R | GTCTTGGCTGCCTCTCAGTT | ChIP-qPCR |

**Figure S1.**

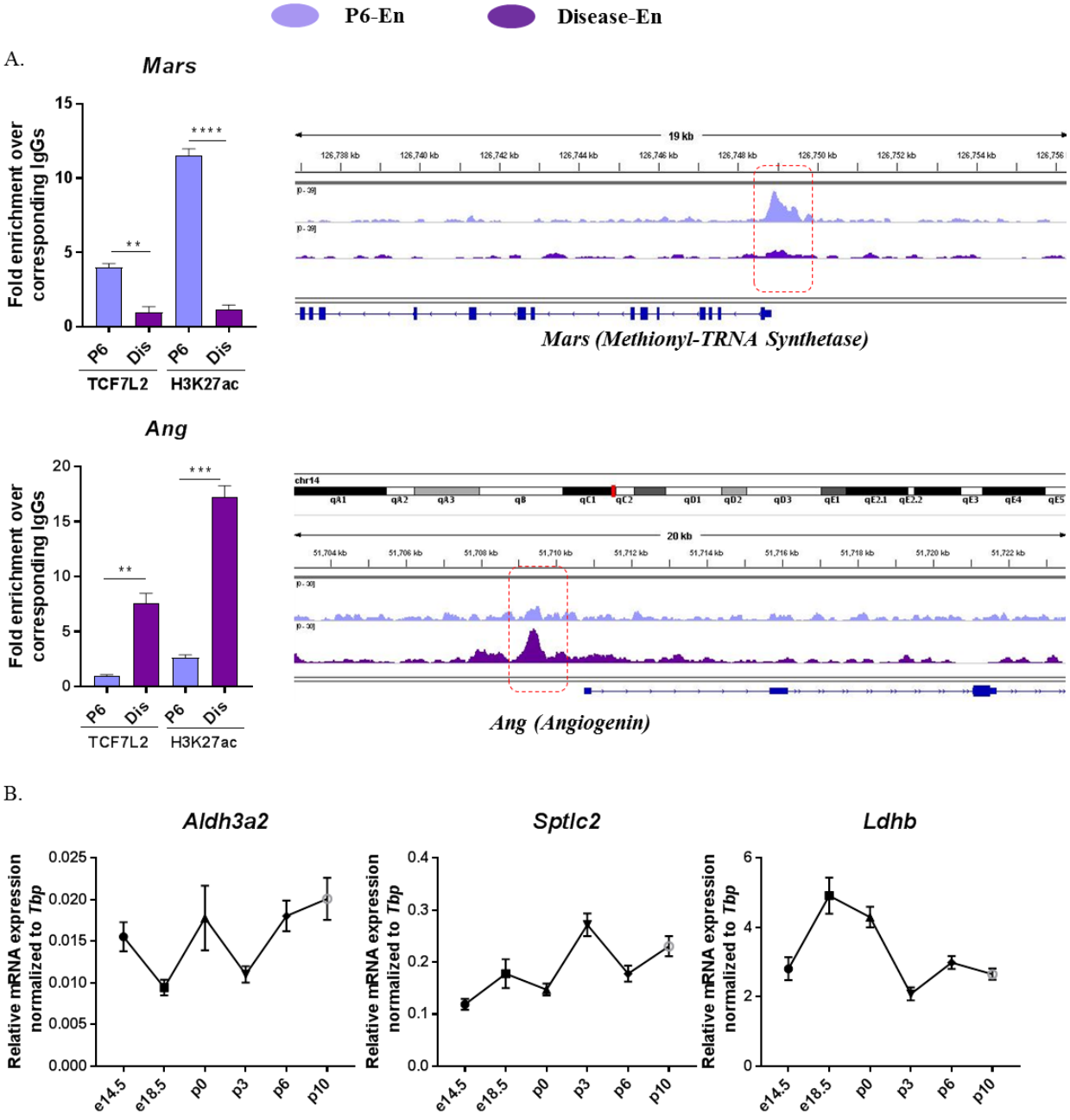


**Fig. S1:. TCF7L2 specifically partakes in regulating metabolism in neonatal hearts.** A. TCF7L2 occupancies on differentially-bound regions in neonatal and diseased hearts for *Mars* (neonatal-specific) and *Ang* (disease-specific) genes, along with corresponding ChIP-qPCR validations in neonatal (P6) and Wnt-activated (disease) hearts, n=3. B. qPCRs depicting expression trends of some exemplary metabolic genes- *Aldh3a2* (aldehyde metabolism), *Sptlc2* (fatty acid metabolism) and *Ldhb* (glucode metabolism), across murine late developmental and early postnatal stages. *Tbp* was used as house-keeping gene, n≥3.

**Figure S2.**

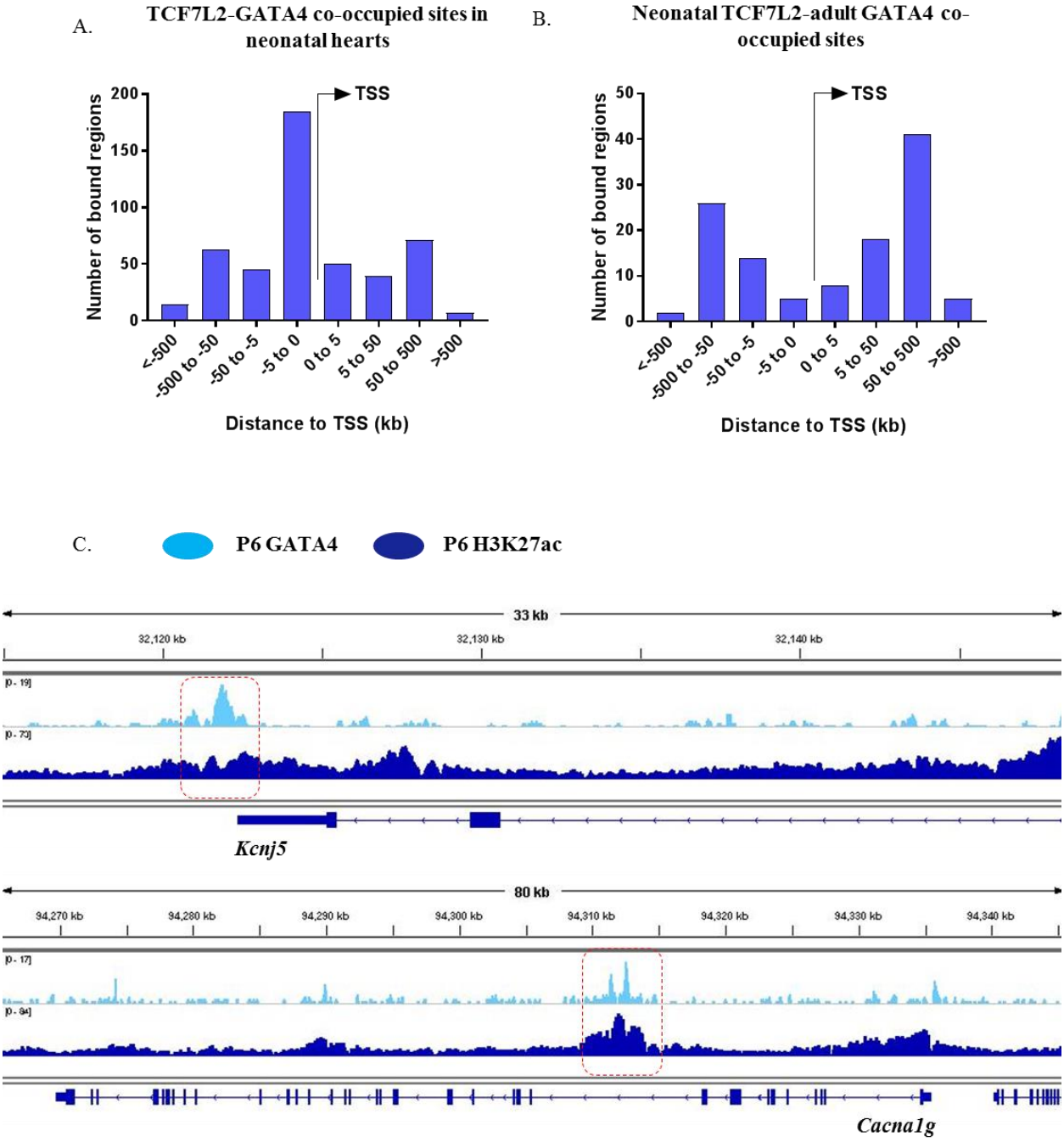


**Fig. S2: GATA4 provides cardiac specificity to TCF7L2 in the neonatal, regenerative heart.** A. Overview of TCF7L2-GATA4 co-occupied regions in neonatal hearts showing proximal occupancy B. Overview of neonatal TCF7L2-adult GATA4 co-occupied regions showing distal occupancy. C. IGV occupancy profiles showing enrichment of H3K27ac on GATA4-bound regions- *Kcnj5* and *Cacna1g*: genes essential for cardiac conduction.

## References


1. Bayat, H. *et al.* Progressive heart failure after myocardial infarction in mice. *Basic Res. Cardiol.* **97,** 206–213 (2002).
2. Struthers, A. D. Pathophysiology of heart failure following myocardial infarction. *Heart* **91,** ii14–ii16 (2005).
3. Fausto, N., Campbell, J. S. & Riehle, K. J. Liver regeneration. *Hepatology* **43,** (2006).
4. Kholodenko, I. V. & Yarygin, K. N. Cellular Mechanisms of Liver Regeneration and Cell-Based Therapies of Liver Diseases. *BioMed Research International* **2017,** (2017).
5. Steinhauser, M. L. & Lee, R. T. Regeneration of the heart. *EMBO Mol. Med.* **3,** 701–712 (2011).
6. Quaife-Ryan, G. a. *et al.* Multi- & ellular Transcriptional Analysis of Mammalian Heart Regeneration. *Circulation* (2017).
7. Miyaoka, Y. *et al.* Hypertrophy and Unconventional Cell Division of Hepatocytes Underlie Liver Regeneration. *Curr. Biol.* **22,** 1166–1175 (2012).
8. Relaix, F. & Zammit, P. S. Satellite cells are essential for skeletal muscle regeneration: the cell on the edge returns centre stage. *Development* **139,** 2845–2856 (2012).
9. Ebrahimi, B. Cardiac progenitor reprogramming for heart regeneration. *Cell Regeneration* (2018). doi:10.1016/j.cr.2018.01.001
10. Amini, H., Rezaie, J., Vosoughi, A., Rahbarghazi, R. & Nouri, M. Cardiac progenitor cells application in cardiovascular disease. *J. Cardiovasc. Thorac. Res.* **9,** 127–132 (2017).
11. Zelarayán, L. C. *et al.* Beta-Catenin downregulation attenuates ischemic cardiac remodeling through enhanced resident precursor cell differentiation. *Proc. Natl. Acad. Sci. U. S. A.* **105,** 19762–19767 (2008).
12. Baurand, A. *et al.* β-catenin downregulation is required for adaptive cardiac remodeling. *Circ. Res.* **100,** 1353–1362 (2007).
13. Noack, C. *et al.* Krueppel-like factor 15 regulates Wnt/β-catenin transcription and controls cardiac progenitor cell fate in the postnatal heart. *EMBO Mol. Med.* **4,** 992–1007 (2012).
14. Porrello, E. R. *et al.* Transient regenerative potential of the neonatal mouse heart. *Science* **331,** 1078–80 (2011).
15. Quaife-Ryan, G. A. *et al.* Multicellular transcriptional analysis of mammalian heart regeneration. *Circulation* **136,** 1123–1139 (2017).
16. N., P., A., K., I., B. & D., P. Neonatal myocardial infarction secondary to umbilical venous catheterization: A case report and review of the literature. *Paediatrics and Child Health* **14,** 539–541 (2009).
17. Iyer, L. M. *et al.* A context-specific cardiac β-catenin and GATA4 interaction influences TCF7L2 occupancy and remodels chromatin driving disease progression in the adult heart. *Nucleic Acids Res.* (2018). doi:10.1093/nar/gky049
18. Gessert, S. & Kühl, M. The multiple phases and faces of Wnt signaling during cardiac differentiation and development. *Circ. Res.* **107,** 186–199 (2010).
19. Ozhan, G. & Weidinger, G. Wnt/β-catenin signaling in heart regeneration. *Cell Regen.* **4,** 1–12 (2015).
20. Aisagbonhi, O. *et al.* Experimental myocardial infarction triggers canonical Wnt signaling and endothelial-

to-mesenchymal transition. *Dis. Model. Mech.* **4,** 469–483 (2011).

21. Weise, A. *et al.* Alternative splicing of Tcf7l2 transcripts generates protein variants with differential promoter-binding and transcriptional activation properties at Wnt/β-catenin targets. *Nucleic Acids Res.* **38,** 1964–1981 (2009).
22. Hansson, O., Zhou, Y., Renström, E. & Osmark, P. Molecular function of TCF7L2: Consequences of TCF7L2 splicing for molecular function and risk for type 2 diabetes. *Current Diabetes Reports* **10,** 444–451 (2010).
23. Lee, M. *et al.* Tcf7l2 plays crucial roles in forebrain development through regulation of thalamic and habenular neuron identity and connectivity. *Dev. Biol.* **424,** 62–76 (2017).
24. Shu, L. *et al.* TCF7L2 promotes beta cell regeneration in human and mouse pancreas. *Diabetologia* **55,** 3296–3307 (2012).
25. Brade, T., Männer, J. & Kühl, M. The role of Wnt signalling in cardiac development and tissue remodelling in the mature heart. *Cardiovasc. Res.* **72,** 198–209 (2006).
26. Giordano, F. J. Oxygen, oxidative stress, hypoxia, and heart failure. *Journal of Clinical Investigation* **115,** 500–508 (2005).
27. Walton, C. B. *et al.* Cardiac angiogenesis directed by stable Hypoxia Inducible Factor-1. *Vasc. Cell* **5,** (2013).
28. J. Patterson, A. & Zhang, L. Hypoxia and Fetal Heart Development. *Curr. Mol. Med.* **10,** 653–666 (2010).
29. Frietze, S. *et al.* Cell type-specific binding patterns reveal that TCF7L2 can be tethered to the genome by association with GATA3. *Genome Biol.* **13,** R52 (2012).
30. Norton, L. *et al.* Chromatin occupancy of transcription factor 7-like 2 (TCF7L2) and its role in hepatic glucose metabolism. *Diabetologia* **54,** 3132–3142 (2011).
31. Hatzis, P. *et al.* Genome-wide pattern of TCF7L2/TCF4 chromatin occupancy in colorectal cancer cells. *Mol. Cell. Biol.* **28,** 2732–2744 (2008).
32. Ang, Y. S. *et al.* Disease Model of GATA4 Mutation Reveals Transcription Factor Cooperativity in Human Cardiogenesis. *Cell* **167,** 1734–1749.e22 (2016).
33. Schlesinger, J. *et al.* The cardiac transcription network modulated by gata4, mef2a, nkx2.5, srf, histone modifications, and microRNAs. *PLoS Genet.* **7,** (2011).
34. He, A. *et al.* Dynamic GATA4 enhancers shape the chromatin landscape central to heart development and disease. *Nat. Commun.* **5,** (2014).
35. Makinde, A. O., Kantor, P. F. & Lopaschuk, G. D. Maturation of fatty acid and carbohydrate metabolism in the newborn heart. in *Molecular and Cellular Biochemistry* **188,** 49–56 (1998).
36. Lopaschuk, G. D. & Jaswal, J. S. Energy metabolic phenotype of the cardiomyocyte during development, differentiation, and postnatal maturation. in *Journal of Cardiovascular Pharmacology* **56,** 130–140 (2010).
37. Sethi, J. & Vidal-Puig, a. Wnt signalling and the control of cellular metabolism. *Biochem J.* **427,** 1–17 (2010).
38. Sawada, A. *et al.* Redundant Roles of Tead1 and Tead2 in Notochord Development and the Regulation of Cell Proliferation and Survival. *Mol. Cell. Biol.* **28,** 3177–3189 (2008).

39. Kaneko, K. J., Kohn, M. J., Liu, C. & DePamphilis, M. L. Transcription factor TEAD2 is involved in neural tube closure. *Genesis* **45,** 577–587 (2007).
40. Xin, M. *et al.* Hippo pathway effector Yap promotes cardiac regeneration. *Proc. Natl. Acad. Sci.* **110,** 13839–13844 (2013).
41. Zhou, Q., Li, L., Zhao, B. & Guan, K. The hippo pathway in heart development, regeneration, and diseases. *Circ. Res.* **116,** 1431–47 (2015).
42. Bruneau, B. G. The developmental genetics of congenital heart disease. *Nature* **451,** 943–948 (2008).
43. Mercola, M., Ruiz-Lozano, P. & Schneider, M. D. Cardiac muscle regeneration: Lessons from development. *Genes Dev.* **25,** 299–309 (2011).
44. De Anda, F. C. *et al.* Cortical neurons gradually attain a post-mitotic state. *Cell Res.* **26,** 1033–1047 (2016).
45. Aranda-Anzaldo, A. The post-mitotic state in neurons correlates with a stable nuclear higher-order structure. *Communicative and Integrative Biology* **5,** 134–139 (2012).
46. Gilsbach, R. *et al.* Distinct epigenetic programs regulate cardiac myocyte development and disease in the human heart in vivo. *Nat. Commun.* **9,** (2018).
47. Narlikar, L., Sakabe, N. J. & Blanski, A. a. Genome-wide discovery of human heart enhancers --- Genome Research. *Genome Res.* **20,** 381–392 (2010).
48. May, D. *et al.* Large-scale discovery of enhancers from human heart tissue. *Nat. Genet.* **44,** 89–93 (2012).
49. Daskalopoulos, E. P., Hermans, K. C. M., Janssen, B. J. a & Matthijs Blankesteijn, W. Targeting the Wnt/frizzled signaling pathway after myocardial infarction: A new tool in the therapeutic toolbox? *Trends Cardiovasc. Med.* **23,** 121–127 (2013).
50. Hirotani, S. *et al.* Inhibition of glycogen synthase kinase 3beta during heart failure is protective. *Circ. Res.* **101,** 1164–74 (2007).
51. Gougelet, A. *et al.* T-cell factor 4 and β-catenin chromatin occupancies pattern zonal liver metabolism in mice. *Hepatology* **59,** 2344–2357 (2014).
52. Zhao, C. *et al.* Dual regulatory switch through interactions of Tcf7l2/Tcf4 with stage-specific partners propels oligodendroglial maturation. *Nat. Commun.* **7,** 1–15 (2016).
53. Kojima, T. *et al.* FOXO1 and TCF7L2 genes involved in metastasis and poor prognosis in clear cell renal cell carcinoma. *Genes Chromosom.* **49,** 379–389 (2010).
54. Ishiguro, H. *et al.* Nuclear expression of TCF4/TCF7L2 is correlated with poor prognosis in patients with esophageal squamous cell carcinoma. *Cell. Mol. Biol. Lett.* **21,** 5 (2016).
55. Piquereau, J. *et al.* Postnatal development of mouse heart: Formation of energetic microdomains. *J. Physiol.* **588,** 2443–2454 (2010).
56. Nielsen, R. *et al.* Genome-wide profiling of PPARγ:RXR and RNA polymerase II occupancy reveals temporal activation of distinct metabolic pathways and changes in RXR dimer composition during adipogenesis. *Genes Dev.* **22,** 2953–2967 (2008).
57. Cardamone, M. D. *et al.* GPS2/KDM4A pioneering activity regulates promoter-specific recruitment of PPARγ. *Cell Rep.* **8,** 163–176 (2014).
58. Hang, C. T. *et al.* Chromatin regulation by Brg1 underlies heart muscle development and disease. *Nature*

**466,** 62–67 (2010).

59. Stratton, M. S. *et al.* Signal-Dependent Recruitment of BRD4 to Cardiomyocyte Super-Enhancers Is Suppressed by a MicroRNA. *Cell Rep.* **16,** 1366–1378 (2016).

60. Bartholomeeusen, K., Xiang, Y., Fujinaga, K. & Peterlin, B. M. Bromodomain and extra-terminal (BET) bromodomain inhibition activate transcription via transient release of Positive Transcription Elongation Factor b (P-TEFb) from 7SK small nuclear ribonucleoprotein. *J. Biol. Chem.* **287,** 36609–36616 (2012).

# 6. Chapter 3: Role of Krueppel-like factor 15 (KLF15) in cardiac homeostasis and disease

## 'SHISA3: A novel KLF15 and Wnt signaling target in cardiac endothelial cell remodeling'

Claudia Noack[1,3]*, Lavanya M. Iyer[1,3]*, Norman Y. Liaw[1,3], Denise Hartung[1,3], Eric Schoger[1,3], Sara Khadjeh[2,3], Eva Wagner[2,3], Monique Woelfer[1,3], Maria-Patapia Zafiriou[1,3], Gerd Hasenfuss[2,3], Wolfram-Hubertus Zimmermann[1,3] and Laura C. Zelarayán[1,3]
* Authors contributed equally.

Affiliations:
[1] Institute of Pharmacology and Toxicology, University Medical Center Goettingen, Georg-August University, Goettingen, Germany

[2]Department of Cardiology and Pneumology, University Medical Center Goettingen, Georg-August University, Goettingen

[3]DZHK (German Center for Cardiovascular Research), partner site Goettingen, Germany

**Abstract:** Sustained cardiac stress promotes the transition from an adaptive response to irreversible heart failure. More detailed knowledge of the underlying mechanisms governing this transition will enable identification of suitable targets, preventing this progression. Here, we show age-specific transcriptional functions mediated by KLF15 that are crucial for cardiac homeostasis. We report that KLF15 continuously activates cardiac metabolism, but represses pathological pathways dictating cardiomyocyte de-differentiation and endothelial cell (EC) remodeling, in an age-dependent manner. Our integrative genomic and transcriptomic analyses reveal novel target genes directly bound, and either activated or repressed by KLF15 in the adult heart. We further present a cooperative program inducing aberrant EC remodeling, caused by a reduction of KLF15 with a concomitant activation of Wnt signaling. Within this program, we unearth a so far uncharacterized cardiac gene - *Shisa3*, with immature EC characteristics, which is expressed in the developing heart and is upregulated in cardiac hypertrophy, ischemia and failure. Importantly, we demonstrate that the KLF15- and Wnt co-dependent SHISA regulation occurs also in the human myocardium. Altogether, our results unravel and characterize a previously unknown cardiac gene *Shisa3*, and underscore its significance in EC homeostasis of the adult heart, controlled by KLF15-Wnt dynamics.

## Introduction

Sustained pathophysiological stress promotes the transition of initially adaptive hypertrophy and remodeling, into a decompensated stage with cardiac contractile dysfunction- a process termed as maladaptive remodeling [1]. This process is characterized by myocardial de-differentiation consisting of changes from a highly organized striated sarcomeric structure, to dense, disorganized complex, along with metabolic and molecular changes, reminiscent of fetal cardiomyocytes [2]. Moreover, pathological tissue remodeling is often associated with impaired myocardial vascularization, changes in the extracellular matrix composition and fibrosis- all resulting in loss of contractile muscle and severe heart failure. Thorough understanding of molecular mechanisms protecting homeostatic pathways that orchestrate and control the onset of maladaptive processes will finally provide valuable information in the design of novel treatment strategies preserving myocardial function.

Krueppel-like factor (KLF) 15 is a DNA-binding transcriptional regulator involved in gene activation and repression [3, 4]. Its main roles have been described in glucose and lipid metabolism, cell differentiation and aging [5-10]. Specifically in the adult heart, KLF15 is known to repress major hypertrophic signaling pathways during pathological remodeling by inhibiting MEF2 and GATA4-dependent transcriptional activities [7], by binding to myocardin-related transcription factors (MRTFs), thereby preventing SRF mediated transcription [11, 12]; and by disrupting p300-mediated acetylation of p53 [13]. Moreover, KLF15 plays a role in cardiac fibrosis. We previously demonstrated that KLF15 represses Wnt/β-catenin (canonical) signaling and controls progenitor cell fate in the adult heart [8]. Importantly, KLF15 expression is reduced in human cardiomyopathies [13, 14] and its overexpression seems to protect the heart upon mild cardiac hypertrophy induction [11, 15], which has been encouraging further investigation of the function of KLF15 in the stressed heart. Despite previous research, specific roles of KLF15 and its targets in transcriptional networks coordinating adaptation pathways controlling tissue homeostasis and de-differentiation in the postnatal heart were not elucidated.

To understand the homeostatic role of KLF15 in the heart during postnatal murine life, our study investigated unbiased cardiac expression profiles lacking KLF15. These uncovered age-specific transcriptional functions of KLF15 necessary for homeostasis in the unstressed heart- playing early activation roles in cardiac metabolism and late inhibitory roles in tissue remodeling pathways. Our integrative analyses identified cardiac target genes either activated or repressed upon direct KLF15 DNA-binding. We further elaborated the pathways and TFs networks

controlled by KLF15, leading to maladaptive tissue and endothelial remodeling and found a synergistic role of KLF15-mediated Wnt signaling regulation of endothelial cell reprograming. This analysis enabled us to discover a novel cardiac fetal gene with an endothelial signature, *Shisa3*, activated in pathological remodeling and reciprocally regulated by Wnt and KLF15, in an evolutionarily conserved manner. These findings contribute to the understanding of homeostatic mechanisms in favorable tissue remodeling.

## Results

### KLF15 maintains cardiac homeostasis by repressing developmental reprogramming pathways and activating metabolism in the postnatal heart

Given the relevance of KLF15 in the healthy and diseased mammalian heart [7, 12, 13, 16, 17], we aimed to define its age-specific, homeostatic, repressive and activating roles in the growing postnatal heart.

Thus, we wanted to investigate the molecular events orchestrated by KLF15, responsible for the development of the cardiac phenotype. Since KLF15 has repressive functions on gene regulation, especially hypertrophic genes, we tested the hypothesis that transcriptional de-repression upon loss of KLF15, results in progressive molecular changes, leading to adverse cardiac remodeling. To define the mechanisms leading to the onset of cardiac remodeling, we studied sequential transcriptional changes by performing transcriptome-wide sequencing (RNA-seq) of *Klf15* KO heart ventricles and compared to wild-type (WT) postnatal hearts. We selected 10 days (P10), 4 and 20 weeks (w) stages to study differential transcriptomic changes. The selection was based on the physiological *Klf15* expression, which was low at P10 and high at 4w and 20w. Moreover, 4w and 20w were selected based on the onset of cardiac failure in *Klf15* KO mice- normal (4w) versus impaired (20w) cardiac function.

To define global similarities and differences among the different stages, we performed principal component analysis (PCA) on the transcriptome datasets and displayed the results as biplots. PCA depicted 6 groups of transcriptomes belonging to 3 different ages and genotypes (Fig. S1A). WT and *Klf15* KO hearts were differentially grouped at all ages. As expected, WT early (P10) and late (4 and 20w) postnatal transcriptomes grouped separately, according to their maturation state. Interestingly, P10, 4 and 20w *Klf15* KO heart transcriptomes were closely grouping in proximity to early postnatal, but *not* to late postnatal stages (4 and 20w) in WT hearts. This suggests that *Klf15* KO hearts undergo tissue remodeling similar to early, normal

postnatal hearts. Further, read counts grouped closely for 4w and 20w hearts and not P10, indicating the overall differences in the transcriptomes of P10 in comparison to the adult hearts (Fig. S1B).

**Figure 1**

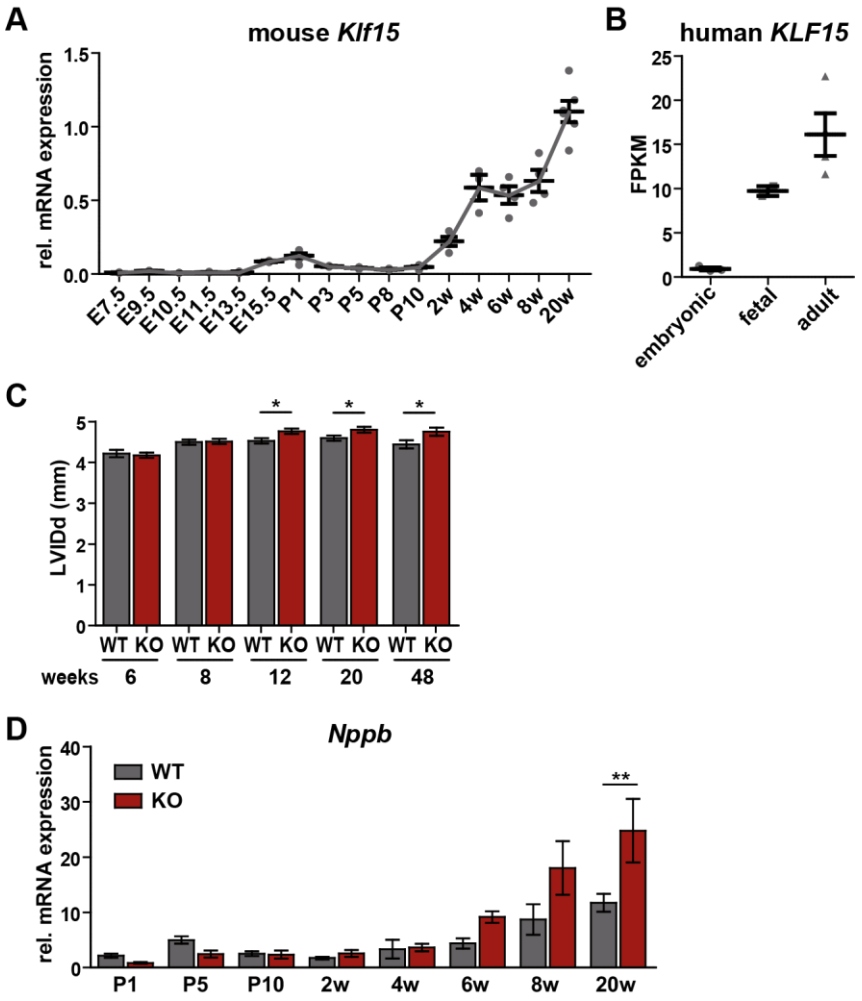


**Figure 1: *Klf15* in the mouse and human heart. a,** qPCR showing increasing transcript levels of *Klf15* across murine cardiac embryonic, postnatal and adult stages; normalized to *Actb*; n=3/stage (embryonic tissue were pooled as followed per N: E7.5 20 embryos; E9.5-11.5 8-10 hearts; E13.5-15.5 4-6 hearts). **b,** Fragments Per Kilobase of transcript per Million mapped reads (FPKMs) of *KLF15* expression in human embryonic, fetal and adult hearts, showing its increasing expression similar to *Klf15* in murine hearts, n=3. **c,** Left Ventricular Inner Diameter in diastole (LVIDd) in 6, 8, 12, 20 and 48 weeks-old WT and *Klf15* KO mice, depicting chamber dialation in 12 weeks and older *Klf15* KO animals; n≥12. **d,** *Nppb* transcript levels in WT and *Klf15* KO postnatal hearts; n≥12. 1-way ANOVA with Bonferroni's multiple comparison test, *p≤0.05, **p≤0.01.

Compared to control WT, we identified 92, 183 and 220 upregulated genes at P10, 4 and 20w, respectively indicating an increasing tendency of its repressive roles during heart growth. In contrast, 318, 254 and 359 downregulated genes were detected in *Klf15* KO hearts at P10, 4 and

20w, respectively, indicating a stable, activating role, postnatally (n=3/stage, $p<0.05$ and $\log_2FC \geq 0.5$). At P10, only one Gene Ontology (GO) biological process was identified for upregulated genes in *Klf15* KO- namely developmental pattern formation, due to upregulation of the Iroquois Homeobox (IRX) transcription factors. Upregulated genes in 4w *Klf15* KO hearts clustered into GO including chromatin modifications, developmental processes, cell cycle, cell communication, muscle contraction and endothelial development. At 20w, genes encoding for cell growth, cardiac muscle and endothelial development were upregulated in *Klf15* KO hearts (Fig. 2A). GO corresponding to downregulated genes in *Klf15* KO hearts included mainly amino acid, carbohydrate and fatty acid metabolism, independent from the age, suggesting a consistent regulation of KLF15 in these processes (Fig. 2B). Heatmaps depicting normalized counts of differentially expressed genes (DEGs) for all ages are shown in Fig. S1C. In line with activation of developmental processes, fetal genes that are re-activated in the remodeled heart (i.e *Nppa, Nppb, Ankrd1, Acta1, β-MHC*), were upregulated between 4 and 20w, but *not* in P10 *Klf15* KO hearts, in accordance with the onset of heart dysfunction (Fig. 2C). Moreover, microtubule densification and increased DNA cycling, characteristics of hypertrophied and decompensated hearts, were increased in *Klf15* KO CMs at 20w (Fig. 2D, E and S2). These observations indicate that the loss of *Klf15* sequentially activates age-dependent, typical adaptation mechanisms leading to pathological heart remodeling.

To understand the dynamics of these adaptation mechanisms, we next analyzed the genes that were commonly regulated among the different ages of *Klf15* KO hearts. We discovered that only a few upregulated genes (7 genes) overlapped between all the ages, further suggesting a stage-specific, *repressive* action of KLF15 on cardiac developmental processes. A higher overlap between 4 and 20w (23 genes) was observed, which explains their similar grouping observed in Fig. S1B, expectedly annotating to tissue remodeling processes specially in branching morphogenesis (e.g *Ckap4, Myot, Dysf, Cenpa*). In contrast, downregulated genes showed more overlap between all the ages (53 genes) and mainly categorized into amino acid, carbohydrate and fatty acid metabolism (e.g *Aldh2, Abhd1, Fah, Ldhd*), suggesting a persistent, *activating* function of KLF15 in cardiac metabolism, independent of the age (Fig. 2F).

**Figure 2**

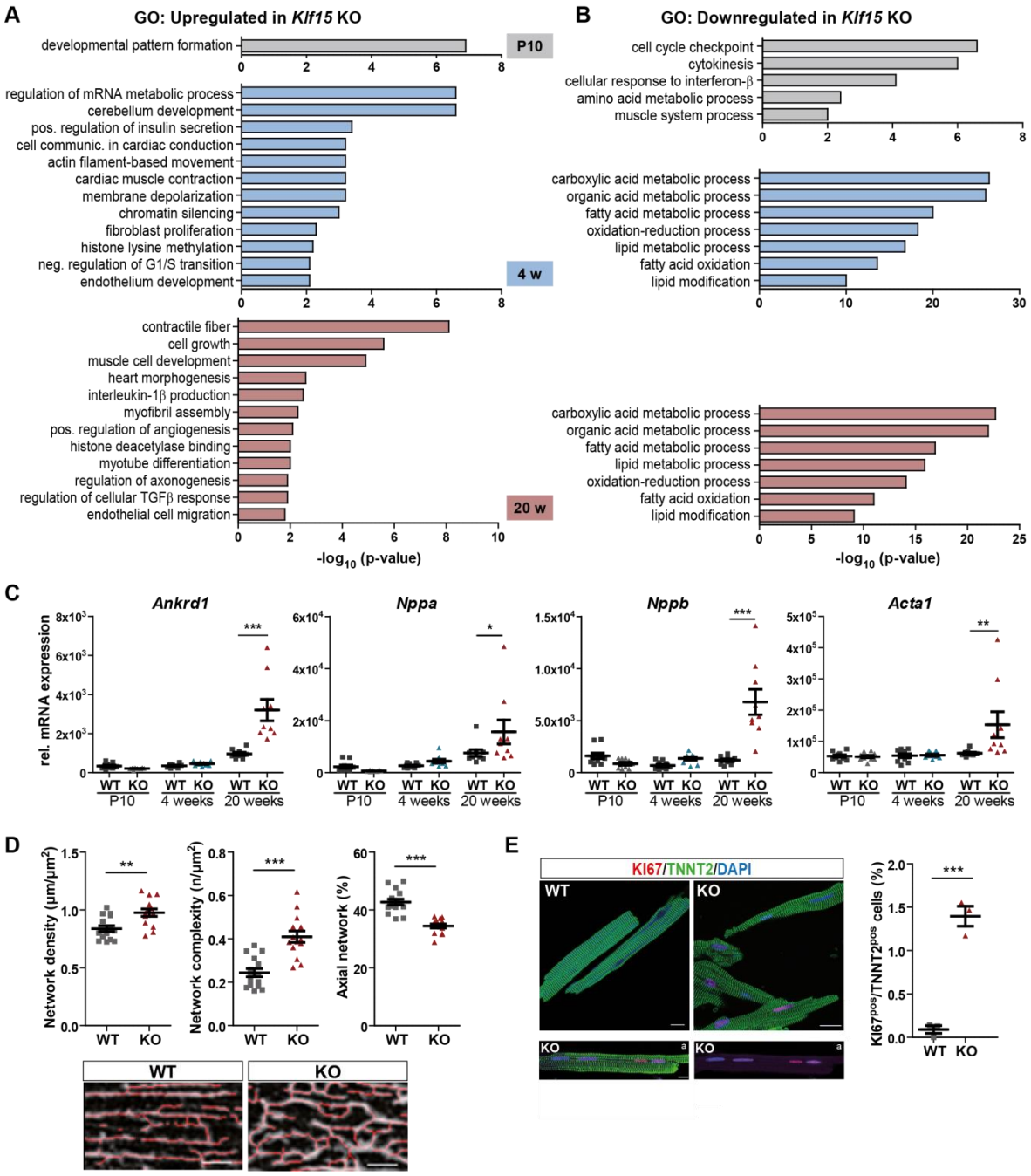


**Figure 2: Transcriptomic profiles of *Klf15* KO postnatal hearts.** Gene ontology (GO) (-$\log_{10}$ (p-value)) biological processes of upregulated (**a**) and downregulated (**b**) genes in postnatal day 10 (P10), 4 and 20 weeks-old *Klf15* KO murine cardiac ventricles. Differentially expressed genes (DEGs) with $\log_2$FC>±0.5 and p<0.05 were considered. **c,** qPCR validations of genes associated to heart remodeling in P10, 4w and 20w *Klf15* WT and KO mice. Increased expression is observed only at 20 weeks of age, normalized to *Tata-binding protein* (*Tbp*). **d,** Representative immunofluorescence (IF) images showing α-Tubulin staining and quantification of cytoskeletal network densities, complexities and axial networks in isolated cardiomyocytes (CM) of 20w *Klf15* KO mice, showing cytoskeletal remodeling in KO CM. **e,** Representative IF images and quantification showing increased cell cycling in isolated CM of 20w *Klf15* KO hearts. Red, green and blue indicate KI67, TNNT2 and DAPI staining,

respectively, n=3/≥10 cells. GO are informed as -$\log_{10}$ (p-value). Statistics in (C) and (D): Student's *t*-test, *p≤0.05, **p≤0.01, ***p≤0.001, p<0.05. Scale bar in (D): 5 μm, (E): 20 μm.

## KLF15 directly represses the developmental canonical Wnt pathway in a cardiac cell-specific manner

We further explored direct repressive or activating functions of KLF15 on the regulatory regions of the identified DEGs. To that end, we integrated a published ChIP-seq dataset [16] with our RNA-seq results by overlapping KLF15-bound genes in the adult heart (2,363 genes), with the DEGs (up or down) in 4w and 20w KO hearts. P10 DEGs were not included due to their distinct transcriptional signatures in comparison to 4w and 20w hearts. This analysis showed that bound genes, which were downregulated in the absence of KLF15 (74 genes), categorized again to amino acid, carbohydrate and fatty acid metabolism. This data validates that KLF15 functions as a transcriptional activator on those set of genes, by directly binding to their regulatory regions. Representative KLF15 occupancies are depicted for amino acid and fatty acid metabolic gene promoters of *Aldh9a1* and *Fads1*, in the adult heart, respectively (bound and activated) (Fig. S3A). Upregulated genes in *Klf15* KO hearts, which were bound by KLF15 (48 genes), were enriched in cellular remodeling processes including G-protein coupled receptor and Wnt signaling pathways, indicating that KLF15 functions as a direct chromatin-associated repressor of these pathways (Fig. 3A).

We observed that the promoter region of the classical Wnt target *Axin2*, which is normally expressed lowly in the normal adult heart, showed KLF15 binding and low H3K27ac, a histone marker for transcriptionally active chromatin regions. Moreover, this binding coincided with the occupancy of TCF7L2 (an activated mediator of the Wnt canonical signaling in pathological remodeling) in the diseased heart along with increased H3K27ac recruitment (Fig. S3B). These observations are in line with previous data from our group- showing Wnt canonical repression mediated by KLF15, which binds to TCF7L2. We now showed for the first time, that this repression, at least for a set of genes (55 genes), takes place by directly binding to the regulatory regions of the cardiac chromatin. Representative KLF15 occupancies are depicted for *Axin2* gene promoter (bound and repressed) in the adult heart. Altogether, these data show that repressive functions of KLF15 are necessary to silence developmental remodeling cascades, including the Wnt canonical signaling in the healthy adult heart.

Since KLF15 is highly expressed in other organs such as liver and kidney (Fig. 3B), we next investigated whether the absence of KLF15 affects Wnt target expression in these organs. Expression of *Tcfl2* and its known ubiquitous target *cMyc* revealed that de-repression of the Wnt canonical cascade takes place *specifically* only in the heart (Fig. 3C). Although, TCF7L2 expression via immunofluorescence in ventricular sections is difficult to detect, *Kfl15* KO mice showed a significantly higher signal in cardiac Troponin T (CTNT)-positive CMs, with typically elongated nuclei, as well as in interstitial cells (Fig. 3D). Since KLF15 is also highly expressed in cardiac fibroblasts, we tested the regulation of Wnt signaling in this specific cell population. KlLF15 inhibits connective tissue growth factor (CTGF). Therefore, the absence of KLF15 increased its levels [17]. We observed that isolated cardiac fibroblasts from *Klf15* KO hearts showed the expected CTGF upregulation in cultured fibroblasts (Fig. 3E). However, expression of TCF7L2 and *cMyc* were not altered in *Klf15* KO fibroblasts, indicating that KLF15-mediated Wnt regulation is not relevant in fibroblasts.

**Figure 3**

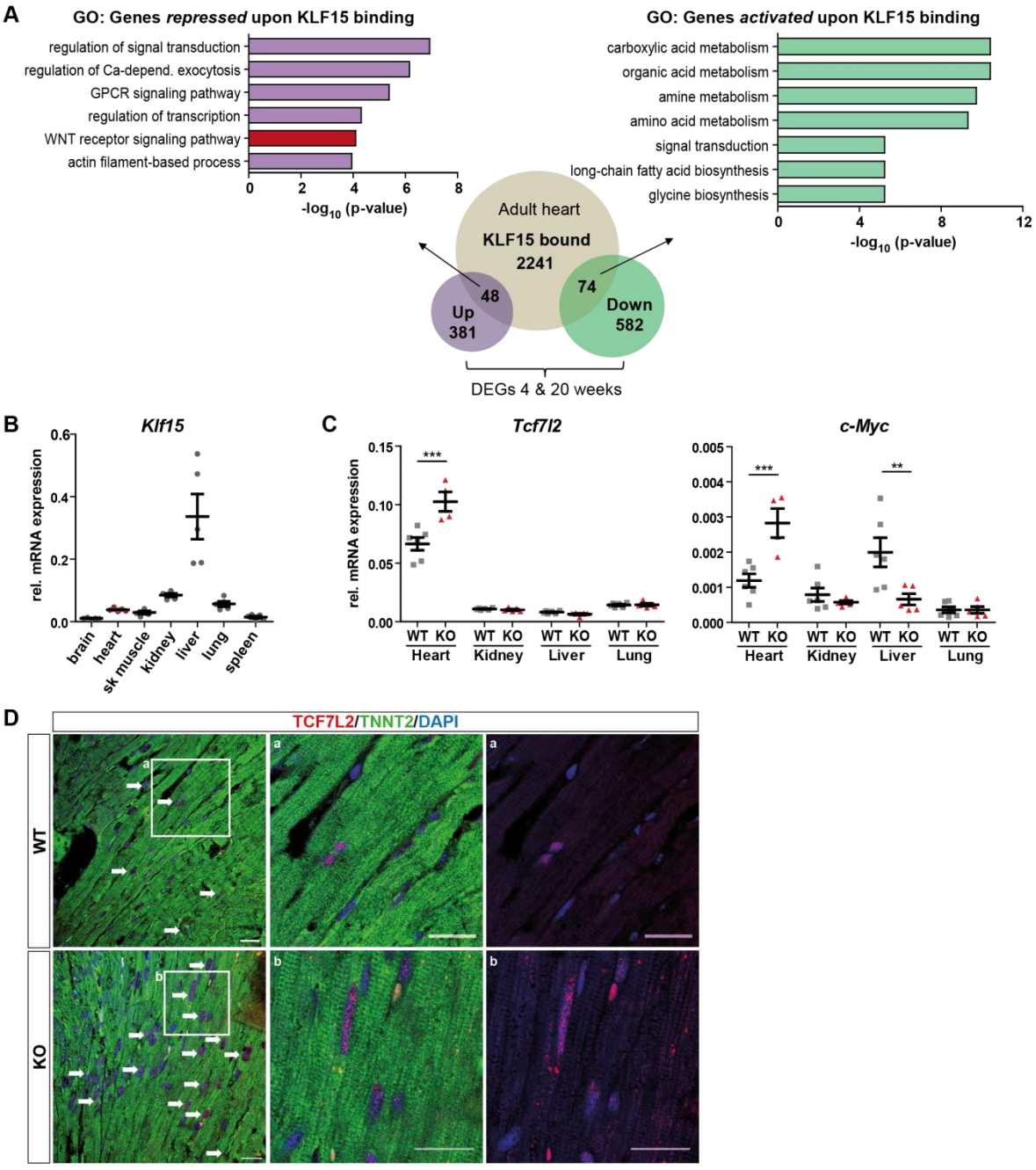


**Figure 3: Genome-wide activation and repression functions of KLF15 in the adult heart. a,** Venn diagram and GO biological processes of genes directly bound by KLF15 (ChIP-seq of KLF15 in the adult heart) and transcriptionally repressed or activated (DEGs from RNA-seq in 4w and 20w *Klf15* KO mice hearts) are shown. Repression of Wnt signaling pathway by KLF15 is highlighted by red bar. **b,** qPCR showing *Klf15* expression in different adult murine organs; normalized to *Actb* expression, n=5. **c,** qPCR showing increased expression of Wnt targets *Tcf7l2* and *c-Myc* specifically in the adult heart upon loss of *Klf15*; normalized to *Actb*, n≥5, Student's *t*-test, **p≤0.01, ***p≤0.001. **d,** Representative IF images showing increased TCF7L2 (magenta) in TNNT2 (green)-positive CM of 20w *Klf15* KO heart tissue. White arrows indicate TCF7L2 expression in CM; DAPI is in blue, n=3, scale bar: 50 µm.

**Canonical and non-canonical Wnt components are sequentially de-repressed in heart tissue upon KLF15 loss**

The Wnt pathway is well known to be involved in pathological tissue remodeling. Thus, we aimed to better understand the dynamics of Wnt pathway de-repression triggered by KLF15 loss contributing to tissue remodeling. We analyzed age-specific pathway enrichment using GSEA [18]. At P10, no significantly enriched pathways were observed. At 4w, Wnt nuclear (β-catenin-dependent, canonical) was significantly enriched along with hematopoietic and immunological processes. Wnt pathway was also enriched at 20w, but genes contributing to this enrichment were different than in 4w, and corresponded to Wnt non-canonical components. In accordance with the activation of tissue remodeling and metabolic processes, inflammatory, hypertrophic, metabolic and sarcomeric reorganization pathways (Thromboxane, G-protein, insulin/glucagon, RhoA signaling, respectively) were also found enriched at 20w in *Klf15* KO hearts (Fig. 4A, B). Validation of this data confirmed upregulation of reported Wnt canonical targets *Axin2*, *CD44* and *Sox4* in both 4 and 20 weeks old *Klf15* KO hearts*;* and non-canonical target *Wnt5b* only in 20 weeks old *Klf15* KO hearts (Fig. 4C). Further, TCF7L2 and WNT5b proteins were upregulated in 20 weeks old *Klf15* KO hearts (Fig. 4D). Interestingly, we observed an upregulation of novel, putative, cardiac Wnt non-canonical targets-*Shisa3* and *Dact3* in 20w *Klf15* KO hearts (Fig. 4E). SHISA3 upregulation was also validated at the protein level. These factors were so far, not described in the context of cardiac biology. Thus, we first tested their expression in cardiac tissue. We detected very low *Shisa3* and *Dact3* expression in the embryonic heart, increasing in the fetal heart and significantly decreasing in the healthy adult heart (20w) (Fig. 4F). These data suggest that *Shisa3* and *Dact3* may be a part of the activated fetal gene program in *Klf15* KO ventricles. Altogether, this indicates that cardiac-specific Wnt canonical activation occurred between P10 and 4w, which is followed by a consequent activation of Wnt non-canonical pathway and progression towards heart failure between 4w and 20w of age in *Klf15* KO mice, strongly supporting its contribution to heart remodeling downstream of KLF15.

## Figure 4

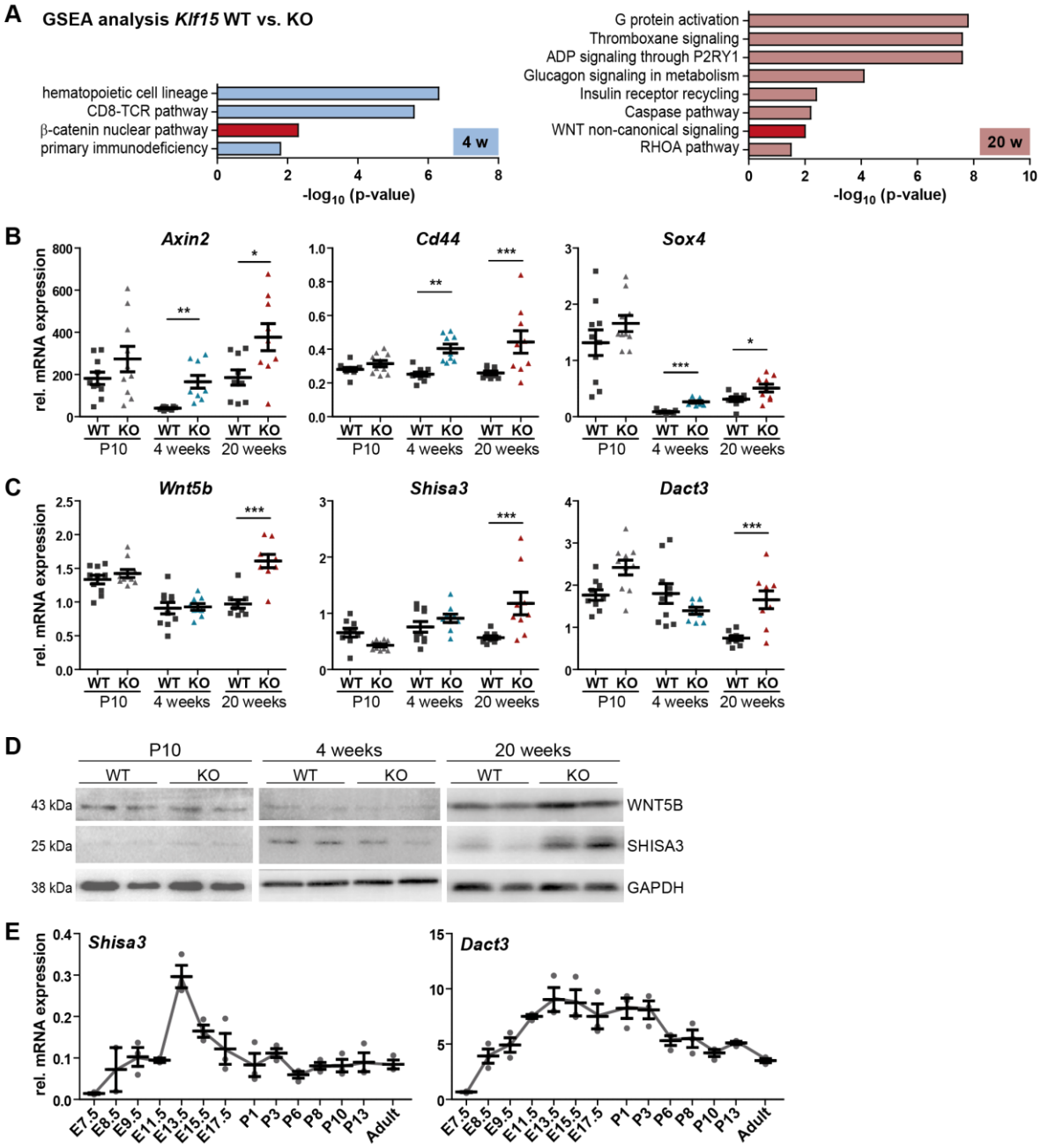


**Figure 4: Sequentially de-repression of canonical and non-canonical Wnt signaling upon loss of KLF15 in the adult heart. a,** Gene Set Enrichment Analysis (GSEA) showing enrichment of the Wnt/β-catenin nuclear pathway gene set (as compared to WT) in 4w hearts as well as enrichment of the Wnt signaling gene set corresponding to non-canonical pathway in 20w *Klf15* KO heart tissue. **b,** qPCR validations of canonical (*Axin2, Cd44, Sox4*) and **c,** non-canonical (*Wnt5b*) Wnt targets and Wnt modulators *Shisa3* and *Dact3* in P10, 4w and 20w *Klf15* KO hearts; normalized to *Tbp* n≥9; Student's *t*-test, *p≤0.05, ***p≤0.001. **d,** Immunoblots depicting WNT5B and SHISA3 protein levels in P10, 4w and 20w *Klf15* WT and KO hearts; GAPDH was used as loading control, representative n=2 are shown. **e,** qPCR analysis depicting increasing fetal and decreasing adult cardiac *Shisa3* and *Dact3* expression, normalized to *Tbp*, n=3 (embryonic tissues were pooled as followed per N: E7.5-8.5 20 embryos; E9.5-11.5 8-10 hearts; E13.5-15.5 4-6 hearts).

**KLF15 loss revealed *Shisa3 as* a novel cardiac gene with endothelial signature and upregulated in pathological remodeling**

Next, we were interested in the expression of *Shisa3* in the context of pathological heart remodeling, upon experimentally validated induced pressure overload (by transaortic constriction (TAC)) and myocardial infarction (MI). We found *Shisa3* significantly upregulated in WT hearts upon TAC, already 1 week after induction and 4 weeks post-MI, and this upregulation was exacerbated in TAC/MI *Klf15* KO hearts (Fig. 5A). Interestingly, analysis of SHISA3 expression revealed its localization in interstitial, (CTNT-negative) cells in adult heart sections, as demonstrated by immunofluorescence analysis in *Klf15* KO and WT hearts. In the healthy adult heart, the number of SHISA3 positive (CTNT-negative) cells was very low, but they were increased in *Klf15* KO left ventricular myocardium. Further confirming the transcriptomic data, SHISA3 (CTNT-negative) expressing cells were significantly increased in WT hearts upon TAC and MI, which were more abundant in *Klf15* KO hearts (Fig. 5B). Next, we specifically isolated non-CMs after 2 weeks of induced TAC in WT mice, and found significant upregulation of *Shisa3* (Fig. 5C). In order to identify the nature of the SHISA3 cells, we isolated non-CMs cell fraction from *Klf15* KO hearts and tested for co-localization of the non-CMs marker Actin, alpha 1, skeletal muscle (ACTA1)- known to be activated in the heart upon remodeling. *In vitro*, SHISA3-positive cells, which were increased in *Klf15* KO non-CM cultures, were not co-localizing with ACTA1 (Fig. 5D). *In vivo*, SHISA3 cells showed no co-localization with POSTN-positive cells in the *Klf15* KO infarcted heart, (Fig S4) confirming that they were not originating from the fibroblastic lineage. Next, we tested Endomucin (EMCN) and PECAM-1 co-expression, both markers of early and late endothelial lineage, respectively. Although co-expression of PECAM-1 and SHISA3 was not evident, we observed a co-localization of SHISA3 and EMCN *in vivo*, in *Klf15* KO hearts, and also in WT hearts upon TAC and MI (Fig. 5E). Accordingly, expression of *Pecam-1* and *Emcn* were significantly increased in WT ventricles 8 weeks post-TAC, where *Shisa3* expression was also found increased (Fig. 5F). This is in line with our previous observations showing increased PECAM-1-positive cells in *Klf15* KO adult hearts [8]. Validating the role of EMCN-positive cells in hypertrophic remodeling, we also found its increased expression in 1 week post-TAC cardiac ventricular tissue (Fig. 5G).

Next, in order to identify transcription factors (TFs) that might contribute to the observed age-specific appearance of increased endothelial phenotype, we performed TRANSFAC motif search analysis on the promoters of dysregulated genes in *Klf15* KO hearts. We identified in 4w and 20w-

specific upregulated DEGs, TFs closely associated to muscle and endothelial/hematopoietic development, lipid metabolism and chromatin remodeling (MYOGNF1, GATA1, TAL1, SP3, CDX2, CEBPδ and YY1) [19-21]. Along with this observation, we validated the upregulation of angiogenic factors *Angpt2, Edn3*, *Tnfrsf12a* at 4 and 20w. At P10-specific upregulated DEG promoters, we observed a significant enrichment of TFs involved in cellular stress, neuronal differentiation and lipid homeostasis (NFκB, HIF1α, BRN2 and SREBP1) [22-24]. Only significantly enriched motifs appearing in the top 10 are depicted ($p<0.05$) (Fig. 5H). These data further support that loss of KLF15 mediates an age-dependent de-repression of TFs, leading to tissue remodeling, with a strong endothelial signature. Altogether, our results report that SHISA3 is a novel marker of pathological tissue remodeling and that these cells belong to an early endothelial cell (EC) lineage, which are increased upon loss or reduction of KLF15.

Figure 5

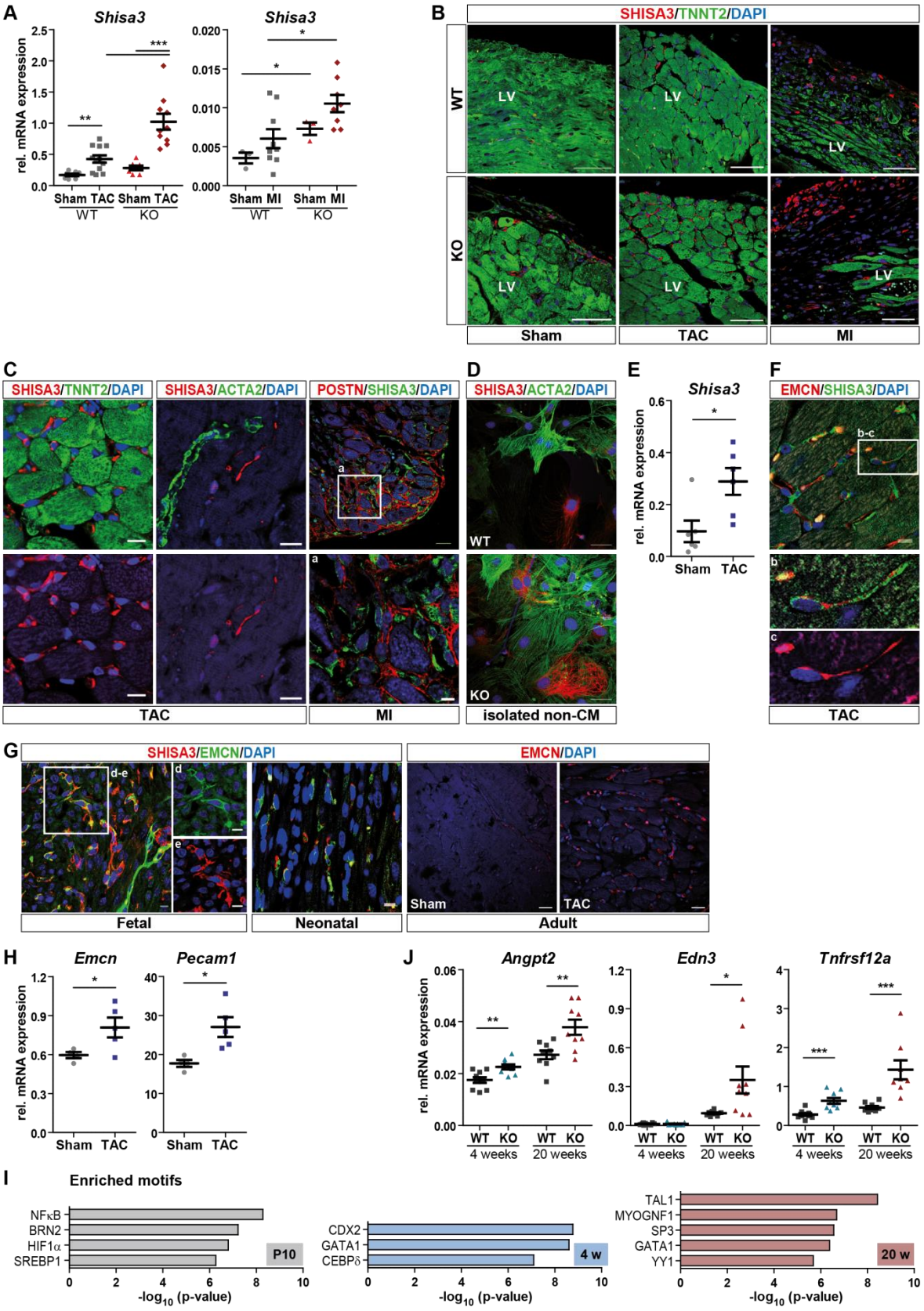
A
Shisa3
rel. mRNA expression
Sham TAC Sham TAC
WT KO
Shisa3
Sham MI Sham MI
WT KO
B
SHISA3/TNNT2/DAPI
WT
KO
LV
Sham
TAC
MI
C
SHISA3/TNNT2/DAPI
SHISA3/ACTA2/DAPI
POSTN/SHISA3/DAPI
TAC
MI
D
SHISA3/ACTA2/DAPI
WT
KO
isolated non-CM
E
Shisa3
rel. mRNA expression
Sham TAC
F
EMCN/SHISA3/DAPI
b-c
TAC
G
SHISA3/EMCN/DAPI
d-e
Fetal
Neonatal
EMCN/DAPI
Sham
TAC
Adult
H
Emcn
Pecam1
rel. mRNA expression
Sham TAC
Sham TAC
J
Angpt2
Edn3
Tnfrsf12a
rel. mRNA expression
WT KO WT KO
4 weeks 20 weeks
I
Enriched motifs
NFκB
BRN2
HIF1α
SREBP1
P10
CDX2
GATA1
CEBPδ
4 w
TAL1
MYOGNF1
SP3
GATA1
YY1
20 w
-log10 (p-value)

**Figure 5: SHISA3 in cardiac endothelial remodeling in disease. a,** qPCR analysis showing increased *Shisa3* expression 2 weeks post-TAC in WT mice and its exacerbated upregulation in *Klf15* KO TAC hearts. Similar *Shisa3* upregulation was observed in 4 weeks post-MI hearts, n≥7 for TAC and n≥4wfor MI. **b,** Representative IF images showing increased SHISA3 (red) expression in interstitial, TNNT2 (green)-negative cells of 2 weeks post-TAC and 4 weeks post-MI in left ventricular (LV) sections. This increased expression was further augmented in the corresponding *Klf15* KO ventricles, n=3. **c,** Representative IF images showing SHISA3 (red) expression in interstitial, TNNT2 (green)-negative and ACTA2 (green)-negative cells of 2 weeks post-TAC as well as in POSTN-(red)-negative cells in 4 weeks post-MI hearts. **d,** Representative IF images depicting increased SHISA3 (red) expression in isolated non-CM of adult *Klf15* KO hearts, which do not co-localize with ACTA2 (green) cells, n=5. **e,** Quantification by qPCR showing increased *Shisa3* expression in non-CM cells of 2 weeks post-TAC hearts; n=6. **f,** Representative IF images showing co-localization of SHISA3 (green) with the endothelial marker Endomucin (EMCN, red) in of 2 weeks post-TAC hearts. **g,** Representative IF images showing co-localization of SHISA3 (red) and Endomucin (EMCN, green) in fetal (E18) and neonatal (P5) as well as EMCN (red) in adult (20w) sham and TAC hearts. **h,** qPCR showing increased *Emcn* and *Pecam1* expression in 8 weeks post-TAC heart tissue; n≥4. **i,** Motif search analyses depicting enriched endothelial and hematopoietic transcription factors specifically in upregulated DEGs of 4wand 20 weeks-old *Klf15* KO hearts. **j,** qPCR validation of upregulated angiogenic factors *Angpt2, Edn3, and Tnfrsf12a* at 4w and 20w *Klf15* KO hearts, n≥9. qPCR in (A), (D), (G), and (I) were normalized to *Tbp*; (A) 1-way ANOVA with Bonferroni's multiple comparison test, (D), (G), and (I) Student's *t*-test, *p≤0.05, **p≤0.01, ***p≤0.001. Scale bar in (B): 50 µm, (C): 20 µm, (D): 10 µm, (E): 10 µm, (F, fetal): 20 µm, (F, neonatal): 10 µm, (F, adult): 20 µm; white boxes in (C/a) and (E/a-d) show higher magnification of the selected area.

## KLF15 and Wnt reciprocally regulate their cardiac target gene *Shisa3*

SHISA members were described as modulators of the Wnt signaling in the context of development [25]. In this study we showed that *Shisa3* expression is stimulated in the stressed heart, along with a loss of KLF15 expression and Wnt canonical activation. We previously demonstrated that a mouse model of Wnt canonical activation mediated by β-catenin stabilization (β-cat$^{\Delta ex3}$) and TCF7L2 upregulation, recapitulated the molecular hallmarks of pressure overload and also showed increased *Shisa3* expression [26]. In this mouse model, interstitial SHISA3 (CTNT-negative) expressing cells were significantly increased in ventricular myocardium in comparison to control hearts, although to a lesser extent than in *Klf15* KO hearts (Fig. 6A). We also found increased SHISA3 protein levels in β-cat$^{\Delta ex3}$ hearts (Fig. 6B). Given the similarity to the *Klf15* KO hearts, we investigated GO of commonly upregulated genes in β-cat$^{\Delta ex3}$ and *Klf15* KO hearts. Interestingly, we found enrichment of cell growth, muscle development and blood vessel morphogenesis processes (Fig. 6C). Next, we overlapped genes bound by TCF7L2 [26] and KLF15 [16] in the adult heart and observed that they were enriched in developmental processes including Wnt signaling activation and vasculogenesis (Fig. 6D). Moreover, motif analysis on common upregulated DEGs in *Klf15* KO and β-cat$^{\Delta ex3}$ hearts showed again, TFs associated with muscle and endothelial development (Fig. S4).

Aiming to investigate whether *Shisa3* expression depends on Wnt canonical activation, we tested its expression in a developmental cardiac environment, upon Wnt modulation *ex vivo*. Embryonic mouse hearts post-coitum (E)14.5 were isolated and cultured under a rotating culture system for 24h in WNT3A-containing medium or normal culture medium as control ($n \geq 5$, 3 independent experiments). Upregulation of the Wnt target gene *Axin2* and *Shisa3* was confirmed by qPCR analysis, confirming Wnt activation and *Shisa3* regulation in response to Wnt activation, respectively (Fig. 6E). Of note, the observed, high dispersion in expression is due to the technique, which does not allow for a homogenous incubation of the conditional medium with all ventricular cells in a 3D system. Immunofluorescence analysis revealed that SHISA3-expressing cells were negative for CTNT, as detected in the adult heart and were uniformly localized in the periphery of the ventricle in the control heart. Hearts upon WNT3A treatment showed increased SHISA3-expressing cells in ectopic location (Fig. 6F). In line with the analysis in the postnatal heart, we observed SHISA3/EMCN positive cells, as well as cells individually expressing SHISA3 or EMCN, indicating that double-positive cells are cells in transition (Fig. 6G).

## Figure 6

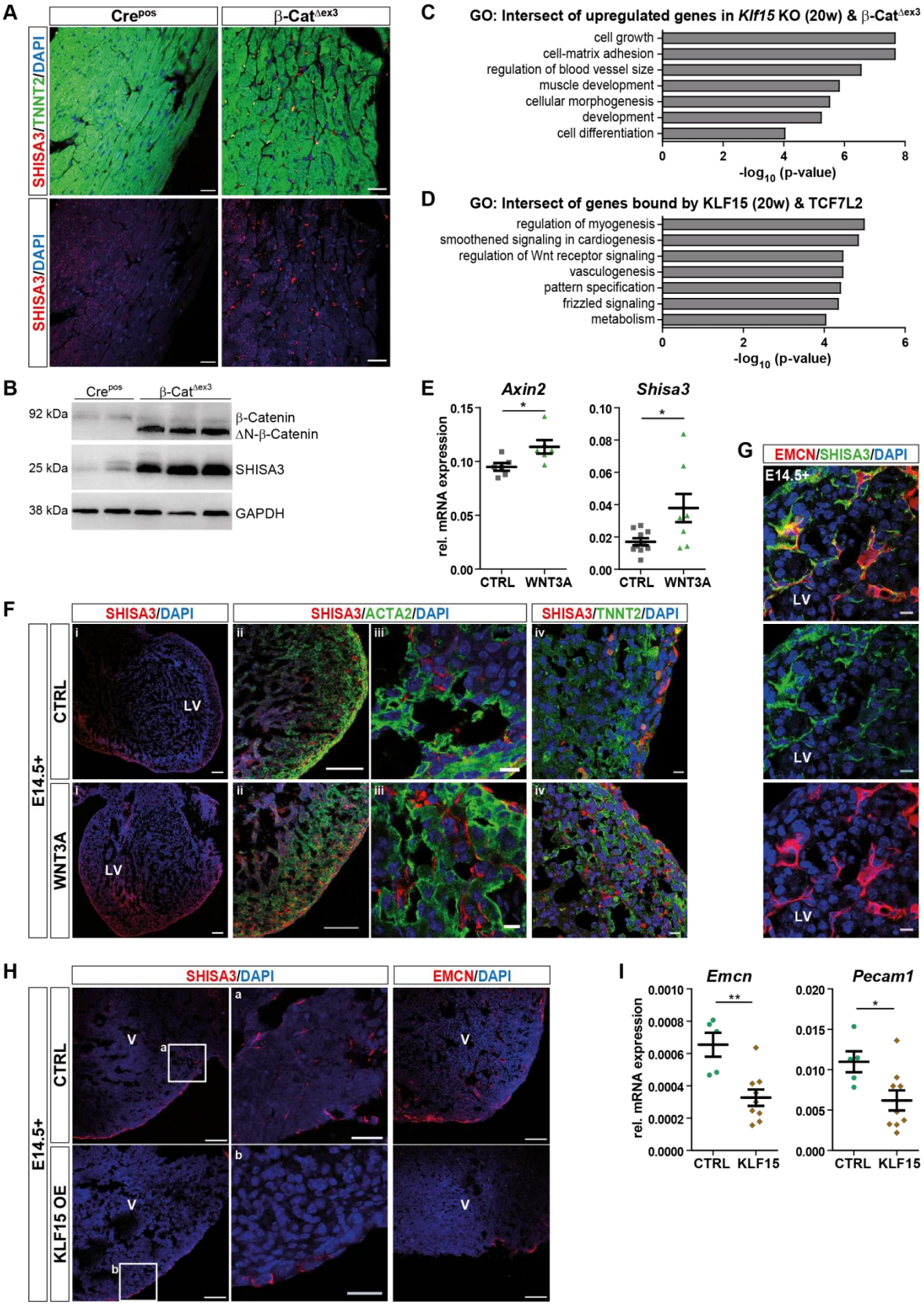
A
Cre^pos
β-Cat^Δex3
SHISA3/TNNT2/DAPI
SHISA3/DAPI
B
Cre^pos
β-Cat^Δex3
92 kDa
β-Catenin
ΔN-β-Catenin
25 kDa
SHISA3
38 kDa
GAPDH
C
GO: Intersect of upregulated genes in Klf15 KO (20w) & β-Cat^Δex3
cell growth
cell-matrix adhesion
regulation of blood vessel size
muscle development
cellular morphogenesis
development
cell differentiation
0
2
4
6
8
-log10 (p-value)
D
GO: Intersect of genes bound by KLF15 (20w) & TCF7L2
regulation of myogenesis
smoothened signaling in cardiogenesis
regulation of Wnt receptor signaling
vasculogenesis
pattern specification
frizzled signaling
metabolism
0
2
4
6
-log10 (p-value)
E
Axin2
Shisa3
rel. mRNA expression
0.15
0.10
0.05
0.00
0.10
0.08
0.06
0.04
0.02
0.00
*
*
CTRL
WNT3A
CTRL
WNT3A
F
SHISA3/DAPI
SHISA3/ACTA2/DAPI
SHISA3/TNNT2/DAPI
E14.5+
CTRL
WNT3A
i
ii
iii
iv
LV
G
EMCN/SHISA3/DAPI
E14.5+
LV
LV
LV
H
SHISA3/DAPI
EMCN/DAPI
E14.5+
CTRL
KLF15 OE
V
a
b
I
Emcn
Pecam1
rel. mRNA expression
0.0010
0.0008
0.0006
0.0004
0.0002
0.0000
0.020
0.015
0.010
0.005
0.000
**
*
CTRL
KLF15
CTRL
KLF15

**Figure 6: *Shisa3* is co-regulated by Wnt canonical signaling and KLF15 in cardiac tissue. a,** Representative IF images showing increased SHISA3 (red) expression in TNNT2 (green)-negative non-CM of murine cardiac tissue from a mouse model with inducible CM-specific β-catenin stabilization (β-Cat$^{\Delta ex3}$) with Wnt canonical activation and corresponding controls (Cre$^{pos}$); DAPI (blue) for stained nuclei, n=3. **b,**Immunoblots showing increased SHISA3 expression protein in β-Cat$^{\Delta ex3}$ hearts; GAPDH was used as loading control. **c,** GO biological processes of commonly upregulated genes between 20w *Klf15* KO and β-Cat$^{\Delta ex3}$ hearts, p<0.05. **d,** GO biological processes of genomic regions commonly bound by KLF15 in the healthy adult and TCF7L2 in Wnt-activated (β-Cat$^{\Delta ex3}$), diseased adult hearts, p<0.05. **e,** qPCR validating an increase in *Axin2* and *Shisa3* expression in E14.5 embryonic hearts treated with WNT3A conditioned medium *ex vivo;* normalized to *Tbp*, n≥6. **f,** SHISA3 expression in control (CTRL) and WNT3A conditioned medium-treated E14.5 hearts showing increased SHISA3-positive, TNNT2- and ACAT2-negative cells upon WNT3a treatment, n=3/≥8 hearts per group and experiment. **g,** SHISA3 and EMCN expression in control (CTRL) and WNT3A-treated E14.5 hearts showing partial co-localization. **h,** Representative IF images showing a markedly reduced SHISA3 and EMCN expression (red) in KLF15 OE embryonic cardiac ventricles (v) vs. GFP-control electroporated hearts; white boxes (a-b) depict a higher magnification of the SHISA3-expressing cells; DAPI (blue) as nuclear stain, n≥5/2 independent experiments. **i,** qPCR validation of the endothelial cell markers *Emcn* and *Pecam1* downregulation upon *Klf15* OE in E14.5 hearts *ex vivo*, n≥5. qPCR in (E) and (I) were normalized to *Tbp*; Student's *t*-test, *p≤0.05, **p≤0.01. Scale bars in (A): 50 µm; (F): 100 µm (SHISA3), 200 µm (SHISA3/ACTA2) and 10 µm (SHISA3/TNNT2). Scale bar in (A), (F), and (G): 20 µm.

We next asked whether TCF7L2 would directly bind to *Shisa3* regulatory regions. Analysis of published TCF7L2 ChIP-seq data from heart ventricular tissue showed no binding of TCF7L2, neither at proximal nor at distal regions of *Shisa3* gene body. Only putative binding sites for the Wnt target c-Myc were identified, along with YY1 and TAL1, which were also identified by the TRANSFAC motif search analysis. Interestingly, ChIP-seq data showed a clear binding for KLF15, which correlated to H3K27me3, a known histone modification highly associated with transcriptional repression [27, 28], at the *Shisa3* 5´proximal regulatory region in the normal adult heart (Fig. 7A). This data suggests that downstream Wnt canonical transcriptional mediators, other than TCF7L2, activate *Shisa3* expression; and that repression of *Shisa3* in the adult heart may be mediated by direct KLF15 binding to its promoter region. To functionally test if KLF15 directly represses *Shisa3* in the heart, we ectopically overexpressed *Klf15* in fetal hearts at E14.5 by electroporation and cultured them for 24 h (*Klf15* OE). Successful gene transfer by electroporation was checked by qPCR quantification of *Klf15* transcripts (Fig. 7B). Immunofluorescence analysis of these hearts showed that ectopic *Klf15* OE in embryonic hearts markedly reduced the expression of *Shisa3* in comparison to control electroporated hearts at the site of electroporation (Fig. 7C). Moreover, expression of *Pecam-1* and *Emcn* were significantly reduced upon KLF15 overexpression (Fig. 7D). EMCN-expressing cells were also found reduced in KLF15 OE embryonic hearts at the site of electroporation (Fig. 7E). These data strongly suggest that a combination of high levels of Wnt transcriptional activity, along with low *Klf15*

expression coordinates a cascade of TFs promoting the expression of *Shisa3*, which contributes to the maladaptive, pathological, endothelial remodeling in the stressed adult heart.

**Figure 7**

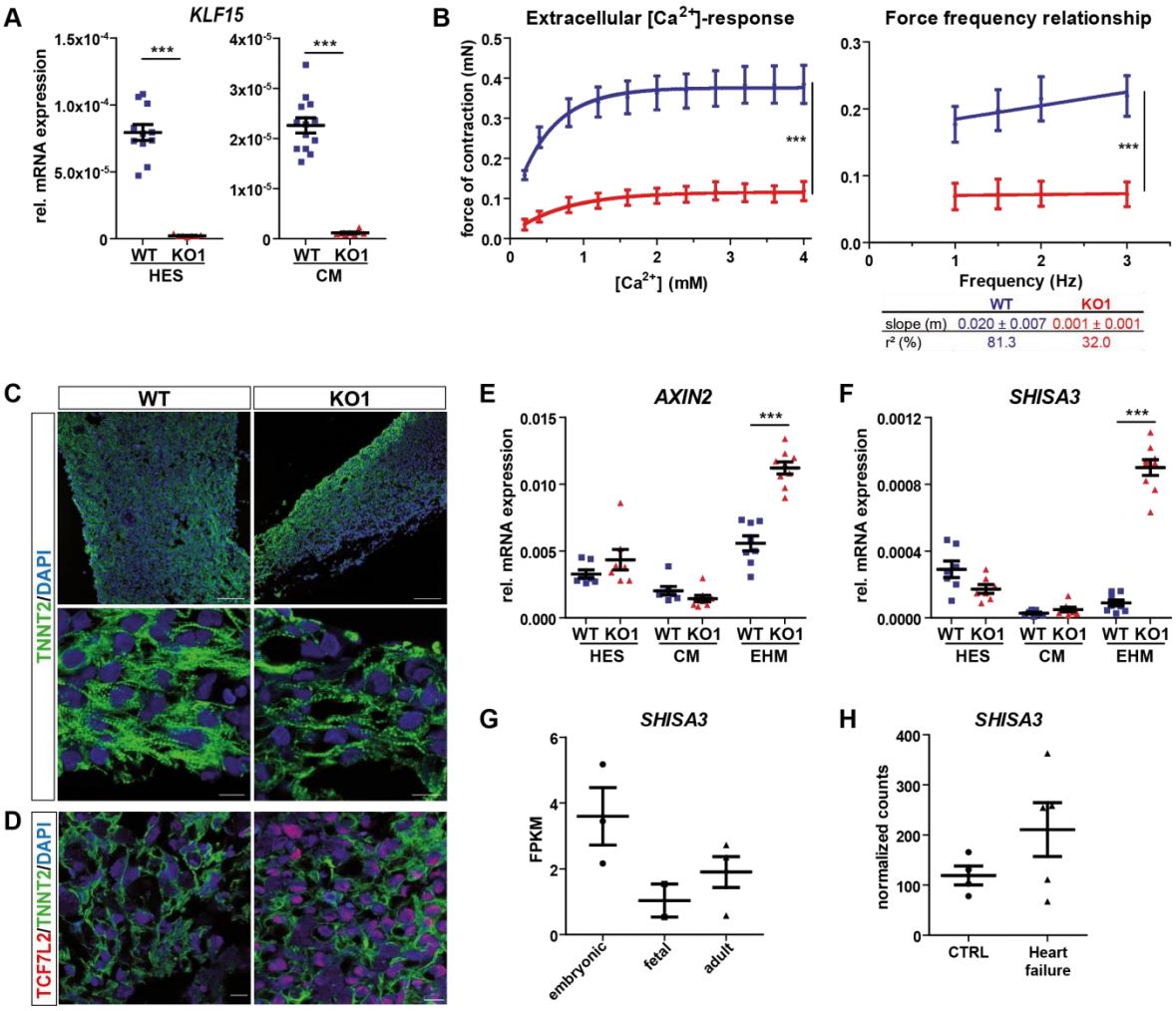


**Figure 7: KLF15 loss in human cells mimics murine function in myocardium. a,** qPCR validating loss of *KLF15* transcript in both human embryonic stem cells (HES) and HES-derived cardiomyocytes (CM) in *KLF15* KO line no. 1 compared to *KLF15* WT controls ; n≥7. **b,** *KLF15* KO1 EHMs exhibit reduced extracellular $Ca^{2+}$ response and force-frequency relationship; n=3; 2-way ANOVA with Tukey's multiple comparison test, ***p≤0.001. **c,** Representative IF from Engineered Human Myocardium (EHM) (WT and KO1) showing TNNT2 expression and significantly increased TCF7L2 expression in TNNT2-positive cells in *KLF15* KO EHMs (**d**). **e,** qPCR showing upregulated Wnt target gene *AXIN2* expression in *KLF15* KO EHMs, but not in HES and the 2D CMs. **f,** qPCR showing upregulation of *SHISA3* only in *KLF15* KO EHM tissues, n≥9. **g,** FPKMs of *SHISA3* expression in human embryonic, fetal and adult hearts, n=3. **h,** Normalized counts of *SHISA3* in healthy and failing human left ventricular cardiac tissue, n=3. qPCR in (A), (E) and (F) were normalized to GAPDH; Student's *t*-test, ***p≤0.001. Scale bar in (C) and (D): 20 µm.

**SHISA re-expression is a feature of human myocardial remodeling**

To test the relevance of KLF15 loss in humans, we generated a homozygous knockout hESC line [29]. *KLF15*-KO hESCs underwent differentiation into morphologically normal CMs, thus indicating that KLF15 is not essential in human CM lineage specification. Next, engineered human myocardium (EHMs) were generated from both WT and *KLF15*-KO-derived CMs. Significantly impaired functional performance and a blunting of the positive force-frequency relationship was apparent in EHMs generated with *KLF15*-KO CMs (Fig. 8B, S5B). Morphologically, *KLF15*-KO-EHMs do not show major differences relative to WT-EHMs (Fig. 8C, S5C). Immunofluorescence assessment of TCF7L2 expression (representing Wnt canonical activation) showed significantly higher nuclear expression in CTNT-positive cells of *KLF15*-KO EHMs compared to WT-EHMs (Fig. 8D)Activation of Wnt canonical signaling as indicated by *AXIN2* transcript upregulation, was also observed in *KLF15*-KO EHMs, but not in 2D embryonic KLF15-KO CMs (Fig. 8E).. All these observations support Wnt canonical activation. Our findings collectively indicate that in the EHM model, KLF15 showed a strong, conserved, repressive function on the Wnt canonical signaling pathway, regulating tissue homeostasis similar to the mouse heart.

SHISA homologs were reported also in human cells [25, 30]. We found that expression of human *(h)SHISA2* and *3* in ventricular myocardium decreased from embryonic to adult postnatal heart, similar to the mouse heart. Interestingly, *hSHISA2* expression was significantly upregulated in left ventricles of patients with heart failure, whereas *hSHISA3* showed a non-significantly increased expression (N=5/per group Fig. S5D). Moreover, activation of *hSHISA3* was also detected in *KLF15*-KO EHMs, while *KLF15*-KO embryonic CMs showed no significant changes as compared to controls (Fig. 8F). Interestingly, normalized counts of *hSHISA2*, but not 3 were significantly upregulated in human heart failure (Fig. S5E). In line with the mouse data, expression of *hSHISA2* and *3* was detected in non-CM human cell fraction negative for ACTA1 (Fig. S5F). Analysis of published transcriptomic data showed a relevant expression of hSHISA3 in highly irrigated tissues such as gastrointestinal organs; kidney, lung and heart including ventricles and vasculature (aorta and coronary arteries) (Fig. 8G). All these data indicate a strong, evolutionarily conserved *SHISA* re-activation in the adult heart upon pathological stress and strongly suggest the contribution of SHISA to vascular remodeling, further supporting its dependency on Wnt signaling and KLF15 expression.

**Figure 8**

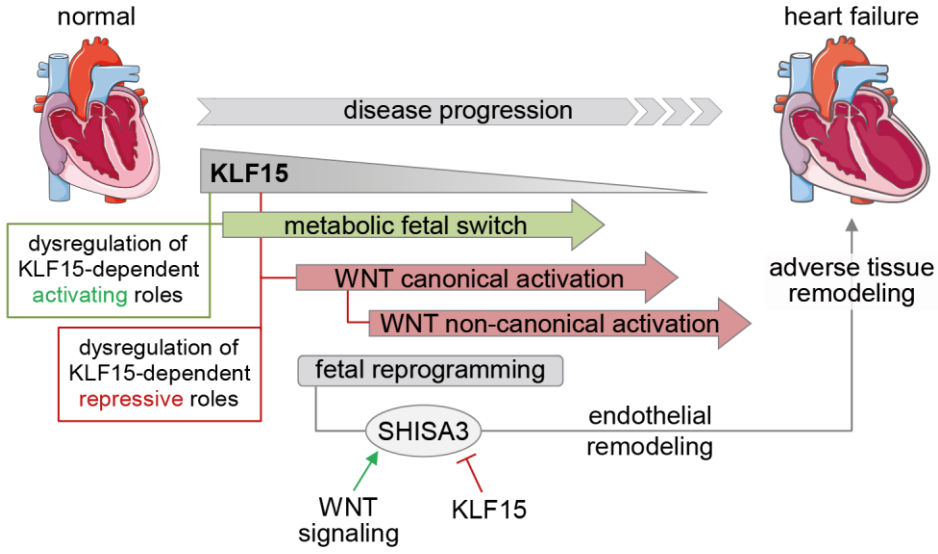


**Figure 8: Schematic representation of the findings.** Our results revealed age-specific, dynamic, transcriptional functions mediated by KLF15, crucial for cardiac homeostasis. We report that postnatally, KLF15 persistently activates cardiac metabolism, but represses in an age-dependent manner, pathological, hypertrophic pathways associated with fetal gene reprogramming, including the Wnt pathway. Within this specific program, we identified a so far uncharacterized cardiac gene - *Shisa3*, normally expressed in the developing heart and upregulated in cardiac remodeling, showing endothelial characteristics. KLF15 and Wnt signaling reciprocally regulate SHISA3 expression and induce an endothelial transcriptional program in cardiac remodeling. Heart illustrations were taken from Servier Medical Art (https://smart.servier.com).

## Discussion

The roles of KLF15 in gluconeogenesis, adipogenesis, muscle hypertrophy and circadian rhythm[5-7] have been well characterized. In the adult heart, KLF15 is known to repress major hypertrophic signaling pathways during cardiac stress; however its homeostatic role remained elusive[7, 12, 13, 15]. Our study demonstrated age-specific transcriptional functions of KLF15, which are essential for homeostasis in the unstressed postnatal heart. Our previous and current findings demonstrated that loss of KLF15 resulted in reduced systolic function and chamber dilation beyond 12 weeks at baseline[8]. Other groups have reported either mild cardiac hypertrophy[7] or no phenotype[13, 16] in *Klf15* KO mice without exposure to stress stimuli. This can be due to the use of younger mice. Mechanistically, we showed that the absence of KLF15 resulted in a downregulation of metabolic pathways including amino acid, carbohydrate and fatty acid metabolism, occurring early after birth and independent of age. These observations strongly support a continuous, activating function of KLF15 in regulating cardiac metabolism which is in line with previous findings[5, 6, 16]. However, it seems not to result in immediate major functional

changes. In contrast, genes categorized under developmental tissue remodeling processes were upregulated later between 4w and 20w. This was accompanied by the onset of fetal reprogramming and CMs structural changes, which are characteristics of maladaptive hypertrophy, and resulting in heart failure in *Klf15* KO mice. This revealed essential KLF15 stage-specific repressive action on tissue remodeling processes. Interestingly, KLF15 has no relevant roles in cardiac development indicating its exclusive role in repressing "adaptation" pathways in the fully mature heart, consequently leading to the development of pathological remodeling upon its absence.

In agreement with our previous work showing an inhibitory role of KLF15 on the Wnt pathway, we now showed that Wnt canonical activation occurred at 4w, but not early, in hearts lacking KLF15. This suggests that regulation of Wnt signaling in early postnatal life is guaranteed by additional factors. In the adult heart, quiescent Wnt signaling is essential for homeostasis and its re-activation results in cardiac developmental reprogramming along with severe heart failure[23, 46]. Activation of Wnt signaling in *Klf15* KO hearts, accompanied by TCF7L2 upregulation, coincided with chromatin remodeling processes, cell cycle activation and cardiac de-differentiation. This is similar to the changes observed upon cardiac Wnt signaling activation, mediated by β-catenin stabilization (β-cat$^{\Delta ex3}$), which results in TCF7L2 upregulation and induces increased active chromatin and developmental gene program activation[23]. Interestingly, a sequential activation of Wnt non-canonical *Wnt5b* and inhibitors *Shisa3* and *Dact3*[47-49] was observed at 20w, but not at earlier stages. This is similar to the initial activation of Wnt/β-catenin signaling during heart development followed by Wnt non-canonical pathway activation, which serves to repress the canonical signaling and regulates cell polarity[50]. In line with this finding, *Klf15* KO hearts at 20w showed upregulation of cell growth and CM cytoskeletal re-organization, similar to hearts with cardiac Wnt signaling activation[23]. Moreover, it is tempting to speculate that activation of Wnt canonical repressors (*Wnt5b*, *Shisa3* and *Dact3*) constitutes a feedback mechanism trying to modulate abnormal Wnt activity. Altogether, this suggests a strong contribution of aberrant Wnt canonical and non-canonical activation to maladaptive tissue remodeling in *Klf15* KO hearts. We don't exclude the contribution of other pathways to the *Klf15* KO cardiac phenotype. In fact, by *de novo* motif search analysis, we identified MEF2 and GATA motifs in upregulated DEGs in *Klf15* KO hearts at 4w and 20w, which fits with KLF15's repressive function on these genes[7].

We previously characterized a Wnt transcriptional inhibitory nuclear complex including KLF15, β-catenin and TCF7L2[8]. In our present study, we showed that KLF15 occupied regulatory regions of classical Wnt targets and tissue remodeling genes containing TCF7L2 binding sites. In the healthy heart, these regions showed low TCF7L2 occupancy and characteristics of silenced chromatin as indicated by low H3K27ac binding. This supports the repressive function of KLF15 on Wnt target activation at the chromatin level in the healthy hearts. Importantly, our study showed that although KLF15 is highly expressed in other organs, dysregulation of Wnt canonical signaling is observed specifically in the heart. This data indicates an exquisite regulation mediated by KLF15 on Wnt signaling and may provide new therapeutic targets for controlling cardiac-specific gene activation, considering the ubiquitous nature of Wnt signaling. *KLF15* expression is known to be reduced not only in mouse, but also in human cardiovascular diseases[13, 16, 17]. However, the mechanism in human cells remained elusive. We showed that similar to the *Klf15* KO mouse model, the lack of KLF15 did not affect cardiomyocyte generation or Wnt signaling regulation after 2D differentiation in immature cardiomyocytes. However, after 3D maturation, *KLF15* KO EHMs showed impaired contractile performance as well as activation of Wnt canonical signaling with TCF7L2 upregulation and target gene activation. Accordingly, Wnt activation results in electrical remodeling in the murine adult heart [46]. These data showed a role for KLF15 in human tissue and indicate that KLF15-dependent Wnt regulation is conserved in human cells and serves as an entry point for further pharmacological investigation.

The analysis of common downstream signaling pathways triggered by the lack of KLF15 and activation of the Wnt canonical signaling, uncovered a KLF15 and Wnt co-regulation of SHISA3. We showed that *Shisa3* is a fetal gene silenced in the homeostatic adult heart, but upregulated in the diseased adult mouse and human heart. The SHISA protein family comprises 5 sub-families in vertebrates [47]. The founding member of this family, *Xenopus Shisa1*, plays a role in head maturation during development, through inhibition of Wnt and FGF signaling[48], however the role of *Shisa* members in cardiac biology was uncovered. Our study shows for the first time, that *Shisa3* belongs to the reactivated developmental cardiac gene program in the stressed heart and that KLF15 and Wnt are important regulators of its expression. Interestingly, SHISA3 expressing cells showed characteristics of EC lineage, as demonstrated by a co-localization with the early mouse and human EC marker EMCN[33, 34]. Moreover, SHISA3 and

EMCN showed partially overlapping expression, unearthing the existence of a novel precursor cellular-transition state contributing to early EC development.

Similarly to SHISA3, EMCN expression is high in fetal heart, very low in the healthy adult heart, but increased in the hypertrophic heart, along with an upregulation of PECAM1 expression. The role of EMCN in heart failure is unknown. However, data are available that support its role in tumor angiogenesis and EC regulation[33, 51]. Further supporting an EC fate promotion, our transcriptome and motif search analysis revealed genes and TFs closely associated to endothelial development[52, 53] in upregulated DEGs in *Klf15* KO hearts. The new data is well-consistent with our previous work, in which we showed that *Klf15* KO heart progenitors have increased endothelial signature along with PECAM1 upregulation and this was mediated by Wnt activation [8]. Accordingly, WNT3A canonical signaling controls embryonic EC homeostasis[54, 55]. In the fetal heart, SHISA3 expression was stimulated by activation of WNT3A canonical signaling and conversely, ectopic expression of KLF15 reduced not only SHISA3, but also EMCN and PECAM1 expression. This mimicked the situation in the adult heart, in which KLF15 is highly expressed and Wnt signaling and SHISA3 low. All these results fit with the notion that the EC program is controlled synergistically by multiple TFs[53] and that KLFs members exert distinct biological functions in ECs homeostasis[19]. Thus, our results suggest that Wnt canonical signaling and KLF15 control SHISA3 expression and influence EC homeostasis in the stressed heart, where imbalanced angiogenesis drives the progression to heart failure[56-59]. In the healthy heart, SHISA3 is repressed by reciprocally low Wnt canonical transcriptional activity and high KLF15 expression. In contrast, reduced levels of KLF15 along with Wnt activation in the stressed heart led to increased SHISA3 expression. Increased SHISA3 expression in this context may impair proper EC maturation. Similar to mouse, we showed that human SHISA3 was expressed at low levels in fetal and adult ventricles and increased in patients with heart failure, where KLF15 is known to be downregulated and Wnt activated[13, 16, 23]. Consistently, SHISA3 was upregulated in *KLF15* KO EHM along with Wnt activation. In humans, SHISA3 has been previously associated with cancer and human arteriovenous EC identity[29, 60, 61], indicating a role in angiogenesis-related processes.

In summary, our work revealed a tissue- and age-specific role of KLF15-mediated Wnt repression in the postnatal heart affecting tissue remodeling. We identified a novel Wnt and KLF15 common target gene belonging to the SHISA family and attributed its contribution to EC homeostasis in the pathological mouse and human heart (summarized in Fig. 9). SHISA3 may

represent an early immature EC marker. Since myocardial perfusion is a key requisite for heart homeostasis and this is challenged upon pathophysiological stresses[1, 56-59], this work undoubtedly paves the basis for unraveling the initial mechanisms of EC remodeling, which will help to identify efficient targets maintaining a favorable angiogenetic balance in tissue remodeling and adaptation.

## Materials and Methods

### Mouse strains

The generation of C57BL/6 Klf15 loss-of-function (*Klf15* KO) and the heart-specific β-catenin gain-of-function (β-cat$^{\Delta ex3}$) mouse models have been previously described[8, 23]. For transgene induction in β-cat$^{\Delta ex3}$, heart-specific expression of the Cre recombinase under control of the *Myh6* promoter was activated by administration of Tamoxifen (T5648, 30 mg/kg body weight/day; Sigma–Aldrich) i.p. for 3 days. Littermates being WT at the β-catenin locus and positive for Cre recombinase were used as control for β-cat$^{\Delta ex3}$ mice. Genotyping primers are listed in Supplementary Information, Table S1. WT C57BL/6 embryonic, fetal and neonatal hearts were microdissected and pooled for mRNA isolation.

### Heart cell isolation and immunocytochemistry

For cardiomyocyte isolation, hearts were retrogradely perfused by a modified Langendorff solution (NaCl 120.4wmM; KCl 14.7 mM; $KH_2PO_{4w}$0.6 mM; $Na_2HPO_{4w}$0.6 mM; $MgSO_{4w}$1.2 mM; Na-HEPES 10 mM; $NaHCO_3$ 4.6 mM; taurine 30 mM; 2,3-butanedione-monoxime 10 mM; collagenase type II (600 U/mL); glucose 5.5 mM, pH 7.4) for 7 min at 37°C at a flow rate of 4wmL/min. The residual tissue was removed using a 100 μm cell strainer (BD Falcon, 352360). Bovine calf serum (10 %, Gibco) and 12.5 μM $CaCl_2$ in perfusion buffer was used to inhibit collagenase activity. For non-cardiomyocyte isolation mice were anesthetized and hearts dissected, minced and digested with collagenase type II/trypsin. Cells were cultivated in DMEM/F12 (Gibco) supplemented with 10 % FCS/L-glutamine/antibiotics/100 μM ascorbic acid. For immunofluorescence (IF), isolated cells were plated on laminin (L2020, Sigma-Aldrich) coated glass coverslips, fixed with 4w% PFA, followed by PBS washing and permeabilization with 0.2 % BSA and 0.3 % Triton in PBS for 10 min. Cells were then blocked with 5 % BSA and 0.1 % Triton at RT. Primary and secondary antibodies (Supplementary Information, Table S3) were diluted in 2 % BSA and 0.1 % Triton in PBS. Coverslips were

mounted with ProLong Gold medium containing DAPI (Invitrogen) and imaged in Zeiss LSM 710 NLO confocal microscope.

### *Ex vivo* fetal heart culture and treatment

Culture bottles were prepared with 3 mL DMEM-GlutaMAX medium containing 4.5 g/L D-glucose–pyruvate (Gibco), 10% FBS (Gibco), 1% MEM-NEAA, 100 U/ml Penicillin (Gibco), 100 µg/ml Streptomycin (Gibco). WNT3A-containng medium was collected from L- Wnt3a cells (ATCC, CRL-2647), sterile filtered and mixed with fresh medium (1:1). Bottles were placed in the incubator to stabilize the gas mixture (60% $O_2$, 5% $CO_2$, 35% $N_2$). Pregnant mice were culled upon isoflurane narcosis by cervical dislocation. Uteruses were dissected and embryos at E14.5 were isolated and placed in pre-warmed PBS. Embryo dissection was performed under magnification at 37°C on a warming plate. For conditional medium culture, embryos were placed in culture bottles containing control (CTRL) or WNT3A-conditional medium and cultured at the aforementioned gas mixture for 30 h at 37°C. For *Klf15* overexpression, a solution containing *Klf15* cDNA-containing pcDNA3.1 plasmid at a final concentration of 1,5 □g/□l in 10 □l PBS and 0,2 □l Fast Green (SIGMA) was prepared and load onto a glass microcapillary. As control a GFP-reporter plasmid pLP-EGFP-C1 (Clontech) was used at same concentration. The solution was injected into the left ventricular heart chamber with a micromanipulator (Eppendorf) and subsequently electroporated in a cuvette containing Tyrode's solution with a total of 8 pulses at 75 V, 50 ms duration and an interval of 1 s in an ECM 830 Electro Square Porator (BTX Harvard Apparatus). Left ventricular heart chamber was considered the site of electroporation. After electroporation the hearts were placed immediately in warm medium and transferred to culture bottles for culturing as mentioned above. Successful electroporation was monitored by GFP expression and qPCR. After culture, the hearts were rinsed in DEPC-PBS and either snap-frozen for RNA isolation or fixed in 4% PFA for IF. Of note, the observed high dispersion in expression is due to the technique, which does not allow for a homogenous incubation of the conditional medium with all ventricular cells in a 3D system.

### RNA-sequencing (RNA-seq) and data analyses

Total RNA-seq was performed at the Transcriptome and Genome Analysis Laboratory (TAL), University Medical Center Goettingen, in biological triplicates with each individual sample consisting of a pool from 3 different hearts of the same age and genotype to minimize biological variation. Total RNA from P10, 4wweeks and 20 weeks old murine heart tissue from *Klf15* WT

and KO animals was extracted. Quality and integrity were assessed by Bioanalyzer (Agilent). Libraries were prepared and cDNA libraries were amplified and the size range of final cDNA libraries was determined by applying the DNA 1000 chip on the Bioanalyzer 2100 from Agilent (280 bp). cDNA libraries and sequenced by using the cBot and HiSeq 4000 Illumina (SR; 1x50 bp; 51 cycles with single indexing; 6 GB ca. 30-35 million reads per sample). Sequence reads were aligned to the mouse reference assembly (UCSC version mm9) using TopHat[62]. For each gene, the number of mapped reads was counted using 'htseq-count'[63]; and 'DESeq2'[64] was used to analyze the differential expression. Gene ontology (GO) analyses were performed using default parameters and stringency in 'ClueGO': a Cytoscape plug-in[65]. The significant 'GO Biological Processes' were shown with $p \leq 0.05$. Gene Set Enrichment Analysis was performed with GSEA[112] based on the entire RNAseq profile. Pathways were retrieved from Molecular Signature database (MSigdb)[113]. Pathway datasets are referred to as follows: PID_BETA_CATENIN_NUC_PATHWAY and PID_WNT_SIGNALING_PATHWAY. The gene sets included in the analysis were limited to those that contained between 50 and 500 genes. Permutation was conducted 1000 times according to default-weighted enrichment statistics and by using a signal-to-noise metric to rank genes according to their differential expression levels across the *Klf15* WT and KO groups. Significant gene sets were defined as those with nominal p-value $\leq 0.05$. Motif search on differentially expressed genes was performed using default parameters of the 'TRANSFAC' tool on 'GATHER'[66]. Only significantly enriched motifs are shown.

**Chromatin immunoprecipitation-sequencing (ChIP-seq) and data analyses**

Published KLF15 ChIP-seq data in the normal adult heart was obtained from GSM1901940. Published TCF7L2 ChIP-seq data in the diseased heart was obtained from GSE97761. Sequence reads were aligned to the mouse reference assembly (UCSC version mm9) using Bowtie2.0[67]. Peak calling was performed with Model Based Analysis of ChIPseq (MACS2) version 2.1.0.20140616.0[68]. Integrative Genomics Viewer (IGV) was used to view and represent bigwig file tracks[69]. Genes proximal to the bound chromatin regions were identified by GREAT[70] using 'Basal plus extension' method where each genomic region is overlapped with genes which are 5 kb upstream and 1 kb downstream (proximal), plus up to 1000 kb (distal). Gene ontology/pathway analyses for gene lists were performed using default parameters and stringency in 'ClueGO' and the significant 'Gene Ontology Biological Processes' were shown

with $p \leq 0.05$. To integrate ChIP-seq with RNA-seq, BioVenn web application was used to compare, create and analyze Venn diagrams showing commonly or differently bound genes between two or more datasets [71].

**Generation of the KLF15-hESC line**

The use of human embryonic stem cells (hESCs) was approved according to the German Stem Cell Act by the Robert Koch Institute to WHZ (permit #12, reference number 1710-79-1-4-16). Generation of the *KLF15* KO hESC line by CRISPR/Cas9n has been described elsewhere [44]. In brief, sgRNAs targeting the transcription start site of human *KLF15* was designed and cloned into modified pX335A vectors containing a GFP-T2A-puromycin cassette and SpCas9-D10A nickase[72]. HES2 cells were electroporated (Human Stem Cell Nucleofector kit 1, Lonza), selected after 24 h and colonies were picked for genotyping. Genomic integrity was demonstrated by standard G-banding karyotype analysis of the KO line. Pluripotency was assessed by IF using the stemness markers OCT4, TRA1-60, SSEA-4. Assessment by flow cytometry showed at least 99.3 % OCT4wand 88.1 % TRA1-60 positive cells. Spontaneous differentiation capacity into all three germ layers was tested by formation of embryoid bodies.

**Generation of Engineered Human Myocardium (EHM)**

HES2-hESCs were differentiated by Wnt signaling pathway modulation, and EHM were generated as previously described[44, 45]. KLF15 WT and KO hESC-derived CMs were digested with a custom mixture of Accutase cell detachment solution (Merck), 0.025 % Trypsin (Gibco) and 20 µg/mL DNase I (Calbiochem) at RT. Human foreskin fibroblasts (HFFs; ATCC SCRC-1041) were digested from monolayer culture with TrypLE (Gibco) at 37°C, and filtered through a 20 µm cell strainer to remove excess extracellular matrix. CMs and HFFs were interspersed within a bovine type I collagen hydrogel (0.3 mg/EHM; Collagen Solutions, UK), with each construct comprising of $1.25 \times 10^6$ total cells (70 % CMs, 30 % HFFs). The final EHM mastermix were cast into silicone molds and permitted to condense at 37°C for 1 h, after which Iscove's Modified Delbucco's Medium with GlutaMAX Supplement (IMDM; Gibco) containing 1% MEM-NEAA (Gibco), 1% Pen./Strep. (Gibco), 300 µM L-Ascorbic Acid (Sigma), 4% B27 Supplement minus Insulin (Gibco), and growth factors IGF-1 (100 ng/mL), FGF-2 (10 ng/mL), $VEGF_{165}$ (5 ng/mL) and TGF-β1 (5 ng/mL; Peprotech) was overlaid. A media change was performed the day after casting. Two days thereafter at day three post-casting, EHMs were manually transferred onto silicone auxotonic stretchers (preload) and permitted to develop for four weeks. Media changes with IMDM without TGF-β1 were then performed every second day.

**Contractile force assessment of EHM**

Isometric force assessment of EHMs was performed in a 37°C thermo-regulated organ bath (Fohr Medical Instruments, Germany) containing carbogen (95% O2, 5% CO2) saturated Tyrode's solution (119.8 mM NaCl, 5.4 mM KCl, 1.05 mM MgCl2, 0.2 mM CaCl2, 0.42 mM NaH2PO4, 22.6 mM NaHCO3, 5.05 mM glucose, and 0.28 mM ascorbic acid). EHMs were electrically field stimulated with monophasic pulses of 200 mA, 5 ms, and 1.5 Hz. Baths were initially adjusted to 1.8 mM Ca2+ and each EHM incrementally lengthened according to the Frank-Starling principle to achieve the maximum contractile force (Fmax). A Ca2+ concentration response (0.2-4 mM) was performed to determine the $[Ca2+]_{EC50}$, and assessment of the force-frequency response (1, 1.5, 2 and 3 Hz) was performed at this Ca2+ concentration.

**Statistical analyses**

G-Power3.1 was used to determine the sample size for animal studies. For ChIP-seq and RNA-seq analyses, q-value (to call peaks) and adjusted p-value of $\leq 0.05$ was considered for statistical significance respectively. Unpaired Student's *t*-test, 1-way ANOVA followed by Bonferroni's multiple comparison test, or 2-way ANOVA with Tukey's multiple comparison test (GraphPad Prism 6.0) were used where appropriate for statistical analysis. Data are presented as mean±SEM, with p-values $\leq 0.05$ considered statistically significant.

**Acknowledgements**

The authors thank Ines Mueller, Daniela Liebig-Wolter, and Daria Reher for superb technical assistance, the Collaborative Research Center (CRC) (Sonderforschungsbereiche (SFB)) 1002 service units (S01 Disease Models for echocardiography measurements and analysis; S02 High resolution fluorescence microscopy for advancing cell staining and cytoskeleton analysis and INF Information infrastructure for providing platform structure) and Dr. Gabriela Salinas (Head of Transcriptome and Genome Analysis Laboratory, Georg-August University Goettingen) for her advice on our RNAseq.

**Author contributions**

CN and LCZ initiated the study and developed the concept of the paper. CN, LMI, NYL, DH, ES, SK, EW, MW, MPZ and LCZ performed experiments. SK and GH provided support with human data. WHZ provided expertise in EHM data discussion. CN, LMI, NYL, MPZ and LCZ

analyzed, interpreted and discussed the data. CN, LMI and LCZ wrote the manuscript. All authors revised the manuscript.

**Funding**

This work was supported by a Deutsche Forschungsgemeinschaft (DFG) grant (ZE900-3 to LCZ), CRC1002 (Project C07 to LCZ), German Heart Research Foundation (F/29/7 to LCZ) and the German Center for Cardiovascular Research (DZHK). The funders had no role in our study design, data collection, analysis and/or decision to publish. Funding for open access charge was provided by internal institutional funding (UMG).

**Competing financial interests**

The authors declare no competing financial interests

**References**

1. Denise Hilfiker-Kleiner, U.L., HelmutDrexler Molecular Mechanisms in Heart Failure: Focus on Cardiac Hypertrophy, Inflammation, Angiogenesis, and Apoptosis. *Journal of the American College of Cardiology* **48**, A56-A66 (2006).
2. Joshua Bloomekatz, M.G.-S., Neil C Chi Myocardial plasticity: cardiac development, regeneration and disease. *Current Opinion in Genetics & Development* **40**, 120-130 (2016).
3. Bieker, J.J. Kruppel-like factors: three fingers in many pies. *The Journal of biological chemistry* **276**, 34355-34358 (2001).
4. Miller, I.J. & Bieker, J.J. A novel, erythroid cell-specific murine transcription factor that binds to the CACCC element and is related to the Kruppel family of nuclear proteins. *Molecular and cellular biology* **13**, 2776-2786 (1993).
5. Gray, S. *et al.* Regulation of gluconeogenesis by Kruppel-like factor 15. *Cell metabolism* **5**, 305-312 (2007).
6. Mori, T. *et al.* Role of Kruppel-like factor 15 (KLF15) in transcriptional regulation of adipogenesis. *The Journal of biological chemistry* **280**, 12867-12875 (2005).
7. Fisch, S. *et al.* Kruppel-like factor 15 is a regulator of cardiomyocyte hypertrophy. *Proceedings of the National Academy of Sciences of the United States of America* **104**, 7074-7079 (2007).
8. Noack, C. *et al.* Krueppel-like factor 15 regulates Wnt/beta-catenin transcription and controls cardiac progenitor cell fate in the postnatal heart. *EMBO Mol Med* **4**, 992-1007 (2012).
9. Mallipattu, S.K. *et al.* Kruppel-like Factor 15 (KLF15) Is a Key Regulator of Podocyte Differentiation. *The Journal of biological chemistry* **287**, 19122-19135 (2012).
10. Meng, G., Zhong, X. & Mei, H. A Systematic Investigation into Aging Related Genes in Brain and Their Relationship with Alzheimer's Disease. *PloS one* **11**, e0150624 (2016).
11. Zhang, L. *et al.* KLF15 Establishes the Landscape of Diurnal Expression in the Heart. *Cell reports* **13**, 2368-2375 (2015).

12. Leenders, J.J. *et al.* Regulation of cardiac gene expression by KLF15, a repressor of myocardin activity. *The Journal of biological chemistry* **285**, 27449-27456 (2010).
13. Haldar, S.M. *et al.* Klf15 deficiency is a molecular link between heart failure and aortic aneurysm formation. *Science translational medicine* **2**, 26ra26 (2010).
14. Wang, B. *et al.* The Kruppel-like factor KLF15 inhibits connective tissue growth factor (CTGF) expression in cardiac fibroblasts. *Journal of molecular and cellular cardiology* **45**, 193-197 (2008).
15. Leenders, J.J. *et al.* Repression of cardiac hypertrophy by KLF15: underlying mechanisms and therapeutic implications. *PloS one* **7**, e36754 (2012).
16. Prosdocimo, D.A. *et al.* Kruppel-like factor 15 is a critical regulator of cardiac lipid metabolism. *The Journal of biological chemistry* **289**, 5914-5924 (2014).
17. Lu, Y. *et al.* Kruppel-like factor 15 is critical for vascular inflammation. *The Journal of clinical investigation* **123**, 4232-4241 (2013).
18. Gao, L., Guo, Y., Liu, X., Shang, D. & Du, Y. KLF15 protects against isoproterenol-induced cardiac hypertrophy via regulation of cell death and inhibition of Akt/mTOR signaling. *Biochemical and biophysical research communications* **487**, 22-27 (2017).
19. Fan, Y. *et al.* Kruppel-like factors and vascular wall homeostasis. *Journal of molecular cell biology* **9**, 352-363 (2017).
20. Sequeira, V., Nijenkamp, L.L., Regan, J.A. & van der Velden, J. The physiological role of cardiac cytoskeleton and its alterations in heart failure. *Biochimica et biophysica acta* **1838**, 700-722 (2014).
21. Liu, Z., Yue, S., Chen, X., Kubin, T. & Braun, T. Regulation of cardiomyocyte polyploidy and multinucleation by CyclinG1. *Circulation research* **106**, 1498-1506 (2010).
22. Kubin, T. *et al.* Oncostatin M is a major mediator of cardiomyocyte dedifferentiation and remodeling. *Cell stem cell* **9**, 420-432 (2011).
23. Iyer, L.M. *et al.* A context-specific cardiac beta-catenin and GATA4 interaction influences TCF7L2 occupancy and remodels chromatin driving disease progression in the adult heart. *Nucleic acids research* (2018).
24. Creyghton, M.P. *et al.* Histone H3K27ac separates active from poised enhancers and predicts developmental state. *Proceedings of the National Academy of Sciences of the United States of America* **107**, 21931-21936 (2010).
25. He, T.C. *et al.* Identification of c-MYC as a target of the APC pathway. *Science* **281**, 1509-1512 (1998).
26. van de Schans, V.A., Smits, J.F. & Blankesteijn, W.M. The Wnt/frizzled pathway in cardiovascular development and disease: friend or foe? *Eur J Pharmacol* **585**, 338-345 (2008).
27. Brade, T., Manner, J. & Kuhl, M. The role of Wnt signalling in cardiac development and tissue remodelling in the mature heart. *Cardiovascular research* **72**, 198-209 (2006).
28. Subramanian, A. *et al.* Gene set enrichment analysis: a knowledge-based approach for interpreting genome-wide expression profiles. *Proceedings of the National Academy of Sciences of the United States of America* **102**, 15545-15550 (2005).
29. Chen, C.C. *et al.* Shisa3 is associated with prolonged survival through promoting beta-catenin degradation in lung cancer. *American journal of respiratory and critical care medicine* **190**, 433-444 (2014).

30. Maffei, R. *et al.* Increased SHISA3 expression characterizes chronic lymphocytic leukemia patients sensitive to lenalidomide. *Leukemia & lymphoma* **59**, 423-433 (2018).
31. Nandi, S.S. & Mishra, P.K. Harnessing fetal and adult genetic reprograming for therapy of heart disease. *Journal of nature and science* **1** (2015).
32. Snider, P. *et al.* Origin of cardiac fibroblasts and the role of periostin. *Circulation research* **105**, 934-947 (2009).
33. Liu, C. *et al.* Human endomucin is an endothelial marker. *Biochemical and biophysical research communications* **288**, 129-136 (2001).
34. Brachtendorf, G. *et al.* Early expression of endomucin on endothelium of the mouse embryo and on putative hematopoietic clusters in the dorsal aorta. *Developmental dynamics : an official publication of the American Association of Anatomists* **222**, 410-419 (2001).
35. Muller, A.M. *et al.* Expression of the endothelial markers PECAM-1, vWf, and CD34 in vivo and in vitro. *Experimental and molecular pathology* **72**, 221-229 (2002).
36. Fan, C. *et al.* Novel roles of GATA1 in regulation of angiogenic factor AGGF1 and endothelial cell function. *The Journal of biological chemistry* **284**, 23331-23343 (2009).
37. Ema, M. *et al.* Combinatorial effects of Flk1 and Tal1 on vascular and hematopoietic development in the mouse. *Genes & development* **17**, 380-393 (2003).
38. Min, Y., Li, J., Qu, P. & Lin, P.C. C/EBP-delta positively regulates MDSC expansion and endothelial VEGFR2 expression in tumor development. *Oncotarget* **8**, 50582-50593 (2017).
39. Karra, R., Knecht, A.K., Kikuchi, K. & Poss, K.D. Myocardial NF-kappaB activation is essential for zebrafish heart regeneration. *Proceedings of the National Academy of Sciences of the United States of America* **112**, 13255-13260 (2015).
40. Guimaraes-Camboa, N. *et al.* HIF1alpha Represses Cell Stress Pathways to Allow Proliferation of Hypoxic Fetal Cardiomyocytes. *Developmental cell* **33**, 507-521 (2015).
41. Goodall, J. *et al.* Brn-2 expression controls melanoma proliferation and is directly regulated by beta-catenin. *Molecular and cellular biology* **24**, 2915-2922 (2004).
42. Hosogane, M., Funayama, R., Shirota, M. & Nakayama, K. Lack of Transcription Triggers H3K27me3 Accumulation in the Gene Body. *Cell reports* **16**, 696-706 (2016).
43. Lutz, M. *et al.* Transcriptional repression by the insulator protein CTCF involves histone deacetylases. *Nucleic acids research* **28**, 1707-1713 (2000).
44. Noack, C., Haupt, L.P., Zimmermann, W.H., Streckfuss-Bomeke, K. & Zelarayan, L.C. Generation of a KLF15 homozygous knockout human embryonic stem cell line using paired CRISPR/Cas9n, and human cardiomyocytes derivation. *Stem cell research* **23**, 127-131 (2017).
45. Tiburcy, M. *et al.* Defined Engineered Human Myocardium With Advanced Maturation for Applications in Heart Failure Modeling and Repair. *Circulation* **135**, 1832-1847 (2017).
46. Jeong, M.H. *et al.* Cdon deficiency causes cardiac remodeling through hyperactivation of WNT/beta-catenin signaling. *Proceedings of the National Academy of Sciences of the United States of America* **114**, E1345-E1354 (2017).

47. Furushima, K. *et al.* Mouse homologues of Shisa antagonistic to Wnt and Fgf signalings. *Developmental biology* **306**, 480-492 (2007).
48. Yamamoto, A., Nagano, T., Takehara, S., Hibi, M. & Aizawa, S. Shisa promotes head formation through the inhibition of receptor protein maturation for the caudalizing factors, Wnt and FGF. *Cell* **120**, 223-235 (2005).
49. Jiang, X. *et al.* DACT3 is an epigenetic regulator of Wnt/beta-catenin signaling in colorectal cancer and is a therapeutic target of histone modifications. *Cancer cell* **13**, 529-541 (2008).
50. Cohen, E.D., Tian, Y. & Morrisey, E.E. Wnt signaling: an essential regulator of cardiovascular differentiation, morphogenesis and progenitor self-renewal. *Development* **135**, 789-798 (2008).
51. Park-Windhol, C. *et al.* Endomucin inhibits VEGF-induced endothelial cell migration, growth, and morphogenesis by modulating VEGFR2 signaling. *Scientific reports* **7**, 17138 (2017).
52. Jo, A. *et al.* The versatile functions of Sox9 in development, stem cells, and human diseases. *Genes & diseases* **1**, 149-161 (2014).
53. De Val, S. & Black, B.L. Transcriptional control of endothelial cell development. *Developmental cell* **16**, 180-195 (2009).
54. Wang, H. *et al.* Gene expression profile signatures indicate a role for Wnt signaling in endothelial commitment from embryonic stem cells. *Circulation research* **98**, 1331-1339 (2006).
55. Yang, D.H. *et al.* Wnt5a is required for endothelial differentiation of embryonic stem cells and vascularization via pathways involving both Wnt/beta-catenin and protein kinase Calpha. *Circulation research* **104**, 372-379 (2009).
56. De Boer, R.A., Pinto, Y.M. & Van Veldhuisen, D.J. The imbalance between oxygen demand and supply as a potential mechanism in the pathophysiology of heart failure: the role of microvascular growth and abnormalities. *Microcirculation* **10**, 113-126 (2003).
57. Hilfiker-Kleiner, D., Limbourg, A. & Drexler, H. STAT3-mediated activation of myocardial capillary growth. *Trends in cardiovascular medicine* **15**, 152-157 (2005).
58. Itescu, S., Kocher, A.A. & Schuster, M.D. Myocardial neovascularization by adult bone marrow-derived angioblasts: strategies for improvement of cardiomyocyte function. *Annals of hematology* **81 Suppl 2**, S21-25 (2002).
59. Diaz-Sandoval, L.J. & Losordo, D.W. Gene therapy for cardiovascular angiogenesis. *Expert opinion on biological therapy* **3**, 599-616 (2003).
60. Pei, J. & Grishin, N.V. Unexpected diversity in Shisa-like proteins suggests the importance of their roles as transmembrane adaptors. *Cellular signalling* **24**, 758-769 (2012).
61. Aranguren, X.L. *et al.* Unraveling a novel transcription factor code determining the human arterial-specific endothelial cell signature. *Blood* **122**, 3982-3992 (2013).
62. Trapnell, C., Pachter, L. & Salzberg, S.L. TopHat: discovering splice junctions with RNA-Seq. *Bioinformatics* **25**, 1105-1111 (2009).
63. Anders, S., Pyl, P.T. & Huber, W. HTSeq--a Python framework to work with high-throughput sequencing data. *Bioinformatics* **31**, 166-169 (2015).

64. Love, M.I., Huber, W. & Anders, S. Moderated estimation of fold change and dispersion for RNA-seq data with DESeq2. *Genome biology* **15**, 550 (2014).
65. Bindea, G. *et al.* ClueGO: a Cytoscape plug-in to decipher functionally grouped gene ontology and pathway annotation networks. *Bioinformatics* **25**, 1091-1093 (2009).
66. Chang, J.T. & Nevins, J.R. GATHER: a systems approach to interpreting genomic signatures. *Bioinformatics* **22**, 2926-2933 (2006).
67. Langmead, B. & Salzberg, S.L. Fast gapped-read alignment with Bowtie 2. *Nature methods* **9**, 357-359 (2012).
68. Feng, J., Liu, T., Qin, B., Zhang, Y. & Liu, X.S. Identifying ChIP-seq enrichment using MACS. *Nature protocols* **7**, 1728-1740 (2012).
69. Thorvaldsdottir, H., Robinson, J.T. & Mesirov, J.P. Integrative Genomics Viewer (IGV): high-performance genomics data visualization and exploration. *Briefings in bioinformatics* **14**, 178-192 (2013).
70. McLean, C.Y. *et al.* GREAT improves functional interpretation of cis-regulatory regions. *Nature biotechnology* **28**, 495-501 (2010).
71. Hulsen, T., de Vlieg, J. & Alkema, W. BioVenn - a web application for the comparison and visualization of biological lists using area-proportional Venn diagrams. *BMC genomics* **9**, 488 (2008).
72. Zhang, M. *et al.* Recessive cardiac phenotypes in induced pluripotent stem cell models of Jervell and Lange-Nielsen syndrome: disease mechanisms and pharmacological rescue. *Proceedings of the National Academy of Sciences of the United States of America* **111**, E5383-5392 (2014).

**Supplemental Figure 1**

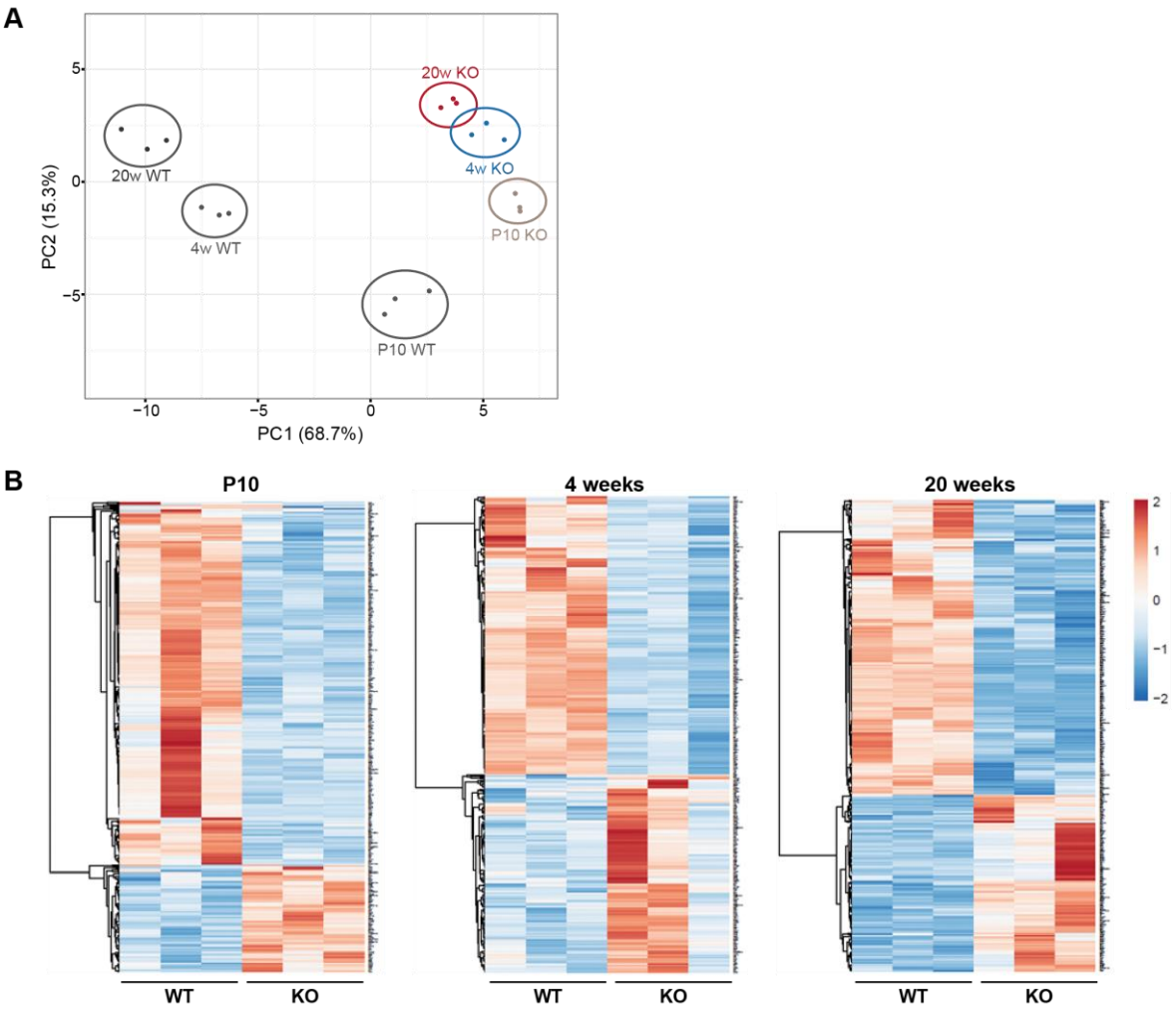


**Supplementary Figure 1: Global transcriptomic changes in hearts with KLF15 loss of function. (A)** PCA plot depicting differential grouping of P10, 4 and 20 weeks-old *Klf15* WT and KO murine hearts, based on read counts. Transcriptionally, P10 samples cluster together with 4 and 20 weeks *Klf15* KO hearts, suggestive of immaturity upon loss of *Klf15* in adult murine hearts**. (B)** Heatmaps illustrating all DEGs with $\log_2$FC>±0.5 and p<0.05 in P10, 4 and 20 weeks-old *Klf15* WT and KO hearts.

## Supplemental Figure 2

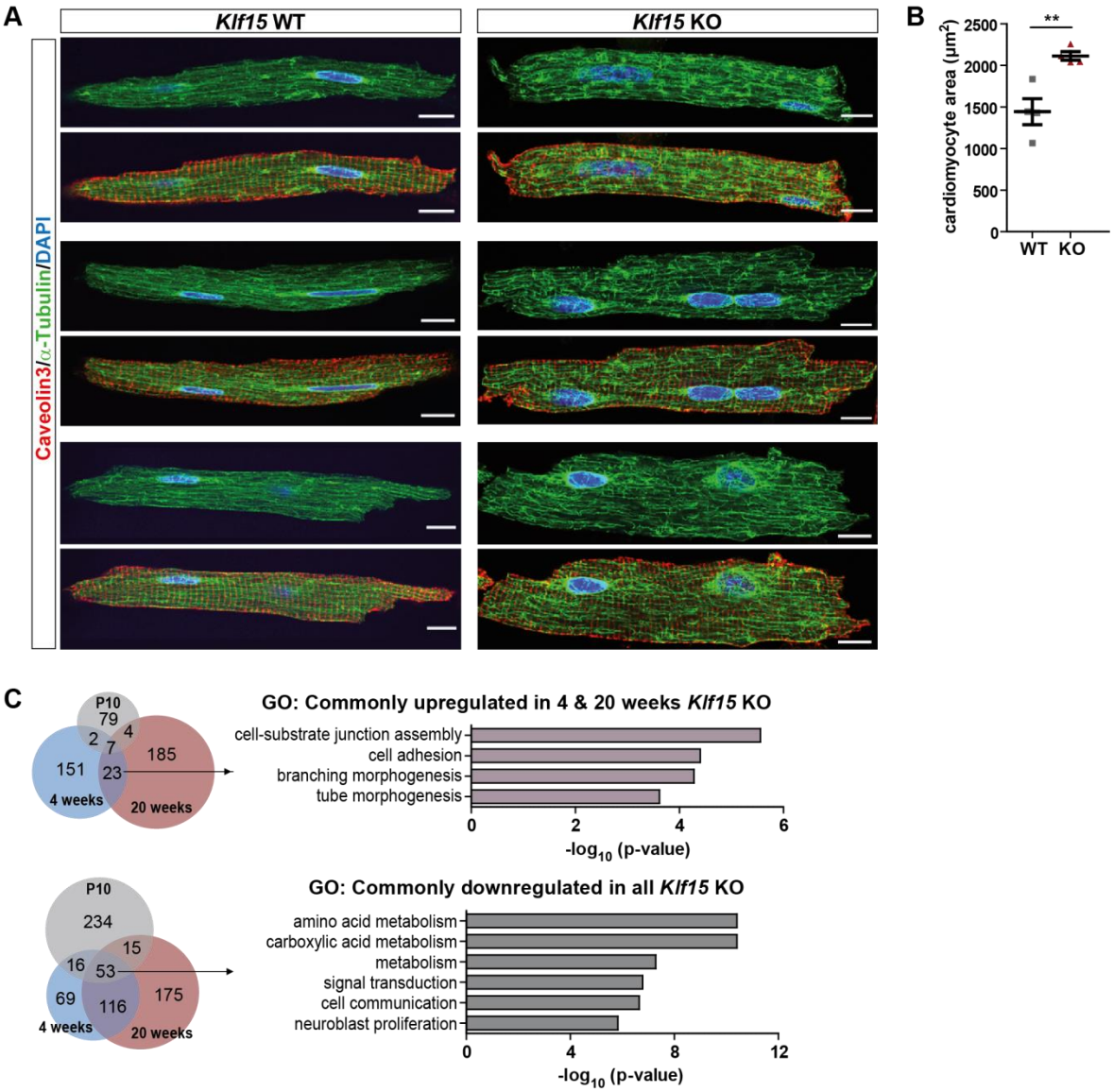


**Supplementary Figure 2: Cytoskeletal remodeling in *Klf15* KO cardiomyocytes. (A)** Representative IF images showing visibly increased cytoskeletal density and junctions in isolated CM from *Klf15* KO mice hearts and corresponding controls (quantified in Fig. 1d). Caveolin3 (red) marks the CM membrane, α-Tubulin (green) stains the microtubule cytoskeleton and DAPI (blue) marks the nuclei; n=3 animals per group of isolation. Scale bar: 10 µm. **(B)** Quantification of CM longitudinal area in isolated CM of WT and *Klf15* KO hearts. 3 hearts per group, n≥10 cells; Student's *t*-test, **p≤0.01. **(C)** Venn diagram showing common DEGs (up or down) in P10, 4w and 20w *Klf15* KO hearts. GO biological processes of commonly upregulated genes in 4 and 20 weeks; and commonly downregulated genes in all ages of *Klf15* KO hearts are depicted. GO are informed as -$\log_{10}$ (p-value).

## Supplemental Figure 3

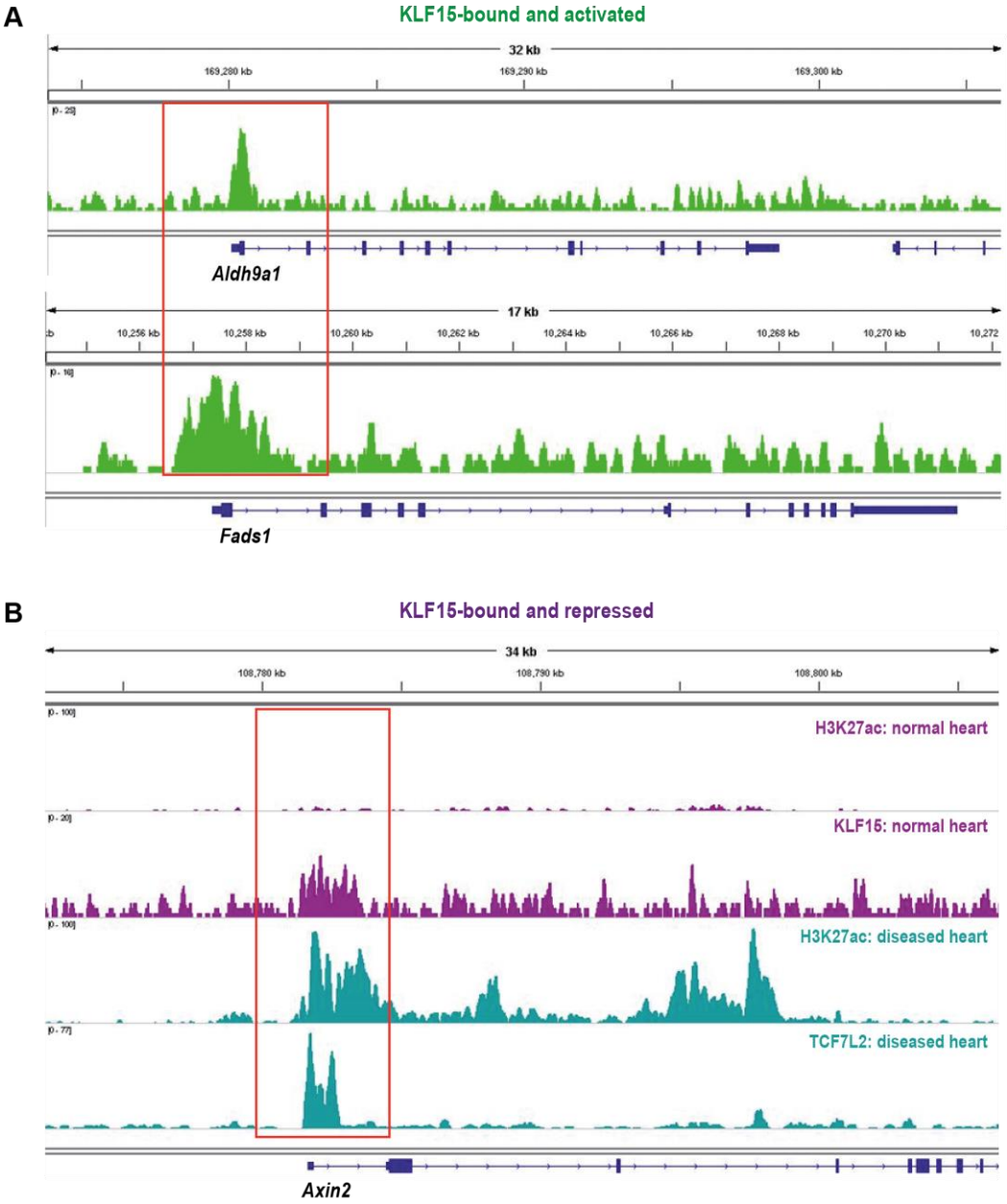


**Supplementary Figure 3: KLF15 chromatin binding activates and represses specific gene sets in the adult heart. (A)** IGV occupancy profiles of *Aldh9a1* and *Fads1*, metabolic genes bound and activated by KLF15. **(B)** IGV occupancy profiles of *Axin2* promoter, of KLF15 and H3K27ac in the normal adult, and TCF7L2 and H3K27ac in the diseased adult hearts. Red boxes highlight specific regions of binding.

## Supplemental Figure 4

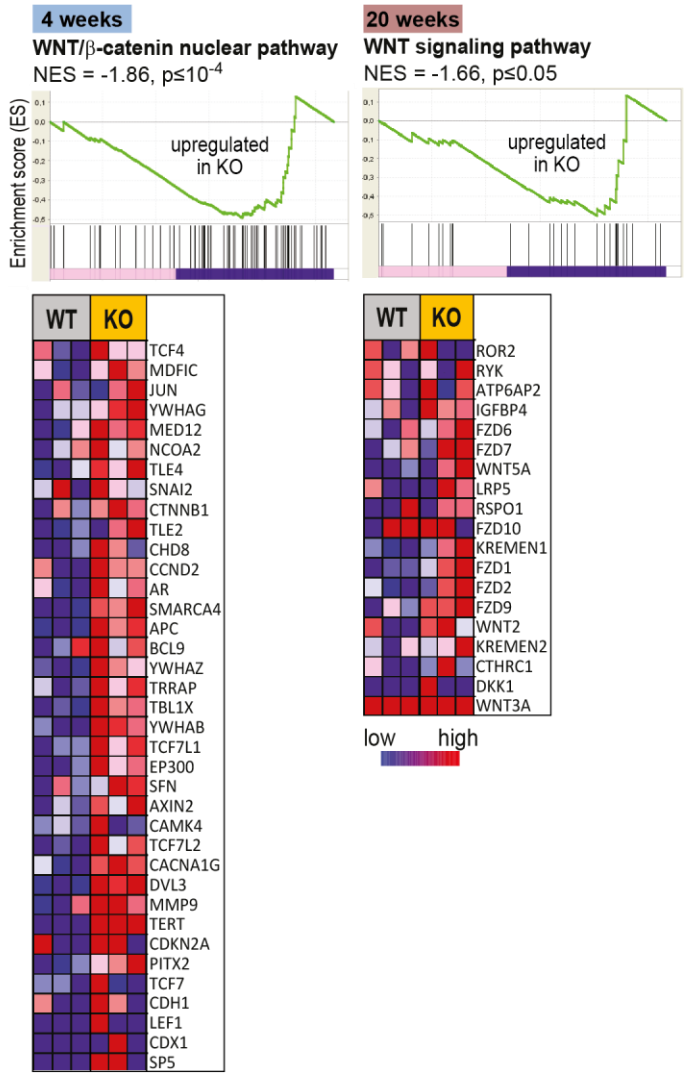


**Supplementary Figure 4: Gene Set Enrichment Analysis (GSEA) in *Klf15* KO hearts.** GSEA showing enrichment of the Wnt/β-catenin nuclear pathway gene set (as compared to WT) in 4w hearts as well as enrichment of the Wnt signaling gene set corresponding to non-canonical pathway in 20w *Klf15* KO heart tissue. The enrichment score (ES, green line) reflects the degree to which the gene set is over-represented at the top or bottom of the ranked list of genes. A positive value indicates correlation with 'WT'-phenotype, a negative value with 'KO'-phenotype. Heat maps of the genes contributing most to the high enrichment score of the gene set; expression values are shown for each replicate within a condition and are represented as range of colors (from red to blue) showing the range of expression values (high, moderate, low, and lowest).

**Supplemental Figure 5**

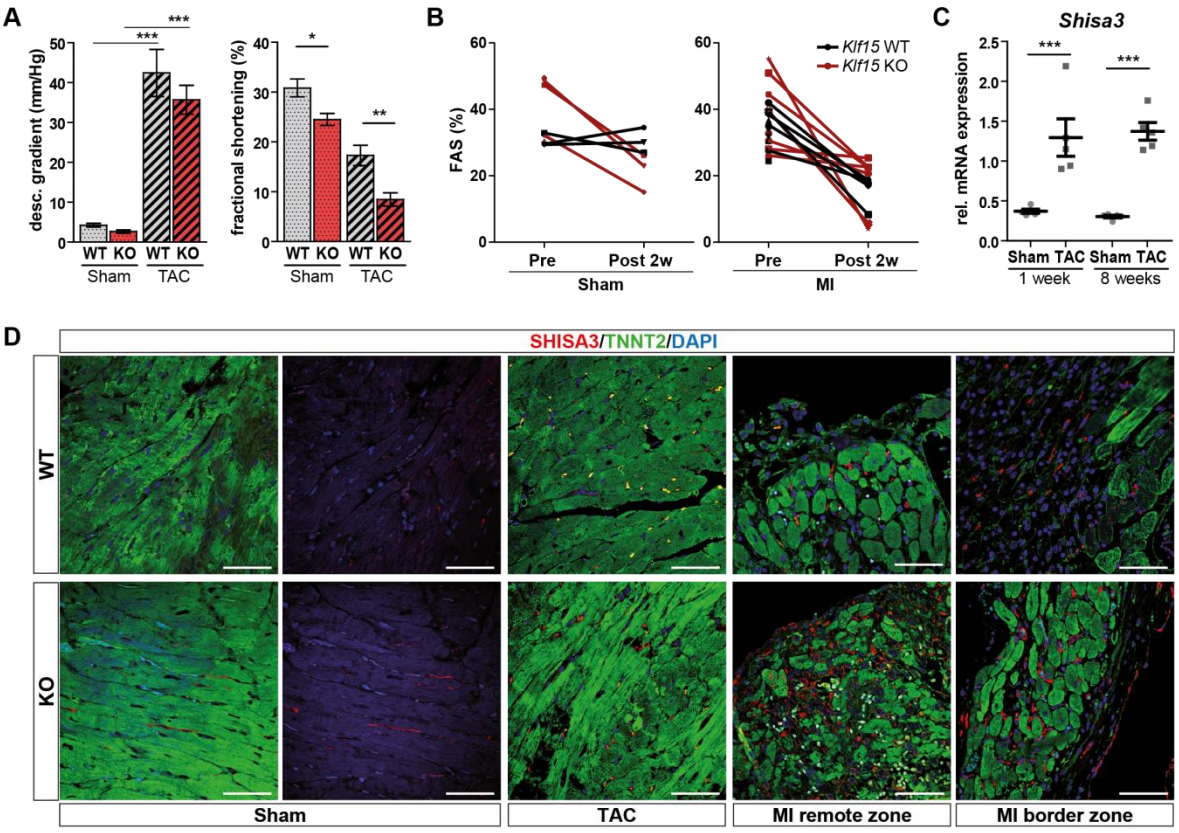


**Supplementary Figure 5: SHISA3 is upregulated in pathological cardiac remodeling. (A)** Functional data measured by Doppler echocardiography confirming successful TAC intervention. Despite having similar aortic gradients, *Klf15* KO hearts showed a stronger deterioration in heart function upon TAC; n≥8. **(B)** Functional data measured by echocardiography confirming successful MI induction. **(C)** Upregulated *Shisa3* expression upon TAC in WT mice was already evident 1 week post-TAC and persisted till 8 weeks after TAC; n=5. **(D)** Representative IF images showing increased SHISA3 (red) expression in interstitial, TNNT2 (green)-negative cells of 2 weeks post-TAC and 4 weeks post-MI heart sections. This increased expression was further augmented in the corresponding *Klf15* KO ventricles, n=3; Scale bar 100 µm. Statistics in (A)-(C): 1-way ANOVA with Bonferroni's multiple comparison test, *p≤0.05, **p≤0.01, ***p≤0.001.

## Supplemental Figure 6

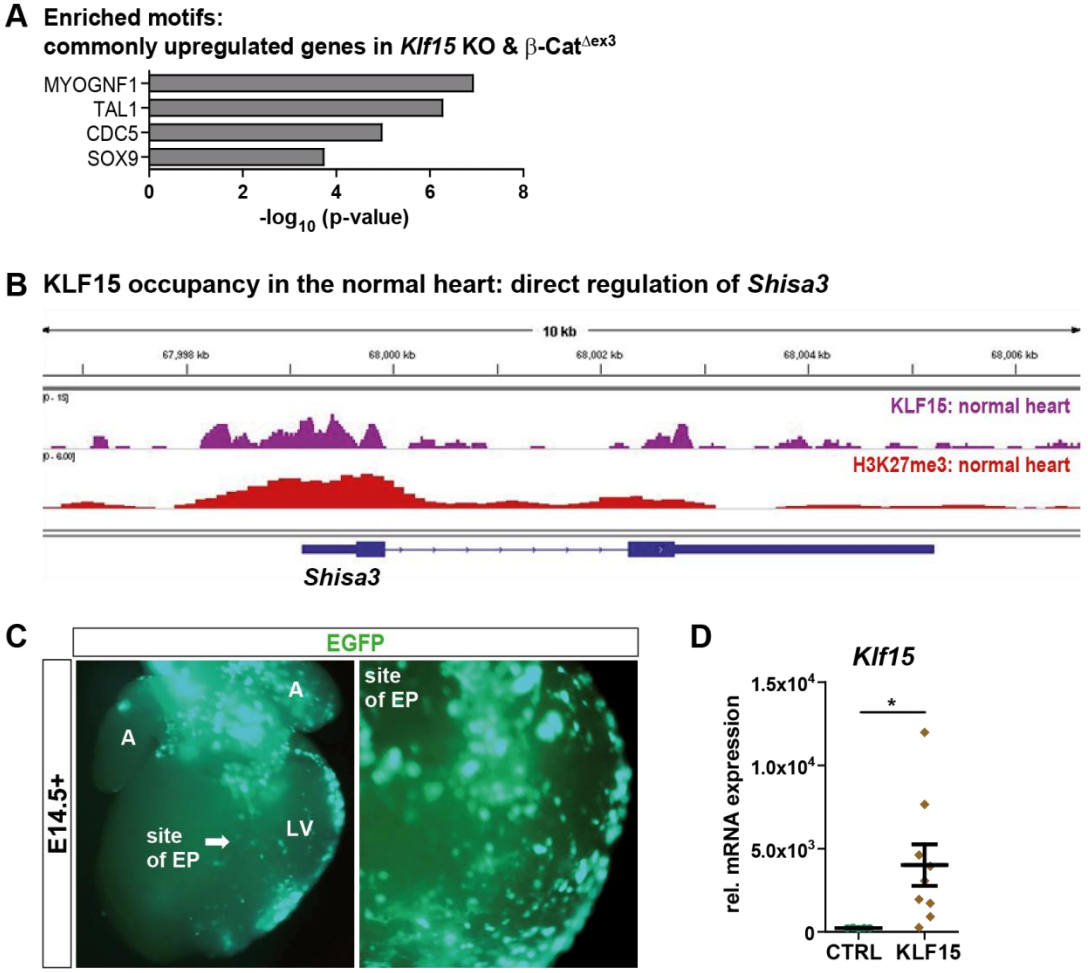


**Supplementary Figure 6: *Shisa3* is regulated by KLF15 in cardiac tissue. (A)** Motif search analyses using TRANSFAC of commonly upregulated genes in *Klf15* KO and β-Cat$^{\Delta ex3}$ (Wnt activated) hearts. **(B)** Integrative Genomics Viewer (IGV) occupancy profile illustrating KLF15 binding to *Shisa3* promoter in the adult heart. **(C)** Representative figure of a GFP-electroporated fetal heart at 14.5 after 24 h showing the site of electroporation (EP). Atria (A); Left ventricle (LV). **(D)** qPCR validation of *Klf15* overexpression (KLF15-OE) in E14.5 mouse heart tissue compared to GFP-electroporated controls (CTRL) of *ex vivo* heart cultures, n≥5.

**Supplemental Figure 7**

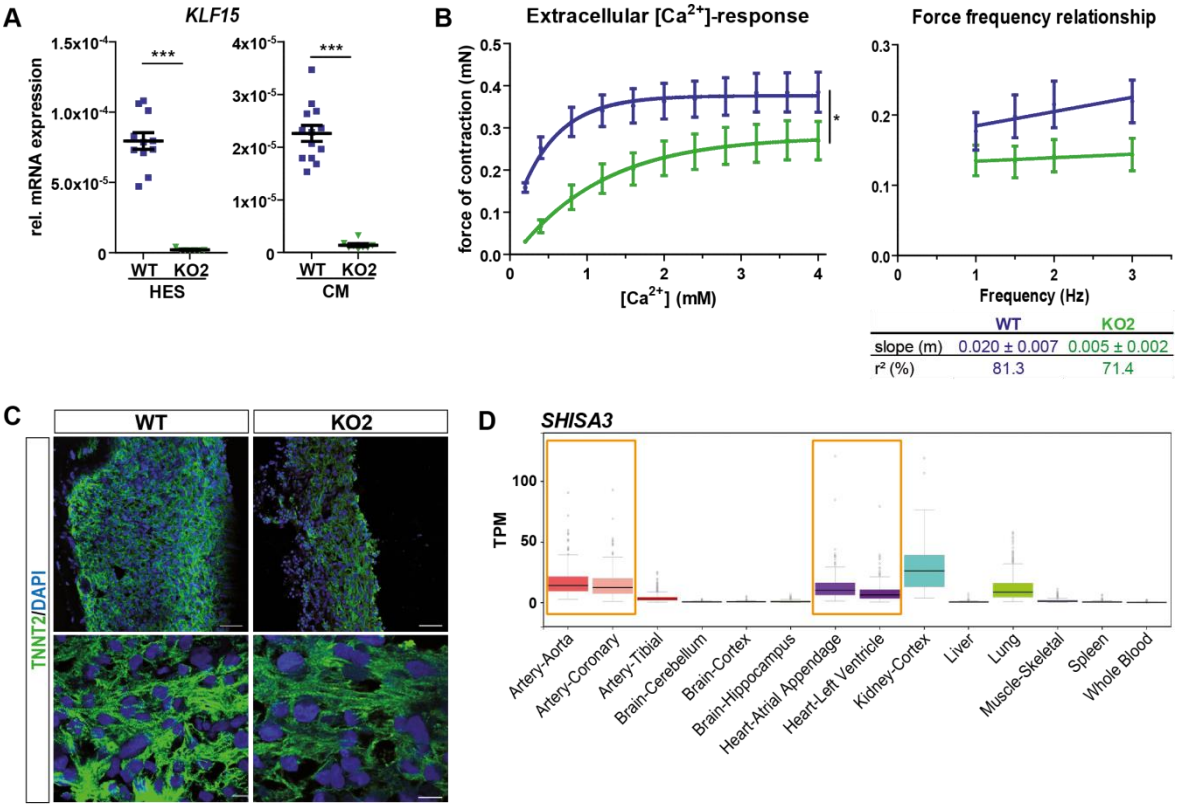


**Supplementary Figure 7: KLF15 loss in human cells mimics murine function in myocardium. (A)** qPCR validating reduced *KLF15* mRNA expression in both human embryonic stem cells (HES) and HES-derived cardiomyocytes (CM) in KLF15 KO line no. 2 compared to KLF15 WT controls; normalized to *GAPDH*; n≥7; Student's *t*-test, ***p≤0.001. **(B)** KLF15 KO2 EHMs exhibit blunted extracellular $Ca^{2+}$ response and force-frequency relationship; n=3; 2-way ANOVA with Tukey's multiple comparison test, *p≤0.05. **(C)** Representative IF from Engineered Human Myocardium (EHM) (WT and KO2) showing TNNT2 expression. **(D)** Analysis of publicly available transcriptomic data (GTEx project) showing expression of *SHISA3* in different tissues and its relevant expression in ventricles and vasculature (aorta and coronary arteries); expression values are shown in Transcripts Per Million (TPM); box plots as median and 25$^{th}$ and 75$^{th}$ percentiles.

# 7. Discussion

TCF7L2, the main Wnt signaling transcriptional effector, is expressed in multiple tissues in a context-specific manner and has known roles in influencing global chromatin profiles[53,54,91]. However, its stage-specific transcriptional functions in cardiac homeostasis were never investigated before. Therefore, in addition to studying the direct role of TCF7L2 in heart development and disease, this study also investigated the changes occurring at the chromatin level, across different cardiac contexts. At the chromatin level, the heart employs distinct chromatin remodelers like BAF60c (BRG1 Associated factor 60c), BRG1 (Brahma-Related Gene 1) and CHDs (Chromodomain Helicase DNA Binding Proteins) at every developmental/specification stage at proximal as well as distal enhancers, thereby potentiating precise, temporal association of cardiac TFs like TBX5, GATA4, MEF2C and SRF for accurate cardiac gene transcription[17,19,20,114]. These remodelers further recruit histone modifiers, which acetylate and/or methylate the chromatin, establishing an epigenetic landscape, thereby creating the "histone-code" of the genome, eventually 'read' by the TFs. The binding of TFs further promotes recruitment of more histone modifiers, creating a gene-expression-loop.

The following sections discuss and summarize the findings of this thesis regarding the transcriptional role of Wnt signaling across different stages of the mammalian myocardium.

## 7.1 Adulthood

The adult heart constitutes a fully mature, functional myocardium with efficient contractile properties and elevated metabolism. This constitutively operational state is carefully monitored and driven by the timely synergy between major cardiac TFs, which provide the necessary genomic profiles to coordinate cardiac gene transcription. Wnt signaling, being a pro-proliferative, developmental pathway is known to be quiescent in the adult CMs[12]. This Wnt inactivation was also reported to be crucial for CM differentiation. Hence, it is not surprising that we also observed almost no or basal expression of TCF7L2 in the adult cardiac ventricular tissue as well as in isolated adult CMs. However, despite the basal activity, comparing its expression within the cardiac chambers- atria and ventricles in the healthy adult heart revealed its specific expression only in the ventricles (previous results, data not shown), suggesting its homeostatic role in the healthy adult working myocardium. Following this observation, only cardiac ventricular tissues were used for all subsequent experiments. Encouraged by its basal ventricular expression, ChIP-seq was attempted for TCF7L2 in the adult cardiac ventricles; however, only

~200 peaks were detectable, mostly in known target gene promoters like *Axin2* and *SP5*. However, these regions were not enriched for H3K27ac; and in an inactive state, TCF7L2 is known to be bound to repressors like HDAC, TLE and Groucho proteins[115]. Moreover, our and previous studies have shown that the mRNA levels of Wnt target genes *Axin2, Lef1* are all basal/negligible in the healthy adult heart.

In the first chapter of this thesis, GATA4 motifs were found enriched in TCF7L2-bound regions in the diseased cardiac ventricles. Curiosity regarding the relevance of GATA4 within the Wnt nuclear complex of the adult heart prompted IP experiments, revealing a clear interaction between GATA4 and B-catenin in the normal adult heart. This was surprising for two reasons: a. since GATA4 motifs were identified in TCF7L2-occupied regions in the diseased hearts, there was an expectation that the interaction occurred instead between GATA4 and TCF7L2; and b. GATA4 is known to drive hypertrophic responses in diseased heart. Hence, the interaction was expected in the diseased, rather than in the healthy heart. This suggests the involvement of other co-factors to this Wnt-GATA4 complex, which restrict the activity of the Wnt pathway in the adult heart. On this note, previous data had revealed Krueppel-like factor 15 (KLF15) as a common interacting partner between B-catenin, TCF7L2 and Nemo-like kinase (NLK) in adult murine heart tissue. Notably, NLK is a known inhibitor of the B-catenin-TCF7L2 complex. This study had provided the first evidence for the role of KLF15 as a cardiac nuclear Wnt inhibitor and revealed that lack of KLF15 led to increased Wnt target genes activation in the adult heart, along with aberrant tendencies of KLF15 KO cardiac progenitor cells (CPC) to commit towards endothelial-like fate rather than myocyte-like fate. It was further shown that at baseline, KLF15 KO mice exhibited reduced cardiac performance at 12 weeks of age and later. Moreover, the lack of KLF15 resulted in exacerbated pathological responses post-pressure overload and upon Angiotensin II treatment, all signifying the importance of KLF15 in cardiac homeostasis[64]. Apart from these previous studies, other groups had also reported KLF15 as a repressor of maladaptive hypertrophic pathways in the heart, essential for homeostasis. In the normal heart, KLF15 was shown to inhibit Myocardin (MYOCD), thereby repressing the activation of SRF and its pathological gene transcription; and that its loss led to increased association of MYOCD and SRF, thereby promoting cardiac dysfunction[63,116]. An interesting study demonstrated the direct role of KLF15 in regulating the cardiac circadian rhythm by binding to relevant genomic regions in the adult heart[61]. Owing to the above reasons, this thesis aimed at studying the age-specific

roles of KLF15 in cardiac development, maturation and homeostasis, thereby closely examining its importance in stage-specific cardiac functions. Firstly, KLF15 expression was tested in murine cardiac tissue across different developmental and adult stages. This revealed an increasing trend towards adulthood, consistent with its proposed homeostatic role in the adult hearts.

Interestingly, KLF15 was shown to bind to *Gata4* promoter, suppressing its expression for cardiac homeostasis[117]. Moreover, KLF15 was observed bound to the Wnt target- *Axin2* promoter too. Notably, upon overlapping published ChIP-seq datasets for KLF15 and GATA4 in the healthy adult hearts, an extensive intersect was observed (data not shown, unpublished work), further supporting the existence of a cardiac-specific Wnt repressive complex in the healthy adult heart. Experiments are ongoing to investigate the nature of this probable interaction. Further, ChIP-seq experiments in KLF15 KO hearts for TCF7L2, GATA4 and H3K27ac could strongly determine the consequences of losing a Wnt-repressor KLF15 on the cardiac chromatin landscapes occupied by an activator like TCF7L2.

**7.2 Disease**

Different components of the Wnt signaling pathway are reported to be reactivated in the diseased hearts by multiple research groups. Changes in Wnt proteins like GSK3β and Protein Kinase B (PKB) have been shown to induce a cytoplasmic stabilization of B-catenin, propelling a hypertrophic response in an injured myocardium[104,118,119]. Additionally, soluble Frizzled-related proteins (sFRPs), competitors of Wnt ligand binding to Frizzled (FZD) receptors, are shown to be upregulated in the myocardium post-infarct. Studies have also demonstrated a protective role of sFRP1 in the heart, post-injury[41,120]. On the other hand, the group of M. Blankesteijn has thoroughly studied and shown the important presence of Wnt signaling in myocardial would healing, especially with FZD2 receptor[11,103,121]. Despite controversial claims regarding both deteriorative as well as protective roles of the Wnt pathway in the failing heart, it was interesting to observe a common trend which was being recurrently suggested by data from research groups worldwide: that B-catenin cytoplasmic/nuclear accumulation in the CMs was detrimental for the adult heart. This activation could be due to lack of repressors or hyper-activation of mediators in the heart. However, still, there was no strong evidence for its downstream implications (especially at the chromatin level) in pathogenesis of heart disease.

**Activation due to lack of repressors**

KLF15 KO mice exhibited poor cardiac performance 12 weeks of age onwards, where increased Wnt activity was detected. In order to get deeper insights into the chromatin-linked transcriptional role of KLF15, published KLF15 ChIP-seq data in adult heart tissue was overlapped with own RNA-seq data of different WT and KO murine ages (P10, 4 weeks and 20 weeks old, due to different *Klf15* expression levels at these three ages). This integrative analysis revealed a persistent, transcriptionally activating function of KLF15 on the control of cardiac metabolic processes across all ages, along with an age-dependent repressive role on pathological gene programs in the heart. This present study is the first to identify direct KLF15 target genes and characterize their functional relevance, in an age-dependent manner.

At P10, lack of KLF15 did not result in major differences in cardiac transcriptomes, with preserved cardiac function. This corroborates the finding that KLF15 was not expressed at P10 and hence, its loss was not injurious to the heart. At 4 weeks, again with preserved heart function, KLF15 loss led to an increase in B-catenin dependent Wnt signaling (and validated by its increased targets *Axin2, CD44* and *Sox4*). At 20 weeks, the heart deteriorated further, with a concomitant increase in B-catenin independent (non-canonical) Wnt pathway components (e.g *Wnt5b*). Within this network, *Shisa3*, a cytoplasmic Frizzled inhibitor previously identified in *Xenopus* and in *in vitro* malignant cells[122,123], was identified. Studies have repeatedly addressed the repressive role of non-canonical Wnt on their B-catenin-dependent (canonical) counterparts[124,125], leading us to hypothesize that *Shisa3* could belong to the non-canonical Wnt circuit within the heart. Moreover, there was no information regarding *Shisa3* and its function in the heart, rendering it as an attractive target that deserved further investigation.

Expression analyses revealed that *Shisa3* was mainly a developmental gene (unpublished data), which was re-activated in heart disease. Further, Shisa3-positive cells showed an endothelial-like feature, with their remarkable co-localization with early endothelial markers like Endomucin (*Emcn*). This was in line with the finding that pressure-overload in the adult heart increased endothelial reprogramming (based on increased *Emcn* levels) and hence, *Shisa3* may be part of this aberrantly reactivated program. Interestingly, KLF2 and KLF4 were recently shown to be indispensable for the maintenance of the endothelial and vascular networks and that an endothelial deletion of these factors resulted in increased mortality in mice[126,127]. Multiple groups have also shown that KLF15 regulates vascular smooth muscle cell identity and protects from

vascular inflammation and dysfunction[128,129]. However, a direct link between KLF15 and endothelial reprogramming via Wnt activation was never shown before, especially in myocardial homeostasis.

In the quest to identify what exactly regulates *Shisa3* directly in the heart, *in silico* as well as *ex vivo* experiments were performed. Notably, a direct binding of KLF15 to *Shisa3* promoter was detected in the published ChIP data in the adult heart. Strikingly, *ex vivo* embryonic heart culture experiments revealed that the overexpression of KLF15, particularly in the heart, *repressed Shisa3* expression; while activating Wnt signaling by treating the cultured hearts with Wnt-conditioned medium, *increased Shisa3* expression. Importantly, these results also showed a conserved reactivation of Wnt signaling as well as *SHISA* in Engineered Human Myocardial (EHM) tissue upon loss of KLF15 in CMs.

**Activation due to overexpression of mediators**

The fact that Wnt signaling components are activated during heart disease is not new. The results of this thesis confirmed an upregulation of TCF7L2 and total B-catenin in both murine and human heart disease, as reported recently also by Hou and colleagues[44]. In addition to total B-catenin, p-S675-B-catenin (phosphorylation at serine 675$^{th}$ residue- leading to its activation and nuclear translocation) was also upregulated- which was not reported before in the heart.

However, this activation could be either a cause, or a consequence of pathological remodeling, or both. Hence, in order to clearly define Wnt's role in this process, an inducible CM-specific stabilization of B-catenin was achieved in the adult heart. The reason for choosing adult hearts was because tweaking B-catenin levels during development has been shown to be embryonically lethal, given its crucial role in mesoderm formation[35,130]; and that the adult heart was a suitable environment to study disease mechanisms, if any.

Inducing CM-B-catenin stabilization (gain of function: B-cat GOF) led to severe mortality within the first week post-tamoxifen (TX) administration in mice. Time-point analyses revealed a decline in cardiac function along with CM hypertrophy and fibrosis, and an increased expression of Wnt target gene transcription, 3 weeks post-induction. These findings indicated that simply activating Wnt signaling in the adult myocardium triggered detrimental pathological responses, culminating in heart failure. Given that Wnt signaling is known to be a developmental pathway, essential for cardiac regenerative responses post-injury, the above results point to the

repercussions of hyper-activating a regenerative pathway in the wrong context (in the adult CMs); leading to hypertrophic remodeling. Interestingly, activating B-catenin in the endothelial cells of the adult heart also led to severe cardiac dysfunction[131]. In line with the above findings, another study showed that loss of B-catenin in Periostin (POSTN)-expressing fibroblasts attenuated fibrotic responses in the adult heart, ameliorating its function post-stress[42].

To truly understand the mechanisms triggered upon B-catenin stabilization in the adult CMs, gene ontology analyses were performed. Genes annotating to cardiac development (*Myh7, Hand2, Tbx20, Sox4, Cacna1g, Bambi*), cytoskeletal remodeling (*Dstn, Rock2, Wnt11*), cell cycle (*Ccnd2, Ccng1, Mki67*), vascular development (*Edn3, Angpt1, Vav1*) and Wnt pathway (*Axin2*) were all upregulated in B-cat GOF hearts. The upregulation of these processes could also be well validated with immunofluorescence stainings, immunoblots and qPCRs. Within this dataset, an increase in *Shisa3* (the newly found fetal gene upregulated in KLF15 KO hearts) was also observed in this model with direct Wnt activation. As expected, p-S675-B-catenin, total B-catenin and TCF7L2 protein expressions were increased in these B-cat-GOF-diseased cardiac ventricles; whereas *Tcf7l2* transcript levels remained unchanged, owing to its numerous isoforms contributing to the challenges of measuring changes in *Tcf7l2* gene expression[47–49].

To understand the chromatin-associated role of TCF7L2 in heart disease, ChIP-seq was performed both for TCF7L2 and H3K27ac in B-cat-GOF hearts. Not only was there a global increase in H3K27ac occupancy, but also specifically on TCF7L2-occupied regions in diseased compared to healthy adult hearts, suggesting an overall and TCF7L2-specific increase in transcriptional activity in the disease genome. This is in line with the massive increase in cell-cycle activity and developmental processes in the GOF diseased hearts. Differential H3K27ac binding analyses further revealed an enrichment of TCF7L2 along with other pathological TFs like PPARG[132] and STAT1[133] specifically in the diseased, and not in the normal heart. Not only for H3K27ac, but TCF7L2-bound regions were also enriched for RNAPII and H3K4me1, along with a significant overlap with DNAse-seq accessible chromatin regions in the adult heart, further supporting its transcriptionally activating function.

The most striking observation was that TCF7L2 occupied distal enhancer regions (based on the enrichment of H3K27ac) in diseased hearts. Promoter-based, proximal TCF7L2 occupancies have been long reported in different malignant cells[91]. However, in 2012, Frietze and colleagues

experimentally demonstrated the binding of TCF7L2 to distal enhancer regions in several human carcinoma cells[50], augmenting the validity of our findings of its activity at enhancers in the diseased myocardium. The distal-disease enrichment of TCF7L2 is particularly remarkable because important chromatin remodelers like BRG1 (Brahma-Related Gene 1) and BRD4 (Bromodomain-containing protein 4) have been strongly implicated to act on distal enhancer regions, propelling heart disease progression[19,23]. Therefore, TCF7L2 could potentially be associated to chromatin remodelers, *specifically on distal regions* in the diseased hearts. ChIP-seq experiments for BRG1 and/or BRD4 occupancies in B-cat-GOF hearts could reveal important insights into this novel putative mechanism.

Consistent with transcriptomic data, TCF7L2-occupied regions annotated mainly to cardiac developmental processes and despite its prominent role in tumor biology and proliferation, 'heart failure' was the most significant disease ontology in B-cat-GOF failing hearts, hinting at its context-specificity. It was interesting to observe that the overlap between TCF7L2-bound genes and the upregulated genes in these diseased hearts was not enormous. This could be explained by the presence of other Wnt effectors like LEF1, which could possibly also be involved in part, to mediate downstream Wnt actions in the diseased myocardium.

Only 68 out of the 376 upregulated DEGs coincided with TCF7L2-bound genes. These 68 genes annotated to heart developmental processes. On the other hand, the 308 upregulated genes that were *not* bound by TCF7L2 annotated mainly to mitotic cell-cycle processes, which could be attributed to direct effects of B-catenin-activation (given its important role in promoting cell-cycle), not involving TCF7L2. Experiments determining the genomic occupancy of B-catenin and comparing with that of TCF7L2 could clarify the TCF7L2-independent and B-catenin-dependent transcriptional activation observed in these hearts.

Having successfully identified cardiac targets of TCF7L2, the search for *cardiac-specific* targets unfolded. An important study in 2014 had mapped TCF7L2 targets in a similar B-cat-GOF transgenic murine model, but in the liver[105]. This dataset provided the basis for discerning liver-specific and cardiac-specific TCF7L2 target genes. While enrichments were expectedly observed on the promoters of classical targets *Axin2, SP5* and *Lef1* in both the heart and liver; there was a prominent trend: liver-specific regions (e.g *Aldoa, Aldob, Aldh3a2, Acer3, Smpd4*) annotated to cholesterol, steroid and glucose metabolism; and heart-specific regions (e.g *Hand2, Tbx20, Dstn,*

*Rock2*) annotated to cardiac morphogenesis. Notably, TCF7L2 was shown to interact with HNF4a and FOXA2, both factors crucial for hepatocyte homeostasis, in liver cells[90]. These informative cues prompted the hunt for the cardiac interaction partners of TCF7L2.

Unbiased *de-novo* motif search on TCF7L2-bound heart regions unearthed indeed, an enrichment of cardiac master TFs like GATA4 and NKX2-5 motifs. Given the known antagonistic relationship of GATA4 and Wnt signaling; and that GATA4 is known to mediate pathological disease responses in hypertrophic hearts, this finding was stifling. To delve deeper into the mechanism of this putative association, published GATA4 ChIP-seq dataset[92] in the normal adult heart was overlapped with the TCF7L2-disease regions. This revealed a 30% overlap between the two. It could either be an activating or a repressive association. To answer this, luciferase assays were performed and the results were astonishing: upon addition of GATA4 to commonly bound, Wnt-driven TCF7L2-GATA4 cardiac enhancers (enhancers upstream of *Hand2* and *Tbx20*), the firefly luciferase activity was repressed. This repressive association was also validated with ChIP-qPCRs. Curiously, this finding was in line with the observation that GATA4 interacted with B-catenin in the healthy adult heart, where Wnt signaling was quiescent (described in the "adulthood" section previously). Further IP experiments indicated a *loss* of GATA4-B-catenin interaction in diseased hearts (both in experimental and B-cat-GOF cardiac disease models), strongly suggesting a repressive role of GATA4 on Wnt-occupied genomic regions in the adult heart, the loss of which triggers Wnt activation and pathological remodeling. It is possible that other pathological cardiac chromatin players mentioned before like BRD4 and/or BRG1 could instead supersede and associate to TCF7L2, steering towards heart failure.

More importantly, in line with previous studies from our group[43], cardiac performance could be rescued post-injury by inactivating B-catenin. This also reduced the expression of the identified TCF7L2-cardiac-disease target genes, confirming the important role of TCF7L2 in mediating Wnt-related pathogenesis in the adult myocardium. Additionally, ChIP-qPCR experiments for testing GATA4 occupancy on the commonly TCF7L2-GATA4-bound *Hand2* and *Tbx3* loci validated an enrichment of GATA4 in the healthy adult, its loss in disease; and importantly, a *re-enrichment* in the B-catenin inactivated, rescued hearts.

### 7.3 Development and Regeneration

The development of the cardiovascular system demands precise, phase-specific regulation of Wnt signaling, given that it has been shown to both promote as well as restrict CM specification[12]. Elevated Wnt/β-catenin pathway activity has been reported in the developing heart using numerous TCF/LEF reporter lines. Despite evidences showing its activity in the pericardium, endocardial cushions, cardiac mesoderm, and the early outflow tract, only a basal activity was reported in the ventricular myocardium. Wnt signaling has been shown to regulate the development of the heart's anterior portion including the outflow tract and the right ventricle. The deletion of β-catenin in the SHF (Second Heart Field) caused a dramatic reduction in both the levels of Isl1 (Islet-1) expression and the numbers of cells that express Isl[13,134]. Even though the overall transcriptional activity of the Wnt pathway is often gauged by B-catenin localization, phosphorylation or interacting partners and TCF/LEF reporter lines; the Wnt related TFs LEF1 (Lymphocyte Enhancer Factor-1) and TCF7L2 (Transcription Factor 7-like 2, formerly known as TCF4) mediate most downstream nuclear activating functions[45,46,135–137] of the pathway, while TCF7 and TCF7L1 are predominantly repressive[138,139] on Wnt target loci.

TCF7L1 was shown to inhibit CM specification after an initial induction, promoting endothelial cell differentiation in zebrafish[138,140]. LEF1 was shown to be important for axial and paraxial mesoderm differentiation in *Xenopus* embryos. Embryos lacking LEF1 failed to develop major blood vessels of the heart and the heart itself[141]. While TCF7L2 has been implicated as a significant player in forebrain development and ectodermal maintenance[85], there has been no evidence regarding the role of TCF7L2 in heart or mesodermal development, despite the known relevance of Wnt signaling in this process. Moreover, the significance of TCF7L2 was never investigated in the working myocardium, either in heart development or in other cardiac contexts.

Results of this thesis indicate that TCF7L2 expression increased postnatally until P6 (postnatal day 6) and is very low at baseline in the adult heart. Considering that the CMs in the developing heart gradually lose their ability to proliferate (around P7 in mice)[37], this increasing cardiac TCF7L2 expression trend from development to early neonatal life was surprising. This is because TCF7L2 has been implicated as a strong mediator of mitotic Wnt activity in several malignancies and also in stem cell population maintenance[85,86,135]. In the neonatal cardiac tissue,

TCF7L2 displayed a very high overall protein expression at murine P6. Further immunostainings revealed that TCF7L2 was expressed in cardiac Troponin T (cTNT)-positive CMs, both at P3 and P6, but very low at P0 (similar to total protein expression). At P6, the CMs are already specified, yet possess the ability to proliferate and populate the growing myocardium, with a switch in metabolic responses, required to generate adequate contractile forces of the beating adult heart. Further, KI67 (a mitosis marker[142]) immunostainings also revealed robust KI67 expression in TNNT2-positive cells at P6, demonstrating ongoing cell-cycle activity in the CMs at this age. It seems that TCF7L2 is crucial for CM function once they *have already attained a certain specification* in the developing/maturing mammalian myocardium. This could suggest the involvement of other Wnt mediators during the initial phase of cardiac development.

TCF7L2 possesses a strikingly unique tendency of interacting with cell-specific TFs to control cell-specific gene transcription[53,57,105]. In the quest to unravel its cardiac interaction partners, the first chapter of this thesis identified GATA4 using *de novo* motif search analyses on TCF7L2-occupied regions in the diseased myocardium. GATA4 is one of the most important cardiac TFs, necessary to maintain cardiac function, at every stage of life[28,29]. With respect to Wnt pathway and cardiac maturation, GATA4 has often been demonstrated to act antagonistically, wherein, increased GATA4 and decreasing Wnt was essential for CM maturation and vice-versa for proliferation of pro-cardiogenic cells[143]. However, its direct interaction with Wnt nuclear components was never shown before. Interestingly, in P6 hearts, an interaction between GATA4 and B-catenin was observed, despite a high Wnt activity (as opposed to the low Wnt activity in the healthy adult heart) and TCF7L2 expression at this stage. This signifies a mix and clash of maturation as well as developmental (based on increased CM cycling) transcriptional states in the neonatal, regenerative hearts.

Intrigued by the peculiar neonatal heart interaction profile, both RNA-seq; and ChIP-seq for TCF7L2, GATA4 and H3K27ac were performed. P6 transcriptomes grouped distinctly in comparison to normal and diseased adult hearts. Interestingly, transcriptomic data revealed that the Wnt-activated (B-cat GOF) hearts were enriched specifically for immune, angiogenesis and muscle developmental process and P6 hearts for aldehyde and fatty acid metabolic processes. Notably, P6-Disease commonly enriched transcripts (in comparison to the healthy adult heart) annotated expectedly to cell cycle, Wnt signaling pathway and chromatin reorganization processes- highlighting the similarities between these two cardiac states. With respect to the

genomic occupancy profiles, it was interesting to observe that in neonatal P6 hearts, TCF7L2 not only occupied proximal promoter-based genomic regions, but these regions annotated primarily to metabolic processes, along with heart development, Wnt signaling and cell-cycle activity (corroborating RNA-seq results). The maturing CMs switch from glucose to fatty-acid oxidative metabolism, with a tendency to reactivate glucose metabolism in heart disease[144]. TCF7L2 binding was also observed on classical Wnt target gene promoters of *Axin2* and *SP5*, showing increased Wnt transcriptional activity. Within the metabolic genes cohort, TCF7L2 bound predominantly to aldehyde and fatty-acid metabolic genes like *Aldh3a2* and *Sptlc2* respectively. Given the need for neonatal hearts to progress and build a fully mature, robust, contractile myocardium, and at the same time, grow in size by proliferating CMs. The enrichment of metabolic as well as cell-cycle processes implicates the important role of TCF7L2 in mediating this response.

Consistent with the indispensable role of GATA4 in heart homeostasis, GATA4-occupied regions (e.g *Myl2, Nr3c2*) annotated mainly to heart structure development, CM contraction and metabolism in P6 hearts. This is the first study to profile the genomic landscapes of GATA4 and TCF7L2 occupancies in the neonatal mammalian myocardium, directly identifying their downstream target genes, essential for regenerative responses. The fact that GATA4 occupied ~18,000 regions in comparison to a mere 1200 TCF7L2-bound regions in P6 hearts indicates the necessity and dominance of GATA4 over other TFs in the working myocardium. Strikingly, despite the profound difference in the number of bound-sites, not only was there a considerable overlap (75% of TCF7L2 peaks) between TCF7L2 and GATA4-occupied regions in the P6 hearts, but also a remarkable association of these genes to cardiac developmental and maturation annotations. Moreover, TCF7L2, GATA4 and their commonly bound regions were all highly enriched for H3K27ac, suggesting a transcriptionally active role of their synergy on these loci. However, GATA4 is expressed throughout cardiac development, maturation, homeostasis and disease. This raised a question whether a regeneration-stage specific TF could be involved within this TF-complex at P6. On performing *de novo* sequence-based motif search on both TCF7L2 and GATA4-bound regions in P6 hearts, a common enrichment of TEAD2- a TF, which mediates downstream gene transcription of Hippo pathway, was unearthed. This finding is interesting for a multitude of reasons. Firstly, Hippo pathway is a crucial player in cardiac regeneration post-injury and its activation in the adult heart post-disease has been shown to

improve cardiac performance[98,99]. Secondly, similar to Wnt pathway, Hippo pathway also has multiple TFs (TEAD1-4), mediating its downstream activities. Of these TEADs, TEAD4 is implicated significantly in skeletal myocytes differentiation and maintenance[145]. Moreover, TEAD1, 3 and 4 are expressed in adult tissues[146], whereas TEAD2 is predominantly expressed in developing tissues[96,97,147], suggesting its possible involvement in providing a 'regenerative-context' to this GATA4-B-catenin association in the neonatal hearts (given that this interaction occurred both in P6 and healthy adult hearts). Owing to these reasons, TEAD2 was characterized further in the ventricular myocardium. In line with its known relevance in developing tissues, TEAD2 expression was high throughout early developmental and neonatal stages, becoming low in adult and diseased hearts. Furthermore, IP experiments revealed an interaction between TEAD2 and B-catenin, only in the P6 and not in the adult or diseased hearts, supporting its envisaged role specifically at this age. ChIP-qPCRs for TCF7L2-TEAD2 commonly bound regions in P6 hearts could confirm their synergistic association in the neonatal cardiac chromatin.

### 7.4 Neonatal vs. Disease

Pathological machineries in a failing heart result in an activation of regenerative responses, including developmental transcriptional programs. Despite this activation, the heart proceeds towards dysfunction. Therefore, discerning regenerative and disease states could help explain this inability of the adult heart to cope with stress. Global cardiac chromatin landscapes have been studied and compared in development and disease[15,18]. An interesting study had revealed context-specific genomic occupancies of GATA4 in the fetal, healthy and diseased adult hearts[92]. However, a detailed investigation involving the Wnt pathway was never performed, prior to the present study. Upon performing differential TCF7L2 occupancy analyses in the neonatal and diseased hearts, it became evident that TCF7L2 clearly played distinct roles in both these contexts. While it occupied proximal, promoter-based regions in the neonatal, regenerative hearts; the occupancy was predominantly on distal enhancers in the diseased hearts. This unique trend in the genomic occupancies of TCF7L2 in these two contexts could occur for many reasons. RNAPII (RNA polymerase II), together with the transcription initiation complex components like TAF1 (TATA-Box Binding Protein Associated Factor 1), p300/CBP usually drive promoter-based TF gene responses[148,149]. On the other hand, factors like BRD4 and BRG1 occupy distal enhancer regions and have known roles in cardiac disease progression. Even though TCF7L2 is known to associate with cell-specific TFs; depending on the context within

the same cell- type, TCF7L2 could possess unique interaction partners that are *chromatin remodelers*. Further ChIP and IP experiments can potentially validate this hypothesis. Interestingly, TCF7L2-bound regions in both neonatal and diseased hearts were highly enriched for H3K27ac- indicating the active state of Wnt-based gene transcription.

Delving deeper into the differentially bound TCF7L2 regions in these two cardiac states, biological processes were identified. Strikingly, metabolic processes (predominantly genes annotating for aldehyde and fatty acid metabolism like *Aldh3a2, Sptlc2*) were enriched in P6-specific. Cardiac developmental and angiogenesis processes were enriched in disease-specific regions. Notably, the maturing CM in the neonatal heart tends to switch to fatty acid from glucose metabolism, required for the excessive energy demands in the constitutively beating mature adult heart. The fact that TCF7L2 specifically plays a role on the promoters of metabolic genes in neonatal hearts is a new finding. Interestingly, nuclear B-catenin has been shown to interact with a plethora of metabolism-related TFs like PPARG (Peroxisome Proliferator Activated Receptor Gamma), RXRA (Retinoid X Receptor Alpha), FOXO (Forkhead Box O) and RAR (Retinoic Acid Receptor), especially influencing metabolic gene promoters[95,144]. Hence, it would be logical to speculate a possible interaction of TCF7L2 with the above-mentioned metabolic TFs in neonatal hearts. Given that cardiac regeneration was never investigated before in the context of TCF7L2-metabolism-chromatin, this paves the way for future studies.

Meanwhile, the enrichment of vascular and angiogenesis processes in TCF7L2-bound disease-specific regions (like *Angpt1, Ang, Vav1*) in the heart is also particularly interesting. This is because a recent study demonstrated that B-catenin activation in the endothelial cells of the adult heart led to severe cardiac dysfunction[131]. Additionally, B-catenin was shown to directly interact with ERG (ETS-Related Gene) to regulate endothelial transcription[150]. Moreover, Wnt signaling has been implicated strongly in promoting angiogenesis in several metastatic tumors[151,152].

## 8. Summary of Results

This thesis characterized and identified the stage and context-specific, chromatin-associated roles of nuclear Wnt signaling in the heart. The fetal program reactivation in the diseased heart is never sufficient to fully restore cardiac function and reach its original regenerative capacity

(dashed line in scheme below). This could be attributed to the differential transcriptional and chromatin states in these two situations. In neonatal, regenerative hearts, Wnt activity/TCF7L2 expression is high, along with a GATA4-B-catenin interaction, driving both homeostatic as well as proliferative processes in CMs, necessary for driving maturation and heart growth, at the same time. In this stage, TCF7L2 occupies proximal regions, specifically promoting fatty acid and aldehyde metabolism; and these regions are enriched for H3K27ac. In the healthy adult hearts, Wnt/TCF7L2 is low, devoid of H3K27ac enrichment, owing to the presence of cardiac Wnt repressors like KLF15; again, with an intact GATA4-B-catenin interaction, ensuring homeostasis. Conversely, the diseased myocardium entails a loss of repressors like KLF15 and GATA4; with TCF7L2 overtaking transcriptional roles on distal enhancers. These regions specifically regulate cardiac developmental and vascular/angiogenesis processes, also enriched for H3K27ac. Altogether, this study identified TCF7L2 target genes across different cardiac stages and unraveled novel mechanistic insights into the role of context-specific interaction partners, essential to elicit accurate gene regulation in heart homeostasis and disease.

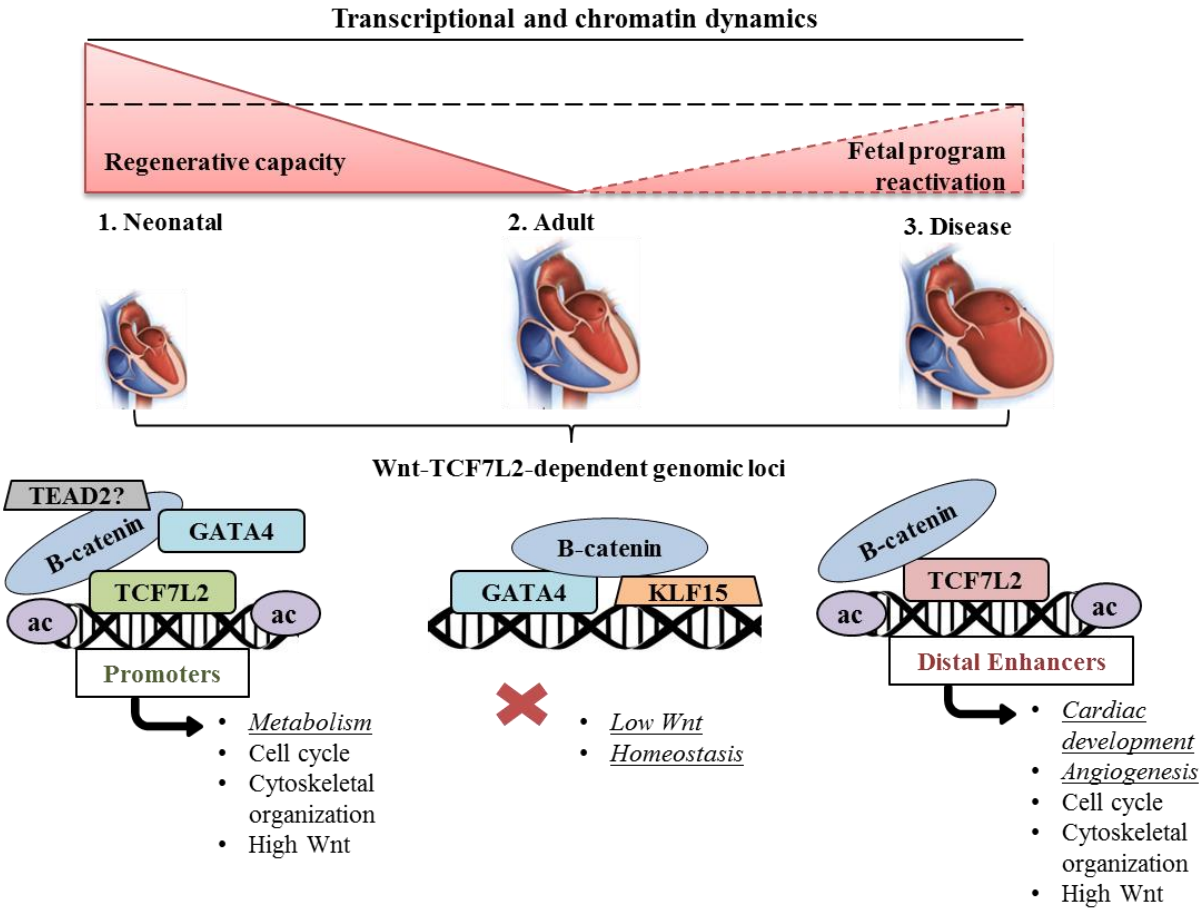

# 9. References (for overall Introduction and Discussion)


1. Szibor, M., Pöling, J., Warnecke, H., Kubin, T. & Braun, T. Remodeling and dedifferentiation of adult cardiomyocytes during disease and regeneration. *Cellular and Molecular Life Sciences* **71,** 1907–1916 (2014).
2. Jiang, F. *et al.* Angiotensin-converting enzyme 2 and angiotensin 1-7: Novel therapeutic targets. *Nature Reviews Cardiology* **11,** 413–426 (2014).
3. Chowdhury, S. K. *et al.* Stress-Activated Kinase Mitogen-Activated Kinase Kinase-7 Governs Epigenetics of Cardiac Repolarization for Arrhythmia Prevention. *Circulation* **135,** 683–699 (2017).
4. Ellison, G. M., Waring, C. D., Vicinanza, C. & Torella, D. Physiological cardiac remodelling in response to endurance exercise training: cellular and molecular mechanisms. *Heart* **98,** 5–10 (2012).
5. Kuwahara, K., Nishikimi, T. & Nakao, K. Transcriptional Regulation of the Fetal Cardiac Gene Program. *Journal of Pharmacological Sciences* **119,** 198–203 (2012).
6. Dirkx, E., da Costa Martins, P. a. & De Windt, L. J. Regulation of fetal gene expression in heart failure. *Biochim. Biophys. Acta - Mol. Basis Dis.* **1832,** 2414–2424 (2013).
7. Chaudhry, H. W. *et al.* Cyclin A2 mediates cardiomyocyte mitosis in the postmitotic myocardium. *J. Biol. Chem.* **279,** 35858–35866 (2004).
8. Woo, Y. J. *et al.* Therapeutic delivery of cyclin A2 induces myocardial regeneration and enhances cardiac function in ischemic heart failure. *Circulation* **114,** (2006).
9. Jessen, J. R. Noncanonical Wnt signaling in tumor progression and metastasis. *Zebrafish* **6,** 21–8 (2009).
10. Zhan, T., Rindtorff, N. & Boutros, M. Wnt signaling in cancer. *Oncogene* **36,** 1461–1473 (2017).
11. Hermans, K. C., Daskalopoulos, E. P. & Blankesteijn, W. M. Interventions in Wnt signaling as a novel therapeutic approach to improve myocardial infarct healing. *Fibrogenesis Tissue Repair* **5,** 16 (2012).
12. Gessert, S. & Kühl, M. The multiple phases and faces of Wnt signaling during cardiac differentiation and development. *Circ. Res.* **107,** 186–199 (2010).
13. Brade, T., Männer, J. & Kühl, M. The role of Wnt signalling in cardiac development and tissue remodelling in the mature heart. *Cardiovasc. Res.* **72,** 198–209 (2006).
14. Mathiyalagan, P., Keating, S. T., Du, X. & El-osta, A. Chromatin modifications remodel cardiac gene expression. *Cardiovasc. Res.* **103,** 7–16 (2014).
15. Han, P., Hang, C. T., Yang, J. & Chang, C. P. Chromatin remodeling in cardiovascular development and physiology. *Circ. Res.* **108,** 378–396 (2011).
16. Iyer, L. M. *et al.* A context-specific cardiac β-catenin and GATA4 interaction influences TCF7L2 occupancy and remodels chromatin driving disease progression in the adult heart. *Nucleic Acids Res.* (2018). doi:10.1093/nar/gky049
17. Tyagi, M., Imam, N., Verma, K. & Patel, A. K. Chromatin remodelers: We are the drivers!! *Nucleus* **7,** 388–404 (2016).
18. Quaife-Ryan, G. A. *et al.* Multicellular transcriptional analysis of mammalian heart regeneration. *Circulation* **136,** 1123–1139 (2017).
19. Hang, C. T. *et al.* Chromatin regulation by Brg1 underlies heart muscle development and disease. *Nature* **466,** 62–67 (2010).
20. Takeuchi, J. K. *et al.* Chromatin remodelling complex dosage modulates transcription factor function in heart development. *Nat. Commun.* **2,** (2011).
21. Bruneau, B. G. The developmental genetics of congenital heart disease. *Nature* **451,** 943–948 (2008).
22. Bartholomeeusen, K., Xiang, Y., Fujinaga, K. & Peterlin, B. M. Bromodomain and extra-terminal (BET) bromodomain inhibition activate transcription via transient release of Positive Transcription Elongation Factor b (P-TEFb) from 7SK small nuclear ribonucleoprotein. *J. Biol. Chem.* **287,** 36609–36616 (2012).
23. Anand, P. *et al.* BET bromodomains mediate transcriptional pause release in heart failure. *Cell* **154,** 569–582 (2013).
24. Creyghton, M. P. *et al.* Histone H3K27ac separates active from poised enhancers and predicts developmental state. *Proc. Natl. Acad. Sci. U. S. A.* **107,** 21931–21936 (2010).
25. Dickel, D. E. *et al.* Genome-wide compendium and functional assessment of in vivo heart enhancers. *Nat. Commun.* **7,** 1–13 (2016).
26. May, D. *et al.* Large-scale discovery of enhancers from human heart tissue. *Nat. Genet.* **44,** 89–93 (2012).
27. Wamstad, J. a., Wang, X., Demuren, O. O. & Boyer, L. a. Distal enhancers: New insights into heart development and

disease. *Trends Cell Biol.* **24,** 294–302 (2014).

28. Schlesinger, J. *et al.* The cardiac transcription network modulated by gata4, mef2a, nkx2.5, srf, histone modifications, and microRNAs. *PLoS Genet.* **7,** (2011).

29. Ang, Y. S. *et al.* Disease Model of GATA4 Mutation Reveals Transcription Factor Cooperativity in Human Cardiogenesis. *Cell* **167,** 1734–1749.e22 (2016).

30. Narlikar, L., Sakabe, N. J. & Blanski, A. a. Genome-wide discovery of human heart enhancers --- Genome Research. *Genome Res.* **20,** 381–392 (2010).

31. Sasaki, T., Hwang, H., Nguyen, C., Kloner, R. a. & Kahn, M. The Small Molecule Wnt Signaling Modulator ICG-001 Improves Contractile Function in Chronically Infarcted Rat Myocardium. *PLoS One* **8,** 2–12 (2013).

32. Inestrosa, N. C. & Arenas, E. Emerging roles of Wnts in the adult nervous system. *Nat Rev Neurosci* **11,** 77–86 (2010).

33. Cohen, E. D. *et al.* Wnt/beta-catenin signaling promotes expansion of Isl-1-positive cardiac progenitor cells through regulation of FGF signaling. *J. Clin. Invest.* **117,** 1794–1804 (2007).

34. Ueno, S. *et al.* Biphasic role for Wnt/beta-catenin signaling in cardiac specification in zebrafish and embryonic stem cells. *Proc. Natl. Acad. Sci.* **104,** 9685–9690 (2007).

35. Lickert, H. *et al.* Formation of multiple hearts in mice following deletion of β-catenin in the embryonic endoderm. *Dev. Cell* **3,** 171–181 (2002).

36. Alexander, J. M. & Bruneau, B. G. Lessons for cardiac regeneration and repair through development. *Trends in Molecular Medicine* **16,** 426–434 (2010).

37. Porrello, E. R. *et al.* Transient regenerative potential of the neonatal mouse heart. *Science* **331,** 1078–80 (2011).

38. N., P., A., K., I., B. & D., P. Neonatal myocardial infarction secondary to umbilical venous catheterization: A case report and review of the literature. *Paediatrics and Child Health* **14,** 539–541 (2009).

39. Uygur, A. & Lee, R. T. Mechanisms of Cardiac Regeneration. *Dev. Cell* **36,** 362–374 (2016).

40. Mercola, M., Ruiz-Lozano, P. & Schneider, M. D. Cardiac muscle regeneration: Lessons from development. *Genes Dev.* **25,** 299–309 (2011).

41. Nakamura, K. *et al.* Secreted frizzled-related protein 5 diminishes cardiac inflammation and protects the heart from ischemia/reperfusion injury. *J. Biol. Chem.* **291,** 2566–2575 (2016).

42. Xiang, F. L., Fang, M. & Yutzey, K. E. Loss of β-catenin in resident cardiac fibroblasts attenuates fibrosis induced by pressure overload in mice. *Nat. Commun.* **8,** (2017).

43. Zelarayan, L. C. *et al.* -Catenin downregulation attenuates ischemic cardiac remodeling through enhanced resident precursor cell differentiation. *Proc. Natl. Acad. Sci.* **105,** 19762–19767 (2008).

44. Hou, N. *et al.* Transcription Factor 7-like 2 Mediates Canonical Wnt/β-Catenin Signaling and c-Myc Upregulation in Heart Failure. *Circ. Hear. Fail.* **9,** 1–9 (2016).

45. Cadigan, K. M. & Waterman, M. L. TCF/LEFs and Wnt signaling in the nucleus. *Cold Spring Harb. Perspect. Biol.* **4,** (2012).

46. Jin, T. & Liu, L. Minireview: The Wnt Signaling Pathway Effector TCF7L2 and Type 2 Diabetes Mellitus. *Mol. Endocrinol.* **22,** 2383–2392 (2008).

47. Weise, A. *et al.* Alternative splicing of Tcf7l2 transcripts generates protein variants with differential promoter-binding and transcriptional activation properties at Wnt/β-catenin targets. *Nucleic Acids Res.* **38,** 1964–1981 (2009).

48. Prokunina-Olsson, L. *et al.* Tissue-specific alternative splicing of TCF7L2. *Hum. Mol. Genet.* **18,** 3795–3804 (2009).

49. Hansson, O., Zhou, Y., Renström, E. & Osmark, P. Molecular function of TCF7L2: Consequences of TCF7L2 splicing for molecular function and risk for type 2 diabetes. *Current Diabetes Reports* **10,** 444–451 (2010).

50. Frietze, S. *et al.* Cell type-specific binding patterns reveal that TCF7L2 can be tethered to the genome by association with GATA3. *Genome Biology* **13,** R52 (2012).

51. Zhao, J., Schug, J., Li, M., Kaestner, K. H. & Grant, S. F. a. Disease-associated loci are significantly over-represented among genes bound by transcription factor 7-like 2 (TCF7L2) in vivo. *Diabetologia* **53,** 2340–2346 (2010).

52. Boccardi, V. *et al.* Potential role of TCF7L2 gene variants on cardiac sympathetic/ parasympathetic activity. *Eur. J. Hum. Genet.* **18,** 1333–1338 (2010).

53. Norton, L. *et al.* Chromatin occupancy of transcription factor 7-like 2 (TCF7L2) and its role in hepatic glucose metabolism. *Diabetologia* **54,** 3132–3142 (2011).

54. Facchinello, N. *et al.* Tcf7l2 plays pleiotropic roles in the control of glucose homeostasis, pancreas morphology, vascularization and regeneration. *Sci. Rep.* **7,** 1–16 (2017).

55. Villareal, D. T. *et al.* TCF7L2 variant rs7903146 affects the risk of type 2 diabetes by modulating incretin action. *Diabetes* **59,** 479–485 (2010).

56. van Es, J. H. *et al.* A Critical Role for the Wnt Effector Tcf4 in Adult Intestinal Homeostatic Self-Renewal. *Mol. Cell. Biol.* **32,** 1918–1927 (2012).

57. Zhao, C. *et al.* Dual regulatory switch through interactions of Tcf7l2/Tcf4 with stage-specific partners propels oligodendroglial maturation. *Nat. Commun.* **7,** 1–15 (2016).

58. McConnell, B. B. & Yang, V. W. Mammalian Krüppel-like factors in health and diseases. *Physiol. Rev.* **90,** 1337–81 (2010).

59. Bieker, J. J. Krüppel-like Factors: Three Fingers in Many Pies. *Journal of Biological Chemistry* **276,** 34355–34358 (2001).

60. Yoshitane, H. *et al.* CLOCK-Controlled Polyphonic Regulation of Circadian Rhythms through Canonical and Noncanonical E-Boxes. *Mol. Cell. Biol.* **34,** 1776–1787 (2014).

61. Zhang, L. *et al.* KLF15 Establishes the Landscape of Diurnal Expression in the Heart. *Cell Rep.* **13,** 2368–2375 (2015).

62. Fan, Y. *et al.* Krüppel-like factors and vascular wall homeostasis. *J. Mol. Cell Biol.* **9,** 352–363 (2017).

63. Leenders, J. J. *et al.* Regulation of cardiac gene expression by KLF15, a repressor of myocardin activity. *J. Biol. Chem.* **285,** 27449–27456 (2010).

64. Noack, C. *et al.* Krueppel-like factor 15 regulates Wnt/β-catenin transcription and controls cardiac progenitor cell fate in the postnatal heart. *EMBO Mol. Med.* **4,** 992–1007 (2012).

65. Prosdocimo, D. a. *et al.* KLF15 and PPAR α Cooperate to regulate cardiomyocyte lipid gene expression and oxidation. *PPAR Res.* **2015,** (2015).

66. Prosdocimo, D. a. *et al.* Kruppel-like factor 15 is a critical regulator of cardiac lipid metabolism. *J. Biol. Chem.* **289,** 5914–5924 (2014).

67. Li, J. *et al.* Sp1 and KLF15 regulate basal transcription of the human LRP5 gene. *BMC Genet.* **11,** 6–13 (2010).

68. Grady, W. M. & Carethers, J. M. Genomic and Epigenetic Instability in Colorectal Cancer Pathogenesis. *Gastroenterology* **135,** 1079–1099 (2008).

69. Sullivan, M., Hahn, K. & Kolesar, J. M. Azacitidine: A novel agent for myelodysplastic syndromes. *American Journal of Health-System Pharmacy* **62,** 1567–1573 (2005).

70. Silverman, L. R. *et al.* Continued azacitidine therapy beyond time of first response improves quality of response in patients with higher-risk myelodysplastic syndromes. *Cancer* **117,** 2697–2702 (2011).

71. Bayat, H. *et al.* Progressive heart failure after myocardial infarction in mice. *Basic Res. Cardiol.* **97,** 206–213 (2002).

72. Struthers, A. D. Pathophysiology of heart failure following myocardial infarction. *Heart* **91,** ii14–ii16 (2005).

73. Fausto, N., Campbell, J. S. & Riehle, K. J. Liver regeneration. *Hepatology* **43,** (2006).

74. Kholodenko, I. V. & Yarygin, K. N. Cellular Mechanisms of Liver Regeneration and Cell-Based Therapies of Liver Diseases. *BioMed Research International* **2017,** (2017).

75. Steinhauser, M. L. & Lee, R. T. Regeneration of the heart. *EMBO Mol. Med.* **3,** 701–712 (2011).

76. Quaife-Ryan, G. a. *et al.* Multi- & ellular Transcriptional Analysis of Mammalian Heart Regeneration. *Circulation* (2017).

77. Miyaoka, Y. *et al.* Hypertrophy and Unconventional Cell Division of Hepatocytes Underlie Liver Regeneration. *Curr. Biol.* **22,** 1166–1175 (2012).

78. Relaix, F. & Zammit, P. S. Satellite cells are essential for skeletal muscle regeneration: the cell on the edge returns centre stage. *Development* **139,** 2845–2856 (2012).

79. Ebrahimi, B. Cardiac progenitor reprogramming for heart regeneration. *Cell Regeneration* (2018). doi:10.1016/j.cr.2018.01.001

80. Amini, H., Rezaie, J., Vosoughi, A., Rahbarghazi, R. & Nouri, M. Cardiac progenitor cells application in cardiovascular disease. *J. Cardiovasc. Thorac. Res.* **9,** 127–132 (2017).

81. Zelarayán, L. C. *et al.* Beta-Catenin downregulation attenuates ischemic cardiac remodeling through enhanced resident precursor cell differentiation. *Proc. Natl. Acad. Sci. U. S. A.* **105,** 19762–19767 (2008).

82. Baurand, A. *et al.* β-catenin downregulation is required for adaptive cardiac remodeling. *Circ. Res.* **100,** 1353–1362 (2007).

83. Ozhan, G. & Weidinger, G. Wnt/β-catenin signaling in heart regeneration. *Cell Regen.* **4,** 1–12 (2015).

84. Aisagbonhi, O. *et al.* Experimental myocardial infarction triggers canonical Wnt signaling and endothelial-to-mesenchymal transition. *Dis. Model. Mech.* **4,** 469–483 (2011).

85. Lee, M. *et al.* Tcf7l2 plays crucial roles in forebrain development through regulation of thalamic and habenular neuron identity and connectivity. *Dev. Biol.* **424,** 62–76 (2017).

86. Shu, L. *et al.* TCF7L2 promotes beta cell regeneration in human and mouse pancreas. *Diabetologia* **55,** 3296–3307 (2012).

87. Giordano, F. J. Oxygen, oxidative stress, hypoxia, and heart failure. *Journal of Clinical Investigation* **115,** 500–508 (2005).

88. Walton, C. B. *et al.* Cardiac angiogenesis directed by stable Hypoxia Inducible Factor-1. *Vasc. Cell* **5,** (2013).

89. J. Patterson, A. & Zhang, L. Hypoxia and Fetal Heart Development. *Curr. Mol. Med.* **10,** 653–666 (2010).

90. Frietze, S. *et al.* Cell type-specific binding patterns reveal that TCF7L2 can be tethered to the genome by association with GATA3. *Genome Biol.* **13,** R52 (2012).

91. Hatzis, P. *et al.* Genome-wide pattern of TCF7L2/TCF4 chromatin occupancy in colorectal cancer cells. *Mol. Cell. Biol.* **28,** 2732–2744 (2008).

92. He, A. *et al.* Dynamic GATA4 enhancers shape the chromatin landscape central to heart development and disease. *Nat. Commun.* **5,** (2014).

93. Makinde, A. O., Kantor, P. F. & Lopaschuk, G. D. Maturation of fatty acid and carbohydrate metabolism in the newborn heart. in *Molecular and Cellular Biochemistry* **188,** 49–56 (1998).

94. Lopaschuk, G. D. & Jaswal, J. S. Energy metabolic phenotype of the cardiomyocyte during development, differentiation, and postnatal maturation. in *Journal of Cardiovascular Pharmacology* **56,** 130–140 (2010).

95. Sethi, J. & Vidal-Puig, a. Wnt signalling and the control of cellular metabolism. *Biochem J.* **427,** 1–17 (2010).

96. Sawada, A. *et al.* Redundant Roles of Tead1 and Tead2 in Notochord Development and the Regulation of Cell Proliferation and Survival. *Mol. Cell. Biol.* **28,** 3177–3189 (2008).

97. Kaneko, K. J., Kohn, M. J., Liu, C. & DePamphilis, M. L. Transcription factor TEAD2 is involved in neural tube closure. *Genesis* **45,** 577–587 (2007).

98. Xin, M. *et al.* Hippo pathway effector Yap promotes cardiac regeneration. *Proc. Natl. Acad. Sci.* **110,** 13839–13844 (2013).

99. Zhou, Q., Li, L., Zhao, B. & Guan, K. The hippo pathway in heart development, regeneration, and diseases. *Circ. Res.* **116,** 1431–47 (2015).

100. De Anda, F. C. *et al.* Cortical neurons gradually attain a post-mitotic state. *Cell Res.* **26,** 1033–1047 (2016).

101. Aranda-Anzaldo, A. The post-mitotic state in neurons correlates with a stable nuclear higher-order structure. *Communicative and Integrative Biology* **5,** 134–139 (2012).

102. Gilsbach, R. *et al.* Distinct epigenetic programs regulate cardiac myocyte development and disease in the human heart in vivo. *Nat. Commun.* **9,** (2018).

103. Daskalopoulos, E. P., Hermans, K. C. M., Janssen, B. J. a & Matthijs Blankesteijn, W. Targeting the Wnt/frizzled signaling pathway after myocardial infarction: A new tool in the therapeutic toolbox? *Trends Cardiovasc. Med.* **23,** 121–127 (2013).

104. Hirotani, S. *et al.* Inhibition of glycogen synthase kinase 3beta during heart failure is protective. *Circ. Res.* **101,** 1164–74 (2007).

105. Gougelet, A. *et al.* T-cell factor 4 and β-catenin chromatin occupancies pattern zonal liver metabolism in mice. *Hepatology* **59,** 2344–2357 (2014).

106. Kojima, T. *et al.* FOXO1 and TCF7L2 genes involved in metastasis and poor prognosis in clear cell renal cell carcinoma. *Genes Chromosom.* **49,** 379–389 (2010).

107. Ishiguro, H. *et al.* Nuclear expression of TCF4/TCF7L2 is correlated with poor prognosis in patients with esophageal squamous cell carcinoma. *Cell. Mol. Biol. Lett.* **21,** 5 (2016).

108. Piquereau, J. *et al.* Postnatal development of mouse heart: Formation of energetic microdomains. *J. Physiol.* **588,** 2443–2454 (2010).

109. Nielsen, R. *et al.* Genome-wide profiling of PPARγ:RXR and RNA polymerase II occupancy reveals temporal activation of distinct metabolic pathways and changes in RXR dimer composition during adipogenesis. *Genes Dev.* **22,** 2953–2967 (2008).

110. Cardamone, M. D. *et al.* GPS2/KDM4A pioneering activity regulates promoter-specific recruitment of PPARγ. *Cell*

*Rep.* **8,** 163–176 (2014).

111. Stratton, M. S. *et al.* Signal-Dependent Recruitment of BRD4 to Cardiomyocyte Super-Enhancers Is Suppressed by a MicroRNA. *Cell Rep.* **16,** 1366–1378 (2016).

112. Subramanian, A. *et al.* Gene set enrichment analysis: a knowledge-based approach for interpreting genome-wide expression profiles. *Proc. Natl. Acad. Sci. U. S. A.* **102,** 15545–15550 (2005).

113. Liberzon, A. *et al.* Molecular signatures database (MSigDB) 3.0. *Bioinformatics* **27,** 1739–1740 (2011).

114. Thompson, B. a., Tremblay, V., Lin, G. & Bochar, D. a. CHD8 Is an ATP-Dependent Chromatin Remodeling Factor That Regulates -Catenin Target Genes. *Mol. Cell. Biol.* **28,** 3894–3904 (2008).

115. Wang, H. & Matise, M. P. Tcf7l2/Tcf4 transcriptional repressor function requires HDAC activity in the developing vertebrate CNS. *PLoS One* **11,** 1–11 (2016).

116. Leenders, J. J. *et al.* Repression of cardiac hypertrophy by KLF15: Underlying mechanisms and therapeutic implications. *PLoS One* **7,** (2012).

117. Fisch, S. *et al.* Kruppel-like factor 15 is a regulator of cardiomyocyte hypertrophy. *Proc Natl Acad Sci U S A* **104,** 7074–7079 (2007).

118. Zhou, J. *et al.* Loss of adult cardiac myocyte GSK-3 leads to mitotic catastrophe resulting in fatal dilated cardiomyopathy. *Circ. Res.* **118,** 1208–1222 (2016).

119. Wu, D. & Pan, W. GSK3: a multifaceted kinase in Wnt signaling. *Trends in Biochemical Sciences* **35,** 161–168 (2010).

120. Sklepkiewicz, P. *et al.* Loss of secreted frizzled-related protein-1 leads to deterioration of cardiac function in mice and plays a role in human cardiomyopathy. *Circ. Hear. Fail.* **8,** 362–372 (2015).

121. van Gijn, M. E. *et al.* The wnt-frizzled cascade in cardiovascular disease. *Cardiovasc. Res.* **55,** 16–24 (2002).

122. Yamamoto, A., Nagano, T., Takehara, S., Hibi, M. & Aizawa, S. Shisa promotes head formation through the inhibition of receptor protein maturation for the caudalizing factors, Wnt and FGF. *Cell* **120,** 223–235 (2005).

123. Furushima, K. *et al.* Mouse homologues of Shisa antagonistic to Wnt and Fgf signalings. *Dev. Biol.* **306,** 480–492 (2007).

124. Nemeth, M. J., Topol, L., Anderson, S. M., Yang, Y. & Bodine, D. M. Wnt5a inhibits canonical Wnt signaling in hematopoietic stem cells and enhances repopulation. *Proc. Natl. Acad. Sci. U. S. A.* **104,** 15436–41 (2007).

125. Bengoa-Vergniory, N., Gorroño-Etxebarria, I., González-Salazar, I. & Kypta, R. M. A switch from canonical to noncanonical wnt signaling mediates early differentiation of human neural stem cells. *Stem Cells* **32,** 3196–3208 (2014).

126. Sangwung, P. *et al.* KLF2 and KLF4 control endothelial identity and vascular integrity. *JCI Insight* **2,** e91700 (2017).

127. Lee, J. S. *et al.* Klf2 Is an Essential Regulator of Vascular Hemodynamic Forces In Vivo. *Dev. Cell* **11,** 845–857 (2006).

128. Lu, Y. *et al.* Kruppel-like factor 15 is critical for vascular inflammation. *J. Clin. Invest.* **123,** 4232–41 (2013).

129. Lu, Y. *et al.* Kruppel-like factor 15 regulates smooth muscle response to vascular injury. *Arter. Thromb Vasc Biol* **30,** 1550–2 (2010).

130. Dunty, W. C. *et al.* Wnt3a/ -catenin signaling controls posterior body development by coordinating mesoderm formation and segmentation. *Development* **135,** 85–94 (2007).

131. Nakagawa, A. *et al.* Activation of endothelial β-catenin signaling induces heart failure. *Sci. Rep.* **6,** (2016).

132. Son, N. H. *et al.* Cardiomyocyte expression of PPAR?? leads to cardiac dysfunction in mice. *J. Clin. Invest.* **117,** 2791–2801 (2007).

133. Mccormick, J. *et al.* STAT1 deficiency in the heart protects against myocardial infarction by enhancing autophagy. *J. Cell. Mol. Med.* **16,** 386–393 (2012).

134. Biechele, T. L. & Moon, R. T. in *Wnt Signaling, Volume I: Pathway Methods and Mammalian Models,* **468,** 99–110 (2008).

135. Reya, T. *et al.* Wnt signaling regulates B lymphocyte proliferation through a LEF-1 dependent mechanism. *Immunity* **13,** 15–24 (2000).

136. Giese, K., Amsterdam, A. & Grosschedl, R. DNA-binding properties of the HMG domain of the lymphoid-specific transcriptional regulator LEF-1. *Genes Dev.* **5,** 2567–2578 (1991).

137. Arce, L., Yokoyama, N. N. & Waterman, M. L. Diversity of LEF/TCF action in development and disease. *Oncogene* **25,** 7492–7504 (2006).

138. Merrill, B. J. *et al.* Tcf3: a transcriptional regulator of axis induction in the early embryo. *Development* **131,** 263–274 (2004).

139. Kim, C. H. *et al.* Repressor activity of Headless/Tcf3 is essential for vertebrate head formation. *Nature* **407,** 913–916 (2000).

140. Yi, F. *et al.* Opposing effects of Tcf3 and Tcf1 control Wnt stimulation of embryonic stem cell self-renewal. *Nat. Cell Biol.* **13,** 762–770 (2011).

141. Roël, G., Gent, Y. Y. J., Peterson-Maduro, J., Verbeek, F. J. & Destrée, O. Lef1 plays a role in patterning the mesoderm and ectoderm in Xenopus tropicalis. *Int. J. Dev. Biol.* **53,** 81–89 (2009).

142. Ladstein, R. G., Bachmann, I. M., Straume, O. & Akslen, L. A. Ki-67 expression is superior to mitotic count and novel proliferation markers PHH3, MCM4 and mitosin as a prognostic factor in thick cutaneous melanoma. *BMC Cancer* **10,** (2010).

143. Martin, J., Afouda, B. a. & Hoppler, S. Wnt/β-catenin signalling regulates cardiomyogenesis via GATA transcription factors. *J. Anat.* **216,** 92–107 (2010).

144. Ahuia, P. *et al.* Transcriptional regulation of cardiac metabolism and mitochondrial biogenesis in response to pathological stress. *J.* **In Press,** (2009).

145. Benhaddou, A. *et al.* Transcription factor TEAD4 regulates expression of Myogenin and the unfolded protein response genes during C2C12 cell differentiation. *Cell Death Differ.* **19,** 220–231 (2012).

146. Liu, R. *et al.* Tead1 is required for maintaining adult cardiomyocyte function, and its loss results in lethal dilated cardiomyopathy. *JCI insight* **2,** 1–15 (2017).

147. Diepenbruck, M. *et al.* Tead2 expression levels control Yap/Taz subcellular distribution, zyxin expression, and epithelial-mesenchymal transition. *J. Cell Sci.* 1523–1536 (2014). doi:10.1242/jcs.139865

148. Curran, E. C., Wang, H., Hinds, T. R., Zheng, N. & Wang, E. H. Zinc knuckle of TAF1 is a DNA binding module critical for TFIID promoter occupancy. *Sci. Rep.* **8,** (2018).

149. Boija, A. *et al.* CBP Regulates Recruitment and Release of Promoter-Proximal RNA Polymerase II. *Mol. Cell* **68,** 491–503.e5 (2017).

150. Shah, A. V. *et al.* The endothelial transcription factor ERG mediates Angiopoietin-1-dependent control of Notch signalling and vascular stability. *Nat. Commun.* **8,** (2017).

151. Zerlin, M., Julius, M. A. & Kitajewski, J. Wnt/Frizzled signaling in angiogenesis. *Angiogenesis* **11,** 63–69 (2008).

152. Goodwin, A. M. & D'Amore, P. A. Wnt signaling in the vasculature. *Angiogenesis* **5,** 1–9 (2002).

# Appendix

Luciferase reporter constructs mentioned in Chapter 1.

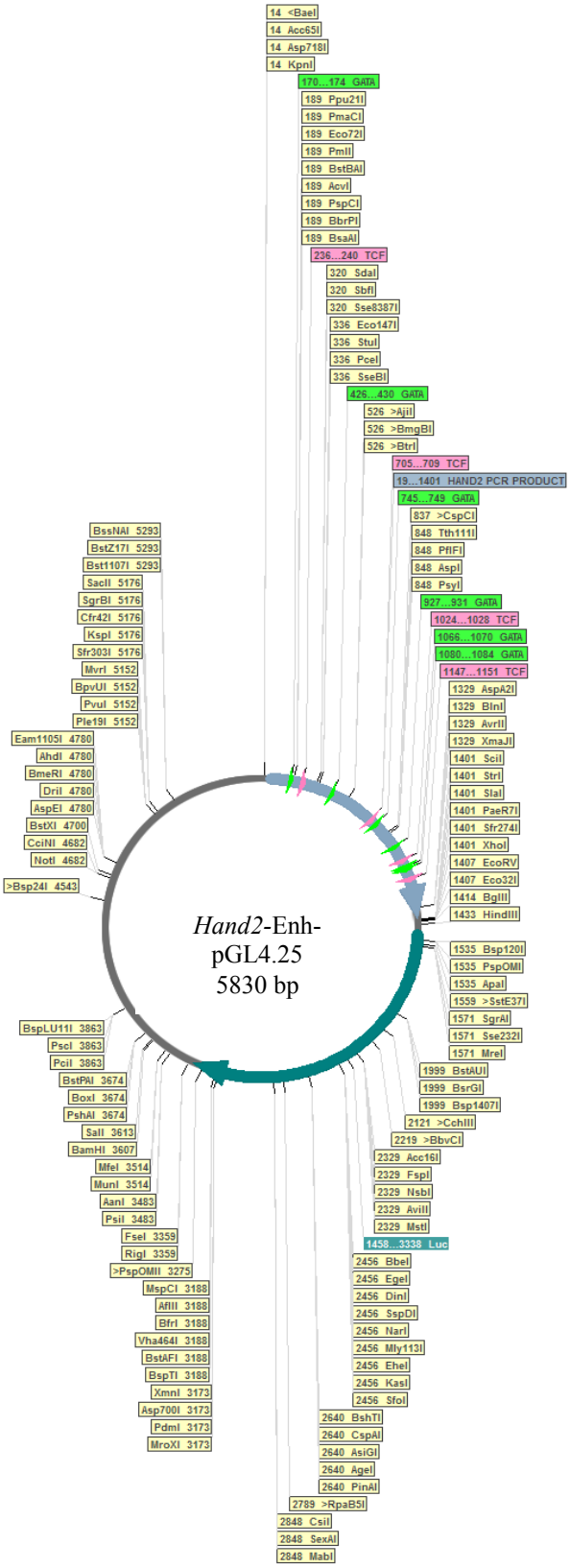

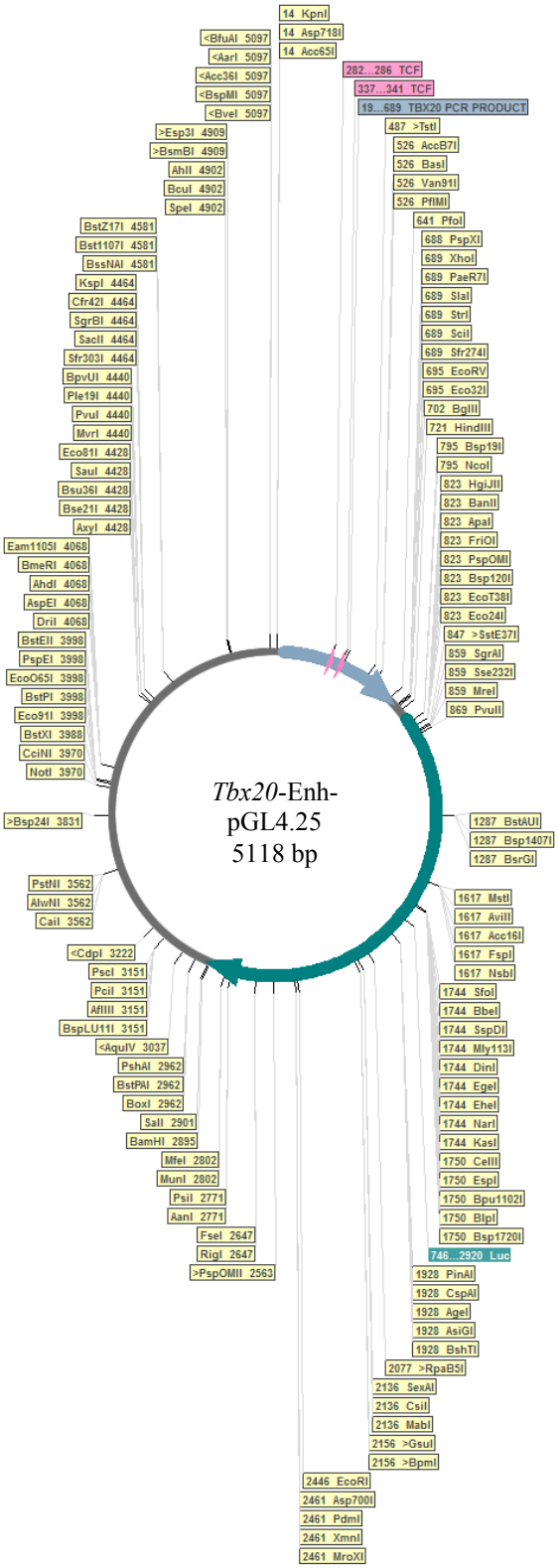
14 KpnI
14 Asp718I
14 Acc65I
<BfuAI 5097
<AarI 5097
<Acc36I 5097
<BspMI 5097
<BveI 5097
>Esp3I 4909
>BsmBI 4909
AhlI 4902
BcuI 4902
SpeI 4902
BstZ17I 4581
Bst1107I 4581
BssNAI 4581
KspI 4464
Cfr42I 4464
SgrBI 4464
SacII 4464
Sfr303I 4464
BpvUI 4440
Ple19I 4440
PvuI 4440
MvrI 4440
Eco81I 4428
SauI 4428
Bsu36I 4428
Bse21I 4428
AxyI 4428
Eam1105I 4068
BmeRI 4068
AhdI 4068
AspEI 4068
DriI 4068
BstEII 3998
PspEI 3998
EcoO65I 3998
BstPI 3998
Eco91I 3998
BstXI 3988
CciNI 3970
NotI 3970
>Bsp24I 3831
PstNI 3562
AlwNI 3562
CaiI 3562
<CdpI 3222
PscI 3151
PciI 3151
AflIII 3151
BspLU11I 3151
<AquIV 3037
PshAI 2962
BstPAI 2962
BoxI 2962
SalI 2901
BamHI 2895
MfeI 2802
MunI 2802
PsiI 2771
AanI 2771
FseI 2647
RigI 2647
>PspOMII 2563
2446 EcoRI
2461 Asp700I
2461 PdmI
2461 XmnI
2461 MroXI
2156 >BpmI
2156 >GsuI
2136 MabI
2136 CsiI
2136 SexAI
2077 >RpaBSI
1928 BshTI
1928 AsiGI
1928 AgeI
1928 CspAI
1928 PinAI
746...2920 Luc
1750 Bsp1720I
1750 BlpI
1750 Bpu1102I
1750 EspI
1750 CelII
1744 NarI
1744 KasI
1744 EheI
1744 EgeI
1744 DinI
1744 Mly113I
1744 SspDI
1744 BbeI
1744 SfoI
1617 NsbI
1617 FspI
1617 Acc16I
1617 AviII
1617 MstI
1287 BsrGI
1287 Bsp1407I
1287 BstAUI
847 >SstE37I
859 MreI
859 Sse232I
859 SgrAI
869 PvuII
823 EcoT38I
823 Bsp120I
823 PspOMI
823 FriOI
823 ApaI
823 BanII
823 HgiJII
795 NcoI
795 Bsp19I
721 HindIII
702 BglII
695 Eco32I
695 EcoRV
689 Sfr274I
689 ScaI
689 StrI
689 SlaI
689 PaeR7I
689 XhoI
688 PspXI
641 PfoI
526 Van91I
526 PflMI
526 BasI
526 AccB7I
487 >TstI
19...689 TBX20 PCR PRODUCT
337...341 TCF
282...286 TCF
Tbx20-Enh-
pGL4.25
5118 bp

## Curriculum Vitae


# Ms. Lavanya Muthukrishnan Iyer (*2 August, 1991)

*PhD Candidate, Institute of Pharmacology and Toxicology, University Medical Center Goettingen,*
*Robert-Koch-Str. 40, 37075 Goettingen, Germany. Tel: +49(0)55139-5777, Fax: +49(0)55139-5699,*
*E-mail: lavanya.iyer@med.uni-goettingen.de*


## Languages spoken

*English, Hindi, Tamil, German.*

## Key skills

RNA-seq, ChIP-seq, bioinformatic data analyses and interpretation, chromatin biology and transcriptomics.

## Academic Qualifications

**2015–Oct 18** **PhD Candidate**
*Institute of Pharmacology and Toxicology, University Medical Center Goettingen, Germany.*
Thesis Supervisor: Priv.-Doz. Dr. Laura Zelarayan
Thesis Title: "Wnt/TCF7L2-dependent transcriptional and chromatin dynamics in cardiac regeneration, homeostasis and disease"

**2013-15** **Masters of Science (Molecular Medicine)**,
*Institute of Pharmacology and Toxicology, University Medical Center Goettingen, Germany.*
Thesis Supervisor: Priv.-Doz. Dr. Laura Zelarayan
Thesis Title: "Role of TCF7L2 in cardiac homeostasis and disease."
**GPA: 1.44** (Highest=1.0)

**2009-13** **Bachelor of Technology (Genetic Engineering)**
*Department of Neurogenetics and Translational Medicine, Institut de Genetique et de Biologie Moleculaire et Cellulaire (IGBMC), Strasbourg, France (thesis)* and *SRM University, Chennai, India (degree).*
Thesis Supervisor: Dr. Jocelyn Laporte
Thesis Title: "Development and characterization of tools for zebrafish congenital myopathy models."
**GPA: 9.54** (Highest=10)

## Awards and Honours

**2018** **Best Science Slam,** German Pharmacology-Toxicology Summit, Goettingen, Germany.

**2017** **Young Investigator Award,** German Center for Cardiovascular Research (DZHK) Retreat, Warnemuende, Germany.

**2013-15** **Erasmus Mundus India4EUII fellowship** for masters program: MSc. Molecular Medicine, Goettingen, Germany.

**2014** **Silver Medal** for academic performance in B.Tech Genetic Engineering, SRM University, India.
**2012** **Indian Academy of Sciences (IAS) fellowship** (Summer Research Program)
**2011** **Best Project Idea,** National conference on Biopharmaceuticals and Healthcare, Bengaluru, India.

## Professional Memberships

**2017 –** European Society of Cardiology (ESC, ID #776451)
**2016 –** Deutsches Zentrum für Herz Kreislauf (DZHK; German Center for Cardiovascular Research)

## Publication(s)

**Iyer, L. M**. *et al.* A context-specific cardiac β-catenin and GATA4 interaction influences TCF7L2 occupancy and remodels chromatin driving disease progression in the adult heart. ***Nucleic Acids Res.*** (2018). 2018 Apr 6;46(6):2850-2867. doi: 10.1093/nar/gky049.

## Selected Conference Presentations

Iyer, LM., Woelfer, M., et al. *"Dynamic Stage-Specific 'Wnt' Chromatin Landscapes Govern Cardiac Development and Disease."* Keystone symposium on Gene control in Development and Disease; Poster Presentation. 23rd-27th March 2018; Whistler, British Columbia, Canada.

Iyer, LM., Noack C., Nagarajan S., et al. *"Activating Wnt/TCFL2 signaling initiates aberrant transcriptional landscapes and pathological remodelling in the adult heart."* Keystone symposium on Molecular Mechanisms of Heart Development; Poster Presentation. 26-30th March 2017; Colorado, USA.

Iyer, LM., Noack C., Kari, V., "*Activation of Wnt/β-catenin/Tcf7l2 signaling initiates aberrant transcriptional landscapes leading to cardiac dysfunction in the adult heart."* German Center for Cardiovascular Research (DZHK) Annual Conference; Oral Presentation. 14-17th September 2016; Bad Aibling, Germany.

## Referees

1. **PD Dr. Laura C. Zelarayan:** Institute of Pharmacology and Toxicology, University Medical Center (UMG), Robert-Koch Str. 40, 37075, Goettingen, Germany; laura.zelarayan@med.uni-goettingen.de; +49(0)55139-20730.
2. **Dr. Jocelyn Laporte:** Department of Neurogenetics and Translational Medicine, IGBMC, 1 Rue Laurent Fries, 67400, Illkirch, Strasbourg, France; jocelyn.laporte@igbmc.fr; +33(0)388653412.